UNIVERSITÉ DE GENÈVE

Section de Biologie
Département de biologie moléculaire

FACULTÉ DES SCIENCES
Professeur Jean-Claude Martinou

LIGHT CHAIN BIOSCIENCE – NOVIMMUNE SA

Docteur Krzysztof Masternak

Targeting CD47 and PD-L1 Immune Checkpoints with Bispecific Antibodies

THÈSE

présentée aux Facultés de médecine et des sciences de l'Université de Genève
pour obtenir le grade de Docteur ès sciences en sciences de la vie,
mention Biosciences moléculaires

par

Elise PENARRIETA

de

Salins (Valais)

Thèse N° 167

GENÈVE

2022

LIFE SCIENCES PhD SCHOOL GENEVA

DOCTORAT ÈS SCIENCES EN SCIENCES DE LA VIE DES FACULTÉS DE MÉDECINE ET DES SCIENCES

MENTION BIOSCIENCES MOLÉCULAIRES

Thèse de Madame Elise PENARRIETA

intitulée :

«Targeting CD47 and PD-L1 Immune Checkpoints with Bispecific Antibodies»

Les Facultés de médecine et des sciences, sur le préavis de Monsieur K. MASTERNAK, docteur et directeur de thèse (Light Chain Biosciences, NovImmune SA, Plan-les-Ouates), Monsieur J.-C. MARTINOU, professeur ordinaire et codirecteur de thèse (Département de biologie cellulaire), Monsieur P. WALKER, docteur (Faculté de médecine, Département de médecine interne des spécialités), Monsieur M. DE PALMA, professeur associé (Institut suisse de recherche expérimentale sur le cancer, Faculté des sciences de la vie, École polytechnique fédérale de Lausanne, Lausanne), autorisent l'impression de la présente thèse, sans exprimer d'opinion sur les propositions qui y sont énoncées.

Genève, le 28 juin 2022

Thèse - 167 -

Le Doyen
Faculté de médecine

Le Doyen
Faculté des sciences

N.B. - La thèse doit porter la déclaration précédente et remplir les conditions énumérées dans les "Informations relatives aux thèses de doctorat à l'Université de Genève".

Abstract

Cancer cells can evade immune system surveillance by creating an immunosuppressive microenvironment and by expressing inhibitory molecules, such as PD-L1 and CD47. The latter is an innate immune checkpoint and a marker of "self" expressed by virtually all cells. Upon its interaction with SIRPα, CD47 protects cells from destruction by innate immune phagocytes, a mechanism that is hijacked by many cancers. In pre-clinical studies, anti-CD47 monoclonal antibodies (mAbs) promoted tumor elimination by increasing phagocytosis of tumor cells and by enhancing antigen cross presentation, thus providing a strong rationale for CD47 targeting in the clinic. A large number of anti-CD47 mAbs and SIRPα-Fc fusion proteins are now being tested in clinical trials. Notwithstanding, monospecific CD47 targeting suffers from important limitations, such as poor pharmacokinetics and hematotoxicity related to the ubiquitous expression of CD47, including on platelets and on red blood cells (the so called "CD47 antigen sink"). CD47-targeting with bispecific antibodies represents an alternative and safer approach, allowing to mitigate the "antigen sink" issues, since CD47 targeting can be restricted to defined cell populations.

In my PhD thesis work, I investigated the anti-tumor efficacy, the pharmacokinetics, and the mechanism of action of CD47|PD-L1 bsAbs in the context of different Fc portions (either active or silenced Fc). As expected, the bsAbs efficiently blocked the PD-1/PD-L1 and CD47/SIRPα interactions on double positive cells and showed minimal binding to PD-L1 negative cells, such as red blood cells. *In vivo*, these bsAbs showed a modest effect on tumor growth in the MC38 syngeneic model, but no difference in anti-tumor efficacy was apparent when comparing a bsAb with an active Fc with its silenced Fc counterpart. However, Fc silencing significantly improved the pharmacokinetics of the CD47|PD-L1 bsAb, confirming the notion that FcgR binding may contribute to antibody elimination, probably by exaggerating the TMDD (target-mediated drug disposition) rate. Finally, I also performed an analysis of the tumor microenvironment and showed that the bsAb treatment enhanced both the innate and the adaptive immune responses, as demonstrated by an increase in M1-like macrophages and CD8+ T cell infiltration.

Résumé

Les cellules cancéreuses peuvent échapper à la surveillance du système immunitaire en créant un microenvironnement immunosuppresseur via l'expression de molécules inhibitrices, telles que PD-L1 et CD47. Ce dernier est un point de contrôle immunitaire inné et un marqueur du « soi » exprimé par pratiquement toutes les cellules. Lors de son interaction avec SIRPα, CD47 protège les cellules de la destruction par les phagocytes ; ce mécanisme est détourné par de nombreux cancers qui peuvent surexprimer CD47. Les anticorps monoclonaux anti-CD47 (mAbs) ont favorisé l'élimination de tumeurs sur des modèles souris, en augmentant la phagocytose des cellules tumorales et en améliorant la présentation croisée d'antigènes exogènes aux lymphocytes T, motivant des études cliniques. Un grand nombre de mAbs anti-CD47 et de protéines de fusion SIRPα-Fc sont actuellement investiguées dans les cancers solides et les hémopathies malignes. Néanmoins, le ciblage de CD47 avec ce type d'approche présente des limites : i) un profil pharmacocinétique peu satisfaisant et ii) une hématotoxicité, liés à l'expression de CD47 par les globules rouges (jouant le rôle de « puits d'antigène » CD47) et les plaquettes. L'utilisation d'anticorps bispécifiques (bsAbs) d'affinités optimisées représente une alternative attractive pour favoriser le ciblage de CD47 sur les cellules tumorales, en atténuant la liaison aux globules rouges.

Dans mon travail de thèse de doctorat, j'ai étudié l'efficacité anti-tumorale, la pharmacocinétique et le mécanisme d'action de bsAbs CD47|PD-L1 possédant différentes parties Fc (capables de se lier ou non aux récepteurs Fc). Les bsAbs bloquent efficacement les interactions PD-1/PD-L1 et CD47/SIRPα sur des cellules tumorales exprimant CD47 et PD-L1 et présentent une faible liaison aux cellules négatives pour PD-L1 dont les globules rouges. *In vivo*, ces bsAb ont montré un effet modeste sur la croissance tumorale dans le modèle syngénique MC38, sans qu'une différence d'activité soit établie entre les différentes bsAbs. Cependant, l'inactivation de la partie Fc a significativement amélioré la pharmacocinétique du bsAb, confirmant que l'engagement des récepteurs Fc contribue à l'élimination des anticorps, probablement en exagérant le taux de TMDD (disposition médiée par la cible). Enfin, j'ai également effectué une analyse du microenvironnement tumoral et montré que le traitement par les bsAbs améliorait à la fois les réponses immunitaires innées et adaptatives, comme en témoigne l'augmentation des macrophages pro-inflammatoires de type M1 et l'infiltration des lymphocytes T CD8+.

Remerciements

Tout d'abord, je tiens particulièrement à remercier le Dr. Krzysztof. Masternak qui a suivi et supervisé ce projet de thèse. Krzysztof, merci pour ta disponibilité et ton soutien. Merci d'avoir su rester constant, compréhensif et optimiste face à toutes les difficultés rencontrées au fil des années. Un grand merci pour l'énergie et le temps que tu as consacré lors de la rédaction et la correction de ce manuscrit.

Je tiens à remercier le professeur Michele De Palma d'avoir accepté de participer à mon jury de thèse. Merci pour le temps consacré à l'évaluation de ce travail.

Je tiens à remercier le professeur Paul Walker pour sa participation à mon jury de thèse ainsi que pour sa participation à l'évaluation de mon projet lors du TAC meeting.

Je tiens à remercier le professeur Jean-Claude Martinou qui est non seulement membre de mon jury de thèse mais aussi le co-directeur de ce projet.

Je tiens à remercier le Dr. Nicolas Fischer pour m'avoir permis de faire ma thèse au sein de Novimmune/LCB.

Un grand merci à la professeur Stéphanie Hugues et à sa doctorante Mengzhu Sun avec lesquelles j'ai collaboré pour l'analyse du microenviroment tumoral. Merci pour vos conseils avisés et votre expertise. Je tiens aussi à remercier tous les autres membres du laboratoire qui, à chacune des expériences, ont été d'une aide précieuse.

Je tiens à remercier Xavier pour sa participation active dans mon projet de thèse. Merci pour toutes tes suggestions et conseils pertinents ainsi que pour tes conseils et corrections lors de la rédaction de ce manuscrit. Merci d'avoir trouvé les bons mots quand il le fallait, et de ne jamais te départir de ton énergie et ta motivation quand il s'agit d'attaquer une nouvelle expérience.

Je souhaite remercier tous les membres de la Biology Section (souvenir d'une époque lointaine à Novimmune). Un merci particulier à Sara qui m'a coachée au tout début de ma thèse et dont j'ai souvent sollicité l'avis et les conseils précieux. Merci à Valéry Moine qui m'a accompagnée lors des premières manips vivo et qui a su rester disponible tout au long de ma thèse (même le dimanche). Merci Ulla et à son équipe, plus particulièrement Nessie, Sébastien et Nicolas sans qui les bras anti-PD-L1 et CD47 décrits dans ce projet n'auraient pas vu le jour. Merci à Giovanni, Pauline et à l'équipe PGN qui m'ont accueillie dans leur labo pour le travail de biologie moléculaire. Merci d'avoir pour votre aide indispensable et votre expertise. Merci à Yves et à toute l'équipe BIP qui m'a chaleureusement accueillie. Merci Guillemette d'avoir toujours trouvé une solution (sauf quand un bsAb ne produit qu'un mAb), de m'avoir toujours proposé ton aide. Un grand merci à Christophe pour m'avoir donné de rigoureuses et solides bases de purification. L'AKTA n'est plus un mystère pour moi. Merci à Tereza pour tes conseils et ta relecture. Un

grand merci à toute l'équipe *vivo* qui m'a apporté une aide des plus indispensables. Merci à Laurence pour ton aide et ta réactivité dans l'écriture des demandes d'expérimentation. Merci à Emeline E. pour ta disponibilité, ton écoute et tes encouragements. Un grand merci à Laura sans qui plusieurs des expériences *vivo* décrites dans ce travail n'auraient pas pu être faites. J'apprécie ta détermination, ton éthique professionnelle et ton énergie quand il s'agit de mener une expérience rigoureusement et efficacement. Un immense merci à Lise et Elise qui m'ont accompagnée durant ces années de thèse. Lise, merci pour ton énergie et tes conseils, merci d'avoir toujours eu le bon mot et le bon coup de gueule dans les moments de doute. Merci pour toutes ces conversations tard le soir à refaire le monde ou plutôt refaire nos thèses. Un grand merci à Elise pour ta bonne humeur et ton optimisme sans faille, c'est un bonheur de t'avoir comme collègue. Merci d'avoir su me comprendre sans forcément devoir m'expliquer. Et comme une PhD avisée me l'a dit autrefois, il y a une lumière au bout du tunnel. D'une manière générale, un grand merci à tous mes collègues de LCB que je n'ai pas cités ici mais dont les encouragements et la bienveillance tout au long de ces années ont été d'une grande aide.

Je tiens également à remercier mes anciens collègues du laboratoire du professeur Ivan Rodriguez, de m'accueillir comme si je n'étais jamais partie et d'être là pour continuer à fêter mon master. Je tiens aussi à remercier mes anciens collègues de MMV et plus particulièrement Fanny et Mélanie.

Je tiens à exprimer toute ma gratitude envers mes amis dont la présence et le soutien ont été mon oxygène et qui ont compris et accepté bien souvent mon absence. Merci à la Bicaudal Team, Florian, Gerda, Mariana, Marie, Stéphanie et plus particulièrement à sa section romande, Gaby, Kevin et Rhéa. Merci à Madlaina et Joël pour tous les moments partagés et vos conseils. Merci à Natalia, Maroussia, Caroline et Karine, des sources d'inspiration et d'énergie indispensables. Merci à la dynastie Kan de m'avoir fait me sentir chez moi et de m'avoir laissé partager d'inestimables moments à vos côtés. Merci Kunthea pour ton soutien sans faille et ton optimisme à tout épreuve. Merci à tous ceux qui ont été là dans les moments clés de ma vie, Seb, Sam, Max, Maria et Vincent. Chenda, les mots me manquent pour exprimer ma gratitude. Merci de m'avoir accompagnée et soutenue à chaque étape, merci pour ton énergie et ton amour.

Un immense et infini merci à mes parents, qui m'ont toujours soutenu sans jamais me mettre la pression. A Mary et à Bruno, qui me permettent de prendre du recul pour continuer d'avancer. Et merci à Léa qui apporte des rires et de la légèreté à ma vie.

Last but not least, merci Luca. Ces années ont été intenses et il n'y que toi qui a pu et su prendre la mesure des moments traversés. Merci d'avoir partagé tout cela à mes côtés et de m'avoir permis d'avancer.

Contents

1. Introduction

Cancer is a leading social, economic and health system burden while also the second highest cause of death worldwide [1]. It is currently estimated to replace ischemic heart disease at number one by the year 2060 [1]. Historical approaches to treat cancer, beyond physical removal by surgery, relied on radiotherapy, chemotherapies as well as hormone therapy [2]. Improvements in the understanding of the biology of cancer have led to more precise sub-classification of cancers and thus increasingly targeted therapies [3]. Recently, immunotherapeutic drugs have deeply changed the approach to cancer treatment [4]. Although this shift has only occurred in the past couple of decades, the first studies on immunotherapy and cancer emerged in the early 1900s with the work of William Coley [5]. Based on observations in some patients where cancer remission was associated with a bacterial infection, he started to assess the link between the intratumoral injection of bacterial suspensions and the anti-tumor response. The lack of reproducibility and consistency in the experiments raised doubts in the scientific community regarding the validity of the approach [5]. At the same time, the rise of radiotherapy, which showed immediate effect on tumor growth, slowed down the development of immunotherapy [6]. The beginning of the 21st century saw a speed up in the transition of several immunotherapy approaches from bench to bedside [4]. Among them was the discovery of T cell immune checkpoints and their role in T cell response inhibition [7], [8]. Targeting inhibitory immune checkpoint with antagonizing monoclonal antibodies (mAb) resulted in tremendous anti-tumoral effects and increased in patients' survival [9], [10]. Yet, failure of treatment in a majority of patients still highlights the needs for new therapeutic strategies. In order to fully appreciate the revolutionary approach of immunotherapy, one must first understand the functioning of the immune system and the tumor ability to evade it.

1.1. Innate and adaptive immune responses

Survival of any organism depends on its ability to live in a hostile environment. The immune system is a complex network of cells and molecules capable of mediating host protection by recognizing and eliminating noxious foreign substances. Immediately following detection of a pathogen or a harmful compound, the immune system begins with a broad response mediated by the innate immunity [11]. A second stage requires the adaptive immune response, which has higher specificity. Components of each response are tightly regulated and dependent on the other to ensure an appropriate balance between pathogen destruction and host tissues protection [11].

Upon detection of a pathogen, a broad array of immune cells are mobilized to fight the threat. The innate immune response is based on cells whose receptors can recognized common patterns expressed by pathogens or damaged cells [11]. This recognition triggers a strong and immediate response to eliminate the danger as well as the production of inflammatory molecules. Cells of the innate immunity also serve a second function - triggering the activation of the adaptive immune response. Innate immune response differs depending on the type of bacteria, fungus, virus or damaged cell encountered so that the reaction can be tailored to the threat [11].

Among the innate immune cells are the phagocytic cells such as macrophages, dendritic cells (DCs), monocytes and neutrophils[11]. These cells are specialized in capturing and engulfing external foreign substances and other cells [11]. Once internalized, the antigens are processed and cleaved into short peptides that are then displayed at the cell surface in the context of the major histocompatibility complex (MHC) [11]. Among the antigen presenting cells (APCs), DCs are critical to initiate the adaptive immune response [11]. Antigen capture together with costimulatory signals from the microenvironment induce maturation of DCs that is characterized by phenotypic and functional changes [12]. During this process, DCs upregulate MHC II, the costimulatory receptor CD40, as well as CD80 and CD86 [12], [13]. Changes in morphology as well as in cell surface receptor expression allow DCs to migrate to secondary lymphoid organs. In lymph nodes, they interact with T cells and provide the required signals via costimulatory molecules and secreted cytokines to trigger their activation [13]. DCs have the ability to process and present external antigens not only in the context of their MHC class II but also in the context of MHC class I (usually dedicated to cytosolic antigen presentation) via a process called cross-presentation. DCs are thus endowed with the ability to initiate both CD4+ and CD8+ T cell response upon antigen presentation in the context of MHC II and MHC I respectively [12]. Interaction between DCs and T cells does not only result in signaling within the T cell but can also trigger a signal back to the DCs to enhance their activation as exemplified by the CD40-CD40L signaling [14].

1.2. Cell mediated adaptive immune response

The adaptive response can be divided into humoral response, which involves B lymphocytes and antigen production, and cellular response mediated by T lymphocytes. Mobilizing the cell-mediated immunity to fight and eliminate cancer is critical for the success of immunotherapy, and thus understanding how the T cells response is regulated is of utmost importance. T cells originate from

hematopoietic stem cells in the bone marrow and migrate to the thymus where they complete their maturation process. Once mature they are released into the circulatory system as naïve cells[11].

1.2.1. T cell priming and activation

T cells are characterized by the expression at their surface of an antigen receptor, the T cell receptor (TCR), involved in antigen recognition and T cell activation [11]. The TCR is an heterodimeric protein composed of α and β chains which are non-covalently associated with the CD3 co-receptor complex and two intracellular zeta chains [15]. TCR αβ chains are involved in antigen recognition while the CD3 and the zeta chains mediate the signal transduction [16], [17]. Activation of naïve T cells occurs in secondary lymphoid organs and requires the accumulation of two different signals resulting from the interaction between the naïve T cell and the activated APC [11]. The first signal is mediated by the interaction between the TCR, and its cognate antigen presented in the context of MHC complex. The second one is mediated by interaction of costimulatory receptors at the surface of T cells, such as CD28, with ligands expressed on activated APCs, such as CD80 and CD86. This second signal amplifies the signaling pathway downstream of the TCR complex [11], [15] and triggers T cell expansion and IL-2 production (IL-2 is the principal cytokine involved in T cell proliferation and differentiation) [11], [18], [19]. T cell activation mediated only by TCR stimulation without costimulatory signals results in anergy: a state where T cells fail to functionally respond to antigen stimulation [20]. T cell activation results in an important process of differentiation and proliferation that is characterized by modification of the expression of cytokines and surface molecules [11]. Activated T cells leave the secondary lymphoid organs (SLOs) and migrate to the site of infection where they can be reactivated upon antigen encounter [11]. In addition to the two signals described above, a third signal mediated by cytokines produced by DCs supports a strong T cell response and expansion [21] (Fig. I).

1.2.2. T cell subsets

T cells subsets are categorized depending on the co-receptor they express, either CD4+ or CD8+. Both subtypes have defined effector functions [11]. CD4+ T cells activate and modulate the activity of other immune cells by secreting various cytokines [22] while CD8+ T cells, or cytotoxic T lymphocytes (CTLs), have the ability to directly kill cells. The third signal mediated by DCs is a critical determinant of the nature of the T cell response for CD4+ and CD8+ T cells. [21], [22]. For CD4+ T cells, the differentiation

and polarization depends on the specific set of cytokines produced by DCs, which differs depending on the type of pathogens encountered [23]. Depending on the set of cytokines, CD4+ T cells acquire distinct functions characterized by different phenotypic and transcriptomic profiles (Fig. I). For instance, Th1 subset produce interferon (IFN) γ which is involved in macrophage activation while Th2 mostly produce interleukin-4 (IL-4), IL-5, IL-13 and IL-19 that are key to activate the eosinophils [11].

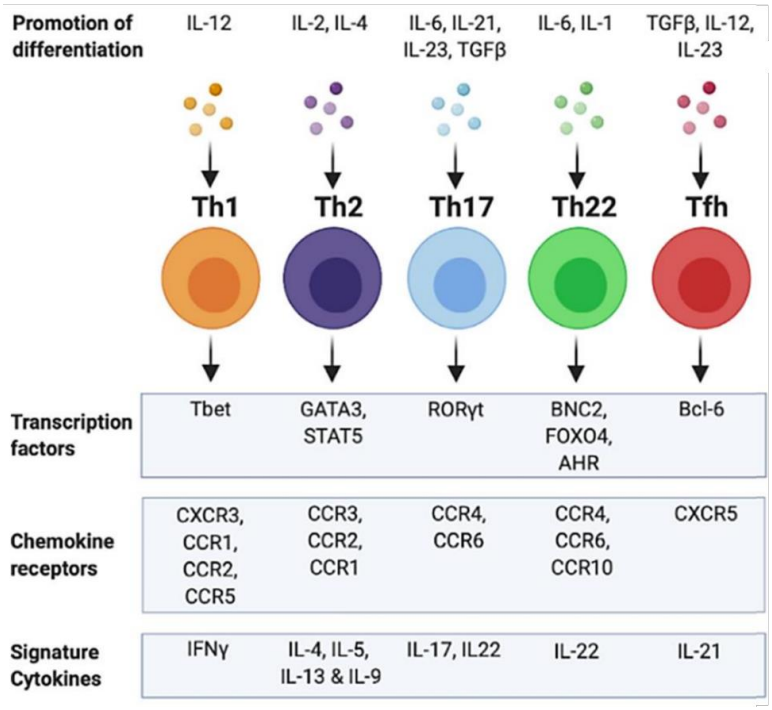

Figure I: The main CD4+ T helper subsets. Modified from [22].

As mentioned above, CD8+ T have the ability to kill target cells upon TCR-MHCI-antigen complex interaction [11] , either via the secretion of cytotoxic compounds (perforin, granzymes A and B) or by inducing apoptosis via Fas-FasL interaction [11]. They also exert pro-inflammatory functions by secreting cytokines such as IFN-γ and Tumor Necrosis Factor (TNF) α [11], [24]. The third signal produced by DCs can either enhance effector functions or promote tolerance of CD8+ T cells [21]. Type I IFN, IFN-γ and IL-12 are triggers of strong CD8+ T cell responses [21].

Another subset of T cells is constituted by regulatory T cells (Tregs), which are immunosuppressive cells involved in maintenance of self-antigen tolerance to avoid autoimmunity [25]. Tregs are characterized by the expression of CD4+ CD25+ and the transcription factor Foxp3+ [26]. In addition, Tregs constitutively express high level of inhibitory receptors such as CTLA-4, PD-1 and LAG-3 [27]–[29]. Tregs dampen effector T cell functions by several mechanisms [30]. As described in the following section, CTLA-4 inhibits the CD28-CD80/ CD86 interaction by decreasing the amount of co-stimulatory molecules on

APCs [31], [32]. In addition, Tregs participate in immunosuppression by secreting IL-10, IL-35 and TGFβ [33] and by depleting IL-2 [34].

Following T cell activation, antigen specific T cells expand and proliferate and give rise to different T subsets of T cells, either effector T cells or memory T cells. Effector T cells represent a short-lived subset of functionally active T cells. Upon antigen clearance, the T cell response contracts and the bulk of effector T cells dies by apoptosis [11], [35]. On the other hand, activated T cells can also differentiate into a long-living T cell subset, called T memory cells, which can persist for years and can reactivate quickly upon antigen re-encounter [11], [36]. Memory T cells can be categorized into three different groups (Fig. II) [11], [36]–[38]. Central memory T cells (T_{CM}), mostly found in the secondary lymphoid organs, are able to quickly proliferate but have poor effector functions. Effector memory T cells (T_{EM}), which can be found both in circulation and in tissues, have a low proliferative ability but high cytotoxic functions. Finally, resident memory T cells (T_{RM}) are only found in tissues, have low proliferative and migratory potential but high effector functions [39].

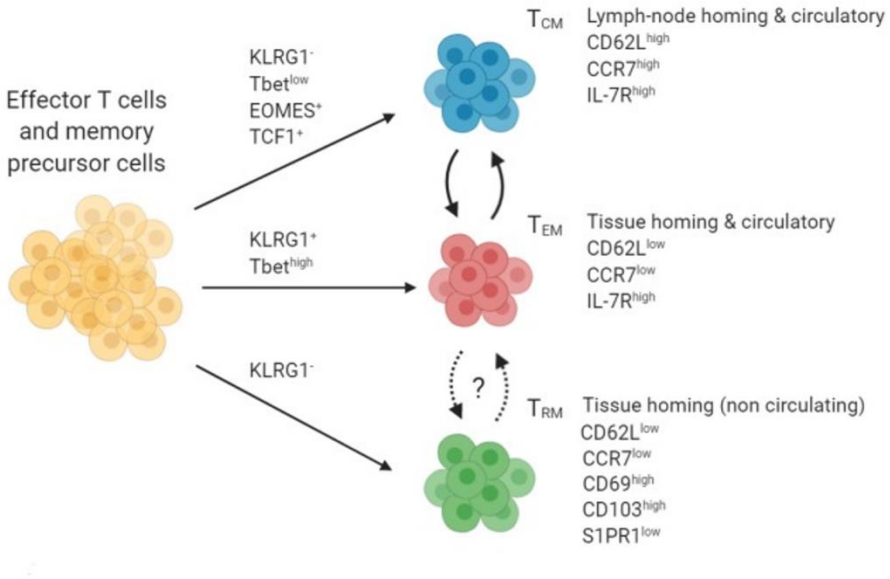

Figure II: The different memory T cell subsets. T_{CM}, T central memory, T_{EM}; T_{RM}, T resident memory; Each subset is defined by different marker and can be found in CD4+ and CD8+ T cells. Modified from [38].

1.2.3. Immune checkpoints

The strength of T cell response is tightly regulated and the final outcome results from a complex balance between the signaling of activating and inhibitory receptors expressed at the surface of T cells (reviewed in: [14], [18], [24], [40]–[43]) (Fig. III). While CD28 expression on T cells is constitutive, the

expression of other activating and inhibitory receptor is mainly dependent on the T cell activation status [18], [40]. The signaling mediated by these different receptors can in turn impact the process of T cell activation and differentiation [18]. Upon binding to their corresponding ligands, stimulatory receptors such as ICOS, CD226, OX-40 or 4-1BB, enhance T cell responses and effector functions [18], [41]. On the other hand, inhibitory surface receptors, called immune checkpoints, such as cytotoxic T lymphocyte antigen-4 (CTLA-4), programmed cell death protein 1 (PD-1), T-cell immunoglobulin and mucin-domain-containing molecule 3 (Tim-3), T-Cell Immunoglobulin and ITIM Domain (TIGIT) or Lymphocyte-activation gene 3 (LAG-3) inhibit T cell effector functions and limit the amplitude and the duration of the T cell response [18], [44], [45]. Thereby, they serve to protect healthy tissue from damages resulting from excessive T cell activation and participate in immune homeostasis and maintenance of self-tolerance [41], [44], [46], [47]. Any disturbance of the expression and/or signaling of immune checkpoints can result in immunopathologies: absence or low expression can lead to autoimmunity while exaggerated expression may inhibit key T cell responses necessary for pathogen elimination [18], [42], [48], [49].

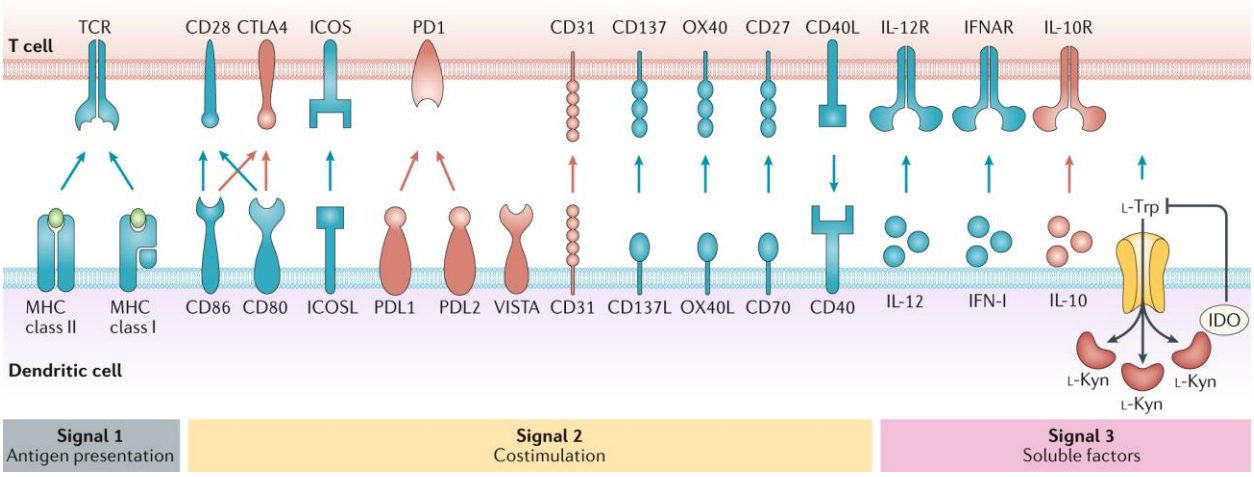

Figure III: T cell activation depends on signal 1, 2 and 3 provided by the dendritic cells. Co-signaling mediated by receptor-ligand interactions either activates (blue) or inhibits (red) the T cell response. Modified from [14].

Activating and inhibitory receptors are critical at various stages of T cell development: T cell activation occurs during priming in the lymph nodes but also at the periphery [18], [43]. Interaction between APCs and effector T cells at the site of inflammation can either result in re-activation or inhibition of T cell responses [11], [43]. Activating and inhibitory receptors also play a role in T cell memory formation [18]. Another layer of complexity is related to the fact that the expression pattern of activating and inhibitory receptors on T cells and of their ligands on immune and non-immune cells is dynamic and

context dependent [18], [50]. The most studied inhibitory immune checkpoints and their ligands are described below.

1.2.3.1. *CTLA-4*

CTLA-4 (or CD152) is a member of the immunoglobulin superfamily and is highly homologous to the costimulatory molecule CD28. CTLA-4 rapidly and transiently expressed on the T cells surface following priming and activation [51]. CTLA-4 binds to the same ligands as the co-stimulatory receptor CD28, i.e., to CD80 (B7-1) and CD86 (B7-2) expressed at the surface of the APCs [31]. CTLA-4 has a 10 to 100 times higher affinity for these ligands and efficiently out-competes CD28 [52]. By preventing the binding of CD80/CD86 to CD28, CTLA-4 inhibits the co-stimulatory signal 2 necessary for T cell activation. In addition, CLTA-4 can also prevent CD28 mediated T cell activation by removing the CD28 ligands from the surface of the APC via a mechanism called transendocytosis [32].

1.2.3.2. *PD-1*

Programmed cell death protein 1 (PD-1; CD279) is a transmembrane co-inhibitory receptor (an immune checkpoint), structurally belonging to the immunoglobulin superfamily. It is upregulated on activated T cells and restrains T cell priming by downregulating the signaling through CD28 and TCR [53]–[55]. PD-1 has two ligands: PD-L1 (CD274) and PD-L2 (CD273), both transmembrane proteins of the immunoglobulin superfamily [56], [57]. PD-L1 is constitutively expressed at low levels on a wide variety of cell types, both of hematopoietic and non-hematopoietic cell lineages, and its expression can be upregulated by IFN-γ and other inflammatory stimuli [58], [59]. On the other hand, PD-L2 expression is more restricted, and is found principally on macrophages, dendritic cells and mast cells [60]. Given the broad distribution of its ligands, PD-1 can inhibit T cell responses in both in the lymph nodes and in the periphery [61], [62]. The PD-1/PD-L1 axis will be described more extensively in the section 4.5.

1.2.3.3. *LAG-3*

LAG-3 (CD223) is part of the immunoglobulin superfamily and is expressed on activated T effector and Tregs [29]. It has several ligands, such as MHCII, galectin-3, lymph node sinusoidal endothelial cell C-type lectin (LSECtin) or fibrinogen-like protein 1 (FGL1) [9]. The binding of LAG-3 to its ligands results in different outcomes depending on the T cells subsets: in effector T cells, it decreases their activity while it increases Tregs activity [45], [63].

1.2.3.4. *TIM-3*

TIM-3 is a transmembrane receptor that belongs to the TIM family of receptors, related to the immunoglobulin superfamily. TIM-3 is expressed at the surface of various immune cells such as T cells, NK cells, or myeloid cells [45], [64]. Galectin-9, Ceacam 1 or high-mobility group box 1 (HMGB1) proteins have been described as TIM-3 ligands [64] and their binding to TIM-3 results in immunosuppression [45], [65].

1.3. Immune response to tumors

1.3.1. The cancer-immunity cycle

Cancer cells are characterized by genomic instability as well as structural alterations [66]. This results in aberrant metabolic and phenotypic characteristics which leads to abnormal and invasive cell proliferation. The expression by tumor cells of mutated genes or usually repressed genes (TSA, tumor-specific antigens, TAA, tumor associated antigens), helps the immune system to recognize them from healthy cells [11]. How the adaptive immune system recognizes and eliminates cancer cells has been conceptualized by Chen and Mellman in 2013 and is represented as a 7 step iterative process called “the cancer-immunity cycle” (Fig. IV) [67]. When the cancer-immunity cycle performs optimally, cancer cells are eliminated by the immune system, resulting in the release of cancer cell antigens (step 1). The newly released antigens are then engulfed by dendritic cells and processed for presentation (step 2). Activated DCs present the antigens to T cells in secondary lymphoid organs (SLOs) such as lymph nodes (LNs) and subsequently activate them (step 3). These activated T cells travel to the tumors (step 4) and infiltrate the tumor bed (step 5). Upon recognition of tumor cells (step 6), T cells destroy them (step 7). The additional release of tumor antigens amplifies the immune response and the cycle starts once again [67].

Each step in the cancer-immunity cycle can be hijacked by cancer cells evading immune destruction (reviewed in [67]). Of note, the anti-tumor immune response has dual, contrasting effects. If the initial immune response is efficacious, it will ultimately result in a strong selective pressure favoring immune escape. The consequence of this is immunoediting: the enrichment in tumor cells capable of evading immune recognition [68]. The interaction between cancer and immune cells in the tumor microenvironment is a dynamic process, important for cancer establishment and progression [69].The following sections will describe the tumor microenvironment and will subsequently focus on PD-L1 and CD47, two immune checkpoint receptors, and on how they could be targeted to restore efficient anti-tumor immunity [67], [70].

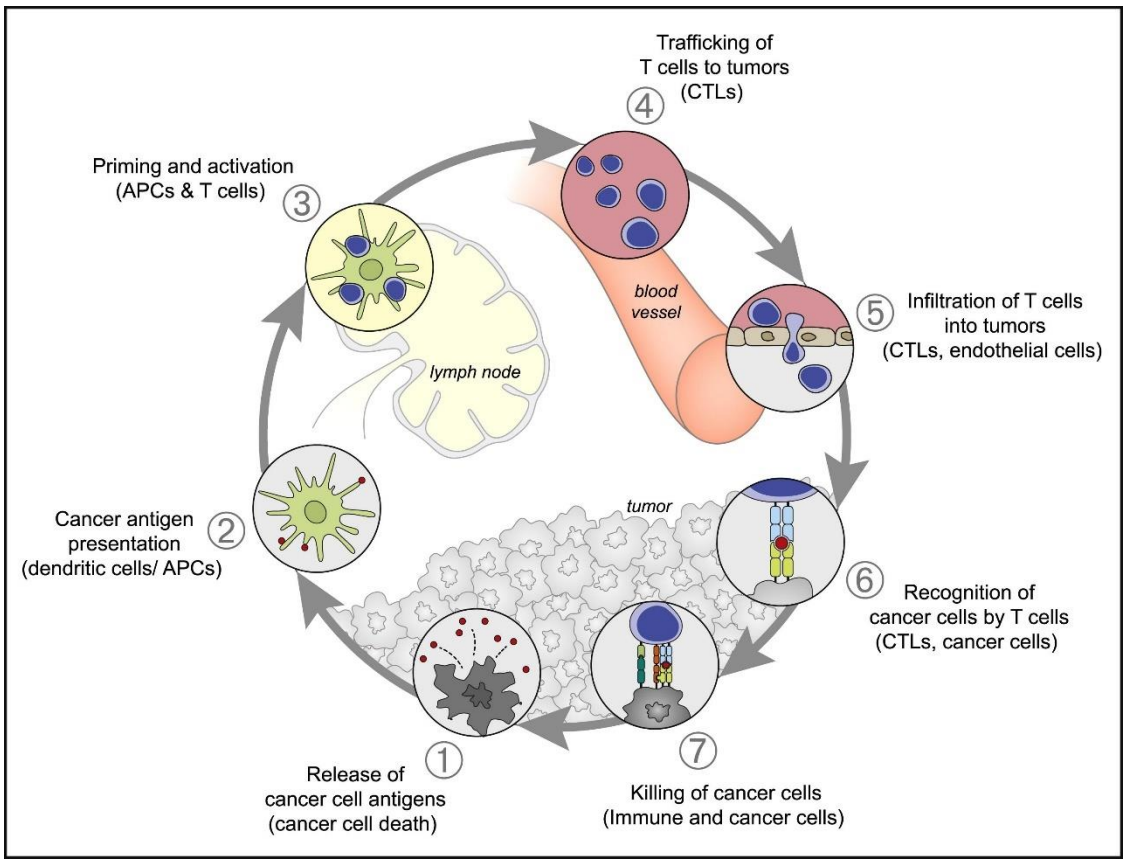

Figure IV : The cancer immunity cycle. Source: [67].

1.3.2. The tumor microenvironment

Tumors are not only composed of cancerous cells but also contain infiltrating immune cells, blood vessels, fibroblasts as well as extracellular proteins, macromolecules, cytokines, and growth factors [71]. This complex network constitutes the tumor microenvironment (TME) (Fig. V) and contributes to tumor progression and immune escape [72]. TME composition is heterogeneous and can vary depending on the cancer type as well as its evolution over time [73]. What is even more complicated, patients with the same type of cancer and the same clinical stage usually have different TMEs and thus potentially different antitumor responses to treatment. The TME has an important role in the modulation of cancer development as it can limit or enhance tumor progression [74]. The immune complexity as well as its organization at the tumor site is described as “the immune contexture” [75]. Its understanding is key to ensure correct classification of patients as well as treatment selection. The development of new therapeutic strategies to tackle cancer depends therefore on a detailed understanding of the TME [69].

The following section will describe the main cell types that can be found in the TME as well as potential therapeutic approaches to target these cell populations with the goal of enhancing anti-tumor responses.

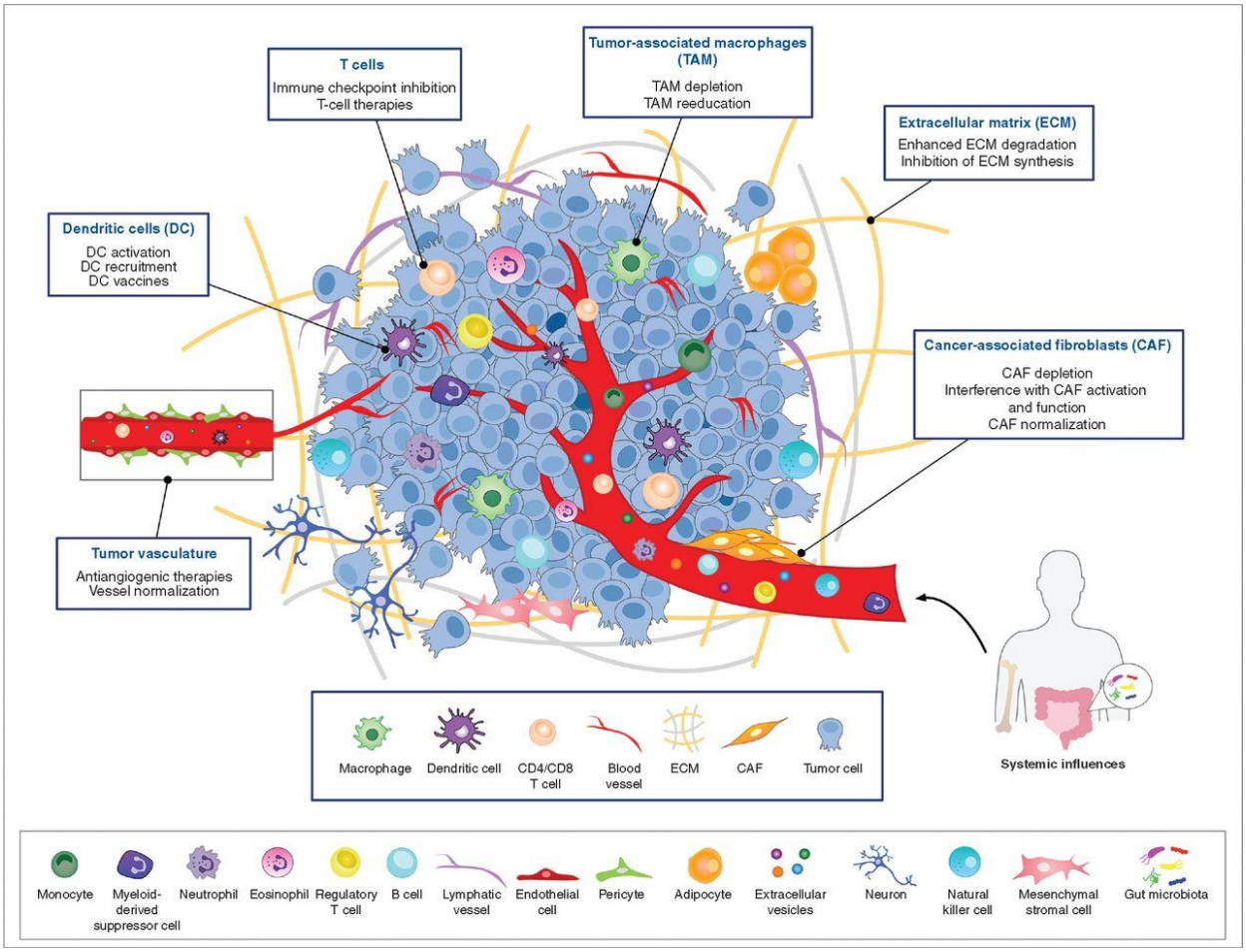

Figure V: The tumor microenvironment. The tumor microenvironment is composed of various cell types (immune and non-immune) as well as extracellular components. Boxes represent various approaches that can be used for therapeutic treatment (source: [71]).

1.3.3. Non-tumor cells in the TME

1.3.3.1. *Neutrophils and monocytes*

Neutrophils, or polymorphonuclear leukocytes, are the most important immune population in the blood. In acute infections, they respond to activating stimuli such as pathogen-associated molecular patterns (PAMPs) or damage-associated molecular patterns (DAMPs) and are rapidly mobilized to the infection site [11]. They are phagocytic cells specialized in engulfing microbes or dying cells but have only a short life span in tissues.

Monocytes, or mononuclear phagocytes, are also blood circulating leukocytes. Upon infection, they migrate to the tissues where they can mature and differentiate into macrophages or dendritic cells (DCs) [11]. They infiltrate the tissues later than neutrophils but have a longer life span. Monocyte populations in the blood are heterogenous and are often divided into classical and non-classical monocytes. The first category has phagocytic and pro-inflammatory properties while the second is involved in tissue repair [11], [76].

In the TME, neutrophils and monocytes may evolve into myeloid-derived suppressor cells (MDSCs), which are generated following a prolonged exposure to signals such granulocyte-macrophage colony-stimulating factor (GM-CSF), IL-6 or VEGF) [77]. MDSCs participate in immune suppression within the TME and are associated with bad prognosis [77]. Yet, No phenotypic markers can help to unambiguously distinguish classical monocytes or neutrophils from their immunosuppressive counterparts, making the analysis of these populations difficult [77]. Targeting MDSCs is challenging due their short life span and unstable phenotypes. Notwithstanding, some approaches that aim to deplete this population are currently evaluated in clinical trials [77].

1.3.3.2. *Macrophages*

Macrophages are professional phagocytes found in tissues [11]. They can arise from blood monocyte maturation or during embryogenesis, from yolk sac or fetal liver precursors [78]. The latter are called tissue resident macrophages and can persist for years. Depending on the organs seeded, they have specialized functions and different names, such as Kupffer cells in the liver or microglia cells in the brain, [11]. Macrophages are highly plastic and heterogenous. Depending on environmental context, they can further differentiate to fulfill several functions [79]. They can promote inflammation and destruction by eliminating damaged cells and pathogen, as well as working as antigen presenting cells that mediate T cell activation [11]. On the other hand, macrophages are also involved in tissue homeostasis, remodeling and repair and act as key mediators of inflammation resolution [79]. A simplistic view based on *in vitro* polarization experiments led to a dichotomous classification of macrophages into either M1 (pro-inflammatory) or M2 (anti-inflammatory) [80]. The M1 state, or “classically activated” macrophages can be differentiated *in vitro* by adding IFN-γ and/or LPS into the culture medium. Inversely, the M2 state, or “alternatively activated” macrophages, arise from induction with L-4, IL-10, or TGFβ [81].

Within the TME, tumor associated macrophages (TAMs) are often associated with either the M1-like or the M2-like phenotype [82]. M1-like TAMs are characterized by secretion of pro-inflammatory cytokines (IFN-γ and TNF-α), increased expression of the major histocompatibility complex II (MHC II) and inducible nitric oxide synthase (iNOS), as well as by increased expression of CD40, CD80 and CD86

costimulatory molecules [83]. M2-like macrophages are characterized by secretion of IL10 and TGFβ, increased expression of CD206 and arginase (Arg1), and are associated with immune suppression and angiogenesis [84]. Yet, the phenotype and the activation state of macrophages *in vivo* are a dynamic continuum rather than defined, fixed states [85]. Adding to this complexity, the presence of a high macrophage infiltrates in the TME is associated with either good or bad prognosis depending on the cancer type [86]. TAMs phenotypes may evolve during tumor progression. For instance, M1-like macrophages are typical to early tumorigenesis. On one hand, during tumor initiation, M1-like macrophages mediate tumor elimination. On the other hand, they promote tumorigenesis by creating an inflamed and mutagenesis-prone microenvironment [87]. During tumor progression, M1 macrophages progressively become pro tumoral M2 macrophages, under the influence of cytokines such as IL-4 secreted by T helper 2 cells or CSF1 produced by tumor cells [88]. Late stage tumors and metastases are mostly infiltrated by M2-like macrophages [89]. Pro-tumorigenic functions mediated by TAMs involve the suppression of adaptive immune response via expression of inhibitory receptors (PD-1, PD-L1), cytokine production (IL-10, TGFβ), and participation to tissue remodeling and angiogenesis (growth factors, proteases and VEGFA secretion) [90]. Reeducating macrophages to favor a M1- over M2-like functions is currently investigated by several approaches. Disruption of CSF-1/CSF-1R or CCL2/CCR2 axis with monoclonal antibodies (mAbs) to limit macrophage recruitment or enhancing macrophage activity with CD47-blocking or CD40 agonist antibodies are some of the examples of immunotherapies currently assessed in clinical trials [83], [91].

1.3.3.3. *Dendritic cells (DCs)*

As described in the first section, DCs are professional antigen presenting cells (APC) that constantly patrol tissues and the circulatory system, where they probe the environment for antigens. DCs efficiently present antigens in the context of MHC class I or MHC class II to activate CD8+ and CD4+ T cells respectively [12]. Cross presentation allows DCs to present internalized antigens via their MHC I and is key for triggering antitumor CD8+ T cell responses [92]. DCs that originate from a common myeloid precursor in the bone marrow differentiate into conventional DCs, while plasmacytoid DCs arise from a lymphoid progenitor [93]. Conventional DCs function mostly as antigen presenting cells and can be subdivided in two categories depending on the T cells they activate, cDCs 1 for CD8+ and cDCs 2 for CD4+ T cells [94]. In contrast, plasmacytoid DCs have weak antigen presentation ability and are specialized in type I IFN secretion [95]. During inflammation, a third subset of DCs can also mature from monocytes after homing in peripheral tissues (monocyte-derived DCs) and is involved in CD8+ T cell activation at the site of

inflammation rather than in SLO [94], [96]. The different subsets of DCs can be differentiated based on expression of transcription factors, phenotypic markers as well as their location [14].

In the TME, the immunosuppressive environment limits and counteracts DC function through several mechanisms [14], [97]. For instance, during tumor progression, the number of cross presenting DCs decreases, thus impairing efficient reactivation of the T cell responses [14]. In addition, the presence of immunosuppressive conditions as well as soluble factors such as VEGF, IL10 or TGFβ impacts DC maturation and antigen presentation functions [98], [99]. Lastly, it has been shown that DCs in the TME can mediate T cell immunosuppression as a consequence of modified metabolic pathways, depleted arginine [100] or expression of inhibitory molecules such as PD-L1 [101]. These DCs become tolerogenic and fail to efficiently activate T cells [99]. Several approaches to overcoming DC tolerance, such as administration of DC activating factors, such as polyinosinic:polycytidilic acid (poly(I:C)) and other Toll like receptor (TLR) agonist, or DC vaccines, are being evaluated in pre-clinical studies and in clinical trials [14], [96], [102].

1.3.3.4. *Natural killer (NK) cells*

NK cells are part of the innate lymphoid family and are mostly found in circulation. During inflammation, they are rapidly recruited to the tissues where they are involved in direct killing of infected cells as well as in secretion of pro-inflammatory molecules such as IFN-γ as well as chemokines [11]. NK cell activation depends on the signaling mediated by their cell surface receptors, classified as either inhibitory or activating, binding to molecules expressed on target cells [11], [103]. Healthy cells mainly express inhibitory receptor ligands, while infected or damaged cells express a higher proportion of ligands binding to NK activating receptors. When the activating signaling is stronger than the inhibitory signaling, it triggers NK cytotoxic response and killing of the target cell. NK cell activation and target cell killing can also occur via antibody-dependent cellular cytotoxicity (ADCC), a process mediated by the Fc parts of IgG antibodies opsonizing the target cell and crosslinking activating Fcγ receptors on the surface of a NK cell.

NK cells infiltration into tumors is usually low but a higher level is usually associated with good prognosis [104], [105]. The efficacy of several anti-tumor monoclonal antibodies has been shown to be depend on ADCC mediated by NK cells [106]. Thus, NK cells can mediate an anti-tumor activity by direct killing, but also by activating and recruiting other immune cells such as DCs [105], [107], [108]. Like in the case of other immune effector cells, NK antitumor activity can be inhibited in the TME by several mechanisms such as the increase in inhibitory ligand expression in tumor cells or by immunosuppressive cytokines [105], [109]–[111]. Some NK cells can also express PD-1, which reduces NK functions upon binding to PD-L1 in the TME [112], [113]. As a consequence, immune checkpoint inhibitors, antibodies

targeting receptors expressed by NK cells or pro-inflammatory cytokines are some strategies currently investigated in clinical trials to enhance NK functions in the TME [110].

1.3.3.5. *Effector T cells*

Tumors can be broadly divided in three categories depending on their T cell infiltration pattern (reviewed in [70], [114]). “Desert” TME displays no T cell infiltration, which can be a consequence of defective DCs-mediated priming. “Immune-excluded” tumors are characterized by the presence of T cells, but their localization is restricted to the periphery of the tumor. This defect in T cell infiltration within the tumor bed might result from a downregulation of adhesion molecules, aberrant chemokine pattern, or the expression of suppressive cytokines that act as a physical barrier. The last category called “Inflamed” tumors display T cell infiltration, yet these T cells fail to control tumor progression.

CD8+ T cells have the ability to kill tumor cells and are thus the main effectors of the anti-tumor response. CTLs infiltration is associated with good prognosis in most cancer types [75], [115]. However, in the TME, chronic antigen stimulation associated with lack of costimulatory signals impairs efficient T cell priming and activation [116]. In addition, interaction with immunosuppressive ligands expressed by immune and non-immune cells, deprivation of nutrients and oxygen as well as inhibitory cytokines progressively drive the T cells in the TME toward a dysfunctional state, called exhaustion [116]–[118]. Exhausted T cells display sustained upregulation of inhibitory receptors (e.g., PD-1, CTLA-4, Tim-3, LAG-3), loss of effector functions, impaired proliferation as well as characteristic metabolic, transcriptional and epigenetic changes [118]–[121]. The path toward a terminally differentiated exhausted phenotype occurs gradually [122]. T cells effector functions such as IL-2 production or proliferative abilities are lost at an early stage, followed by the loss of TNF-α, and finally the loss of IFN-γ expression [122]. Expression of inhibitory immune checkpoint receptors as well as transcriptional profiles differ between early (i.e., reversibly) and terminally dysfunctional T cells [122]–[124]. This results in a coexistence within the TME of different dysfunctional T cell populations with various phenotypic and transcriptomic profiles [124]. Therefore, the analysis of tumor infiltrating T cells and the association of a given CD8+ T cell subset with a specific functional status (effector, pre-dysfunctional, terminally exhausted) is complex and requires the integration of several layers of information [125] (phenotypic markers as well as transcription factors are shared by normal and exhausted cells at different stages and in different contexts [50], [126], [127]). Reversing an exhausted phenotype or “reinvigorating” CD8+ T cells can be sometimes achieved by targeting inhibitory immune checkpoints with monoclonal antibodies (mAbs) [41], [42], [125]. This approach has been fully validated in the clinic for CTLA-4 and PD-1/PD-L1 [41]. The targeting of additional immune checkpoints is currently being investigated in clinical trials [128], [129], [64], [130].

1.3.3.6. *Regulatory T cells*

The presence of Tregs in tumors is associated with a poor clinical outcome [30], [33], [131]. Depletion of Tregs, via mAbs targeting CD25, OX40, or glucocorticoid-induced TNF-related protein (GITR) has shown promising anti-tumor effects in preclinical models, but has not been translated yet into a clinical success [30]. The lack of targeting specificity resulted in the concomitant depletion of effector T cells in the periphery rather than the depletion of Tregs in the TME, and was associated with autoimmunity [131]. In contrast, successful targeting of Tregs has been achieved with anti- CTLA-4 mAbs [8], [132]. Ipilimumab, an anti-CTLA-4 monoclonal antibody, was the first immune checkpoint inhibitor to be approved by the FDA (in 2011). Ipilimumab monotherapy resulted in long term survival of a fraction of metastatic melanoma patients [133]. Ipilimumab is thought to act on the T cells at two different sites: in the TME, which allows to relieve the immune suppression mediated by Tregs, and in the lymph nodes, where it is believed to enhance effector T cell priming and activation [132], [134]. However, the use of CTLA-4 inhibitors in the clinic is often associated with severe immunotoxicity [134].

1.3.4. Non-immune components

1.3.4.1. *Fibroblasts and extracellular matrix*

Fibroblasts are structural cells involved in the production of collagen and extracellular matrix. Upon exposure to growth factors, cytokines and other molecules secreted by the tumor and the immune cells, fibroblast acquire pro-tumorigenic abilities [135]. It has been shown that cancer associated fibroblasts (CAFs) can secrete soluble factors, chemokine and cytokines, enzymes and extracellular matrix components to support tumor progression, angiogenesis and metastasis [136]. However, since CAFs are a phenotypically and functionally heterogeneous population and cannot be easily differentiated from their normal counterparts, the development of targeted treatments might be challenging [137].

1.3.4.2. *Endothelial cells*

Fast growing tumors require enhanced blood to sustain the need for nutrients [138]. Tumor development causes structural stress as well as hypoxic conditions that trigger secretion of proangiogenic factors such as vascular endothelial growth factor (VEGF) and angiopoietin (ANG2) by various types of cell (cancer cells, endothelial cells, stromal cells) [139]. These factors stimulate endothelial cells proliferation and the creation of new blood vessels [140], [141]. Yet, the vasculature that develops in cancer is disorganized and structurally altered, creating an immunosuppressive hypoxic and acidic environment [141], [142]. In addition, endothelial cells within the TME show abnormal expression of surface adhesion

molecules that impair immune cells trafficking and infiltration [143]. Lastly, expression of inhibitory immune checkpoints such as PD-L1 can also be induced on endothelial cells [144].

1.4. Monoclonal antibodies

Antibodies, or immunoglobulins (Ig), are proteins produced by the B cells and are the humoral response against foreign molecules or pathogens [11]. Based on structure and functions, human antibodies can be classified into 5 groups (or called isotypes): IgA, IgD, IgE, IgM and IgG [11]. The latter group is the main class used for therapeutic applications [11], [145], [146]. This section will focus on the IgG subclass and its characteristics.

1.4.1. IgG structure

IgG are Y-shaped proteins composed of two identical heavy chains and two identical light chains linked together by disulfide bonds (Fig. VI) [147]. Each heavy chain displays three constant domains (CH1, CH2 and CH3) and one variable domain (VH). The light chains have two domains, a constant (CL) and a variable domain (VL) [11]. The variable domains (VH and VL) of the antigen-binding fragment (Fab) are the regions that bind to the antigen. Among each variable domain, three hypervariable regions, called complementary determining regions (CDRs), create the antigen binding site (the paratope) and define the antibody specificity. Homodimerization of the CH2 and CH3 domain creates the fragment crystallizable (Fc) domain that mediates the effector functions of the antibody [11].

The IgG isotype can be further divided in subfamilies according to the sequence differences in the Fc part [11]. The Fc part of the antibody can mediate effector functions via binding to Fcγ receptors (FcγRs) or by activation of the complement cascade [148]. Each isotype binds to different receptors with various affinity and thus results in different effector functions. Humans and mice possess four different subgroups: IgG1, IgG2, IgG3 and IgG4 for humans and IgG1, IgG2a, IgG2b, IgG3 in mice [11], [147]. Depending on the FcγR they bind, the IgG are categorized either as active Fc, such as human IgG1 or the mouse IgG2a or effector-reduced, such as the mouse IgG1 and the human IgG4.

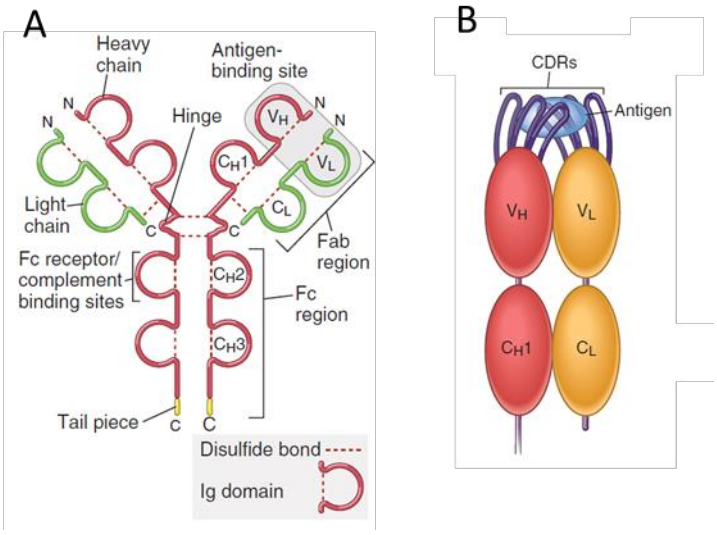

Figure VI: Structure of an antibody molecule and antigen biding sites. (A), Cartoon depicting a secreted IgG molecule. (B) Cartoon depicting the antigen binding site formed by the complementarity determining regions (CDRs). Modified from [11].

1.4.2. Fc gamma receptors (FcγRs)

FcγRs are expressed at the surface of innate immune cells. In mice and in humans, FcγR can be either categorized as activating or inhibitory [149]. Each FcγR has different affinities for different IgG isotypes and a different distribution pattern in immune cells [147]. For example, the mouse FcγRIV has a high affinity for mouse IgG2a and mIgG2b isotype while mouse FcγRIIB preferentially binds to mIgG1 and mIgG3 (Fig. VII) [149]–[151].

Interaction between antibodies and FcγR allows to bridge the adaptive and the innate immune responses [11]. Indeed, the binding of antibodies harboring an active Fc (such as human IgG1 or mouse IgG2a) to FcγRs triggers strong effector mechanisms that lead to the killing of opsonized cell via several mechanisms such as antibody-dependent cell phagocytosis (ADCP) or antibody-dependent cellular cytotoxicity (ADCC) [145], [152].

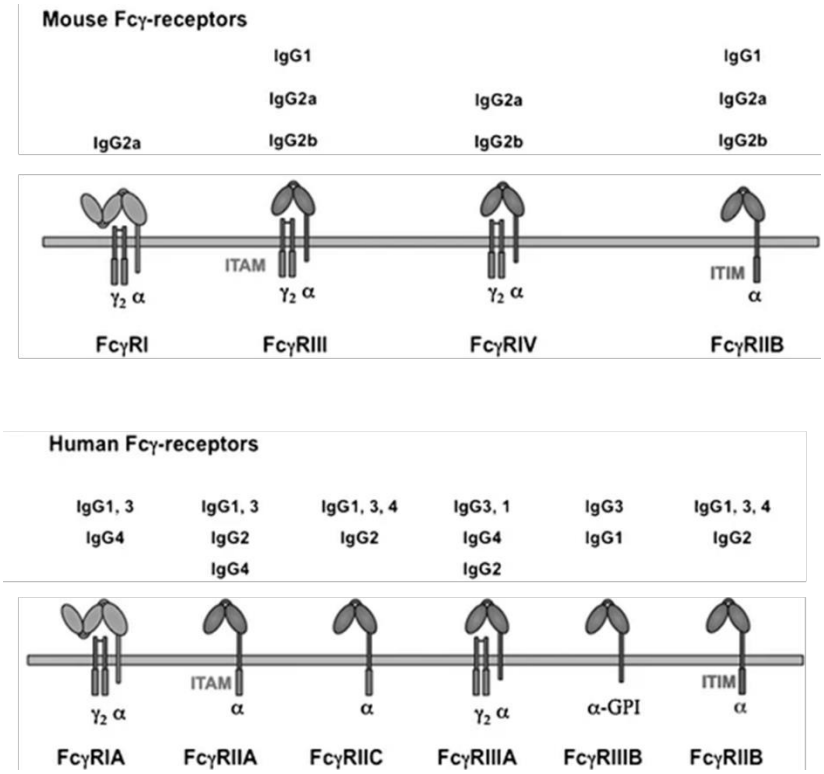

Figure VII: Mouse and human Fcγ receptors. Mouse activating FcγRs: FcγRI, FcγRIII, and FcγRIV. Mouse inhibitory FcγRs: FcγRIIB. Human activating FcγRs family: FcγRIA, FcγRIIA, FcγRIIC FcγRIIIA FcγRIIIB. Human inhibitory FcγRs: FcγRIIB. Modified from [153]

1.4.3. Development of monoclonal antibodies

Acquiring substantial quantities of pure monoclonal antibodies (mAbs) for therapeutic purposes was challenging until the large-scale implementation of the hybridoma technique [154]. Antibodies obtained with this technique were murine IgGs specific to human proteins (therapeutic targets). However, the use and efficacy of mouse antibodies in humans was hampered by their immunogenicity. [155] [146], [156], [157]. Subsequent technological developments partially solved this issue with the creation of chimeric or humanized mAbs with substantially reduced murine sequence content [156], [158]–[161]. Ultimately, the discovery of the phage display technology enabled the generation of fully human antibodies [162]. Libraries of phages expressing antibody fragments (corresponding to the antibody variable regions) can be amplified in bacteria, selected and screened against the desired target *in vitro* [163]–[165]. This method allows for a high throughput screening and a fast generation of fully human monoclonal antibodies.

1.4.4. Monoclonal antibodies targeting immune checkpoints

Nowadays, immune checkpoint blockade with anti CTLA-4 , anti-PD-1 or anti-PD-L1 mAbs is arguably the most widely used immunotherapy approach [146]. While the introduction of ICI therapies revolutionized cancer treatment in a number of indications, ICI therapy works for a fraction of patients and treatment efficacy can decline with time due to resistance mechanisms [155], [166]. Increasing the therapeutic success rate could be achieved by combining ICIs between them or with other types of cancer treatments. In particular, the combination of CTLA-4 and PD-1/PD-L1 blockade resulted in higher efficacy in melanoma or lung cancer, but is also associated with increased toxicities as compared to single agent therapies [167]–[169]

1.4.5. Bispecific antibodies

Bispecific antibodies (bsAbs) allow to engage two different targets either at the surface of the same cell or on two different cells, thus allowing for novel mechanisms of action and more selectivity as compared to mAbs [170]. In addition, they present potential advantages over combinations, such a decreased l toxicity.

Difficulties related to antibody engineering and industrial-scale production limited the development of bsAbs in the 90's. Since then, most of these technical hurdles have been solved and there are currently more than 100 different bsAbs formats available for therapeutic antibody development (Fig. VIII). Each format has its own properties with regards to the structure, flexibility or specificity [171]. BsAbs can be split in two categories: the ones that mimic the native antibody structure and thus have an Fc part, and fragment-based bsAbs which do not have an Fc part (Fig. VIII) [172], [173]. Stability, productivity yield and potential immunogenicity due to engineered (unnatural) antibody sequences remain the main challenges for therapeutic bsAb development. Nonetheless more and more bsAb therapeutics are being tested in the clinic (over 50) and three have already been approved [173], [174]

1.4.5.1. *Kλ body*

Novimmune has developed a phage display platform that allows generating bispecific antibodies composed of a fixed (common) heavy chain associated with two different light chains (one κ and one λ). This bsAb format is referred to as the κλ-body [175]. The two different light chains drive the antigen specificity of the bsAb. The three chains are co-expressed from a single vector which results in an antibody mixture composed of 2 mAbs (one κ and one λ) and a κλ body bsAb. The fact that one of the bsAb arms

bears a k light chain and the other a l light chain allow for a generic three-step purification process with 3 different affinity resins binding to (1) the Fc portion, (2) the κ chain constant region and (3) the λ chain constant region. This approach allows to easily separate the kl bsAb from the two mAbs (ll and kk). κλ bodies are fully native fully human IgGs. The absence of engineered non-native sequences in the kl-body limits the risk of immunogenicity in the clinic.

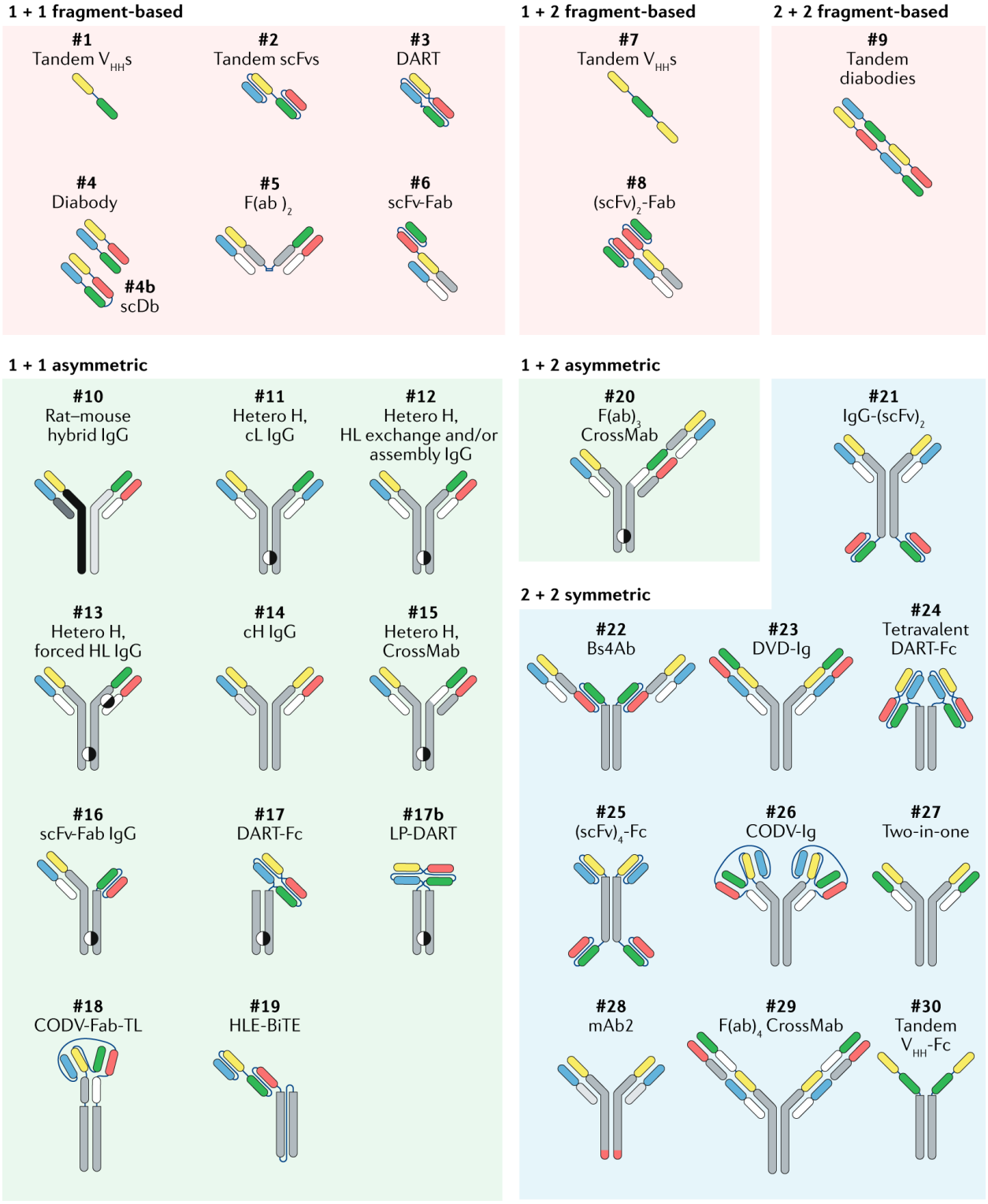

Figure VIII: **Some of the bsAbs formats available**. BsAbs are categorized depending on their structure (source: [172]).

1.5. PD-1/PD-L1 axis

Programmed cell death protein 1 (PD-1; CD279) is a immune checkpoint receptor upregulated following T cell priming and activation [53]–[55]. PD-L1 is the principal ligand for PD-1 and is generally expressed at low levels in various immune and non-immune cells [49]. It is also expressed in some cancer cells and gets often upregulated in the TME, contributing to immunosuppression [58], [59], [176].

1.5.1. Expression and interactions

1.5.1.1. *PD-1 and PD-L1 expression*

PD-1 can be expressed by T cells, B cells, activated monocytes, macrophages, DCs, natural killer (NK) cells [177]. The dynamic of PD-1 expression has been extensively characterized for T cells. Upon T cell activation and TCR signaling, several transcription factors such as NFATc1 or Notch promote a rapid upregulation of PD-1 [62], [178]. Following T cell differentiation and antigen clearance, PD-1 expression is downregulated by another set of transcription factors, such as T-box expressed in T cells (T-bet) or B lymphocyte induced maturation protein 1 (Blimp-1) [178]–[182]. Recently activated T cells express high levels of PD-1 while effector cells (T-bet+) express low levels of PD-1 [62], [116], [183], [184].

PD-L1 is a transmembrane protein that belongs to the immunoglobulin family. It consists of an Ig-V like and Ig-C-like extracellular domain, a transmembrane domain and a cytoplasmic domain which lacks signaling motifs [185]. PD-L1 is constitutively expressed on a wide variety of cell types, both of hematopoietic (i.e. T cells, B cells, macrophages, DCs) and non-hematopoietic lineages (i.e. endothelial cells, mesenchymal stem cells) [60], [177]. Cell surface PD-L1 expression was found to be upregulated by IFN-γ and other inflammatory stimuli [58], [59], [177].

1.5.1.2. *PD-1/PD-L1 interaction in trans*

Upon interaction with PD-L1, the intracellular domains of PD-1 are modified. The cytosolic immunoreceptor tyrosine-based inhibition motif (ITIM) and immunoreceptor tyrosine-based switch motif (ITSM) are phosphorylated, thus triggering the recruitment of two phosphatases, SHP-1 and SHP-2 [181], [186], [187]. These phosphates subsequently restrain T cell priming by inhibiting the signaling downstream of CD28 and TCR [54], [187], [188] . In physiological conditions, PD-1 /PD-L1 interaction can occur in different contexts and sites [189]. In the lymphoid organs, binding of PD-L1 to PD-1 during T cell priming drives an inhibitory signal that limits the extent of priming of naïve T cells [55]. At the periphery, T cells can be reactivated upon the encounter with their cognate antigen [189]. In this context, the PD-1/PD-L1

interaction delivers an inhibitory signal that counteracts the T cell activation during immune responses and inflammation. Specifically, PD-1 signaling inhibits T cell effector functions such as cytokine production and proliferation and modifies T cell metabolism [56], [186]. Thus, the PD-1/PD-L1 immune checkpoint serves to protect tissues from potential damage resulting from excessive and/or persistent T cell activation and is a critical mediator of tolerance and immune homeostasis [180]. [53], [54], [177][56] . PD-1 also enhances tolerance by promoting Tregs differentiation [190].

1.5.1.3. *PD-1/PD-L1 interaction in cis*

Interaction of PD-1 and PD-L1 does not only occur in trans, but also in cis on double positive cells. A recent study showed that the interaction between PD-1 and PD-L1 in cis, either on cancer cells or on APCs, may result in an immunostimulatory effect by preventing the binding of PD-L1 in trans, to PD-1 expressed on T cells [191].

1.5.1.4. *PD-L1/CD80 interaction*

PD-L1 interacts with CD80 in cis on APCs, and this interaction can enhance T cells response [192], [193]. The interaction with CD80 in cis engages PD-L1 and prevents it from interacting in trans with PD-1 on T cells [193]. In addition, the lateral interaction between PD-L1 and CD80 protects CD80 from removal by a CTLA-4 through transendocytosis while still enabling the interaction of CD80 with CD28 [194].

1.5.2. PD-1 and PD-L1 expression in cancer

In the context of cancer, the PD-1/PD-L1 pathway promotes immunosuppression and tumor immune escape. Both PD-1 and PD-L1 are often highly expressed in the TME and their interaction limits local T cell activation and cytotoxic T cell responses [56].

PD-1 gets highly expressed on tumor-reactive T cells in the TME, as a result of chronic antigen exposure and constant TCR signaling [118], [124], [195]. High and sustained PD-1 expression drives T cells toward an exhausted phenotype characterized by the expression of additional immune checkpoints, as well as by a progressive loss of effector functions [116], [118], [119], [196]. In the TME, PD-1 can also be expressed on macrophages and monocytes [197], [198] .High expression of PD-1 on TAMs was found to correlate with M2-like phenotype and inhibition of phagocytic potential [197]. Myeloid-specific deletion of PD-1 resulted in polarization of MDSCs toward pro-inflammatory monocytes and in enhanced tumor control [77].

PD-L1 is expressed on tumor cells and myeloid cells in the TME, such as DCs and macrophages [176], [177], [199]–[201]. Macrophages, monocytes and DCs can upregulate PD-L1 expression following activation [177]. PD-L1 expression on tumor cells can be modulated by several mechanisms (reviewed in [199]), such as oncogenic transcription factors (MYC, RAS, HIF1α) or inflammatory stimuli (IFN-γ, LPS, TNF-α) The latter can also upregulate PD-L1 on immune and non-immune cells such as endothelial cells [144].

1.5.3. Blockade of PD-1/PD-L1 pathway enhances anti-tumor responses

Early studies showed that blocking the interaction between PD-1 and PD-L1 with a monoclonal antibody restored the anti-tumor response by releasing the brake on CD8+ T cell-mediated killing [7]. This approach was rapidly moved to the clinic where anti-PD-1 and then anti-PD-L1 mAbs showed unparalleled anti-tumor activity [10]. In that primary canonical view, PD-L1 is expressed by tumor cells to inhibit T cell activation and to promote T cell exhaustion. While this is certainly true, this view has been complexified by several studies demonstrating the key role of PD-L1 expressed by non-tumor cells both within the TME and in the tumor draining lymph nodes.

1.5.3.1. *Importance of PD-L1 expression is not restricted to tumor cells*

PD-L1 expression on tumor cells has been shown to be a poor predictor of response to PD-/PD-L1 blockade in the clinic, given that anti-PD-L1 mAb efficacy was also observed in patients with PD-L1-negative tumors [202]. Based on this, several preclinical experiments were conducted to understand the importance of PD-L1 expression on host cells versus cancer cells. PD-L1 deletion on either host cells or on tumor cells resulted in a better tumor control, suggesting that both were important for dampening of the antitumor immunity [203]. What is more, some studies showed that PD-L1 expression on host cells, in particular on myeloid cells – and not PD-L1 expressed on tumor cells – was the key target of PD-L1 mAbs [204]–[206]. DCs express high levels of PD-L1 and blocking PD-L1 on DCs seems to be critical for anti-PD-L1 efficacy [101], [207], [208]. Collectively, both PD-L1 on tumor and on host cells inhibit antitumor T cell responses [209], [210].

1.5.3.2. *Lymph nodes are critical for the PD-1/PD-L1 response*

The efficacy of PD-1/PD-L1 blockade relies not only on blocking that immune checkpoint in the TME but also in the tumor draining lymph nodes (TdLN) [206], [208], [210]. Blockade of T cell egress or physical removal of the TdLN abrogated the efficacy of anti-PD-1 treatment [211]. On the other hand, a minute, suboptimal dose of anti-PD-L1 mAb injected directly into a TdLN was shown to be sufficient for

boosting CD8+ T cell responses in the TME [212]. Altogether, these data suggest that blockade of the immune checkpoint PD-1/PD-L1 in the TdLN could be as important as its blockade in the TME [213]–[215].

1.5.3.3. *Early exhausted CD8+ T cells respond to PD-1/PD-L1 blockade*

It is well established that not all CD8+ T cells in the TME are responsive to PD-1/PD-L1 the blockade. Various CD8+ T cells subsets can be found in the TME including tumor reactive T cells, bystander T cells (i.e., not specific for tumor antigens), memory T cells [216], [217]. Exhausted T cells represent a heterogeneous population [218]. Among them, the so called early dysfunctional T cells are characterized by stem-like properties and intermediate expression of inhibitory checkpoints (PD-1+/- Tim-3-TCF-1+) [218]. On the other hand, terminally exhausted T cells in the TME are not able to proliferate and express high level of inhibitory receptors (PD-1++ Tim-3+ TCF-1-) [219], [220]. Recent studies showed that the early dysfunction pool can self-renew or differentiate toward terminally dysfunctional state [221]. This early dysfunctional subset can also respond to PD-1/PD-L1 blockade and expend while terminally exhausted T cells cannot [218], [220], [222]. Yet, it is still unclear what are the characteristics of the subset that reactivates tumor-killing functions upon PD-1/PD-L1 blockade. Due to heterogeneity and possible overlap of different subsets categorized as pre-dysfunctional, the exact identity of the precursor subset which is at the origin of the "reinvigorated" T cells is uncertain [219], [221], [223].

1.5.4. PD-1/PD-L1 inhibitors

In 2014, two anti-PD-1 mAbs, pembrolizumab and nivolumab were approved by the FDA. Their approval was subsequently followed by three anti-PD-L1 mAbs (atezolizumab, durvalumab, avelumab) (Fig. IX) [224]. Therapeutics targeting the PD-1/PD-L1 axis are currently used for the treatment of several cancer types. Recently, a 3rd anti-PD-1 mAb (cemiplimab) has been approved by the FDA [189].

Drug	Nivolumab	Pembrolizumab	Atezolizumab	Avelumab	Durvalumab
Subtypes	**IgG4**	**IgG4**	**IgG1**	**IgG1**	**IgG1**
Binding area	N-loop	C'D loop	CC'FG strands	F and G strands	the N-terminal region, the CC' loop and the
Affinity	3.06 nM	29 pM	1.75 nM	0.046 nM	0.66 nM
Degree of humanization	Fully human	Humanized	Fully human	Fully human	Fully human
Modification	S228P	S228P	Fc engineering	-	Fc engineering
Half life [33]	26.7	25.8	27	6	17
Dosage regimen	3 mg/kg q2w	200 mg q3w	1,200 mg q3w	10 mg/kg q2w	10 mg/kg q2w

Figure IX: Comparison of FDA approved anti-PD-1 and anti-PD-L1 inhibitors. Anti-PD1 (nivolumab and pembrolizumab) and anti-PD-L1 (atezolizumab, avelumab and durvalumab) mAbs showed different characteristics with regards to the epitope they target, or their structure. Modified from [225]

1.5.5. Resistance to immune checkpoint inhibitors

Although strong and consistent responses were observed following CPI treatment in some cases, the majority of patients does not respond [24], [226]. This lack of efficacy is called primary resistance. Additionally, patients that experienced a positive response in the first place, can subsequently develop resistance mechanisms, which is called acquired resistance [227]. In both cases, resistance mechanisms can be intrinsic to the tumor or extrinsic [228]. Among the intrinsic factors are low tumor immunogenicity as well as downregulation of MHC I expression [229]. Similarly, increased expression of inhibitory ligands on tumor cells as well as production of immunosuppressive cytokines (TGF-β, VEGF) by tumor cells following the modification of oncogenic pathways accounts for intrinsic resistance mechanisms. Extrinsic resistance can come from other immunosuppressive cells in the TME, either Tregs, TAMs, or endothelial cells. With regards to the acquired resistance, intrinsic mechanisms can also encompass downregulation or modification of tumor antigens or compensatory upregulation of additional immune checkpoints / ligands [169], [229], [230]

Combination strategies targeting different tumor-promoting pathways and mechanisms aim at to preventing and/or overcoming resistance issues [228]. As a consequence, the bulk of current clinical research investigating PD-1/PD-L1 pathway inhibitors (roughly 4000 active clinical trials [231], [232] involve combinations with other treatment modalities (chemotherapy, radiation, targeted therapies antitumor antibodies or other ICIs, oncolytic viruses, cancer vaccines, bispecific antibodies, etc…)

1.6. CD47/SIRPα axis

CD47 is a broadly expressed cell surface receptor with diverse immune and non-immune functions [233]–[235]. The best described role of CD47 is mediated through its interaction with SIRPα (signal-regulatory protein-α) on myeloid cells, including APCs, such as macrophages and dendritic cells, where it acts as a "don't eat me" signal inhibiting phagocytosis [236]–[241]. CD47 serves therefore as a universal "marker of self" for innate immune recognition [237], [238] [239]. Understandably, the vast majority of cancers overexpress CD47, which helps them escaping phagocytosis and anti-tumor immunity in general [242]. In a broader context, CD47 is now regarded as an important innate immune checkpoint contributing to cancer immune evasion [243]. As a consequence, inhibitors of CD47/SIRPα interaction became a major focus of drug development efforts in the last decade [243]–[245].

1.6.1. CD47 structure and expression

CD47 is a type III transmembrane glycoprotein that belongs to the immunoglobulin superfamily. It consists of V-like extracellular domains, five transmembrane domains and a short cytoplasmic tail. The C terminal part does not have a signaling domain and CD47 signaling occurs via lateral interactions with integrins [246]. The cytoplasmic tail can be alternatively spliced into four isoforms with distinct expression patterns [234], [247]. Besides SIRPα, CD47 interacts with other proteins such as closely related receptor SIRPγ, thrombospondin-1 (TSP-1), a secreted matricellular glycoprotein, and with integrins in cis (i.e., in the same plasma membrane) [248], [249]. Expression of CD47 is elevated on hematopoietic cells and can vary depending on the cell type and the development status. [250], [251]. CD47 expression can also be modulated by other factors, like inflammation or infection [252].

1.6.2. Immune functions of CD47

CD47 is involved in the regulation of various functions important for immune system homeostasis, such as apoptosis, cell adhesion, proliferation, migration, and phagocytosis [233].

1.6.2.1. *CD47 and migration*

CD47 is implicated in leukocyte migration. Neutrophils deficient for CD47 showed impaired transendothelial and transepithelial migration [253], [254] and the absence of CD47 expression in DCs

impairs their migration to secondary lymphoid organs [255]. CD47-SIRPγ interaction plays an important role in T cell transendothelial migration [256].

1.6.2.2. *CD47 and T cell functions*

Some older studies suggest a role of CD47 in T cell differentiation and activation. For instance, anti-CD47 mAbs were shown to enhance the proliferation of activated human T cells *ex vivo* [257]. In contrast, CD47 expressed by naïve T cells inhibited their activation upon interaction with TSP-1 [249], [258] Finally, the TSP1/CD47 interaction has also been shown to promote Treg differentiation [259]. In general, the roles of CD47 in T cell biology are complex and poorly understood, and seem to depend on the immune context and T cell activation status [260].

1.6.2.3. *CD47 and phagocytosis*

The regulation of phagocytosis via interaction with SIRPα is the best characterized function of CD47. SIRPα is a transmembrane receptor expressed principally in neurons and in immune cells of the myeloid lineage such as macrophages, dendritic cells, monocytes and granulocytes [261]. SIRPα is an inhibitory receptor – its cytoplasmic tail contains two immunoreceptor tyrosine-based inhibition motifs (ITIM), which, upon phosphorylation, activate SHP-1 and SHP-2 phosphatases leading to the dephosphorylation of several substrates including myosin IIA, which in turn inhibits the cytoskeleton rearrangement required for phagocytosis [236], [262], [263]. [237]. The role of CD47 to regulate cell phagocytosis has been described at first for red blood cells [240]. In senescent red blood cells, the decrease in CD47 cell surface expression and changes in CD47 membrane mobility modify the balance in favor of pro-phagocytic signals (such as calreticulin) and trigger their removal by splenic macrophages [241], [264]. In normal physiological conditions, pro-phagocytic signals are mostly expressed at the surface of damaged or apoptotic cells but are absent from healthy cells [265]. Blockade of CD47/SIRPα per se is usually not sufficient to trigger phagocytosis and needs to be associated with pro-phagocytic signals, such as Fcγ receptor crosslinking by antibody opsonizing a target cell [266]–[268].

1.6.3. Targeting CD47 in cancer

As mentioned above , the majority of cancer types overexpress CD47, a feature that is associated with poor prognosis [242], [245], [269]–[274]. Likewise, CD47 overexpression is also a common feature of cancer cell lines used in preclinical studies [251], [269], [272], [275], [276].

1.6.3.1. *Preclinical studies*

First preclinical studies evaluating the effect of anti-CD47 mAbs on tumor growth following engraftment of human tumor cells in immunodeficient mice (of note, human CD47 interacts with mouse SIRPα) showed enhanced phagocytosis of cancer cells and impressive tumor regression *in vivo* [269], [270], [272]. These early studies have clearly demonstrated that both the blockade of CD47 on human tumor cells (the "don't eat me" signal) and the engagement of activating Fcγ receptors by the Fc portion of the antibody (the prophagocytic "eat me" signal) were necessary and sufficient for the induction of phagocytosis and for efficient tumor elimination *in vivo* [269], [277]–[279]. In contrast to these early xenograft studies, the therapeutic efficacy of anti-CD47 mAbs in syngeneic models turned out to be generally more mitigated [280], [281] [282]. The reasons for this decreased efficacy with syngeneic models are not known but could be related to the expression pattern of the target antigen in syngeneic versus xenograft models (ubiquitously expressed mouse CD47 versus tumor-restricted human CD47, respectively – the anti-human CD47 mAbs used in xenograft experiments usually do not cross-react with the mouse antigen). Anti-mouse CD47 mAbs used in syngeneic models are thus exposed to the huge "antigen sink" represented by abundant CD47 on healthy tissues, negatively affecting pharmacokinetics and tumor exposure e[237], [283] [243], [279], [284]. Notwithstanding the problems outlined above, the current tendency with preclinical studies of CD47 inhibitors is to use immunocompetent mouse models. Syngeneic models provide a better understanding of the mechanism of action of molecules targeting the CD47/SIRPα pathway, given its complex interactions with the host immune system [285]. Specifically, the concept of CD47 being an immune checkpoint rather than just a "don't eat me" signal downregulating macrophage phagocytosis was developed and adopted thanks recent mechanistic studies in immunocompetent mouse models. Among others, syngeneic mouse studies demonstrated that CD47 blockade effectively promotes adaptive anti-tumor immunity and that it is the T cells and the DCs – rather than macrophages – which are the critical immune effectors of antitumor response induced by CD47 inhibitors [280], [286]–[288].

1.6.3.2. *Targeting CD47 in the clinic*

Therapeutic targeting remains challenging for CD47, due to its ubiquitous expression in healthy tissue. For this reason, the Fc effector functions of most CD47 inhibitors tested in the clinic (CD47 mAbs, SIRPα-Fc fusion proteins) are downregulated or silenced. Clinical studies with these molecules confirmed preclinical observations, namely that CD47/SIPRα blockade is not sufficient *per se* and, for an optimal effect, needs to be combined with prophagocytic signals provided either by chemotherapy or by traditional tumor-targeting IgG1 mAbs (endowed with full Fc effector functionality, e.g., rituximab, refs [268], [279], [289], [290]). On the other hand, current clinical experience with CD47 inhibitors endowed

with IgG1 Fc portion is limited, especially after the early trials with an SIRPα-IgG1Fc experimental drug TTi-621 demonstrated dose limiting toxicities at low doses (0.2 mg/kg, principally thrombocytopenia) [291], [292].

Thus, while human IgG4-Fc based or effector-less CD47 mAbs or SIRPα-Fc fusion proteins display better tolerability in patients (however, still showing unfavorable PK and some residual hematotoxicity issues) their clinical efficacy is limited by the lack of Fc-mediated effector functions [293]–[296]. Nonetheless , despite having a limited efficacy as monotherapy, targeting CD47 with such molecules is a promising approach to enhance anti-tumor activity in combination as demonstrated in several studies [297], [298]. About 10 different anti-CD47 mAbs and 4 SIRPα-Fc fusion proteins are currently at various clinical stages [243], [245]. Among them, the anti-CD47 mAb magrolimab (Hu5F9-G4) is the most advanced molecule, currently in Phase II clinical trials. It is a fully human anti-CD47 mAb with an hIgG4 backbone (i.e., with reduced Fc effector functions) [284], and it has demonstrated promising anti-tumor activity when combined with tumor targeting IgG1 mAbs such as rituximab [293]. A low priming dose is applied in the clinical protocol to mitigate anemia and the treatment still requires a high and frequency/high dose regimen to overcome the CD47 "antigen sink" [293], [294]. Like magrolimab, other CD47 inhibitors such as SIRPα-Fc fusion proteins ALX418 or TTI-622 showed promising anti-tumor efficacy in combination therapies [243], [244], [299], [300]. Current combination strategies are also testing the CD47 targeting in association with immune checkpoint inhibitors, in particular with PD-1/PD-L1 mAbs [242], [243].

1.6.3.3. *Bispecific approach in CD47 targeting*

Bispecific antibodies represent an attractive approach for overcoming the drawbacks associated with broad/ubiquitous expression of the therapeutic target in healthy tissues, and CD47 targeting can be regarded as a paradigm case in this context [245], [301], [302]. Indeed, bsAbs can be designed to associate a high affinity "guide" arm which will drive the binding to the tumor cells with a lower affinity effector arm in this case, an anti-CD47 arm. Such a bsAb is expected to bind and block CD47/SIRPα preferentially on target cells, which increased safety and efficacy by avoiding the "antigen sink" on healthy cells [303]. This selectivity allows for endowing the bsAb with an immunologically active Fc portion to enhance its tumor-killing capabilities. Alternatively, the other arm of a CD47-blocking bsAb could target another immunoreceptor with a more restricted expression pattern, such as PD-L1. Such a bsAb is expected to target both PD-L1 positive tumor and PD-L1 positive immune cells, the latter being particularly abundant in the tumor microenvironment (TME) [304]. The advantage of a CD47|PD-L1 bsAb over a CD47 and PD-L1 mAb combination would be that – while performing the same key function as the PD-L1 mAb, i.e.,

blocking the PD-L1 checkpoint – it would mediate preferential CD47 blockade on PD-L1-positive cells, thus mitigating the "antigen sink" related problems. CD47 arm could also be associated with an arm targeting T cell activating receptors (such as 4-1BB, CD40L). Preclinical studies have shown promising results with different bsAbs targeting CD47 as well as synergistic effects compared to a combination of mAbs [303], [305]–[308]. There are currently about 12 different bsAbs targeting CD47 in clinical trials [301].

1.7. Targeting PD-L1 and CD47 in cancer

Myeloid cells represent an important population infiltrating solid tumors [309], [310]. Thus, combining innate and adaptive checkpoints inhibitors represents a promising approach to enhance anti-tumor responses. In particular, there is a strong rationale for a joint blockade of CD47 and PD-L1. Both PD-L1 and CD47 are overexpressed at the surface of tumor cells [176], [272], [311], [312] and their expression is co-regulated at the transcriptional level by the MYC oncogene and hypoxia, a common feature of solid tumors [313] [314], [315]. In addition, genetic experiments have shown that silencing of both CD47 and PD-L1 in tumor cells leads to strong tumor growth inhibition [316]. And that deletion of CD47 on tumor cells increases the sensitivity to PD-1 blockade, suggesting that CD47 overexpression is a mechanism of resistance to CPI therapies [317]. Last but not least, pre-clinical studies showed that targeting CD47 and PD-L1 with a mAb combination has the potential of enhancing the anti-tumor efficacy compared to either monotherapy [286], [289], [299]. Understandably, co-targeting of CD47 and PD-L1 is now being evaluated in clinical trials [243], [245]. However, as monospecific CD47-inhibitors suffer from poor PK and are associated with hematotoxicity, their clinical success, both as single agents and in combination therapies is not guaranteed [318], [319]. As explained above, problems arising from ubiquitous expression of CD47 could be mitigated, at least partially, with a bispecific approach. Co-targeting CD47 and PD-L1 with bispecific antibodies or SIRPα-Fc fusion proteins has been successfully validated in proof-of-concept (POC) syngeneic experiments [308], [320], [321] and several bispecific experimental drugs have now entered clinical development phase [301] (Fig. X).

Name	Target	Phase	Type of diseases
IBI322	CD47/PD-L1	1	Hematologic Malignancy
HX009	CD47/PD-1	2	Advanced Solid Tumors
PF-07257876	CD47/PDL-1	1	Non-small-cell lung carcinoma/ Squamous cell carcinoma of head and neck
6MW3211	CD47/PD-L1	1/2	Advanced Malignant Neoplasm
SG12473	CD47/PD-L1	1a/1b	Advanced Malignant Tumors
IBC0966	CD47/PD-L1	1/2a	Advanced Malignant Tumors

Figure X: bispecific molecules targeting the CD47/SIRPα and PD-1/PD-L1 axis. Adapted from [301].

2. Aim of the study

Current immunotherapy approaches using immune checkpoint inhibitor (ICI) mAbs have shown clinical activity in different types of cancer. However, positive responses are usually confined to just a subset of patients [322]. In order to improve the efficacy of ICI, a multitude of combination therapies are currently being evaluated in the clinic [323]. The vast majority of ICI combination therapies are built around anti-PD-1 or anti-PD-L1 mAbs, the cornerstone of modern immunotherapy, and include a diverse array of anti-cancer treatments covering various modes of action [231], [232].

Combined targeting of PD1/PDL1 and CD47/SIRPα, an innate immune checkpoint, represents an emerging therapeutic strategy supported by preclinical evidence and the results of early clinical trials [243], [286], [289], [299], [316]. Yet, treatment with CD47-blocking mAbs was found to be associated poor pharmacokinetics (PK) and toxic side effects [291], [318], [319] due to ubiquitous expression of the target (the CD47 "antigen sink"). Various strategies are being used to overcome this issue, among them targeting of CD47 with bispecific antibodies (bsAbs). BsAbs present some potential advantages over mAb combinations, such as new modes of action, increased specificity and reduced toxicity. For instance, when the two target antigens are co-expressed by the same cell, the bsAb allows their co-engagement at the cell surface improving binding selectivity. Thus, bispecific targeting seems particularly appropriate for CD47.

This thesis project evaluated the efficacy of dual blockade of CD47 and PD-L1 with bispecific antibodies in syngeneic mouse models, i.e., in the presence of intact innate and adaptive immunity. Novimmune proprietary κλ-body platform [175] was used to generate various CD47|PD-L1 bispecific IgGs. These bsAbs were designed to have unbalanced affinities: from a mechanistic point of view, an anti-PD-L1 arm of high affinity drives the binding to cells, with the anti-CD47 of lower affinity contributing to cell binding by stabilizing the interaction via avidity [307]. As a result, these bsAbs are expected to block PD-L1 in an indiscriminate manner, i.e., on all PD-L1 expressing cells, while blocking CD47 preferentially on double positive cells, thus alleviating the CD47 antigen sink-related issues.

Many of the tumor-infiltrating immune cells express both CD47 and PD-L1. Thus, PD-L1/CD47 bsAbs target not only PD-L1-positive tumor cells, but also and immune cells in the tumor microenvironment (TME). Taking that into account, the CD47|PD-L1 bsAbs were generated with different Fc effector functions: on one hand, an active Fc portion that could potentially mediate the killing of PD-L1 positive immune cells in the TME through by ADCP and/or ADCC, on the other hand, a silenced Fc portion that would spare PD-L1-positive immune. This antibody toolbox was expected to allow me to assess the importance of the Fc portion for the anti-tumor activity of the bsAbs, but also for their pharmacokinetics

and safety. It is well recognized that the complex network of host cells in the TME plays a key role in cancer immune escape, [69], [75] I therefore took the opportunity to assess the changes induced by bispecific antibody treatment in the immune cells infiltrating the TME.

Last but not least: When looking back at the beginning of my PhD study (2017), a bispecific antibody approach to CD47 and PD-L1 targeting looked innovative and unique. However, in the meantime, three different labs have published *in vivo* studies done with bispecific CD47|PD-L1 molecules and the same cancer model I predominantly used in my study (MC38 in C57/BL6 mice), clearly demonstrating the therapeutic superiority of the bispecific targeting modality over PD-L1 mAb monotherapy, or even over a combination of CD47 and PD-L1 mAbs [320], [321], [324]. The results I obtained during my thesis give a less clear picture.

3. Results

3.1. Generation and characterization of CD47|PD-L1 mIgG2a bispecific antibodies

Bispecific antibodies (bsAbs) identified and generated with the κλ body platform [175] are unmodified, fully human immunoglobulins G (IgGs). They have a common heavy chain and two different light chains that drive the specificity of the arms against the two target antigens (Fig. 1). The fully human format should allow for low immunogenicity in patients. BsAbs generated against mouse targets were made as human-mouse chimeric mIgG2a molecules containing a minimum of human sequences, in order to minimize their immunogenicity in mice. With this approach, the human variable domains (heavy, κ and λ light chains) were associated with mouse heavy and light chain constant domains. Such a chimeric human-mouse mIgG2a molecule is depicted on Fig. 1.

The bsAb generated to target PD-L1 and CD47 are designed with an unbalanced affinity: a high-affinity anti-PD-L1 arm is associated with a lower affinity arm that binds mouse CD47. The reduced affinity for CD47 limits monovalent binding but allows for efficient blocking of CD47 upon coengagement on cells positive for PD-L1. In addition, our aim was that such bsAb has the ability to reach a similar PD-1/PD-L1 blocking level as the anti-PD-L1 mAbs.

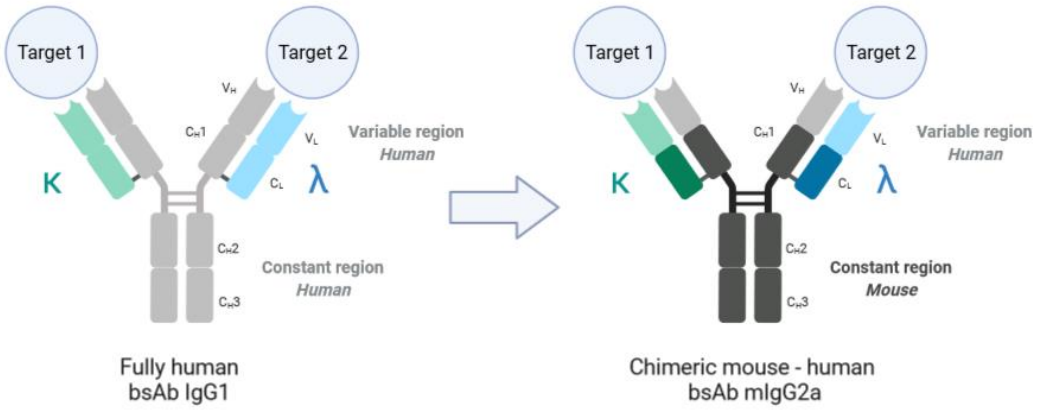

Figure 1: Schematic representation of the bsAb κλ body format as a fully human κλ body (left) or as a chimeric human-mouse κλ body (right). Variable human regions are grafted on constant regions of mouse heavy and light chains. Variable (V_H) and constant (C_H) heavy chains, gray; κ light variable (V_L) and constant (C_L) chains, green; λ light variable (V_L) and constant domain (C_L), blue. Domains of human origin are in light colors while the ones of mouse origin are in dark colors.

3.1.1. PD-L1 and CD47 expressing cells

To test and characterize the different monoclonal antibodies (mAbs) and bispecific antibodies (bsAbs), different cell lines were used (Table 1). Transformed Human Embryo Kidney epithelial cells (PEAK cells) expressing either mouse CD47 (mCD7) or mouse PD-L1 (mPD-L1) were generated. In addition, a panel of mouse cell lines naturally expressing CD47 and/or PD-L1 were selected. The expression of PD-L1 at the cell surface, and of CD47 to a lesser extent, could be modulated by stimulating the cells with recombinant mouse interferon-γ (mIFN-γ) [201], [325]. The target antigen densities characterized by QIFIKIT (DAKO) were summarized in Table 1. All cell lines showed an unbalanced expression of the two targets, with CD47 expression levels consistently higher than PD-L1 levels. A20 and B16F10 cell lines exposed to mIFN-γ showed the least unbalanced ratio of 1.5 CD47 molecules for 1 PD-L1 molecule. These different cell lines were used for selection, screening, and bsAb characterization.

Transfected cell lines			
		WT	
Cell name	**Cell origin**	**# PD-L1**	**# CD47**
PEAK mPD-L1	Human kidney cells transfected with mouse PD-L1	363000	N/A
PEAK mCD47	Human kidney cells transfected with mouse CD47	N/A	414000

Mouse native cell lines					
		WT		+IFN-γ	
Cell name	**Cell origin**	**# PD-L1**	**# CD47**	**# PD-L1**	**# CD47**
4T1	Mammary carcinoma	8000	134,000	28,000	188,000
CT26	Colon carcinoma	7000	88,000	29,000	128,000
L1.2	Pre-B lymphoma	<500	98,000	3000	172,000
MC38	Colon carcinoma	10,000	78,000	42,000	104,000
A20	B cell lymphoma	17,000	23,000	23,000	35,000
B16F10	Skin melanoma	2500	40,500	86,000	130,000
HEPA 1.6	Hepatocellular carcinoma	6000	90,000	80,000	130,000

Table 1: Cell lines details and antigen expression levels determined with QIFIKIT. Cell name and origin of transfected and mouse native cell lines used in this project. On mouse tumor cell lines, PD-L1 and CD47 levels were measured on noninduced cells and on cells exposed for to recombinant mouse IFN-γ (40ng/mL).

3.1.2. Isolation and characterization of anti-CD47 antibody arms

Two anti-mCD47 arms (one κ, named GD1, and one λ named mC2) with different affinities to mouse CD47 were already identified in a previous project [305]. I wanted to isolate a new anti-CD47 arm with a similar affinity as mC2 (λ) but from the κ isotype since the κλ body purification process requires different light chain isotypes. To identify a κ candidate, new CD47 arms with a panel of affinities were generated and reformatted into hIgG1 monoclonal antibodies (mAbs). To assess binding profile, these mAbs were evaluated by flow cytometry analysis on mouse tumor cell lines with known surface expression of CD47. The ability of these mAbs to block mouse CD47 was evaluated on L1.2 cells in a competition assay with soluble SIRPα. All the candidates were able to bind to CD47 expressed at the surface of cells and to block the CD47-SIRPα interaction (Fig. 2A and B). Candidates with a lower binding profile were also the ones with lower blocking ability. Among all the candidates generated, the κ anti-CD47 arm 1E5 displayed similar binding and blocking properties as mC2 (Fig. 2D-H). To measure the affinity and kinetic parameters for CD47, monovalent binding on recombinant mouse CD47 was measured with bio-layer interferometry (Octet, Forte Bio). 1E5 and mC2 showed an equilibrium dissociation constant (K_D) around 100 nM while GD1 has a KD that is in the micromolar range (Fig. 2C). 1E5 and mC2 are referred here as intermediate-affinity CD47 binders, while GD1 is referred as low-affinity CD47 binder.

A

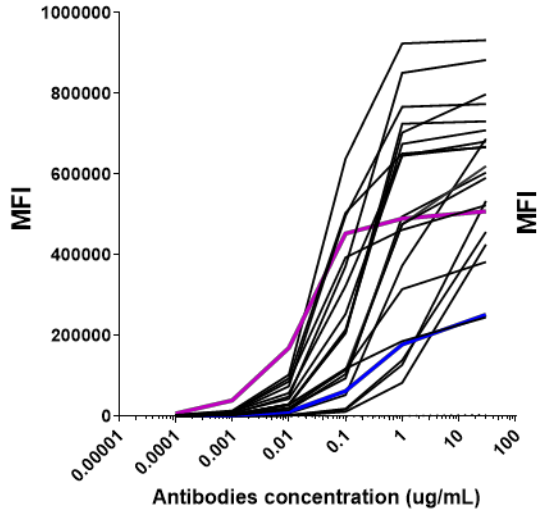

B

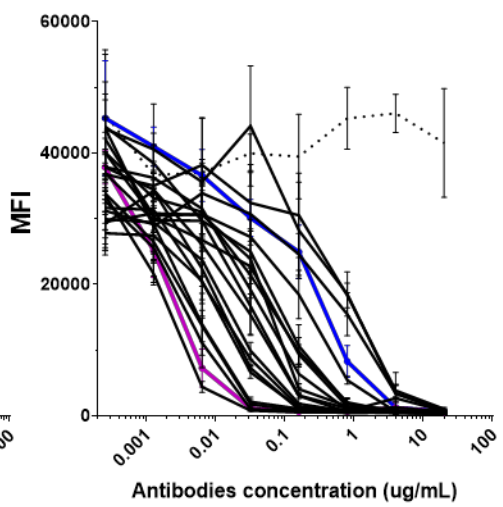

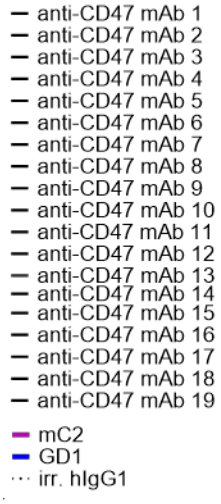

C

Anti-CD47 arm	Affinity for mCD47 (Average K_D, nM)
1E5	126.6 ± 6
mC2	108.2 ± 3
GD1	2130 ± 53

D

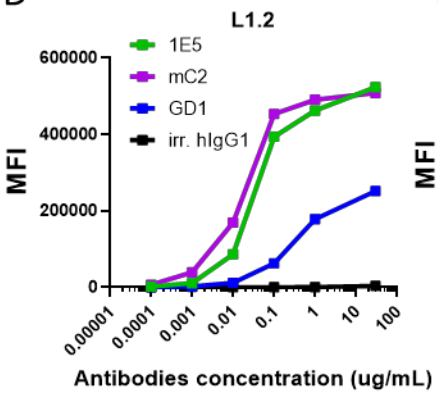

E

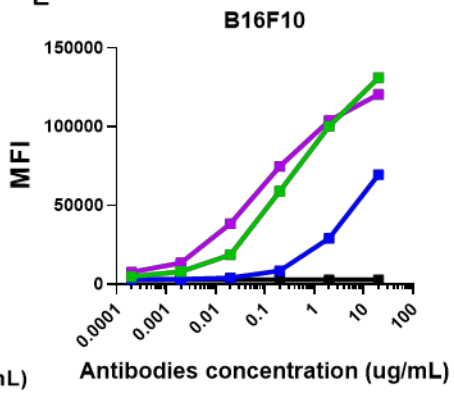

F

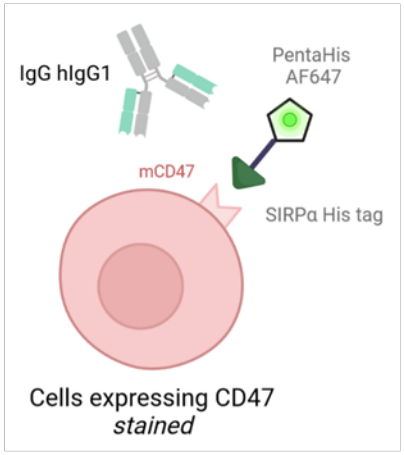

G

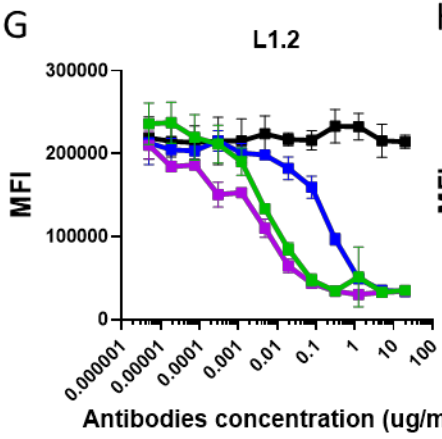

H

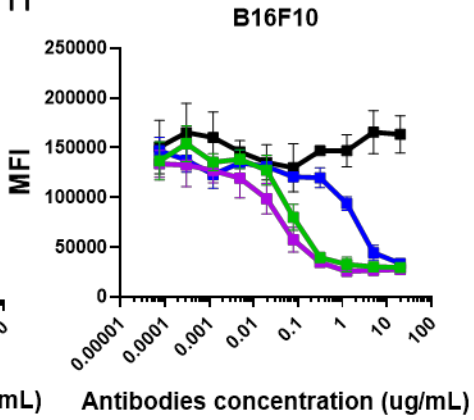

Figure 2 : Generation of a panel of blocking anti-mCD47 mAbs with different affinities. (A) Binding of anti-mCD47mAbs was determined by flow cytometry on L1.2 mouse pre-B cell lymphoma cells and was compared to the previously generated mAbs mC2 (purple) and GD1 (blue). (B) Binding of labeled recombinant mouse SIRPa-HIS to CD47 expressed at the surface of L1.2 cells in the presence of increasing concentration of anti-mCD47 mAbs was assessed using CellInsight CX5 High Content Screening Platform. (C) Affinity of anti-mCD47 arms. The affinity was measured using bio-layer interferometry (Octet, Forte Bio) and expressed as the KD ± SD. Results are representative of two independent experiments. (D-H) Characterization of the final candidates 1E5 (green), mC2 (purple), and GD1 (blue) for binding, to (D) L1.2 cells and (E) B16F10 mouse melanoma cells. Binding results shown are representative of multiple independent experiments (F) Cartoon showing the principle of the CellInsight assay. (G) Blockade of the CD47/SIRPa interaction on L1.2 cells. (H) Blockade of the CD47/SIRPa interaction on B16F10 cells. Blocking data are represented as Mean Fluorescence Intensity (MFI) ± SD of four replicates.

I evaluated the binding of the CD47 mAbs to red blood cells (RBC) since RBC are known to represent an antigen sink for the anti-CD47 antibodies due to the expression of CD47 at their surface and their abundance in the blood. Besides, binding of anti-CD47 mAbs to RBCs and platelets is responsible for toxic side effects observed in the clinic and in preclinical experiments, such as anemia or thrombocytopenia [242]. The binding of the anti-CD47 mAbs to mouse RBCs was assessed by flow cytometry and showed a similar binding for 1E5 and mC2 while GD1 showed reduced binding (Fig. 3A). 1E5 showed strong binding at the concentrations tested (30, 3 and 0.3 ug/mL) while GD1 showed low binding at the lowest concentration. Since the bispecific molecules in this project are designed to bind CD47 with one arm, the monovalent binding of 1E5 and GD1 to RBC was also evaluated. Monovalent constructs (i.e., κλ with an irrelevant arm associated with an anti-mCD47 arm) showed generally lower binding compared to the mAbs, and almost no binding at the lowest concentration (Fig. 3B) This decrease was even more pronounced with the monovalent construct harboring the GD1 low-affinity anti-mCD47 arm. Together, these results showed that monovalent binding to RCBs was significantly reduced as compared to bivalent (mAbs).

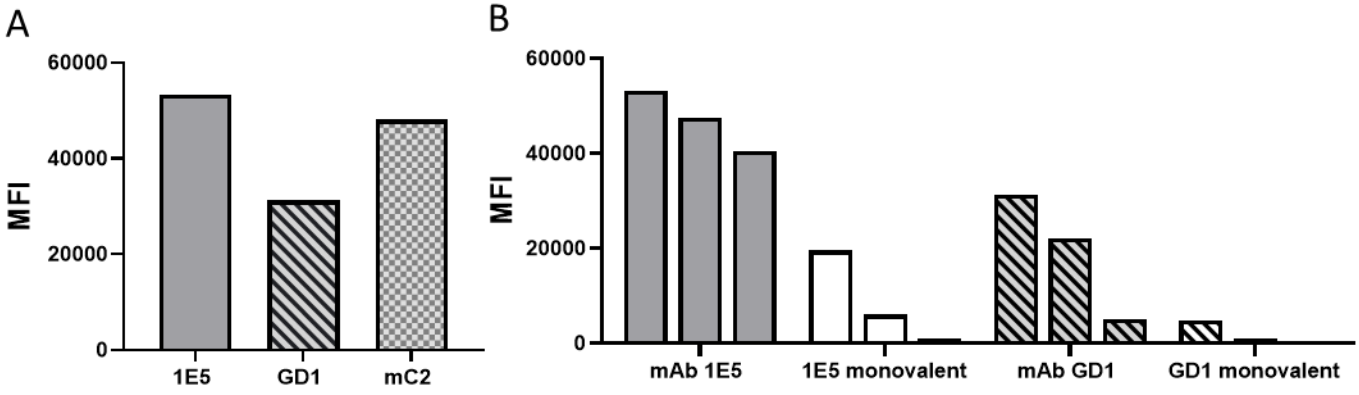

Figure 3: 1E5, GD1, and mC2 mAbs binding to red blood cells (RBCs). (A) mAbs binding to purified RBCs from mce (C57BL/6) was determined by flow cytometry, and the results were reported as the Mean Fluorescence Intensity (MFI). (B) Bivanlent and monovalent binding of the CD47 arms to RBCs were evaluated at 30 ug/mL, 3 ug/mL, and 0.3 ug/mL. Binding results are representative of two independent experiments.

3.1.3. Isolation and characterization of anti-PD-L1 antibody arms

To isolate single-chain variable fragments (scFvs) that specifically bind to the mouse PD-L1 from phage display libraries, several selection strategies were performed on recombinant mouse PD-L1 or on mouse native cell lines, as well as a combination of both approaches. ScFv candidates that bound the recombinant protein and PEAK mPD-L1 cells, were selected. 16 anti-PD-L1 scFv were reformatted into hIgG1 mAb and tested for binding on native mouse cell lines and blocking assay. 13 candidates out of 16 did bind mouse PD-L1 on PEAK mPD-L1 and A20 cells activated with mIFN-γ (Fig. 4A) but did not show binding on control PEAK and on A20 KO-mPD-L1 cells (data not shown). One candidate out of 13 did not bind to the PEAK mPD-L1 but only on native cells (IgG 6) and thus its blocking ability could not be evaluated. Among the reformatted candidates, 12 candidates out of 13 were blockers of the PD-1/PD-L1 interaction (Fig. 4B). However, their binding affinity and blocking properties were weaker compared to the control mAb anti-PD-L1 atezolizumab analog.

To increase the binding and blocking properties, a round optimization (RO) strategy was further performed as described [326]. Following round optimization, a panel of 24 IgGs was identified and tested for binding on mouse PD-L1 and blocking of the PD-1/PD-L1 interaction (Fig. 4C and D). From these 24 IgGs, a selection of 13 IgGs with improved affinity were characterized on mouse native cell lines (Fig. 4E). They showed increased binding compared to the IgGs isolated pre-RO and reached a level of cell binding close to the atezolizumab analog. Accordingly, several of these mabs blocked the PD-1/PD-L1 interaction with potency similar to the atezolizumab analog (Fig. 4F). Finally, a selection of 7 mAbs (4 κ and 3 λ) were chosen to be reformatted into mIGg2a κλ bsAbs.

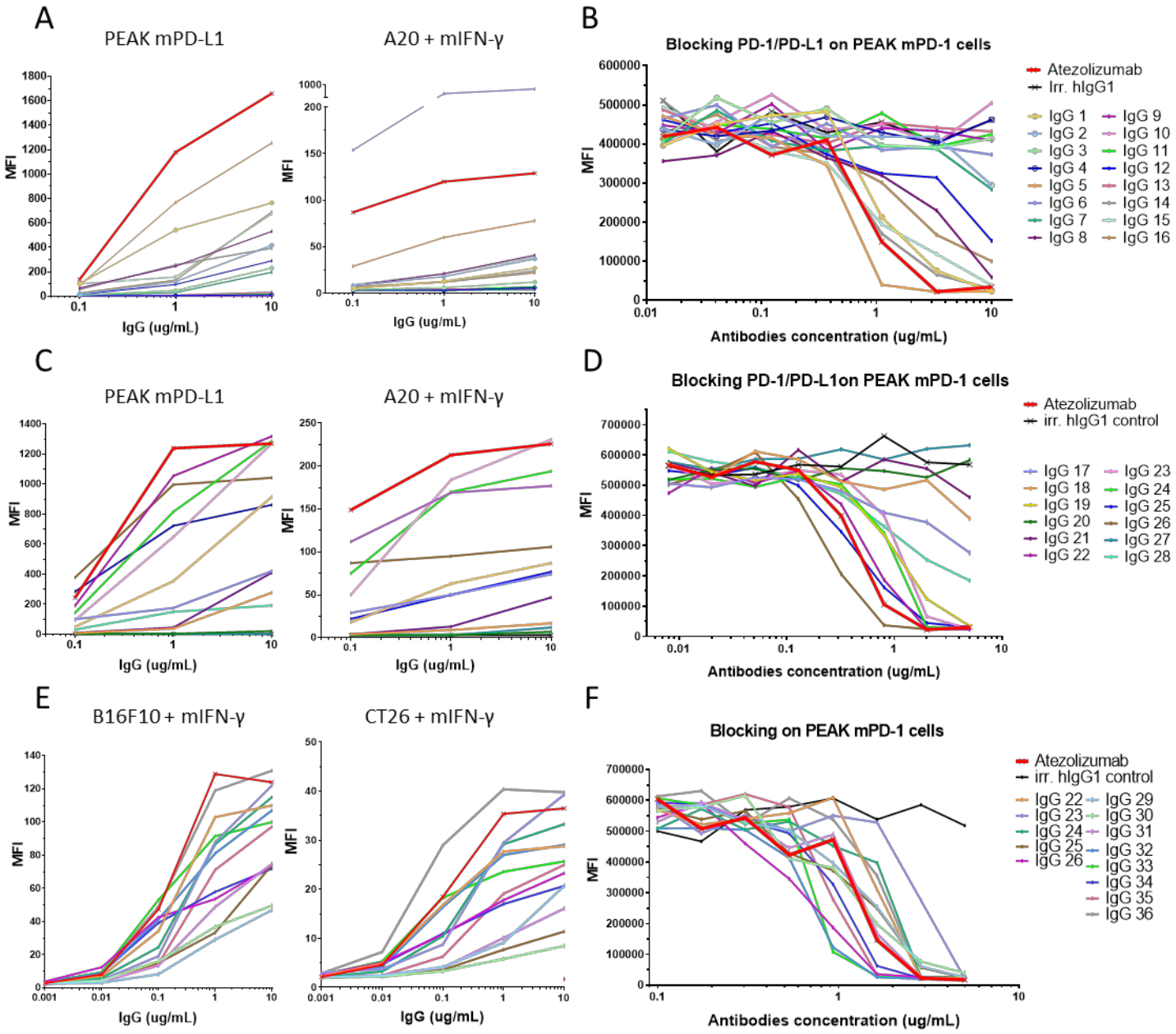

Figure 4: Binding of anti-PD-L1 mAbs and blocking the PD-1/PD-L1 interaction. Characterization of anti-PD-L1 mAb isolated before (A and B) and after RO (C to F) (A) and (C) binding to PEAK mouse PD-L1 and to IFN-γ activated A20 cells was evaluated at 3 concentrations by flow cytometry. (B) and (D) Blockade of PD-1/PD-L1 interaction on PEAK mPD-1 cells. Binding of fluorescently-labeled recombinant mouse PD-L1-Biot to PD-1 on the surface of PEAK mouse PD-1 cells in the presence of an increasing concentration of anti-mouse PD-L1 mAbs was detected using CellInsight CX5 High Content Screening Platform. The most potent candidates were further characterized: (E) Dose-response binding on B16F10 and CT26 cells activated with mouse IFN-γ was assessed by flow cytometry. (F) Blockade of PD-1/PD-L1 interaction on PEAK mPD-1 cells. Binding results are representative of three independent experiments. Blocking data are MFI ± SD of two replicates.

3.1.4. Generation of the 1st wave of CD47|PD-L1bispecific antibodies

Anti-mCD47xmPD-L1 κλ bodies were generated by combining the light chains from the antibodies generated against mCD47 and mPD-L1 with a common heavy chain [175]. The variable heavy and light parts that are from human origin while the constant regions were of mouse origin.

3.1.4.1. *Generation of CD47 hybrid constructs*

The κλ body purification process requires that the two light chains be of the opposing isotype. The GD1 CD47 arm is a kappa light chain that can be associated with the lambda PD-L1 arms while for pairing with the kappa PD-L1 antibody arms, I needed an CD47 light chain with a constant lambda part. GD1 V_H-V_L hybrids were therefore generated, with constant mouse kappa light chain region replaced by constant mouse lambda light chain region (Fig. 5A). Three different constructs were generated, each one having a different framework sequence linking the variable light chain to the constant light chain. The framework four sequence was either fully kappa, fully lambda, or a mix of it (Fig. 5B). The three different hybrids were expressed and purified, with their binding to mouse L1.2 cell line similar to WT GD1 kappa antibody (Fig. 5C).

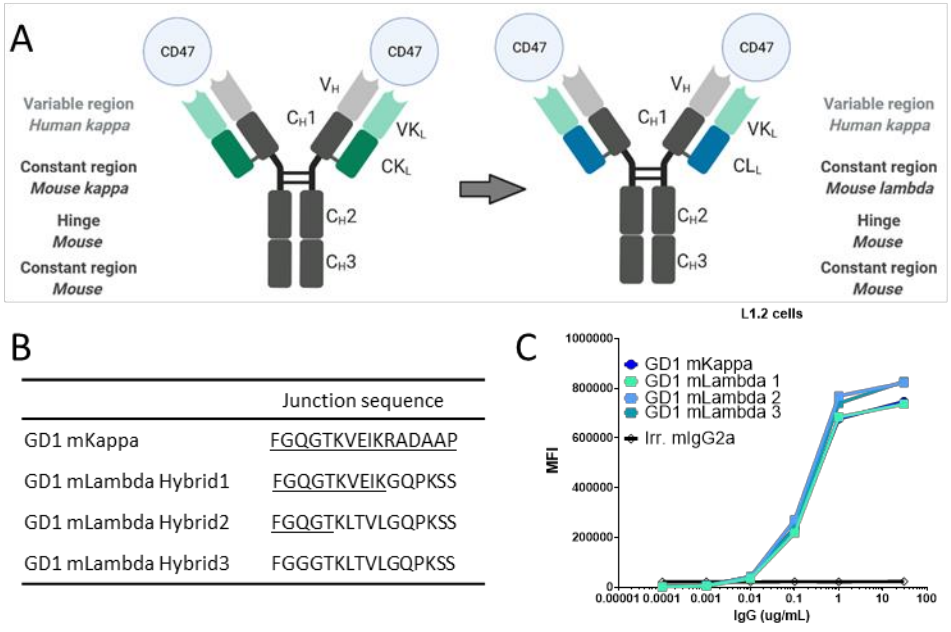

Figure 5: Design and characterization of hybrid constructs. GD1 kappa light chain was converted into different kappa/lambda hybrids. (A) Human variable kappa region was combined with mouse lambda constant regions. (B) The proportion of mouse kappa light chain sequences in hybrid constructs is shown (underlined) (C) Three lambda hybrids were evaluated for binding on L1.2 cell by flow cytometry.

First, GD1 mLambda hybrid 1 sequence was selected to be associated with the PD-L1 kappa sequences. The light chain hybrids expressed as mAbs, or the bsAbs containing the original GD1 mkappa sequences showed no issues in expression and purification. On the other hand, the bsAbs with the GD1 mLambda hybrid 1 were expressed at very poor levels. Unfortunately, the other two GD1 mouse lambda hybrids (2 and 3) were also very poor expressors (data not shown).

3.1.4.2. *Design of new hybrid GD1 constructs for bsAbs generation*

New GD1 lambda hybrid constructs were therefore designed and generated. These constructs contained light chain constant regions of human origin (Fig. 6A), which solved the problem of low bsAb expression. The hybrid construct 1 contained sequences of human origin in the variable and constant light chains, in the CH1 domain, and in the hinge while the CH2 and CH3 domains were from mIgG2a isotype. The hybrid construct 2 was similar except for the hinge that was of mouse origin (Fig. 6A). Among the four mAbs that were generated based on construct 1, a candidate (GD1 λ hybrid 1-3) showed the same binding profile compared to the control GD1 kappa WT (Fig. 6B). This candidate was chosen for the reformatting of the bsAbs that have a kappa PD-L1 arm.

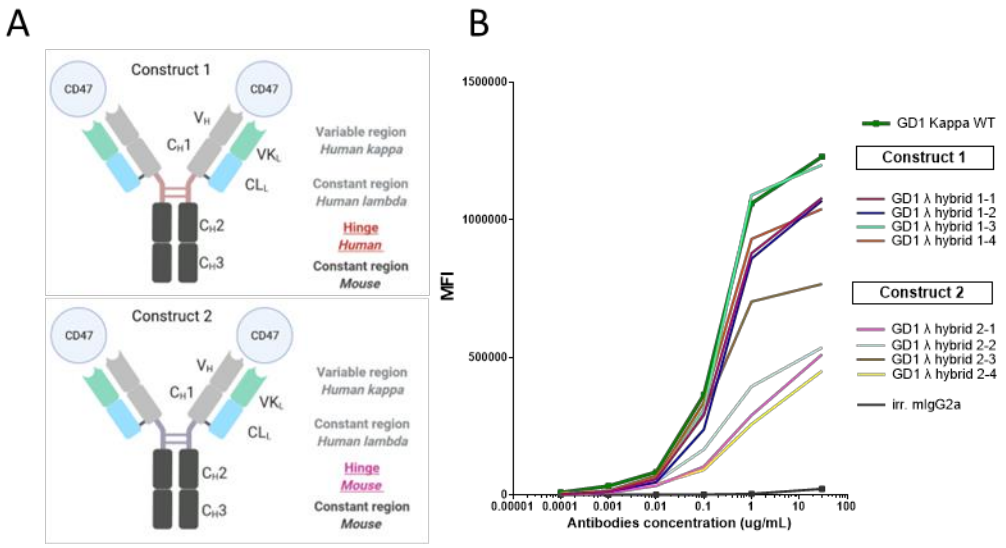

Figure 6: Design and characterization of GD1 chimeric constructs. The part of human sequences was increased as compared to constructs shown in Fig.6. (A) Two types of constructs were designed with constant heavy region 1 and constant kappa regions from human origin. The hinge was of human origin in construct 1 and of mouse origin in construct 2. (B) Binding on L 1.2 cells was evaluated by flow cytometry. Binding results are representative of three independent experiments.

Two different approaches to produce the bsAbs: the GD1 kappa arm was associated with three different lambda PD-L1 arms (Fig. 7A), while the modified GD1 lambda 1-3 was associated with the kappa PD-L1 arms (Fig. 7B).

A

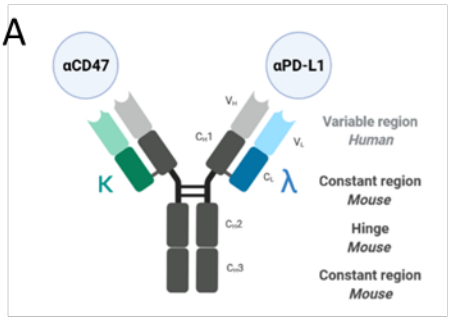

κλ body name	κ arm	κ specificity	λ arm	λ specificity
GD1|1F5	GD1	anti-mCD47	1F5	anti-mPD-L1
GD1|3A9	GD1	anti-mCD47	3A9	anti-mPD-L1
GD1|1F9	GD1	anti-mCD47	1F9	anti-mPD-L1

B

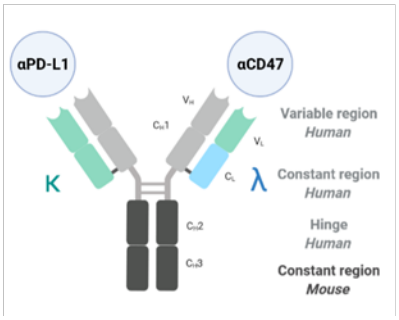

κλ body name	κ arm	κ specificity	λ arm	λ specificity
GD1|1F5	1H6	anti-mPD-L1	GD1 λ 1-3	anti-mCD47
GD1|3A9	1H4	anti-mPD-L1	GD1 λ 1-3	anti-mCD47
GD1|1F9	2E5	anti-mPD-L1	GD1 λ 1-3	anti-mCD47
GD1|1F9	1A7	anti-mPD-L1	GD1 λ 1-3	anti-mCD47

Figure 7: Design of the bsAbs chimeric constructs. (A) BsAbs with a lambda anti-PD-L1 were associated with the anti-CD47 kappa arm. Only the variable regions contained sequences of human origins. (B) The part of human origin sequences was increased the bsAbs with a kappa anti-PD-L1 arm.

3.1.5. *In vitro* characterization of the first wave of bsAbs

3.1.5.1. *Binding to cells*

Binding of the first wave of κλ bodies was evaluated by flow cytometry on different cell lines. Monovalent binding to mCD47 or mPD-L1 was evaluated using transfected PEAK cells. On mPD-L1 expressing cells, monovalent binding of bsAbs as compared to the corresponding mAbs or atezolizumab was lower, yet significant (Fig. 8A and B). On the other hand, only a marginal binding to mCD47 transfected PEAK cells was observed (Fig. 8C), reflecting the unbalanced affinity design of the bsAbs (a high-affinity anti-PD-L1 arm associated to a low-affinity anti-mCD47 arm). To evaluate the effect of the co-engagement, binding of the bsAbs was tested on double positive cells (B16F10 cells activated with IFN-γ, Fig. 8D). The bsAb binding was comparable to atezolizumab analog demonstrating that, while that the PD-L1 arm is the main driver for binding on double-positive to cells, the low affinity CD47 arm (GD1) makes a significant contribution upon co-engagement

3.1.5.2. *Blocking of the CD47/SIRPα interaction*

To test their ability to block the CD47/SIRPα interaction, the bsAbs were tested in a competitive binding assay on L1.2 cells and on IFN-γ induced A20 cells (Fig. 8E and F). L1.2 cells display almost no PD-L1 molecules at cell surface and about 100,000 molecules of CD47 (see Table 1). On the contrary, IFN-γ induced A20 cells display a more balanced expression of the two targets, with about 23,000 copies of PD-L1 and 35,000 copies of CD47. With L1.2 cells, GD1-based bsAbs showed a poor blocking of the CD47/SIRPa interaction similar to the corresponding CD47 monovalent bsAb (Fig. 8E). A superior blocking potency of the bsAbs was apparent on double positive A20 cells, demonstrating the importance of PD-L1 coengagement (Fig. 8E).

3.1.5.3. *Blocking of the PD-1/PD-L1 interaction*

The bsAbs were also tested for their ability to block the PD-1/PD-L1 interaction. When tested on PEAK mPD-L1 cells, the bsAbs appeared as poor blockers (Fig. 8G), with a 100-1000 times lower potency as compared to the atezolizumab analog or 10F.9G2 (a high-affinity rat anti-mouse PD-L1, widely used in syngeneic tumor experiments [204], [327], [328]). To assess the contribution of CD47 engagement, the bsAbs blocking ability was also tested on double-positive IFN-γ induced B16F10 cells. Surprisingly, CD47 co-engagement by the low affinity GD1 arm did not result in a large increase in blocking potency (Fig. 9H) such as previously seen in binding experiments (compare Fig. 8G versus 8B and Fig. 8H to 8D, using the PD-L1 mAbs as benchmarks). Nonetheless, bsAbs bearing the medium-affinity anti-CD47 arm mC2 were significantly more efficacious at PD-1/PD-L1 blocking than the GD1-based bsAbs, demonstrating clearly a contribution of CD47 co-engagement (Fig. 8H).

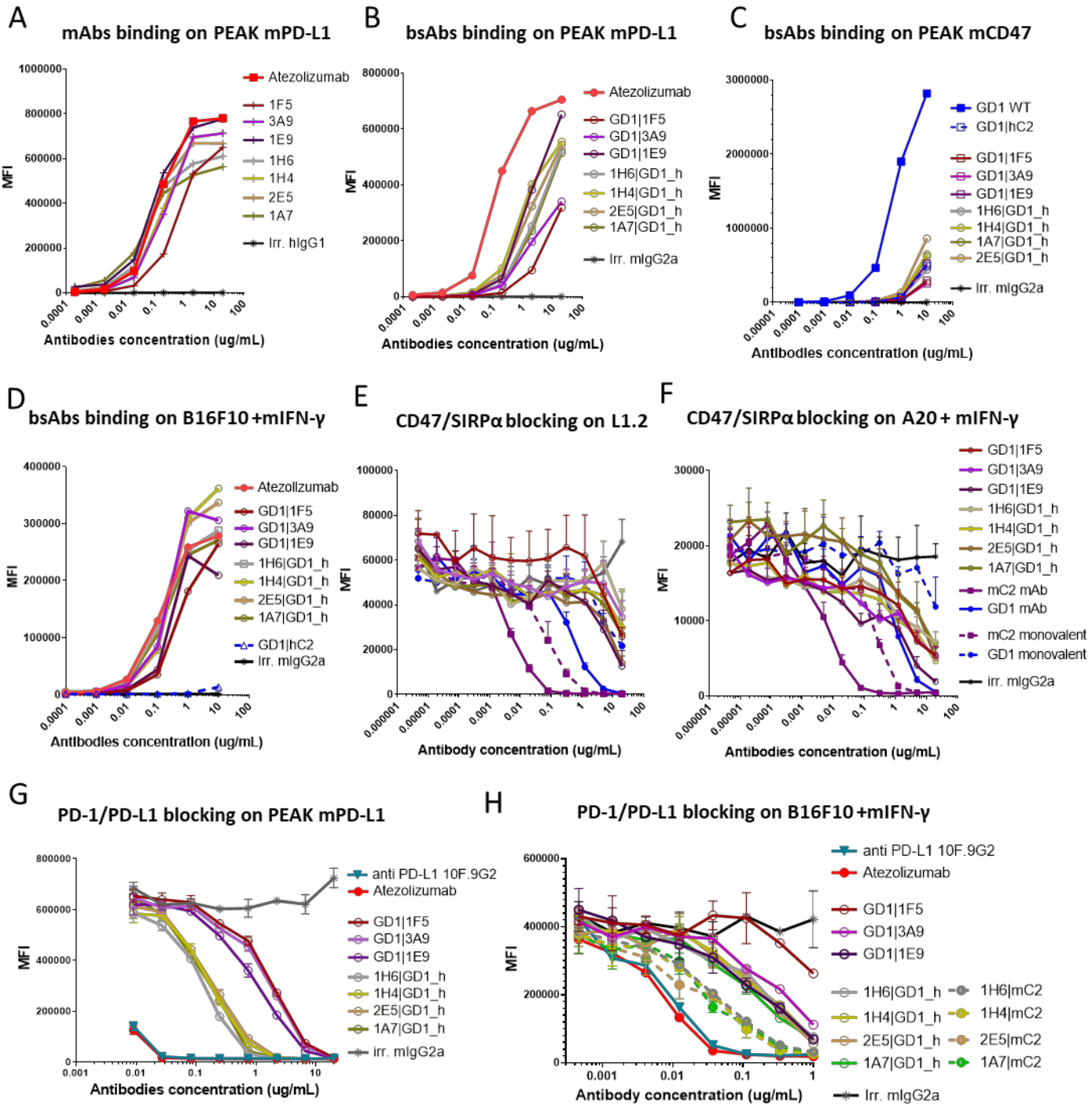

Figure 8: Characterization of the first wave of bsAbs. (A-D) binding was evaluated by flow cytometry with cells expressing PD-L1 or CD47 as well as with double-positive cells. (A) Binding of anti-PD-L1 mAbs on PEAK mPD-L1 cells. (B) Monovalent binding of each arm of the bsAbs was evaluated on (B) PEAK mPD-L1 and on (C) PEAK mCD47. (D) Binding on double-positive B16F10 cells activated with mIFN-γ. (E-F) Blocking of the CD47/SIRPα interaction was assessed with a competitive binding assay. (E) Binding of fluorescently-labeled mouse SIRPα-HIS was measured in the presence of an increased concentration of bsAbs on PD-L1-negative L1.2 cells (F) Binding of fluorescently-labeled mSIRPα hFc, was measured in the presence of an increased concentration of bsAbs double-positive cells A20 cells activated with mIFN-γ. (G-H) Blocking of the PD-1/PD-L1 interaction assessed with a competitive binding assay. (G) . Monovalent blocking evaluated on PEAK mPD-L1 cells. The binding of fluorescently labeled mPD-1 human Fc

was measured in the presence of an increased concentration of bsAbs (H) Blocking upon CD47 co-engagement evaluated on double-positive B16F10 cells activated with mIFN-γ. The binding of fluorescently labeled human PD-1 high-affinity was measured in the presence of an increased concentration of bsAbs. Binding results are representative of three independent experiments. Blocking data are represented as MFI ± SD of two replicates.

3.1.6. Lead optimization of the 1h6 candidate

We sought to further increase the affinity of the PD-L1 arm. Based on binding, blocking, and productivity characteristics, the κ 1h6 anti-PD-L1 antibody was selected for lead optimization. Lead optimization (LO) is a process aiming to increase the affinity of a selected candidate by introducing diversity into the CDRs sequences. To obtain an anti-PD-L1 arm of higher affinity, three phage-display libraries were generated by introducing diversity into the CDR1, CDR2, and/or CDR3 of the variable light chain region of the 1h6 sequence. The three libraries were used for phage-display selections under stringent conditions.

3.1.6.1. *Selection of an anti-PD-L1 lead candidate generated with 1h6 LO.*

Screening of scFv hits was performed with the PD-1/PD-L1 blocking assay and PEAK mPD-L1 cells, activated MC38, and B16F10 cells. Two sets of 20 scFvs identified as potent blockers were reformatted into mAbs for further characterization. The blocking assay on PEAK mPD-L1 showed that all these mAbs blocked the PD-1/PD-L1 interaction (Fig. 9A). Binding to various cell lines was used to further rank these mAbs. Binding to PEAK cells expressing high levels of PD-L1 showed profiles similar to atezolizumab for all but six candidates and was not discriminatory enough (Fig. 9B and E). MC38 cells activated with IFN-γ, provided better resolution (Fig. 9C and F) but even more differences became apparent with non-activated MC38 expressing low amounts of PD-L1 (Fig. 9D and G). Three mAbs from the first set of reformatting and nine candidates from the second set displayed better binding than the parental 1h6 antibody, still without reaching the potency of atezolizumab. The mAb 6E8 showed the best improvement as compared to the parental 1h6 and was thus chosen as the final arm to generate bsAbs

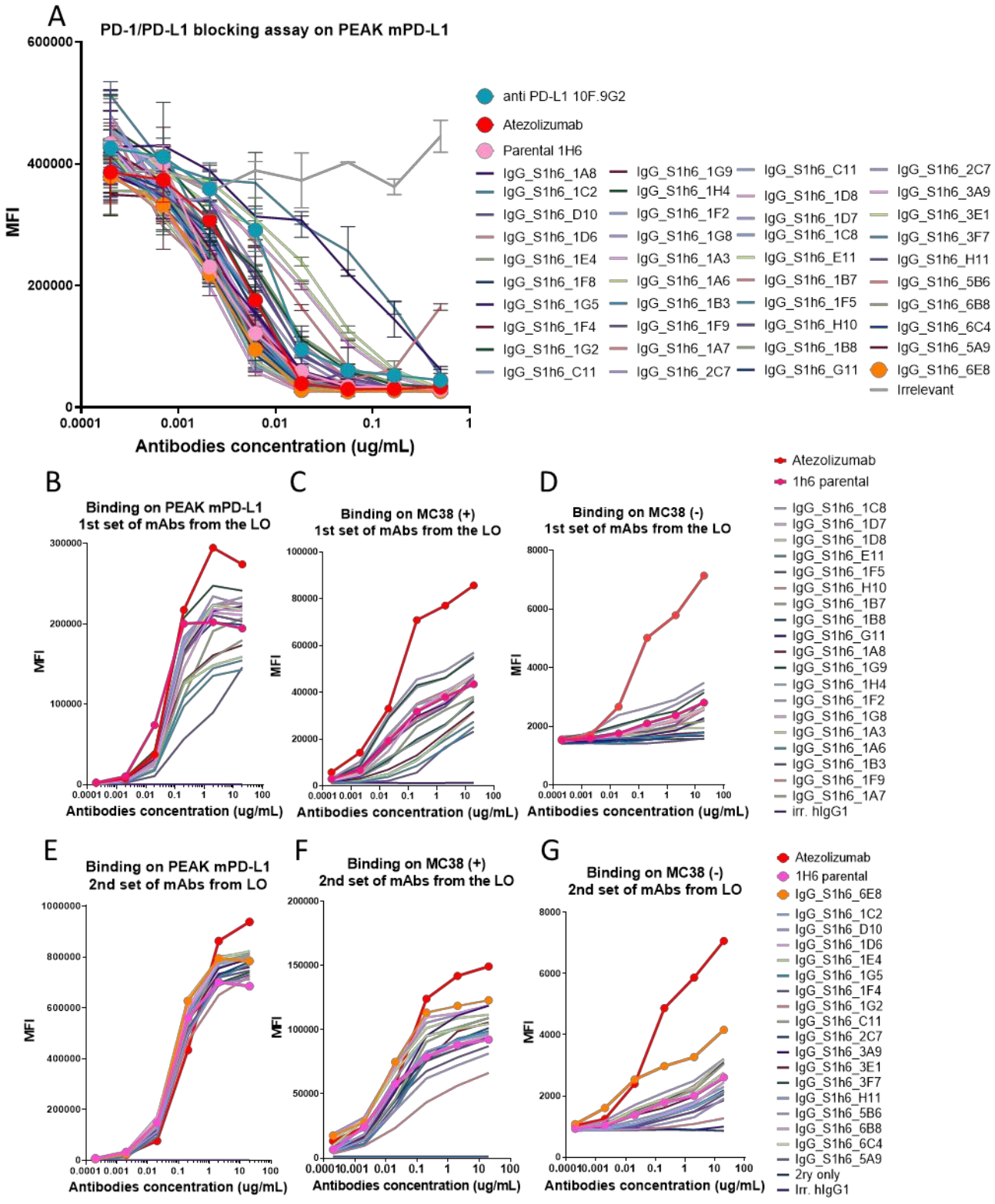
A
PD-1/PD-L1 blocking assay on PEAK mPD-L1
MFI
Antibodies concentration (ug/mL)
anti PD-L1 10F.9G2
Atezolizumab
Parental 1H6
IgG_S1h6_1A8
IgG_S1h6_1C2
IgG_S1h6_D10
IgG_S1h6_1D6
IgG_S1h6_1E4
IgG_S1h6_1F8
IgG_S1h6_1G5
IgG_S1h6_1F4
IgG_S1h6_1G2
IgG_S1h6_C11
IgG_S1h6_1G9
IgG_S1h6_1H4
IgG_S1h6_1F2
IgG_S1h6_1G8
IgG_S1h6_1A3
IgG_S1h6_1A6
IgG_S1h6_1B3
IgG_S1h6_1F9
IgG_S1h6_1A7
IgG_S1h6_2C7
IgG_S1h6_C11
IgG_S1h6_1D8
IgG_S1h6_1D7
IgG_S1h6_1C8
IgG_S1h6_E11
IgG_S1h6_1B7
IgG_S1h6_1F5
IgG_S1h6_H10
IgG_S1h6_1B8
IgG_S1h6_G11
IgG_S1h6_2C7
IgG_S1h6_3A9
IgG_S1h6_3E1
IgG_S1h6_3F7
IgG_S1h6_H11
IgG_S1h6_5B6
IgG_S1h6_6B8
IgG_S1h6_6C4
IgG_S1h6_5A9
IgG_S1h6_6E8
Irrelevant
B
Binding on PEAK mPD-L1
1st set of mAbs from the LO
C
Binding on MC38 (+)
1st set of mAbs from the LO
D
Binding on MC38 (-)
1st set of mAbs from the LO
Atezolizumab
1h6 parental
IgG_S1h6_1C8
IgG_S1h6_1D7
IgG_S1h6_1D8
IgG_S1h6_E11
IgG_S1h6_1F5
IgG_S1h6_H10
IgG_S1h6_1B7
IgG_S1h6_1B8
IgG_S1h6_G11
IgG_S1h6_1A8
IgG_S1h6_1G9
IgG_S1h6_1H4
IgG_S1h6_1F2
IgG_S1h6_1G8
IgG_S1h6_1A3
IgG_S1h6_1A6
IgG_S1h6_1B3
IgG_S1h6_1F9
IgG_S1h6_1A7
irr. hIgG1
E
Binding on PEAK mPD-L1
2nd set of mAbs from LO
F
Binding on MC38 (+)
2nd set of mAbs from the LO
G
Binding on MC38 (-)
2nd set of mAbs from LO
Atezolizumab
1H6 parental
IgG_S1h6_6E8
IgG_S1h6_1C2
IgG_S1h6_D10
IgG_S1h6_1D6
IgG_S1h6_1E4
IgG_S1h6_1G5
IgG_S1h6_1F4
IgG_S1h6_1G2
IgG_S1h6_C11
IgG_S1h6_2C7
IgG_S1h6_3A9
IgG_S1h6_3E1
IgG_S1h6_3F7
IgG_S1h6_H11
IgG_S1h6_5B6
IgG_S1h6_6B8
IgG_S1h6_6C4
IgG_S1h6_5A9
2ry only
Irr. hIgG1

Figure 9: Characterization of mAbs from 1H6 lead optimization. (A) PD-1/PD-L1 blocking characterized with CellInsight competitive binding assay. The binding of fluorescently labeled mouse PD-1 human Fc was measured in the presence of an increased concentration of mAbs (B-F) Binding assessed by flow cytometry on (B, D) PEAK mouse PD-L1 cells, (C,F) MC38 cells activated with mIFN-γ or (D,G) MC38 not activated. Final candidate chosen for bsAb reformatting is represented by a bold orange line (E-G). Binding results are representative of multiple independent experiments. Blocking data are represented as MFI ± SD of two replicates.

3.1.6.2. *Affinity measurements*

In order to better characterize the lead candidate 6E8 compared to the atezolizumab analog, the affinity and binding kinetics were assessed with bio-layer interferometry (Octet, Forte Bio). Atezolizumab and 6E8 showed comparable affinities upon monovalent binding to PD-L1, with a similar K_D (equilibrium dissociation constant, Fig. 10A). In another experiment, the binding kinetic to different mouse PD-L1 proteins was evaluated. Atezolizumab and 6E8 showed different association and dissociation profiles: 6E8 was quicker to associate and dissociate to the proteins (Fig. 10B). This difference (slower K_{off}) probably explains the superior binding observed with atezolizumab in FACS experiments (Fig. 10C and F). Competitive binding assays were also performed, suggesting that 6E8, 10F.9G2, and atezolizumab target the same region of PD-L1 (data not shown).

A

Anti-PD-L1 arm	Affinity for mPD-L1 (Average K_D, nM)	Average K_{ON} (1/Ms)	Average K_{OFF} (1/s)
Atezolizumab	31 ± 4	$1.91x10^5$	$5.91x10^{-3}$
6E8	27 ± 3	$6.2x10^5$	$1.67x10^{-2}$

B

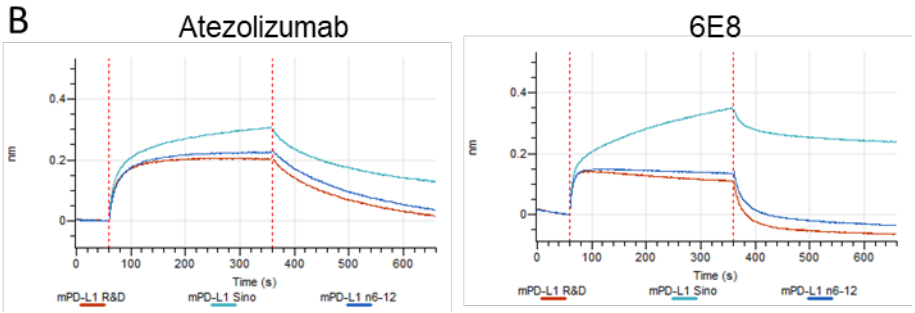

Figure 10: Affinity of the 6E8 antibody to mouse PD-L1 . (A) Affinity was measured using bio-layer interferometry (Octet, Forte Bio) and is shown as the KD ± SD. Results are representative of two independent experiments. (B) Association and dissociation of atezolizumab and 6E8 to three different recombinant mouse PD-L1 proteins was evaluated.

3.1.7. *In vitro* characterization of the 6E8-based bsAbs

The selected 6E8 anti-PD-L1 arm was associated with two previously described anti-mCD47 arms, one of intermediate affinity (mC2, K_D= 108.2 nM), the other of low affinity (GD1, K_D= 2130 nM, Table 2). The mC2 bsAb was made in two versions differing by the Fc region, wild-type mIgG2a with full effector functions, and an mIgG2a version bearing the D265A mutation. This mutation has been described to abrogate the binding to the Fc part to the mouse Fcγ receptors [329].

κλ body name	κ arm	κ specificity	Affinity	λ arm	λ specificity	Affinity	Heavy Chain
6E8|mC2	6E8	anti-mPD-L1	high	mC2	anti-mCD47	intermediate	mIgG2a
6E8|mC2	6E8	anti-mPD-L1	high	mC2	anti-mCD47	intermediate	mIgG2a D265A
GD1|6E8	GD1	anti-mCD47	low	6E8-h	anti-mPD-L1	high	mIgG2a

Table 2: Summary of the generated bsAbs constructs.

3.1.7.1. *Binding to double positive cells*

Binding of the bsAbs the 6E8 mAb was evaluated by flow cytometry. Binding of the 6E8 mAb was similar to atezolizumab while the bsAbs showed a more elevated MFI signal at high antibody concentrations (Fig. 11A and B). That could reflect on one side, the bivalent versus monovalent saturation binding of cell surface PD-L1 (more IgG available for detection reagent in the latter case) and, on the other side, the some monovalent CD47 binding at high bsAb concentrations (a significant part of cell surface CD47 cannot be co-engaged by the bsAbs since the CD47 expression levels are higher than the PD-L1 expression levels, both on MC38+ and B16F10+ cells). By the same token, the difference between 6E8|mC2 and GD1|6E8 MFI signals at high antibody concentrations apparent on Figs 11A and B could be explained by a more efficacious engagement of CD47 by the mC2 antibody arm. The latter is consistent with previously established differences in binding affinities (mC2 K_D = 108.2 nM, GD1 K_D = 2130 nM) and the CD47 monovalent binding shown in Figs 11C and D. In the same set of experiments, the 6E8|mC2 and GD1|6E8 bsAbs were compared with the corresponding bsAbs bearing the parental 1h6 PD-L1 arm. The binding of these bsAbs to MC38(+) and B16F10(+) cells illustrates the effect of PD-L1 affinity increase obtained upon 1h6 LO (Fig. 12E and 12F).

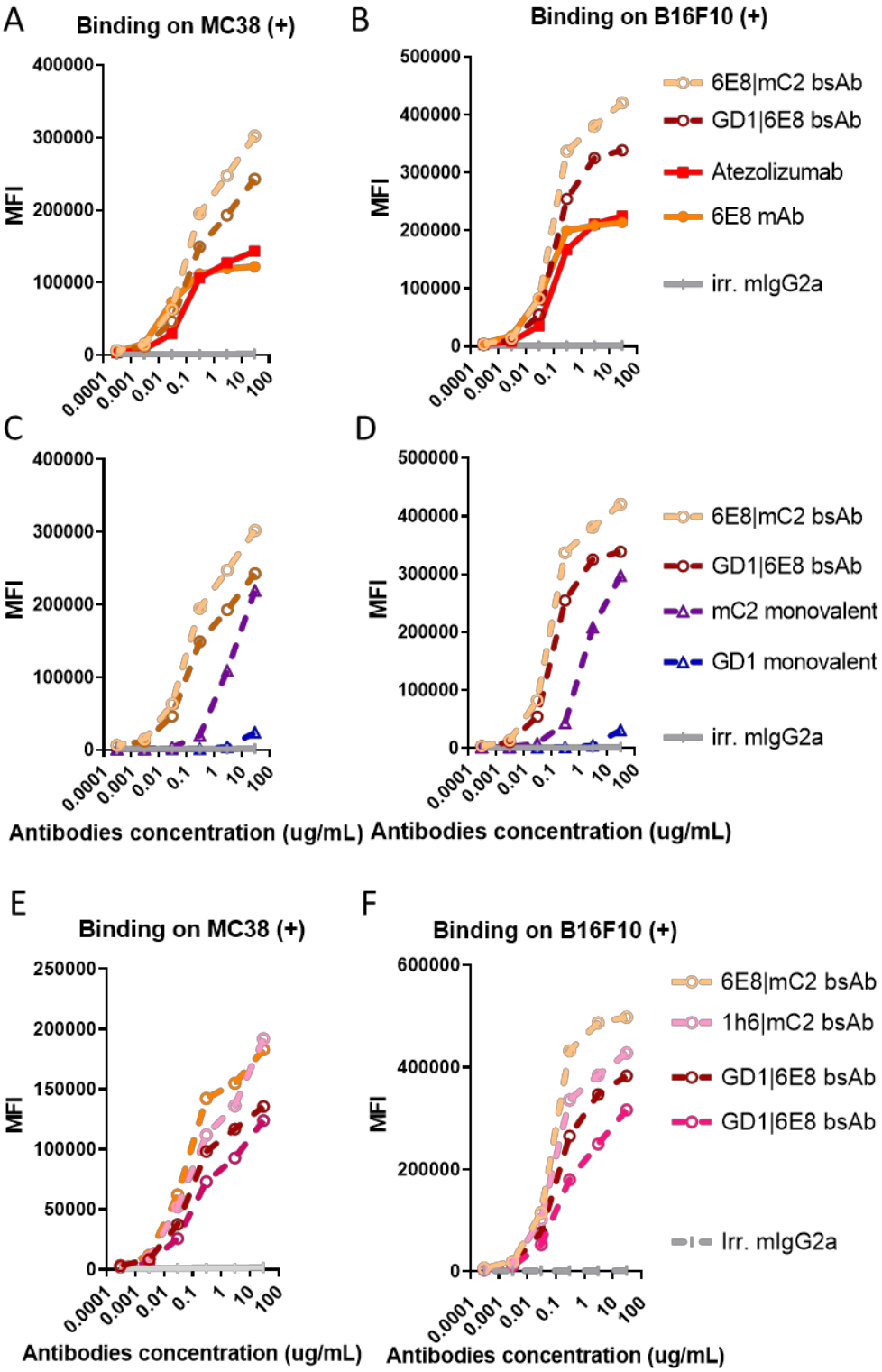

Figure 11: Binding of 6E8|mC2 and GD1|6E8 bsAbs to double positive cells. Binding to MC38 cells (A and C) and B16F10 cells (B and D) activated with mIFN-γ was evaluated by flow cytometry and is shown as mean fluorescence intensity (MFI). BsAb binding was compared to (A-B) anti-PD-L1 mAbs and to (C-D) the corresponding monovalent CD47 antibodies. (E and F) Binding of LO-

derived bsAbs as compared to the corresponding bsAbs with the parental anti-PD-L1 arm 1h6. Binding results are representative of multiple independent experiments.

3.1.7.2. *The bsAbs block the PD-1/PD-and CD47/ SIRPα interactions*

The bsAbs were designed to bind to CD47 and PD-L1 at the surface of the cells and to block the PD-1/PD-L1 and the CD47/SIRPα interactions. I hypothesized that the bsAbs would have an increased blocking ability compared to the corresponding monovalent PD-L1 and CD47 controls. In addition, I assumed that the bsAbs would block the PD-1/PD-L1 interaction similarly to the control mAbs atezolizumab, 6E8, and 10F.9G2. To test this hypothesis, the bsAbs were tested in a competitive PD-1/PD-L1 binding assay on B16F10(+) cells (i.e., activated with IFNγ). Both 6E8|mC2 and GD1|6E8 bsAb induced increased PD-L1 blockade compared to the corresponding monovalent PD-L1 (Fig. 12A). 6E8|mC2 bsAb showed blocking potency similar to the anti-PD-L1 mAbs while GD1|6E8 bsAb was less active, confirming the importance of CD47 co-engagement for efficient CD47 blockade.

The bsAbs were then evaluated in a CD47/SIRPα competitive binding assay on B16F10(+) cells. IFNγ-activated B16F10 cells express higher levels of CD47 than PD-L1 (about 1.5 CD47 molecules for one PD-L1 molecule, see Table 1), therefore not all CD47 can be bound upon coengagement with the high affinity anti-PD-L1 arm. As a consequence, the curve of bsAb-induced CD47 blockade followed a biphasic path: at lower antibody concentrations, PD-L1 coengagement resulted in potent blocking of CD47. On the other hand, at higher antibody concentrations, where no more cell surface PD-L1 was presumably available for antibody binding, the CD47 blockade curves followed the path of monovalent anti-CD47 controls (Fig. 12B).

Overall, these results showed that the bsAbs are able to potently block the PD-1/PD-L1 and CD47/SIRPα interactions and that co-engagement of the cognate target at the cell surface significantly contributes to blocking efficacy.

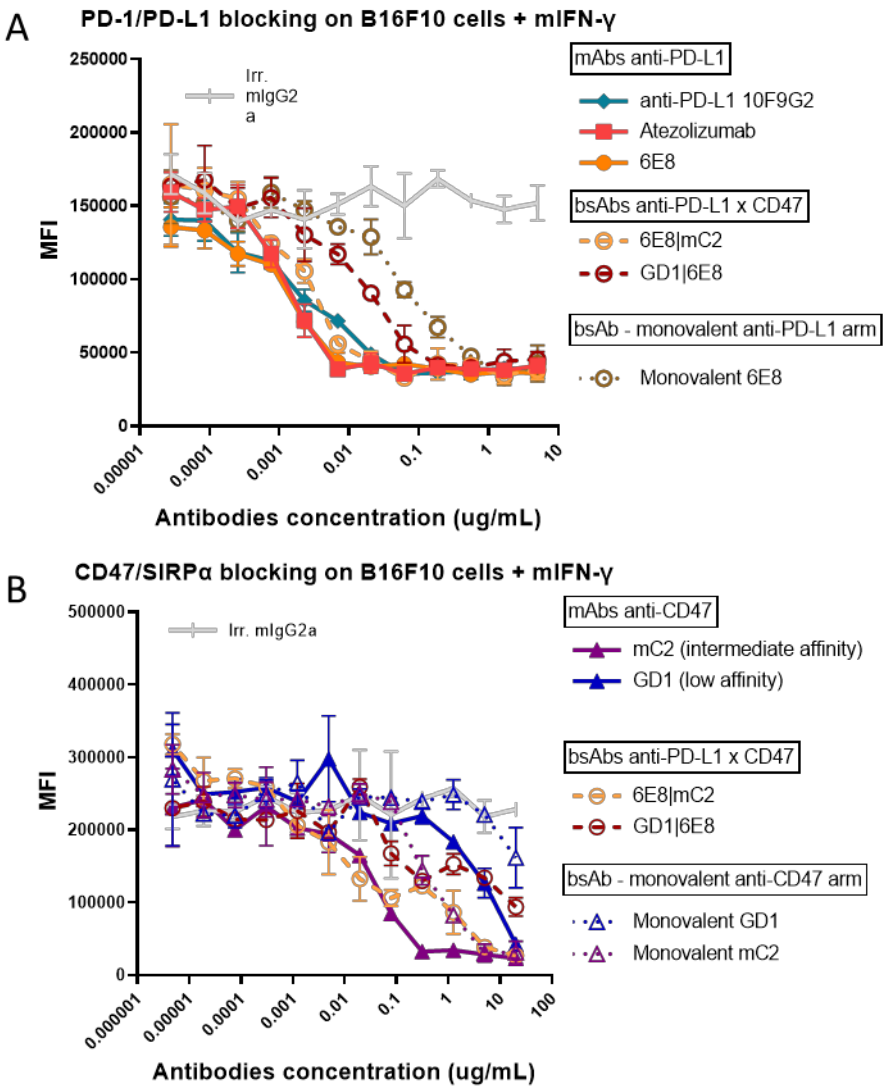

Figure 12: Blocking properties of the bsAbs evaluated in competitive binding assays. PD-L1 and CD47 blocking activity of the bsAbs was characterized using CellInsight CX5 High Content Screening Platform (A) Binding of fluorescently-labeled human PD-L1 high-affinity human Fc was measured in the presence of increased concentrations of bsABs on B16F10 cells activated with mIFN-γ. (B) Binding of fluorescently-labeled mouse SIRPα human Fc, was measured in presence of increased concentration of bsABs on B16F10 cells activated with mIFN-γ. Results are representative of three independent experiments and are plotted as MFI ± SD of two replicates.

3.1.8. Anti-tumor efficacy of 6E8 based bsAbs

Anti-tumoral efficacy of immune checkpoint inhibitors is usually evaluated in syngeneic mouse model. These models involve the engraftment of murine tumor cells into a mouse recipient from the same genetic background with a fully competent immune system, allowing to study the interaction between cancer and the anti-tumor immunity. To study the consequences of concomitant blockade of the innate

CD47/SIRPα and the adaptive PD-1/PD-L1 immune checkpoints on the generation of anti-tumor response, syngeneic mouse models needed to be used. Three different syngeneic models commonly used in *in vivo* preclinical studies were tried in the set-up phase (Table 4) [205], [330]–[333].

	Cell origin	Mouse strain	Characteristics
CT26	Colon carcinoma	BALB/c	Highly immunogenic [334]
4T1	Mammary carcinoma	BALB/c	Poorly immunogenic [334]
MC38	Colon carcinoma	C57BL/6	Highly immunogenic [335]

Table 3: Syngeneic models used in the set up experiment.

3.1.8.1. *Establishment of CT26 and 4T1 tumor models in Balb/c*

As CT26 and 4T1 have never been used before at Novimmune, some setup experiments were required in the first place. To test tumor growth in these two *in vivo* models, varying conditions of tumor inoculation were tried. Specifically, I evaluated different tumor cell loads, as well as two different engraftment sites (thorax and flank, Fig. 13A). CT26 and 4T1 tumor growths were more rapid when implanted in the thorax compared to the flank (Fig. 13B and C), possibly due to a different tissue environment and the degree of vascularization at the site of tumor implantation.

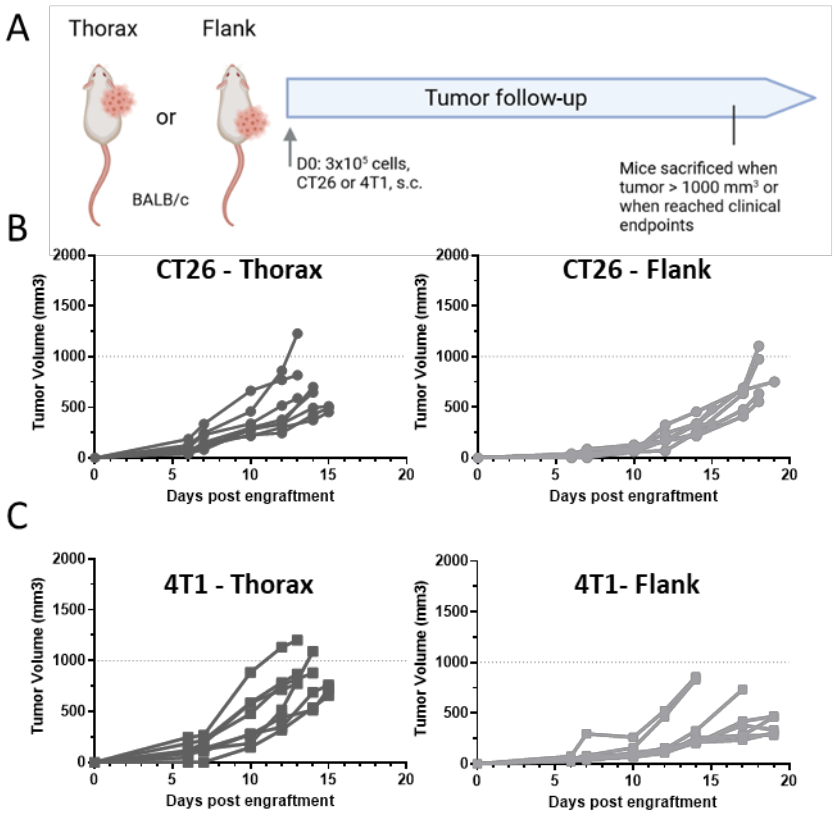

Figure 13: *In vivo* engraftment of CT26 and 4T1 tumor cells. (A) Schematic illustrating the experimental design: $3x10^5$ CT26 or 4T1 cells were injected subcutaneously (s.c.) into BALB/c female mice. Two engraftment sites, either in the thoracic or in the flank region, were evaluated. BALB/c mice (n = 8/group) were inoculated with (B) CT26 or (C) 4T1 cells, and tumor growth was measured at the indicated time points.

The growth kinetic was also influenced by the number of cells engrafted: on day 6, $1x10^6$ of CT26 cells engrafted in the thoracic region resulted in a mean tumor volume about 0,2 cm^3 while $3x10^5$ cells engrafted at the same site yielded smaller tumors, about 0,1 mm^3 (data not shown). For both CT26 and 4T1, high initial tumor cell number resulted in rapid growth and an early onset of tumor ulceration. To slow down tumor growth and to give more time for the immune response to develop, lower numbers of inoculated CT26 and 4T1 cells were tried. The resulting tumors grew more slowly, and, in the CT26 model, the ulceration was restricted to tumors that reached the endpoint volumes. In contrast, 4T1 tumors showed a strong tendency to develop ulcerations even at small volumes and with low number of implanted cells. Due to this limitation, the 4T1 model was not pursued any further. For the CT26 model, the dose of 5000 cells inoculated subcutaneously (s.c.) in the thoracic region resulted in an acceptable tumor growth kinetics and no ulcerations. In these conditions. the tumors started to be measurable between day 8 and 12 and reached a mean volume of about 150 mm^3 on day 14. To evaluate the efficacy

of anti-PD-L1 treatment, a benchmark anti-PD-L1 mAb previously tested in many checkpoint inhibitor preclinical studies (10F.9G2, [204], [327], [328], [336]) was administered intraperitoneally on the day of the recruitment and then a second time, 5 days after the first dose. According to the literature, the CT26 model should respond to the anti-PD-L1 treatment at least partially [331], [337]. Yet, in our hands, the benchmark anti-PD-L1 mAb 10F.9G2 showed no significant impact on tumor growth (Fig. 14).

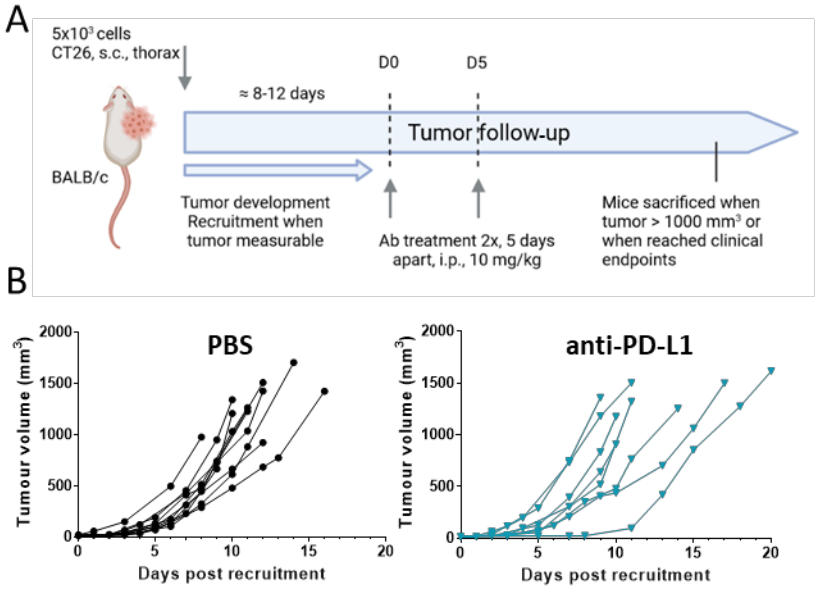

Figure 14: Impact of anti-PD-L1 mAb 10F.9G2 on CT26 tumor growth. (A) Schematic illustrating the experimental design: $5x10^3$ CT26 cells were injected subcutaneously (thorax) into BALB/c female mice (n = 8-10/group). When the tumors were measurable by caliper, mice were randomized into treatment groups and received i.p. 200 µg of anti-PD-L1 (10F.9G2) or PBS on the day of the recruitment and a second time, five days later. (B) Individual tumor growth curves of control and anti-PD-L1 treated groups are shown. Tumor volume was measured at the indicated time points.

3.1.8.2. *Establishment of a MC38 tumor model in C57BL/6 mice*

MC38 model is commonly used model in ICI studies. The literature describes the MC38 model as being generally responsive to anti-PD-L1 or PD-1 mAb treatment, but the therapeutic effect is usually heterogeneous and important variability in tumor growth rate and the effect of PD-1/PD-L1 blockade is also apparent when comparing various published studies [203], [209], [338]. It is well established that several parameters, such as mouse provider, the gut microbiota, or even other less appreciated factors such as housing temperature, could influence tumor growth rates as well as response to the treatment [339]–[341].

Consequently, in the setup phase, we performed several experiments to evaluate how the MC38 model would respond to anti-PD-L1 mAb in our laboratory. Parameters such as *in vitro* cell confluency

before engraftment, the amount of cells injected, as well as two mice providers were evaluated (data not shown). Details of the final experimental protocol, and the results of the final setup experiment are shown in Fig. 15. We demonstrated here some (limited and variable) therapeutic effect of the anti- PD-L1 benchmark mAb 10F.9G2. We also tested a commercially available anti-CD47 mAb MIAP301 known to block the CD47/SIRPα interaction and described by some as having anti-tumor efficacy *in vivo* [280], [342]. An experiment to evaluate the efficacy of a combination mAbs was performed conducted (Fig. 15A). In our hands, MIAP301 didn't show any intrinsic anti-tumor efficacy, either when tested alone, or in combination with the anti-PD-L1 mAb (Fig. 15).

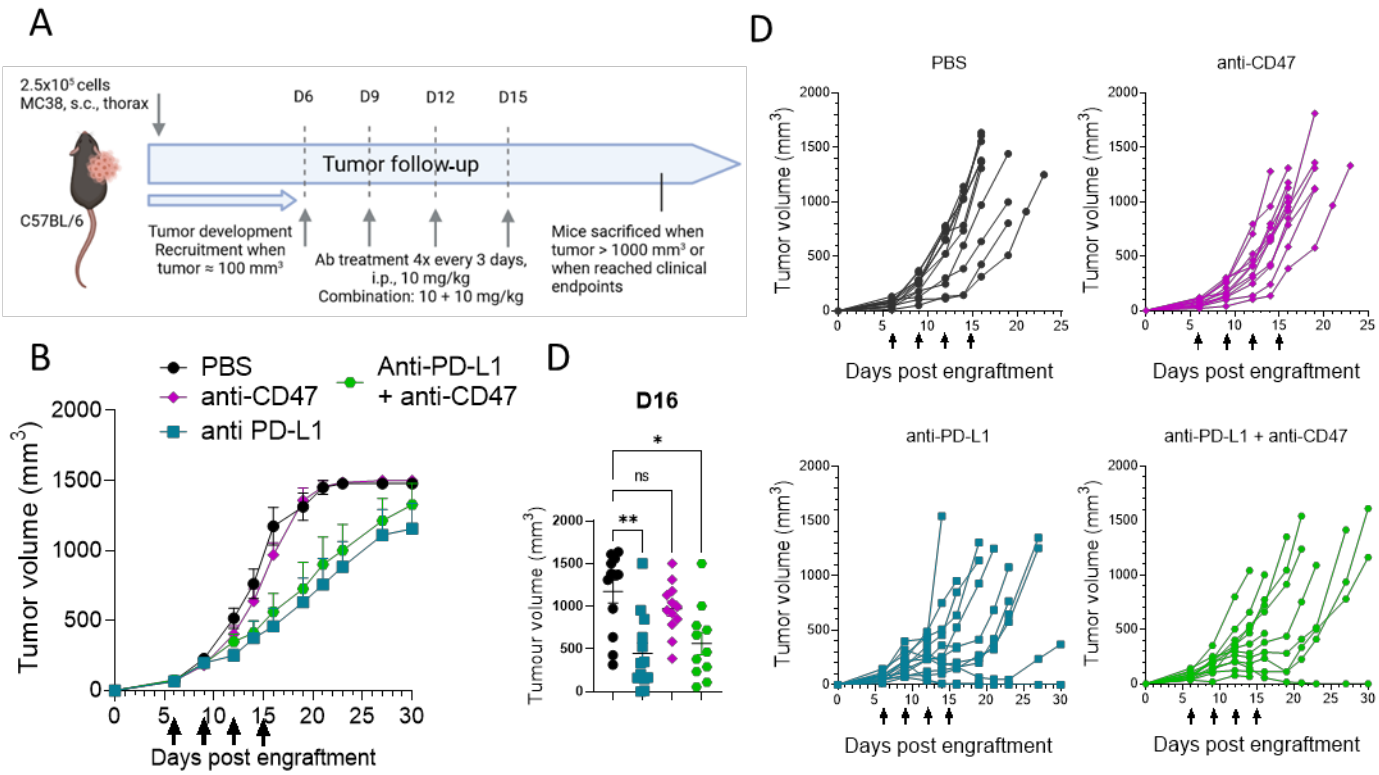

Figure 15: Anti-PD-L1 mAb inhibits MC38 tumor growth. (A) Schematic illustrating the experimental design: 2.5x10^5 MC38 cells were injected subcutaneously (thorax) into C57BL/6 female mice (n = 11-12/group). Mice were randomized into treatment groups on day 6 (mean tumor volume was around 80 mm^3) and were treated i.p. with 200 µg of anti-PD-L1 (10F.9G2), 200 µg of anti-CD47 (MIPA301), 200 µg of anti-PD-L1 + 200 µg of anti-CD47, or PBS on days 6, 9, 12, 15. (B) Tumor growth is shown as average tumor size per group ± SEM. Once a mouse reached the volume endpoint, the subsequent measurements were assigned the maximum value. (C) Individual tumor volumes on day 16 ± SEM (D) Individual tumor growth curves of control and treated groups. n.s., not significant, *P<0.05, **P<0.01 were obtained using the Brown-Forsythe and Welch ANOVA with Dunnett's method for multiple comparison correction.

3.1.8.3. *Anti-tumor efficacy of the bsAb in the MC38 model*

We then tested the two mIgG2a bsAbs, (6E8|mC2 and GD1|6E8) in the MC38 model. Mice with established tumors were treated either with one of the bsAbs or the anti-PD-L1 mAb 10F.9G2, and the tumor growth was monitored (Fig. 16). In the first experiment (Fig. 16A-C) the two bsAbs and the anti-PD-L1 mAb were able to delay tumor growth but the efficacy of the bsAbs was appreciably lower than the efficacy of the PD-L1 mAb (Fig. 16B and C). The two bsAbs showed a similar tumor growth inhibition, in spite of having CD47 arms of different affinity. In a second experiment (Fig. 16D-F), an increased dose of bsAbs was tested (20 mg/kg), but that did not lead to a better therapeutic effect compared to the anti-PD-L1 mAb (Fig. 16E and F).

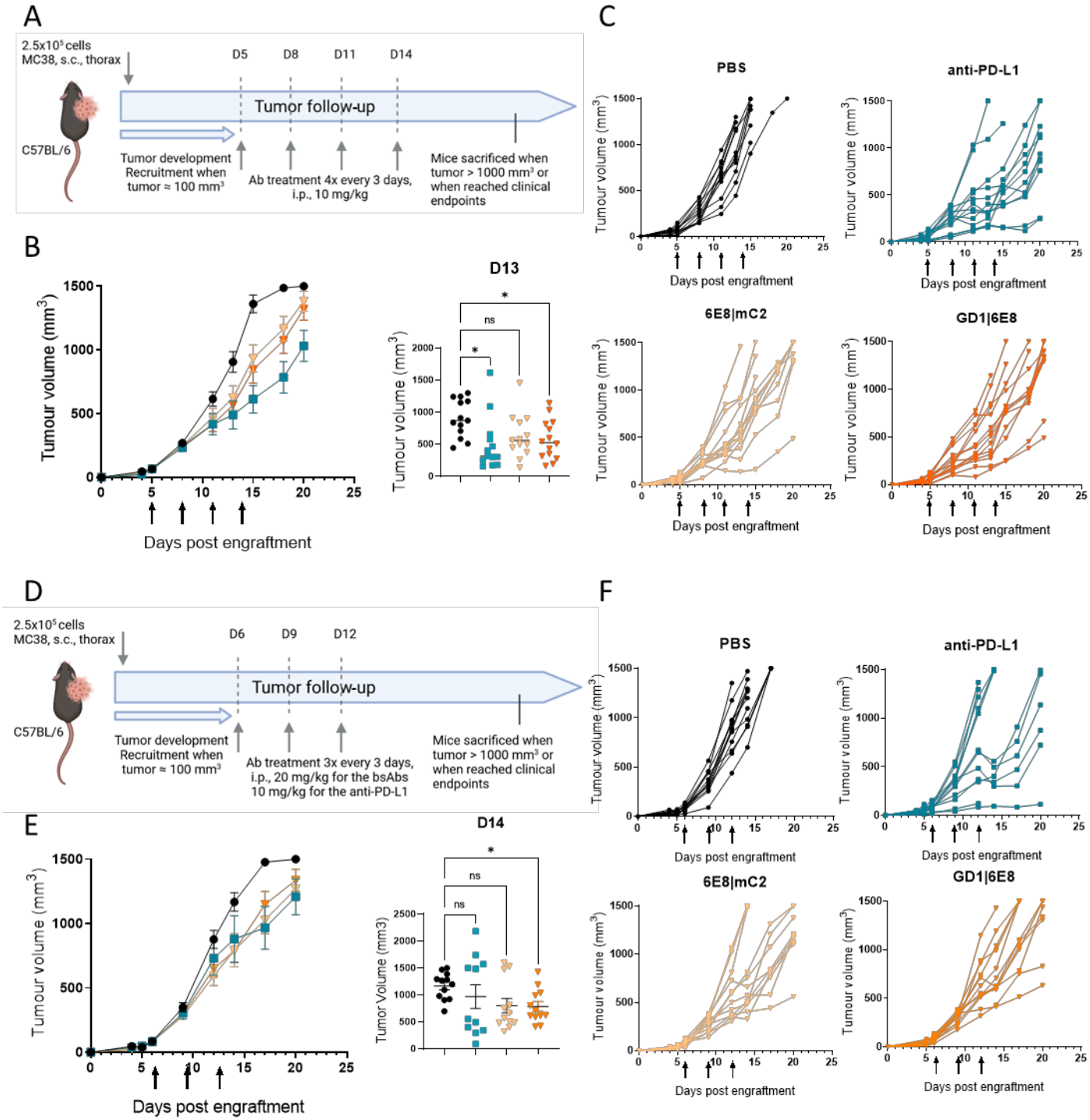
A
2.5x10⁵ cells
MC38, s.c., thorax
D5
D8
D11
D14
Tumor follow-up
C57BL/6
Tumor development
Recruitment when
tumor ≈ 100 mm³
Ab treatment 4x every 3 days,
i.p., 10 mg/kg
Mice sacrificed when
tumor > 1000 mm³ or
when reached clinical
endpoints
B
Tumour volume (mm³)
Days post engraftment
D13
Tumour volume (mm³)
ns
*
C
PBS
anti-PD-L1
6E8|mC2
GD1|6E8
Tumour volume (mm³)
Days post engraftment
D
2.5x10⁵ cells
MC38, s.c., thorax
D6
D9
D12
Tumor follow-up
C57BL/6
Tumor development
Recruitment when
tumor ≈ 100 mm³
Ab treatment 3x every 3 days,
i.p., 20 mg/kg for the bsAbs
10 mg/kg for the anti-PD-L1
Mice sacrificed when
tumor > 1000 mm³ or
when reached clinical
endpoints
E
Tumour volume (mm³)
Days post engraftment
D14
Tumor Volume (mm3)
ns
*
F
PBS
anti-PD-L1
6E8|mC2
GD1|6E8
Tumour volume (mm³)
Days post engraftment

Figure 16: Effect of two anti-PD-L1|CD47 bsAb on MC38 tumor growth. (A) Schematic illustrating the experimental design: $2.5x10^5$ MC38 cells were injected subcutaneously (thorax) into C57BL/6 female mice (n = 13-14/group). Mice were randomized into treatment groups (mean tumor volume around 70 mm^3) and were treated i.p. with 200 µg of anti-PD-L1 (10F.9G2 rat IgG2b), 200 µg of one of the bsAbs mIgG2a, or PBS on days 5, 8, 11, 14. (B) Tumor growth is shown as average tumor size per group ± SEM. Once a mouse reached the volume endpoint, the subsequent measurements were assigned the maximum value. The graph on the right represent the individual tumor volumes on day 13 ± SEM. (C) Individual tumor growth curves of the control and treated groups. (D) Schematic illustrating the experimental design: $2.5x10^5$ MC38 cells were injected subcutaneously (thorax) into C57BL/6 female mice (n = 12/group). Mice were randomized into treatment groups (mean tumor volume around 85 mm^3) and were treated i.p. with 200 µg of anti-PD-L1 (10F.9G2 rat IgG2b), 400 µg of one of the bsAbs (mIgG2a), or PBS on days 6, 9, 12. (E) Tumor growth is shown as average tumor size per group ± SEM. Once a mouse reached the volume endpoint, the subsequent measurements were assigned the maximum value. The graph on the right represent the individual tumor volumes on day 14 ± SEM. (F) Individual tumor growth curves of the control and treated groups. n.s., not significant, *P<0.05, **P<0.01 were obtained using the Brown-Forsythe and Welch ANOVA with Dunnett's method for multiple comparison correction.

3.1.8.4. *Anti-tumor efficacy of the 6E8 mAb in the MC38 model*

I wanted to check the anti-tumor efficacy of mAb 6E8 *in vivo*. In a dedicated MC38 experiment, mAb 6E8 was compared head-to-head with 10F.9G2, and it clearly failed to reach the same in anti-tumor efficacy as that benchmark mAb (Fig. 17). I speculated that the difference in affinity could potentially explain different anti-tumor activity of the two mAbs. The fact that mAb 6E8 is a mouse IgG2a but 10F.9G2 is a rat IgG2b may not explain the difference *in vivo*, since both IgG Fc isotypes interact with mouse FcγRs in a quite similar way (with similar A/I ratios, [336]). I therefore came to the conclusion that 6E8 might be not potent enough candidate for the generation of efficacious CD47|PD-L1 bsAbs.

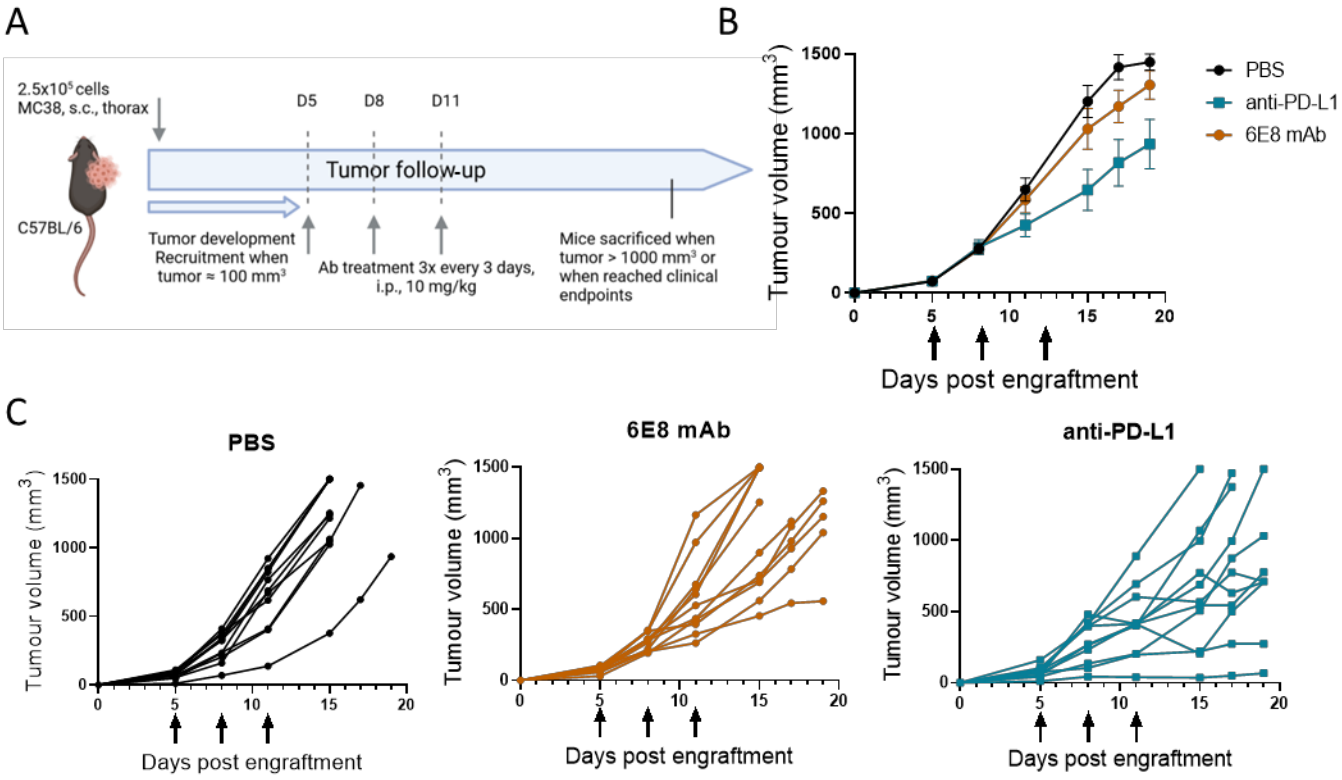

Figure 17: Comparison of *in vivo* efficacy of anti-PD-L1 mAbs. (A) Schematic illustrating the experimental design: 2.5x10^5 MC38 cells were injected subcutaneously (thorax) into C57BL/6 female mice (n = 11/group). Mice were randomized into treatment groups on day 5 (tumor mean volume around 75 mm^3) and were treated i.p. with 200 µg of anti-PD-L1 10F.9G2 (rat IgG2b), 200 µg anti-PD-L1 6E8 mIgG2a, or PBS on days 5, 8, 11 (arrows). (B) Tumor growth is shown as average tumor size per group ± SEM. Once a mouse reached the volume endpoint, the subsequent measurements were assigned the maximum value. (C) Individual tumor growth curves of the control and treated groups.

3.2. Generation and characterization of CD47|PD-L1 hIgG1 bispecific antibodies

3.2.1. Proof of concept bsAb with the atezolizumab PD-L1 arm

Co-targeting PD-L1 and CD47 with bispecific antibodies and Fc-receptor fusions has recently been reported by four different groups and shown to block tumor growth more efficiently than anti-PD-L1 mAbs or even PD-L1 + CD47 mAbs combinations [308], [320], [321], [324]. Two of these publications used a bispecific construct based on atezolizumab [320], [321]. In the *in vitro* experiments shown in Fig. 9, anti-PD-L1 mAb 6E8 showed similar affinity (Fig. 10) and similar PD-1/PD-L1 blocking compared to benchmark anti-PD-L1 antibodies (see Fig. 9A), but lower binding to cells than atezolizumab, especially with non-activated MC38 cells expressing very low levels of PD-L1 (see Fig. 9G). In an attempt to achieve *in vivo* efficacy, I have generated and tested a proof of concept (POC) bsAb containing an atezolizumab-based PD-L1 arm associated to the moderate-affinity anti-CD47 arm 1E5 (comparable to mC2 in terms of affinity and CD47-blocking, see Fig. 2). This bsAb was produced with the knob-into-hole technology [343] as hIgG1.(hIgG1 Fc displays full effector functions in the context of mouse Fc receptors, comparable to mIgG2a and hIgG1 Fc-bearing constructs are often used in translational experiments).

3.2.1.1. *In vitro characterization of the POC molecule*

The binding and blocking properties of the POC molecule (named 1E5|atezolizumab) were evaluated with B16F10 mouse cell line. Binding to B16F10 cells was significantly increased upon IFN-γ-mediated induction of PD-L1 cell surface expression (B16F10+ cells, Fig. 18A). Similar to what was observed previously with the two IgG2a bsAbs (see Fig. 12) 1E5|atezolizumab blocked CD47/SIRPα interaction in a biphasic manner, with PD-L1 coengagement-mediated high potency blockade at lower antibody concentrations, and a less potent blockade at higher antibody concentrations, mediated by the monovalent binding of the 1E5 arm to cell surface CD47 (Fig. 18B). Last but not least, 1E5|atezolizumab showed a similar PD-1/PD-L1 blocking efficacy as the 6E8|mC2 bsAb and PD-L1 mAbs 10F.9G2 and atezolizumab (Fig. 18C).

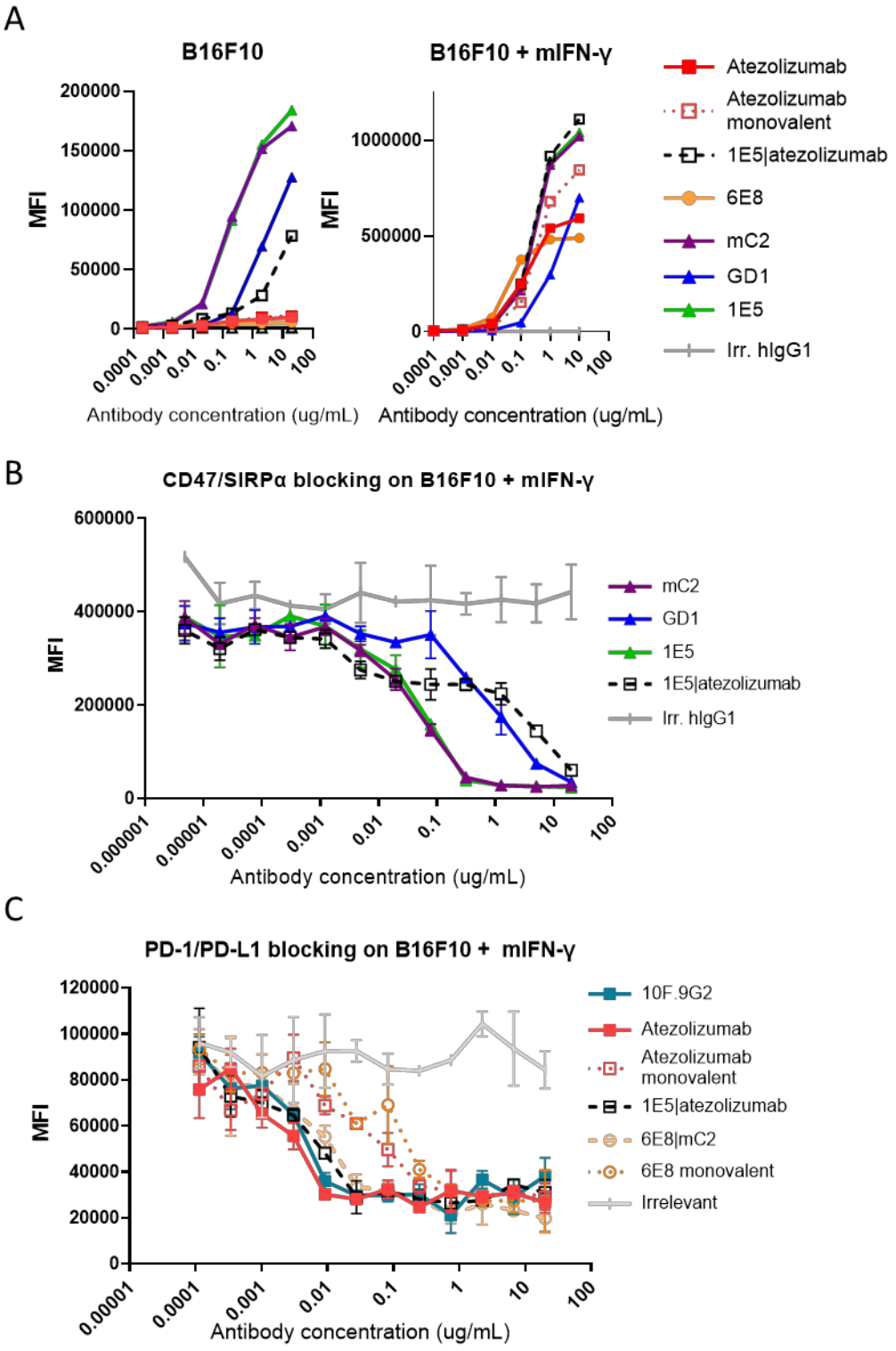

Figure 18: Characterization of the bsAb 1E5|Atezolizumab hIgG1 (A) Binding, reported as mean fluorescence intensity values, was evaluated by flow cytometry on B16F10 cells activated (right graph) or not (left graph) with mIFN-γ and compared to anti-PD-L1 mAbs, 6E8 and atezolizumab and to anti-CD47 mAbs 1E5 and GD1. Results shown are representative of three independent experiments. (B and C) Blocking property of the POC molecule was evaluated in competitive binding assays on B16F10 cells

activated with m-IFN-γ using CellInsight CX5 High Content Screening Platform. (B, C) Binding of fluorescently-labeled mouse SIRPα mouse Fc (B) or human PD-1 high affinity mouse Fc (C) was measured in the presence of increased concentration of antibody. Results shown are representative of two independent experiments and are plotted as MFI ± SD of two replicates.

3.2.1.2. *In vivo characterization of the POC molecule*

The POC bsAb was then evaluated for its ability to inhibit tumor growth in the MC38 tumor model. Mice with established MC38 tumors were treated i.p. either with 1E5|atezolizumab or with the benchmark mAb 10F.9G2 (Fig. 19A). In this experiment, the tumor growth inhibition induced by 10F.9G2 was heterogeneous but overall marginal (not statistically significant) and the POC bsAb was not more efficacious (Fig. 19B, C).

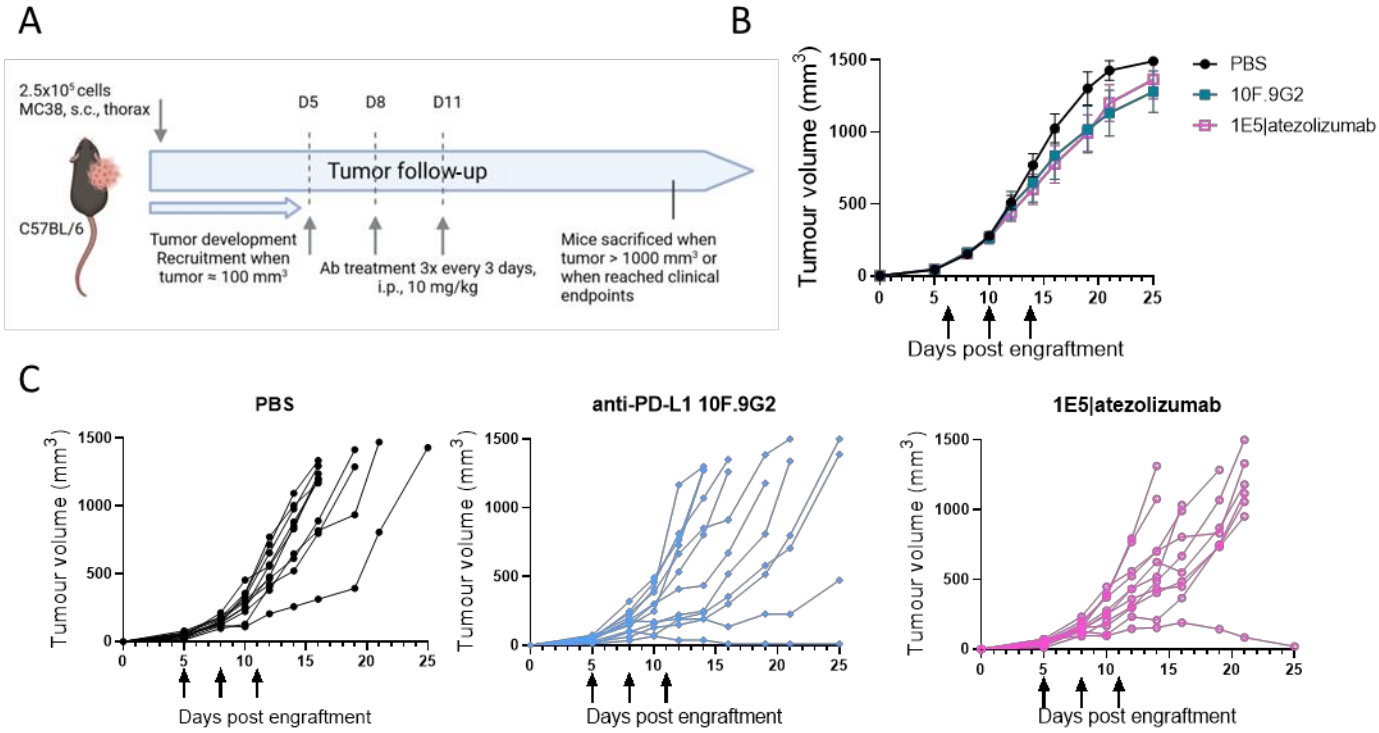

Figure 19: *In vivo* efficacy of 1E5|atezolizumab bsAb (A) Schematic illustrating the experimental design: 2.5x10^5 MC38 cells were injected subcutaneously (thorax) into C57BL/6 female mice (n = 11/group). Mice were randomized into treatment groups on day 5 (mean tumor volume around 50 mm^3) and were treated i.p. with 200 µg of 1E5|atezolizumab (hIgG1), 200 µg of 10F.9G2 (rat IgG2b) or PBS on days 5, 8, and 11. (B) Tumor growth is shown as average tumor size per group ± SEM. Once a mouse reached the volume endpoint, the following measurements were assigned a maximal value. (C) Individual tumor growth curves of control and treated group. Tumor volume was measured at the indicated time points.

3.2.2. Generation of VS9, a new anti-PD-L1 arm

I supposed that a bsAb with an anti-PD-L1 arm of higher affinity than 6E8 or atezolizumab could eventually show superior efficacy *in vivo*. I therefore set out to generate a series of new bsAbs (κλ bodies) based on the recently obtained high-affinity anti-PD-L1 sequence VS9.

3.2.2.1. *Characteristics of the VS9 PD-L1 arm*

To measure the affinity and binding kinetic of the VS9 mAb upon monovalent binding to mouse PD-L1 recombinant protein, bio-layer interferometry (Octet, Forte Bio) was performed. While atezolizumab and 6E8 showed a similar equilibrium dissociation constant (K_D), the VS9 arm was found to be about fifty times more affine (Fig. 20A). Compared to atezolizumab, VS9 showed a much slower dissociation rate (Fig. 20B). Competitive binding assays between the anti-PD-L1 mAbs performed by ELISA showed that the VS9 arm was competing with 6E8 10F.9G2, atezolizumab as well as the MIH5 clone mAb commonly used in FACS experiments for the binding of mouse PD-L1, (data not shown). These results suggest that all these antibodies target the same region on mouse PD-L1.

A

Anti-PD-L1 arm	Affinity for mPD-L1 (K_D, nM)
Atezolizumab	31 ± 4
6E8	27 ± 3
VS9	0.53 ± 0.02

B

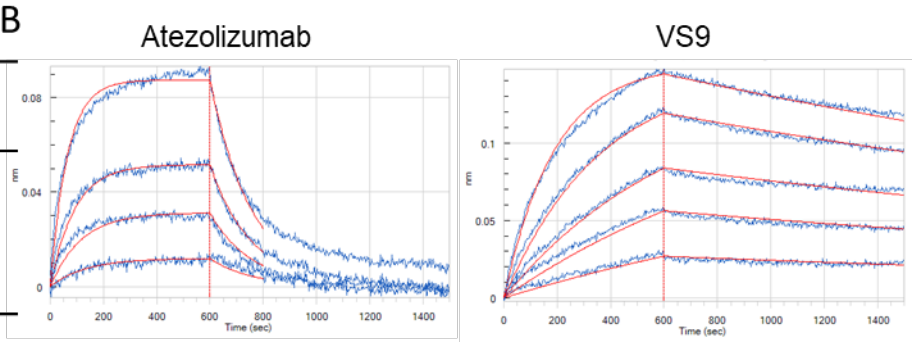

Figure 20: Affinity of anti-mPD-L1 antibodies. (A) Affinity was measured using bio-layer interferometry (Octet, Forte Bio) and is shown as the average K_D ± SD. Results are representative of two independent experiments. (B) Association and dissociation of atezolizumab and VS9 to recombinant mouse PD-L1 protein.

To generated bsAbs, the VS9 anti-PD-L1 arm (λ) was associated with the intermediate affinity anti-CD47 arm 1E5 (κ). Two versions of that bsAb were generated, one with a wild type hIgG1 Fc portion, the other with silenced hIgG1 Fc. Two mutations have been combined to ensure an efficient silencing of the Fc part. The well-known LALA mutation [344], [345] was combined with P329A mutation to fully abrogate Fc mediated effector functions [151], [346]. Antibodies carrying the LALA PA mutation devoid of Fc-mediated effector functions are denoted by an /N at the end of the antibody name. For the sake of this study, an additional bsAb bearing the low affinity anti-CD47 arm GD1 (κ) has been generated (Table 4).

κλ body name	κ arm	κ specificity	Affinity	λ arm	λ specificity	Affinity	Heavy Chain
1E5|VS9	1E5	anti-mCD47	intermediate	VS9	anti-mPD-L1	high	hIgG1
1E5|VS9	1E5	anti-mCD47	intermediate	VS9	anti-mPD-L1	high	hIgG1 LALA PA
GD1|VS9	GD1	anti-mCD47	low	VS9	anti-mPD-L1	high	hIgG1

Table 4: Summary of the bsAbs constructs generated with the VS9 arm.

3.2.3. *In vitro* characterization of the VS9-based bsAbs

3.2.3.1. *Binding of bsAbs to double positive cells*

Binding of the bsAbs to B16F10 and MC38 cells was evaluated by flow cytometry and compared to anti-PD-L1 mAbs (Fig. 21A to C), the CD47 mAb 1E5 and the corresponding monovalent controls (Fig. 21D and E). B16F10 cells activated with mIFN-γ display about 86,000 PD-L1 and 130,000 CD47 molecules while activated MC38 cells display 42,000 PD-L1 for 104,000 CD47 molecules at the cell surface (see Table 1). On both cell types, the bsAbs showed a similar binding profile to atezolizumab and VS9, and increased binding compared to the 6E8 mAb (Fig. 21A and B). On non-activated MC38 cells (10,000 PD-L1 and 78,000 CD47), the difference between the binding of the bsAb and the mAb was more apparent (Fig. 21C).

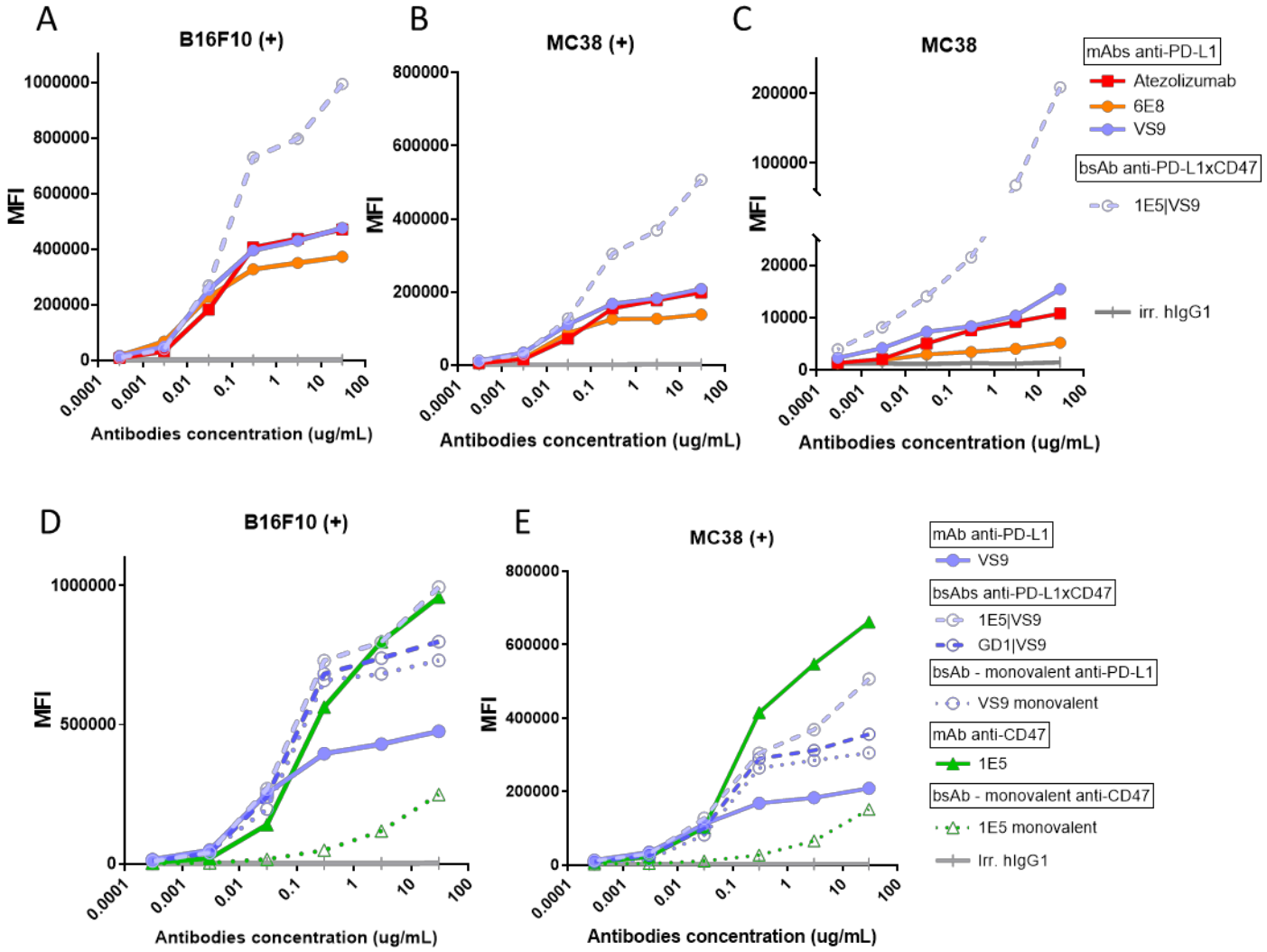

Figure 21: Characterization of the bsAbs generated with the anti-PD-L1 arm VS9. Binding shown as mean fluorescence intensity values, was evaluated by flow cytometry on (A and D) B16F10 activated with mIFN-γ, on (B and E) MC38 cells activated with mIFN-γ and on (C) MC38 cells not activated. Anti-PD-L1 mAbs and the corresponding monovalent bsAbs were run for comparison. Results shown are representative of multiple independent experiments.

3.2.3.2. *Importance of the individual bsAb arms for binding to cells*

To further assess the contribution of individual arms of 1E5|VS9 bsAb to cell binding, CD47 and PD-L1 knockout (KO) cells lines were compared to their double positive (unmodified) counterparts. Both wild type and KO cell lines were activated with mIFN-γ. On wild type HEPA 1.6 cells (80,000 PD-L1 and 130,000 CD47), the presence of CD47 only slightly increased the binding of 1E5|VS9 compared to the CD47-KO cells or the monovalent VS9 antibody (Fig. 22A). The key importance of the anti-PD-L1 arm for cell binding was further highlighted in experiments with PD-L1 KO A20 cells. In the absence of PD-L1 expression, binding of the bsAb was strongly reduced compared to wild type A20 cells (23,000 PD-L1 and

35,000 CD47) (Fig. 22B). Together, these results confirmed that the high affinity anti-PD-L1 arm is the main driver for binding to double positive cells.

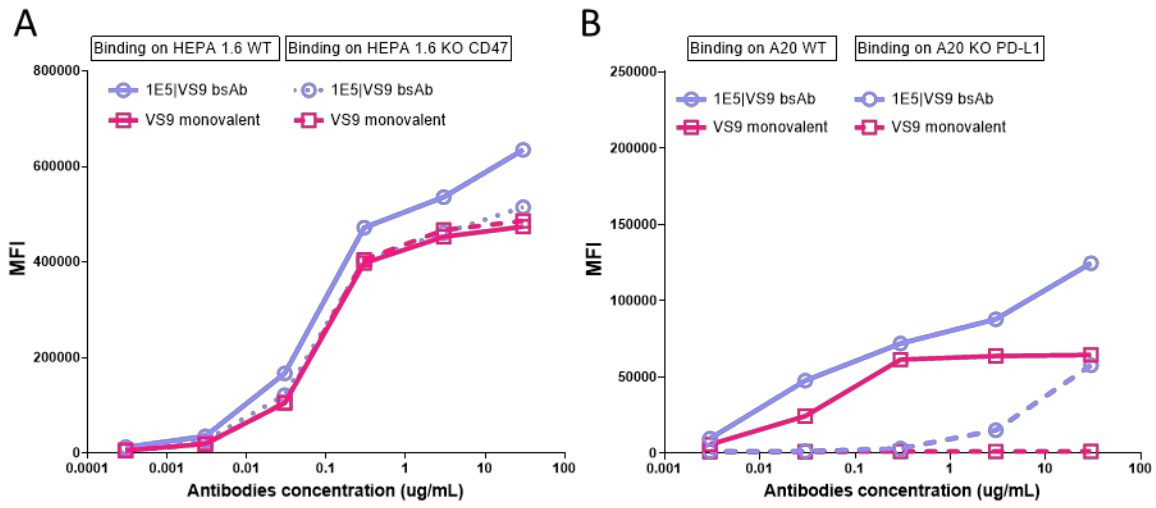

Figure 22: Contribution of individual bsab arms to binding. 1E5|VS9 binding to (A) CD47 KO vs unmodified HEPA 1.6 cells and (B) PD-L1 KO vs unmodified A20 cells VS9 monovalent bsAb was run for comparison. Both KO and WT were active with mIFN-γ. Results are representative of two independent experiments.

3.2.3.3. *Blockade of the PD-L1 / PD-L1 and CD47/SIRPα interactions*

To evaluate the blocking potency of the VS9-based bsAbs, competitive binding assays were performed on B16F10 cells activated with mIFN-γ (Fig. 23). At low concentration, both GD1|VS9 and 1E5|VS9 potently blocked CD47, with a similar efficacy irrespectively of their different affinities to CD47. This is consistent with the idea that CD47 blockade is mainly driven by PD-L1 co-engagement in conditions of low saturation of the target. At higher concentrations, CD47 blockade with GD1|VS9 was less efficacious than with 1E5|VS9 reflecting the monovalent binding of their anti-CD47 arms, in conditions where all the PD-L1 at the cell surface is already saturated.

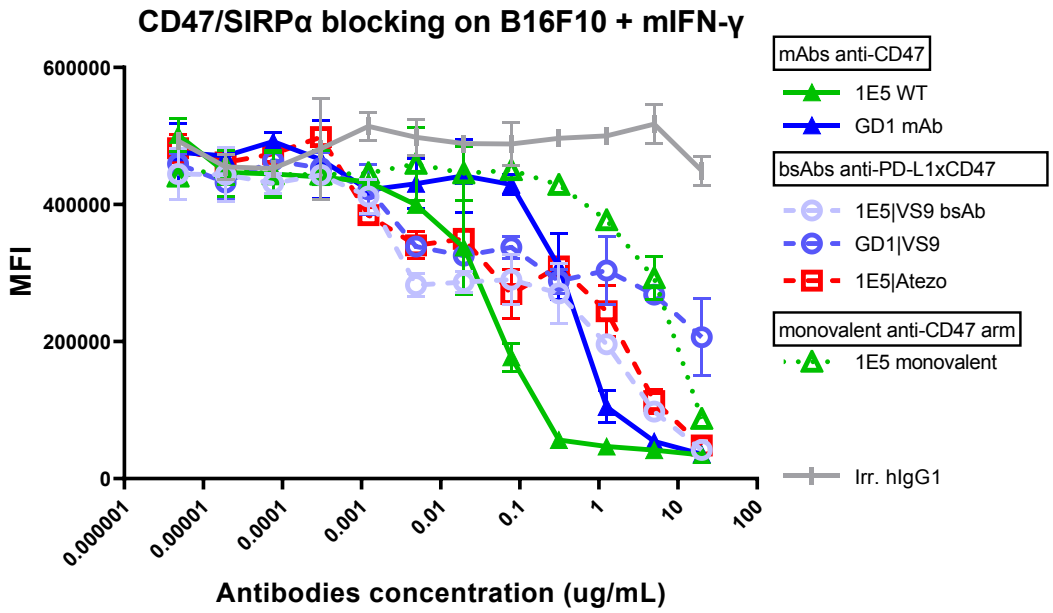

Figure 23: CD47/SIRPα blocking with VS9-based bsAbs. Binding of fluorescently-labeled mouse SIRPα-Fc was measured in the presence of increased concentration of antibodies on B16F10 cells activated with mIFN-γ. Blocking activity of the bsAbs was compared to mAbs and the 1E5 monovalent bsAb. Results shown are representative three independent experiments and are plotted as MFI ± SD of two replicates.

The three classes of bsAbs used in this study, incorporating three different PD-L1 arms, respectively, 6E8, atezolizumab, and VS9, could not be compared head-to-head in a direct binding assay (like FACS) due to different Fc portions implicating different detection reagents (secondary antibodies). In contrast, the PD-1/PD-L1 blocking assay is a competitive binding assay that detects recombinant PD-1-Fc bound to cells, allowing for a head-to-head comparison of PD-1/PD-L1 blockers, irrespectively of their format and molecular structure. 6E8, atezolizumab, and VS9 bsAbs and the corresponding mAbs and monovalent controls were therefore run in parallel in a PD-1/PD-L1 blocking assay with B16F10(+) cells.

Interestingly, the three bsAbs with intermediate affinity CD47 arms 6E8|mC2, 1E5|atezolizumab, and 1E5|VS9 showed indistinguishable blocking potency with B16F10(+) cells (expressing roughly 90,000 and 130,000 PD-L1 and CD47), while a slight but noticeable difference between 1E5|VS9 and GD1|VS9 was apparent, pointing to the contribution of the CD47 arm to PD-L1 blockade upon (Fig. 24A). The importance of CD47 coengagement for PD-L1 blockade is also supported by the comparison between the different bsAbs and their PD-L1 monovalent counterparts (Fig. 24B-D). As anticipated, the contribution of CD47 co-engagement to PD-L1 blockade was inversely proportional to the affinity of the anti-PD-L1 arm

(e.g., compare panels B and D, bsAb vs. monovalent). Finally, the comparison between the monovalent bsAbs and the mAbs confirms the well-appreciated importance of avidity for mAb binding (Fig. 24B-D).

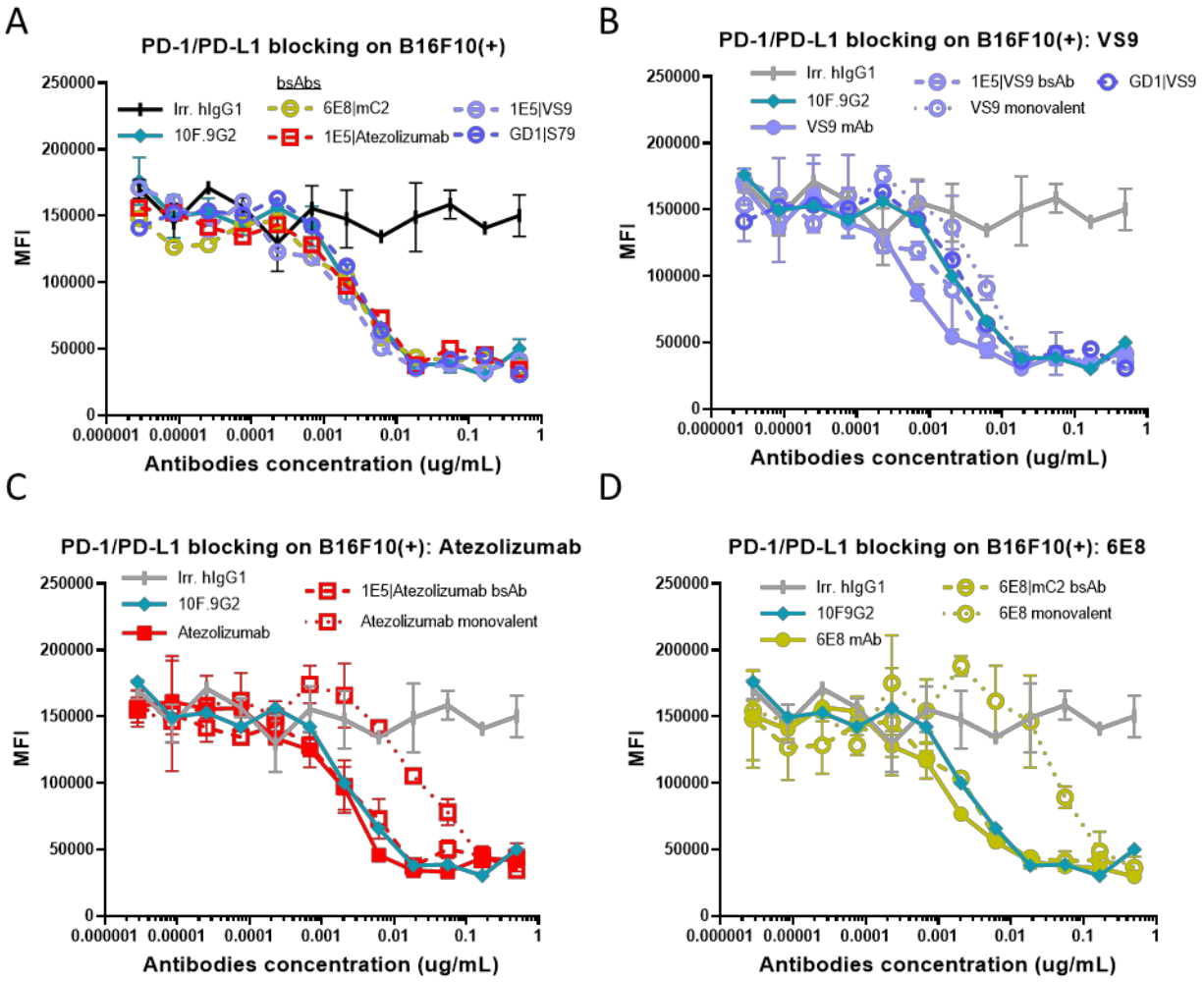

Figure 24: PD-1/PD-L1 blocking properties of the bsAbs used in this study. (A) Binding of fluorescently-labeled human PD-1 high affinity mouse Fc to B16F10+ cells in the presence of increased concentration of various competitor antibodies. (B-D) Results obtained with the three different classes of bsAbs used in this study (VS9, atezolizumab and 6E8 – based) are shown on separate plots for a better legibility. Results representative of teo independent experiments are plotted as MFI ± SD of two replicates.

3.2.4. Anti-tumor efficacy of the VS9 based bsAbs

Since the efficacy of the bsAbs in the MC38 model was not as could be expected based on published studies using the same tumor cell lines and a similar therapeutic approach ([320], [321]), we re-evaluated the experimental conditions of our MC38 model, with a particular focus on tumor implantation site and techniques. The efficacy of immune checkpoint blockade in preclinical models is notoriously variable, often leading to conflicting conclusions from experiments run at different labs. Replicability and

consistency remain a major challenge when working with syngeneic mouse models [339], [340]. We have evidenced here that the position of engraftment and the conditions of *in vitro* culture of cancer cells before engraftment could result in different tumor growth kinetics and could influence the treatment efficacy. In the process, we have learned about the importance of tumor engraftment techniques. Each anatomical site possesses unique immune composition as well different lymphatic and blood vessel structure. However, available literature provides little information about how the tumor growth kinetics and the response to treatment are affected by the depth of the engraftment. The rare studies comparing subcutaneous engraftments at different depths showed the importance of tumor site implantation for tumor growth kinetic as well as for the immunogenicity of the tumors in syngeneic models, thus, consequently, the antitumor responses [347]–[349].

3.2.4.1. *Comparison of the bsAbs efficacy in two different engraftment protocols in the MC38 model*

In collaboration with S. Hugues lab at the CMU, different subcutaneous engraftment techniques as well as different *in vitro* culture protocols were evaluated. Following a new protocol, cells were engrafted in lower back and closer to the skin surface. This engraftment technique was designed as subcutaneous "high" (s.c. "high") in contrast to the engraftment performed previously which was deeper, and thus described as s.c. "deep". We then evaluated the impact of different engraftment protocols on the efficacy of two 1E5|VS9 bsAb versions (active or inactive Fc portion) in the MC38 model. The two protocols of cells engraftment described above were conducted in parallel. The protocol s.c. "deep" resulted in a bigger tumor volume at the endpoint and a comparatively quicker tumor growth. Mice engrafted following the s.c. "deep" protocol were euthanized between day 14 and day 16. On the other hand, the s.c "high" protocol showed a slower tumor growth and a lower maximum volume at the endpoints (Fig. 25B, C). The efficacy of the two bsAbs tested was comparable but depended strongly on the tumor implantation technique. With the s.c. "deep" protocol and fast-growing tumors no therapeutic effect was apparent, while the s.c. "high" protocol resulted in significantly slower growth of tumors, which became even slower following treatment with the bsAbs (Fig. 25B-E). We therefore considered the s.c. "high" protocol as more suitable for future *in vivo* experiments. That said, there was an important tradeoff associated to the s.c "high" protocol: In the s.c. "high" group, as some mice had to be euthanized earlier due to tumor ulceration occurring even at small tumor volumes (ulceration was not observed at all with the s.c. "deep" protocol). Together, the head-to head comparison of the two protocols showed that the position chosen for the MC38 tumor implantation, as well as the injection method, resulted in important differences in tumor growth rate and therapeutic antibody efficacy.

It is well established that the efficacy of antibody treatment depends on the effects mediated through the binding to targets via the variable domains as well as the nature of the Fc part [336]. On the other hand, both the antigen binding part and the Fc part affect antibody pharmacokinetics [350]. We therefore wanted to evaluate the impact of the Fc part on the persistence of the bsAbs in blood. Antibody levels in the plasma were measured by ELISA at 4 different time points (Fig. 25F and G). A later timepoint, on day 26, could be assessed for some mice in the s.c. “high” protocol that responded to antibody treatment, but not for the control group (Fig. 25G). bsAbs blood levels were significantly lower than in the hIgG1 control group, and the concentration of the active Fc bsAb was lower than with the inactive Fc bsAb. For both bsAbs, a rapid drop in concentration was observed 5 days after the last dose, and the active Fc bsAb was under the lower limit of detection. This poor antibody pharmacokinetics probably reflects target-mediated drug disposition (TMDD) mediated principally by the CD47-binding part of the bsAb, and, potentially, anti-drug antibody (ADA) responses directed towards the human sequences contained in the bsAb Fab portions. The disappearance of the bsAbs from the circulation correlated with tumor regrowth in responder animals, suggesting that the loss of tumor control could be due to insufficient antibody exposure.

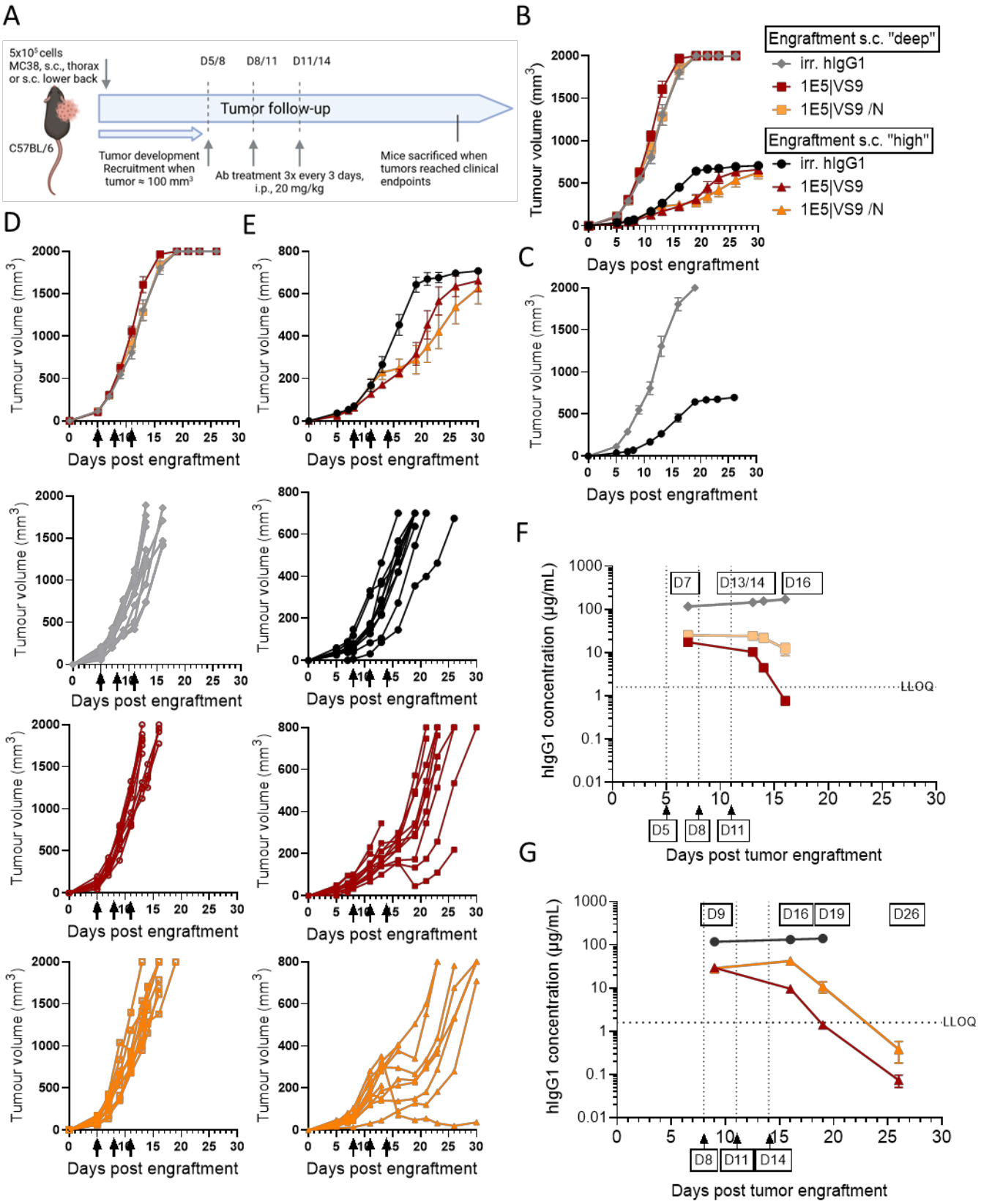
A
5x10⁵ cells
MC38, s.c., thorax
or s.c. lower back
C57BL/6
D5/8
D8/11
D11/14
Tumor follow-up
Tumor development
Recruitment when
tumor ≈ 100 mm³
Ab treatment 3x every 3 days,
i.p., 20 mg/kg
Mice sacrificed when
tumors reached clinical
endpoints
B
Engraftment s.c. "deep"
irr. hIgG1
1E5|VS9
1E5|VS9 /N
Engraftment s.c. "high"
irr. hIgG1
1E5|VS9
1E5|VS9 /N
Tumour volume (mm³)
Days post engraftment
C
Tumour volume (mm³)
Days post engraftment
D
E
Tumour volume (mm³)
Days post engraftment
F
hIgG1 concentration (µg/mL)
D7
D13/14
D16
LLOQ
D5
D8
D11
Days post tumor engraftment
G
hIgG1 concentration (µg/mL)
D9
D16
D19
D26
LLOQ
D8
D11
D14
Days post tumor engraftment

Figure 25: Comparison of two tumor engraftment protocols in the MC38 model. (A) Schematic illustrating the experimental design: $5x10^5$ MC38 cells were injected either in the thorax (s.c "deep") or above the hind leg (s.c. "high") into C57BL/6 female mice (n = 10-11 mice/group). Mice were randomized into treatment groups on day 5 (mean tumor volume around 100 mm3) or on day 8 (mean tumor volume around 60 mm3) depending on the engraftment protocol chosen and were treated i.p. 3 times every 3 days with either 400 µg of the bsAb with active Fc (1E5|VS9), 400 µg of bsAb with the inactive Fc (1E5|VS9 /N) or 400 µg of an irrelevant hIgG1 control antibody on days 5, 8, and 11. (B) Tumor growth is shown as average tumor size per group ± SEM. Once a mouse reached the volume endpoint, the following measurements were assigned a maximal value. (C) Individual tumor growth curves of control groups. (D-E) Tumor growth as average tumor size per group ± SEM and individual curves for mice engrafted with (D) the s.c. "deep" protocol and with (E) the s.c. "high" protocol. Tumor volume was measured at the indicated time points. (F-G) Mean serum concentrations (n = 4-6) ± SEM of bsAbs or irr. hIgG1 were determined using the FastELISA system (RD-Biotech) (F) on day 7, day 13 or 14 and day 16 for mice engrafted with the s.c "deep" technique and (G) on day 9, day 16, day 19 and day 26 for mice engrafted with the s.c "high" technique and treated as depicted in (A).

We also wanted to evaluate the effects of the bsAb on blood cells, especially on RBCs and platelets. To investigate the effect of the bsAbs on blood parameters, blood samples were analyzed at different timepoints (Fig. 26). Mice treated with the active Fc bsAb showed a decrease in red blood cell (RBC) count, in hemoglobin (HGB), in hematocrit (HCT) and in the platelet count (PLT) two day after the last dose. This decrease was correlated with an increase in reticulocytes (RET) count, which was even more pronounced five days after the last dose. On the other hand, the inactive Fc bsAb showed no impact on blood parameters (RBC, HGB, HCT, PLT) except for an increase in the reticulocyte count. These results showed that binding of CD47 on blood cells had a major effect with bsAb endowed with an Fc which is immunologically active. Otherwise, the administration of both bsAbs was well tolerated since no clinical signs were apparent and no body weight loss was observed during the course of the treatment (data not shown).

.

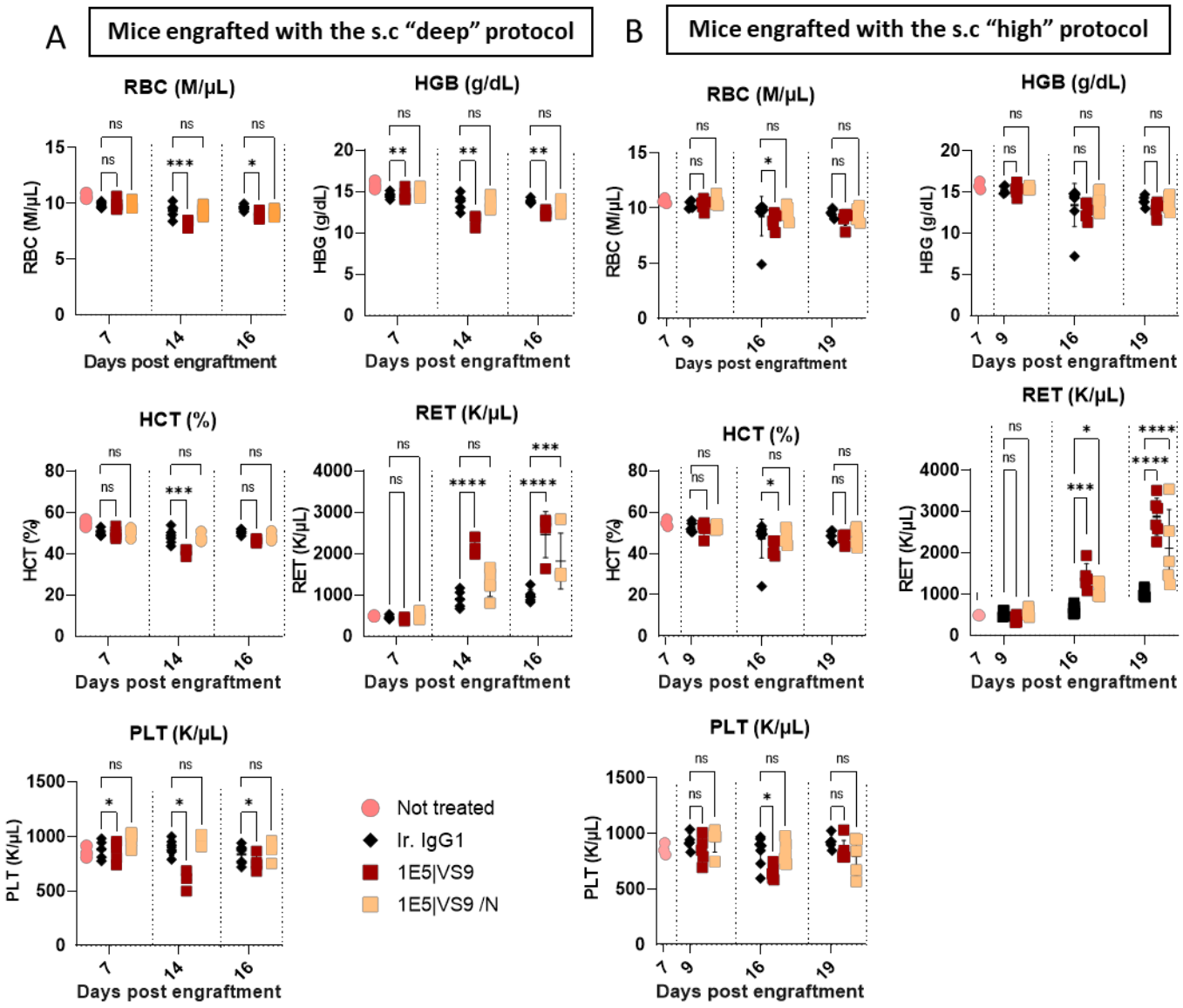

Figure 26: Blood analysis following treatment with bsAbs. Blood was collected at the indicated time points and samples were run on ProCyte Dx Haematology Analyser. Red blood cell (RBC), hemoglobin (HGB), hematocrit (HCT), reticulocytes (RET), platelets, were measured. (n=4-8 mice per group). n.s., not significant, *P<0.05, **P<0.01, ***P<0.001, ****P<0.0001 were obtained using the Kruskal-Wallis ANOVA with Dunn's method multiple comparisons correction. Values are displayed as mean ± SD.

3.2.4.2. *MC38 tumor microenvironment analysis following treatment with bsAbs.*

Anti-tumor efficacy of anti-PD-L1 is linked to the modulation of immune response within the tumors and tumor draining lymph nodes [211]. To evaluate the impact of the CD47|PD-L1 bsAbs on immune subsets within the tumor microenvironment, MC38-bearing mice were treated antibody and the tumors and tumor draining lymph nodes (TdLN) were harvested on day 16. Tumors that ulcerated were

excluded from TME characterization (on day 15, 2 mice per group except for 1E5|VS9 /N where no mice were excluded). The bsAbs and the anti-PD-L1 treatments induced a delay in tumor progression that reached statistical significance in the group treated with the anti-PD-L1 and with the Fc inactive bsAb (Fig. 27B). All the tumors showed high immune cell infiltration, which represented about 50% of the living cells after tumor dissociation (Fig. 27D). This infiltration was significantly increased in the tumors following treatment with anti-PD-L1 mAb and inactive Fc bsAb, where about 65% of the living cells in the tumor were CD45+ cells (Fig. 27E).

Common lineage-defining markers were used to identify the main leukocyte populations (gating strategies are shown in Fig. S1), which revealed that the increase in CD45+ among living cells in all treated groups was mainly due to a higher proportion of infiltrating macrophages and T cells (Fig. 27E and Fig. S2). An increase in natural killer cells (NK) was observed mostly in the group treated with the anti-PD-L1 mAb (Fig. S2). A decrease in dendritic cells (DCs) was observed in all treated groups but was more marked in the two bsAb groups. A decrease in monocytes was also observed in the bsAb groups (Fig. S2). No significant changes were observed at the TdLNs level, except for a negligeable decrease in T cells observed in the group treated with the active Fc bsAb (Fig. S3). The number of neutrophils and B cells in the tumors was generally low and no significant changes were observed in this population while in the TdLN, only the B cells proportion showed a slight tendency to increase in the treatment groups (Fig. S4).

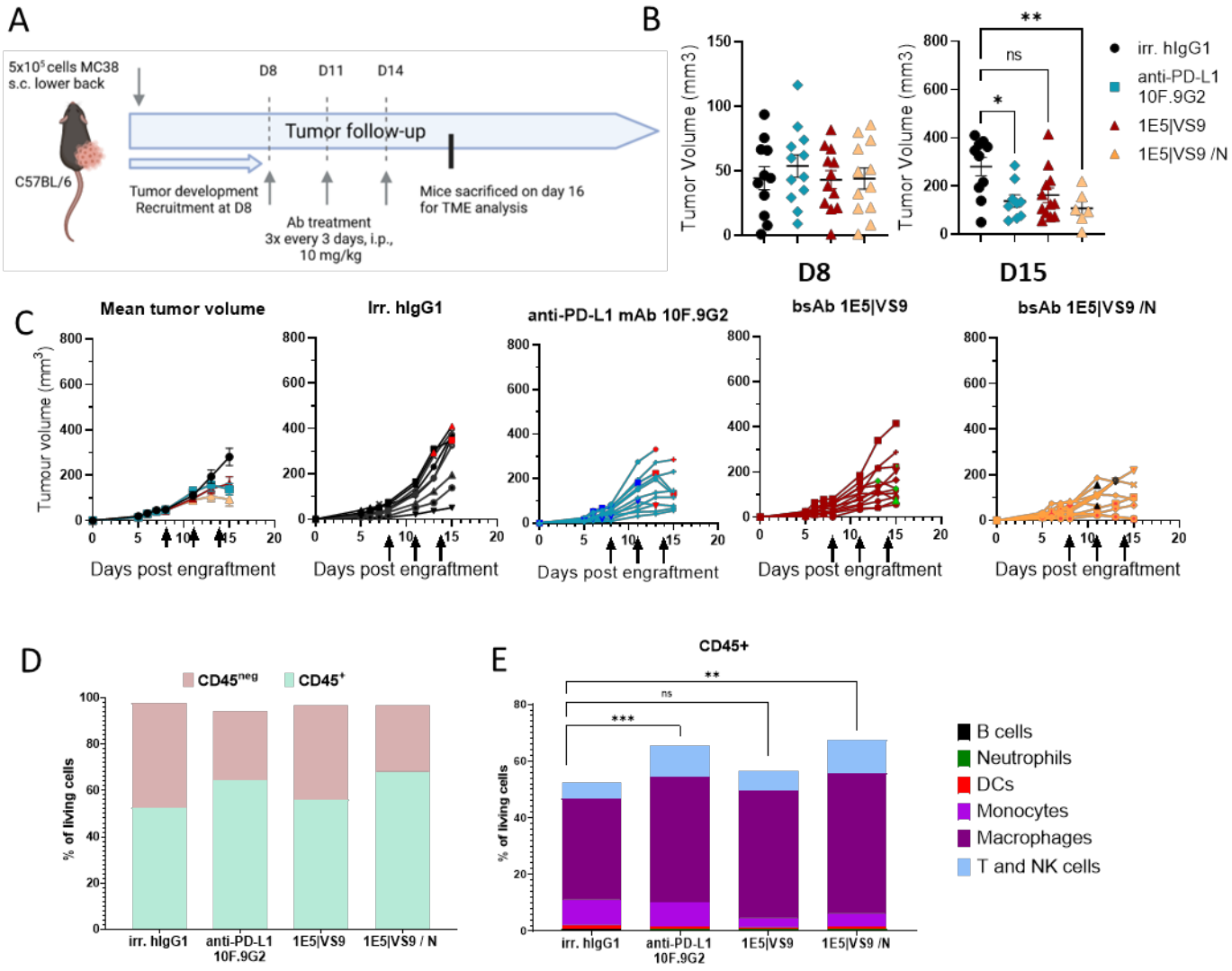

Figure 27: Flow cytometry characterization of intratumoral populations in MC38-bearing mice treated with anti-PD-L1 or the bsAbs. (A) Schematic illustrating the experimental design: 5x10^5 MC38 cells were injected above the hind leg (s.c. "high") into C57BL/6 female mice (n = 11-12 mice/group). Mice were randomized into treatment groups on day 8 (mean tumor volume around 50 mm^3) and were treated i.p with either 200 µg of the bsAb with active Fc (1E5|VS9), 200 µg of bsAb with the inactive Fc (1E5|VS9 /N), 200 µg of an anti-PD-L1 (10F.9G2) or 200 µg of an irrelevant hIgG1 control antibody on days 8, 11, and 14. (B) Individual tumor volume at two time points, D8 and D15 ± SEM. (C) Tumor growth is shown as average tumor size per group ± SEM and as individual tumor growth curves of control and treated groups. On the graph with average tumor size per group, the mice that reached the volume endpoint were assigned the maximum value for the the subsequent measurements. Mice with ulcerated tumors were indicated with a dot of a different color and were excluded from TME analysis. (D) Proportion of CD45+ and CD45^{neg} cells among living cells. (E) Mean proportion of the main immune subgroup among living cells. n.s., not significant, *P<0.05, **P<0.01, ***P<0.001, ****P<0.0001 were obtained using the Brown-Forsythe and Welch ANOVA with Dunnett's method for multiple comparisons correction.

In the subsequent graphs (Fig. 28 to 30), infiltration by individual immune subsets is represented relative to all immune cells (CD45+), instead of living cells (Fig. 27 and S2). Overall, this alternative

representation of immune cell infiltrates revealed the same tendencies as the % of living cells representation discussed above.

Myeloid cells are important modulators of the immune response within solid tumors and high myeloid infiltration is usually correlated with bad prognosis in the clinic [351]. On one hand, myeloid cells can promote tumor elimination via several mechanisms such as phagocytosis or secretion of pro-inflammatory mediators. Yet, they often acquire an immunosuppressive phenotype during tumor development and end up supporting tumor growth. We evaluated how the treatment with bsAbs impacted the myeloid compartment, which represented the major part of the immune infiltrate in MC38 tumors as shown in Fig. 27E. Active Fc bsAb treated group showed a higher proportion of macrophages while a decrease of monocytes was observed in both bsAbs treated groups (Fig. 28A). This may possibly represent a differentiation process where recruited monocytes in the TME give rise to macrophages. Since dendritic cells (DCs) are the most important professional antigen presenting cells bridging the innate and adaptive tumor responses, the impact of antibody treatment on this population was of particular interest. A decrease in DCs in the TME was observed in all treatment groups (Fig. 28A). I speculated that this decrease might be due to DC migration to the TdLNs, however, no corresponding increase in DCs was observed in TdLNs (Fig. S3).

Tumor associated macrophages (TAMs) are a heterogeneous and plastic population which can be polarized toward an activation state following treatment with anti-cancer drugs, including immune checkpoint inhibitors [84], [352]. I therefore evaluated if the antibody treatment induced changes in their phenotype. Strikingly, all treated groups showed an increase in markers associated with M1-like phenotype ($iNOS^+$, $MHCII+CD206^-$) commonly associated with proinflammatory functions [353](Fig. 28B). Conversely, the proportion of macrophages with M2-like phenotype ($MHCII^-CD206^+$), associated with immunosuppressive functions, decreased in all treated groups. Overall, even though the changes of M1-like and M2-like macrophage phenotypes reached statistical significance only in the anti-PD-L1 and the inactive Fc bsAb treated groups, these observations suggest that the blockade of PD-L1 (with or without a concomitant blockade of CD47) induced a shift in the TME towards more tumor-hostile myeloid infiltrates.

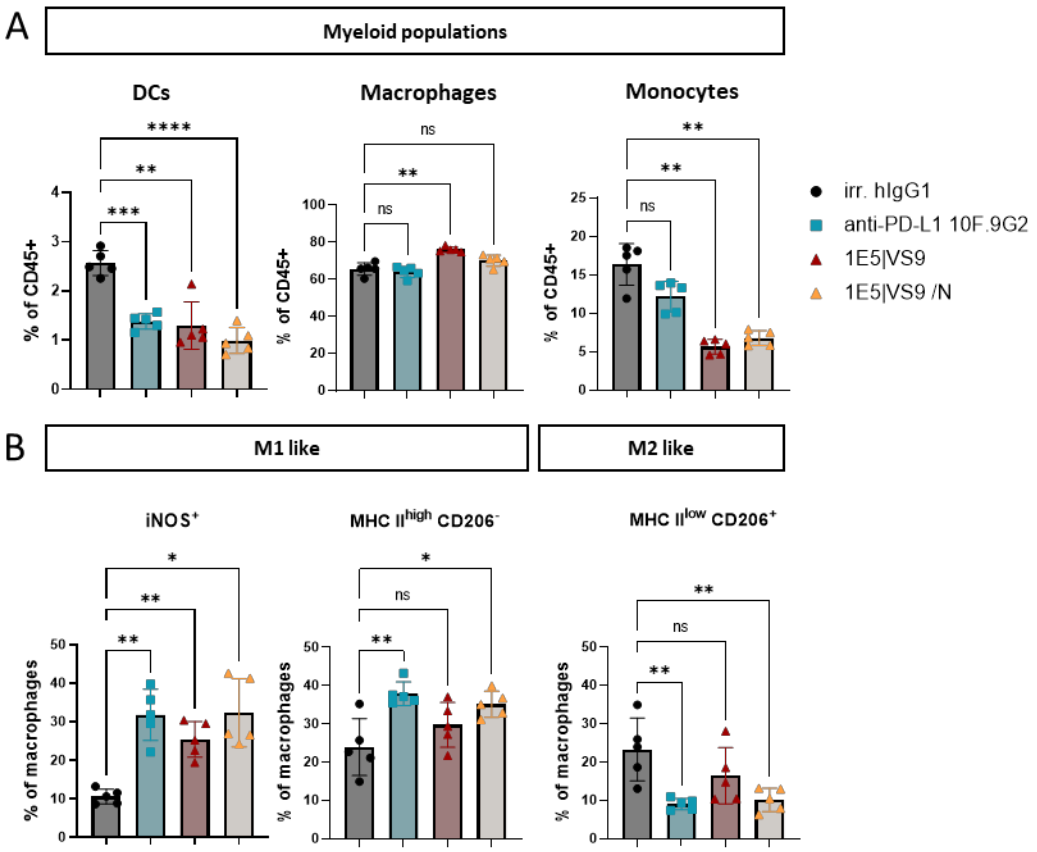

Figure 28: Myeloid populations in the TME showed major changes in response to treatment. (A) Proportion of DCs, macrophages and monocytes among CD45+ cells in the TME. (B) Proportion M1-like (iNOs+, MHC II^{high} CD206-) and M2-like (MHC II^{low}, CD206+) phenotypes among macrophages. n.s., not significant, *P<0.05, **P<0.01, ***P<0.001, ****P<0.0001 were obtained using the Brown-Forsythe and Welch ANOVA with Dunnett's method of multiple comparisons correction. Values are displayed as mean ± SD.

Previous studies have shown CD8+ T cells to be critical for the efficacy of both anti-PD-L1 mAbs, and bispecific molecules targeting CD47 and PD-L1 [320], [324]. We therefore sought to assess the effect of bsAbs on the T cell infiltration in the TME of MC38 tumors. Both bsAbs and the anti-PD-L1 mAb induced an expansion of the T cells compartment, in particular CD8+, which was statistically significant for the groups treated with anti-PD-L1 and with the bsAb with the inactive Fc (Fig. 29A). Overall, CD4+ T cell infiltrations did not increase upon treatment (Fig. 29A). Regulatory T cells (Treg, CD4+Foxp3+) , which represent a highly immunosuppressive CD4+ population that promotes cancer progression [30] were slightly decreased. Conversely, Foxp3^{neg} CD4^{+} T cells showed a tendency to increase in the treatment groups, albeit without reaching statistical significance, Fig. 29B and S5A). Also, the CD4^{+}Foxp3^{+} population showed reduced proliferation (reduced Ki67 signal) in the treatment groups (Fig. 29B). Overall, both the

CD8+:CD4+ and the CD8+:Treg ratios were significantly increased in all treated groups (Fig. 29A and C), indicating that the antibody treatment resulted in a more pro-inflammatory, anti-tumor TME [354].

We analyzed the proportion of effector/effector memory (CD44+ CD62L-) and central memory (CD44+ CD62L+) CD8+T cells in the TME and the TdLN following treatment. No changes were observed in the TME while in the TdLN all the treated groups displayed an increase in the CD8+ T central memory group (Fig. S5 and S6). With regards to CD4+ subsets in the TME, the proportion of effector/effector memory phenotype (CD44+CD62L-) decreased in all treatment groups and no significant change were observed in the TdLNs (Fig. S5 and S6).

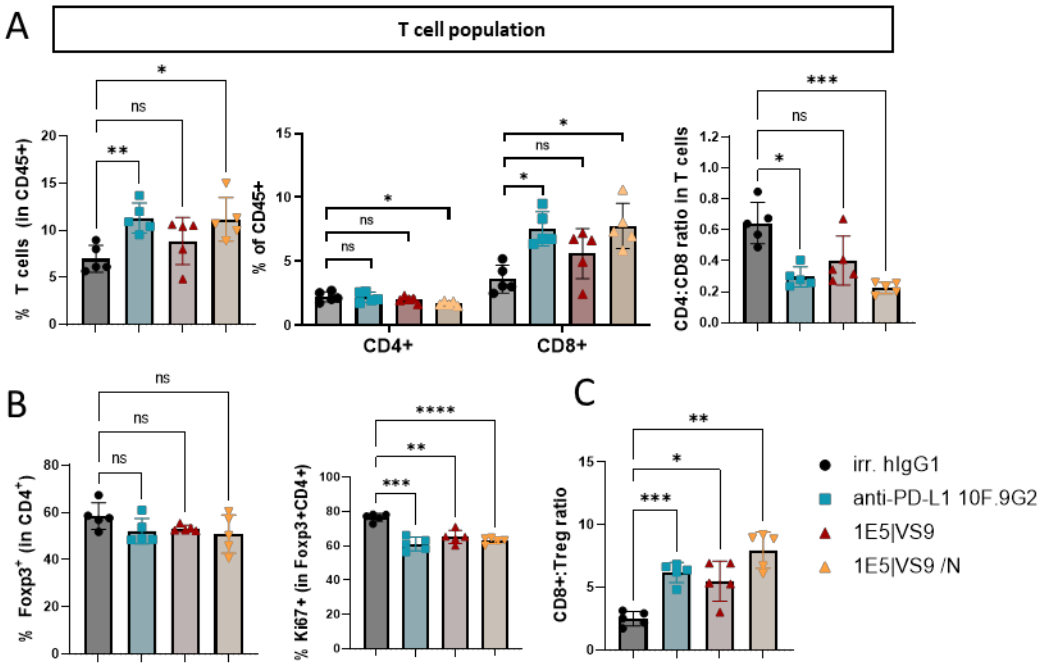

Figure 29: T cells subsets in MC38 tumors following treatment with bsAbs and anti-PD-L1. (A) Proportion of total T cells, CD4+ and CD8+ T cells among CD45+ and the ratio of CD4+ T cells to CD8+T cells (B) Proportion of Foxp3$^+$ CD4+ T and analysis of their proliferative capacity (Ki67+). (C) Ratio of CD8+ T cells to Tregs (CD4+Foxp3+). n.s., not significant, *P<0.05, **P<0.01, ***P<0.001, ****P<0.0001 were obtained using the Brown-Forsythe and Welch ANOVA with Dunnett's method for multiple comparisons correction. Values are displayed as mean ± SD.

Analysis of markers associates with activation or exhaustion state were performed on CD4+ and CD8+ T cell subgroups (Fig. 30 and S7). A significant increase in PD-1 and CD69 expression was observed in the CD8+ T cell subpopulation (Fig. 30A). A small increase in CTLA-4 and Tim3 expression was observed in groups treated with anti-PD-L1 or the inactive Fc bsAb. Less changes were observed on the CD4+ population within the tumor (Fig. S7). On the other hand, upregulation of PD-1 in treated groups was way

more pronounced, and might possibly linked to exhaustion, or, alternatively, an increased activation of the T cells following antibody treatment [62] .

Effector CD8+ T cells are characterized by enhanced proliferative capacity (Ki67+), expression of cytokines such as interferon-γ (IFN-γ) tumor necrosis factor-α (TNF-α) and production of cytotoxic molecules like granzyme B (GzmB) or perforin. An analysis of intracellular cytokines expression on TME cell suspension was performed following *ex vivo* non-specific stimulation with PMA and ionomycin. Functional characteristics of CD8+ T cells gave a complex picture: while the inflammatory cytokine production (IFN-γ and TNF-α) and the expression of Ki67 were decreased, an increase in the granzyme B (GzmB) expression was observed in treated groups compared with the control (Fig. 31B).

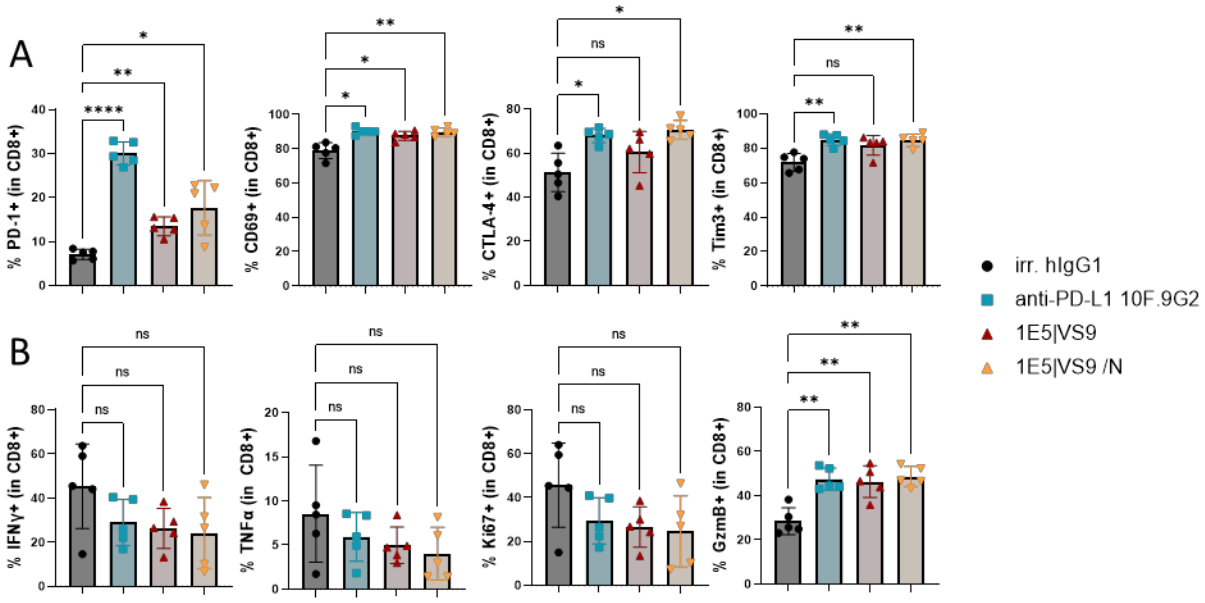

Figure 30: Analysis of activation and exhaustion markers on CD8+ cells from MC38 tumor after *ex vivo* restimulation. (A) Proportion of PD-1+, CD69+, CTLA-4+ positive cells among CD8+ T cells. (B) Cytokine and cytotoxic compound production as well as proliferative ability were assessed by measuring the proportion of IFNγ+, Ki67+, TNFα+ and GzmB+ positive cells among CD8+T cells. n.s., not significant, *P<0.05, **P<0.01, ***P<0.001, ****P<0.0001 were obtained using the Brown-Forsythe and Welch ANOVA with Dunnett's method for multiple comparisons correction. Values are displayed as mean ± SD.

3.2.4.3. *Characterization of tumor microenvironment at two timepoints following treatment with the bsAbs*

In order to characterize the dynamic of the changes in the immune cell infiltration in the MC38 tumors following the treatment with CD47|PD-L1 bsAbs, flow cytometry analysis of the TME was performed at two time points after initiation of the treatment. Tumors and tumor draining lymph nodes (TdLN) were harvested on day 10 and on day 16 post tumor engraftment for analysis. As described previously, some tumors displayed ulceration even at low volumes. This was observed in all groups. These

tumors were excluded from TME characterization. The effect of bsAbs was compared to a PD-L1 antibody (in contrast to previous experiments, the anti-PD-L1 mAb used in the current experiment was the parental mAb VS9 with a silenced Fc portion (VS9 /N).

On day 10, the mean tumor volume was still similar in all groups, while on day 16 the tumors in the three treatment groups were in general significantly smaller than in the control group mice (Fig. 31B and C). The proportion of CD45+ cells among living cells showed that MC38 tumors were highly infiltrated already on day 10, with more than 50% of the cells being CD45-positive. At this early timepoint, the tumors treated with anti-PD-L1 mAb showed more important CD45+ infiltration than in the other groups (Fig. 31D). Compared to D10, the TME at the later time point (D16) showed a relative decrease of immune cell infiltration in the control group and a marked increase in the 1E5|VS9 /N bsAb group, while in the VS9 mAb and the 1E5|VS9 bsAb groups the ratio of CD45+ cells remained about the same (Fig. 31D). The relative decrease of CD45+ cell ratio observed with the control group on D16 could be due to larger tumors, reflecting more vigorous and less restrained tumor growth in the untreated animals. A more detailed analysis of the composition of immune cells infiltrating the TME suggests that the increased immune cell infiltrates seen in the 1E5|VS9 /N bsAb and the VS9 group were mostly composed of macrophages, and, to a lesser extent, of T cells (Fig. S8). The immune cell composition was also analyzed in the TdLNs, but no important differences could be demonstrated when comparing the treatment groups with the control or the earlier (D10) and the later (D16) immune cell infiltrates (data not shown).

The different immune cell subpopulations were also represented and analyzed as percentage of total immune cell infiltrate (CD45+, Fig. S9 to S12). Overall, this alternative representation revealed a similar picture as data discussed above (immune cell subpopulations represented percentage as living cells). When comparing D10 to D16 infiltrates, DCs appeared more abundant at the later time point in the control group, while significantly decreasing in the inactive Fc bsAb group (Fig. S9A). Macrophages which constituted the bulk of immune infiltrates, showed an increased ratio at the later time point, but this did not appear to be treatment-specific (Fig. S10A).

The activation status of the APCs was further characterized (Fig. S9 and S10). An increase in CD86, associated with a little decrease in CD80 expression was observed in all treated groups, both on day 10 and on day 16 (Fig. S9C, D and S10C, D). Markers of macrophage polarization showed an increase of the M1-like signature (iNOS+, MHCII+CD206-) associated with a decrease of M2-like macrophages (MHCII-CD206+) in the three treatment groups, which was accentuated on day 16 as compared to day 10 (Fig.

S10C, D). These results suggested that the treatment with anti-PD-L1 and with the bsAbs induced a shift towards a more pro-inflammatory phenotype.

When comparing day 16 to day 10, a general decrease of T cell ratio within the CD45+ population found in the TME was observed, which was particularly noticeable in the control and in the active Fc bsAb groups (Fig. S12A, B). A marked decrease in CD4+ T cells (which constituted a major part of T cell infiltrate) was apparent in all groups (Fig. S12C, D), while the CD8+ content decreased only in the control group, but stayed generally the same in the three treatment groups (with a minor increase observed in the inactive Fc bsAb group, Fig. S12E, F)

Globally, data summarized above suggest that PD-1/PD-L1 blockade (associated or not with the blockade of CD47/SIRPα) induced changes in the TME of MC38 tumors that could be interpreted as pro-inflammatory and tumor-hostile.

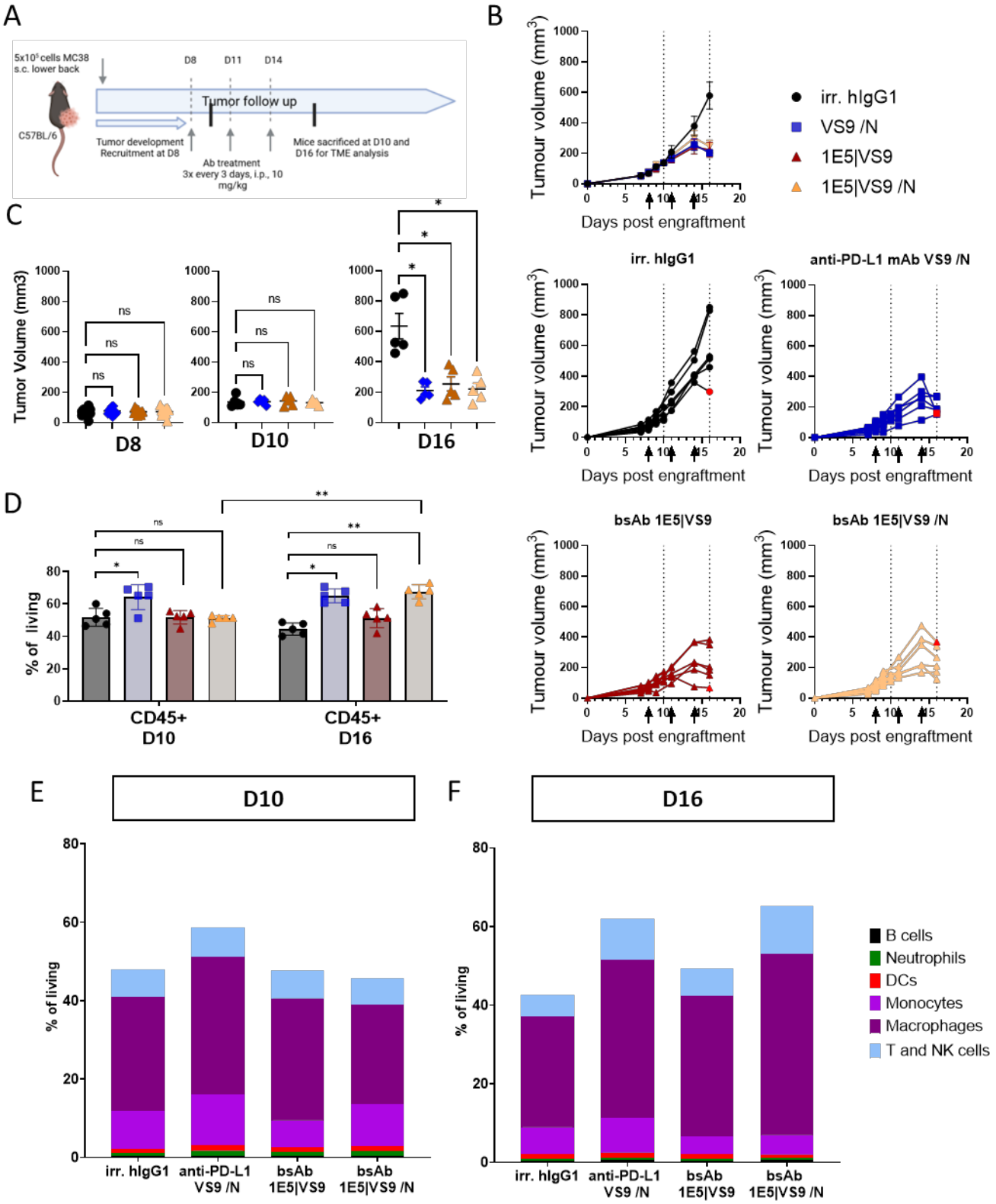

Figure 31: Immune infiltrate in MC38 tumors analyzed at two time points. (A) Schematic illustrating the experimental design: 5x105 MC38 cells were injected above the hind leg (s.c. "high") into C57BL/6 female mice (n = 11-12 mice/group). Mice were

randomized into treatment groups on day 8 (mean tumor volume around 70 mm3) and were treated i.p. with either 200 ug of the bsAb with active Fc (1E5|VS9), 200 µg of bsAb with the inactive Fc (1E5|VS9 /N), 200 µg of an anti-PD-L1 (VS9 /N) or 200 µg of an irrelevant hIgG1 control antibody on days 8, 11, and 14. (B) Tumor growth is shown as average tumor size per group ± SEM and as individual tumor growth curves of control and treated groups. Mice with ulcerated tumors were indicated with a dot of a different color and were excluded from TME analysis. (C) Individual tumor volumes on day 8, 10 and 16 ± SEM. D) Proportion of CD45+ among living cells on day 10 and on day 16. (E-F) Mean proportion of the main immune subgroup among living cells on (E) day 10 and (F) day 16 Values are displayed as mean ± SD. n.s., not significant, *P<0.05, **P<0.01, were obtained using the Brown-Forsythe and Welch ANOVA Dunnett's method for multiple comparison correction in panel (C) and using the 2-way ANOVA with Tukey's test of multiple comparisons in (D).

I also wanted to compare antibody exposure in TME of treated animals. For that goal, cell surface expression of PD-L1 was assessed on CD45+ and CD45- cells by flow cytometry at the two time points

Owing to binding competition between the primary FACS detection reagent (PD-L1 mAb clone MIH5) and the VS9 antibody, free (unbound) cell surface PD-L1 could be detected, which informed about target occupancy by the therapeutic antibody. On day 10, i.e., two days after the first antibody dose, neither immune (CD45+) nor non-immune (tumor, stromal, $CD45^{neg}$) cells were bound by the detection reagent, demonstrating that cell surface PD-L1 was efficiently occupied by the bsAbs and the PD-L1 mAb (Fig. 32). A different picture emerged when evaluating unbound cell surface PD-L1 on D16, i.e., two days after the third and last administration of antibody. While a minimal level of detection reagent bound to cells from the PD-L1 mAb and the inactive Fc bsAb groups, strong binding was detected with cells from the active Fc group, suggesting that the active Fc bsAb was eliminated at a significantly faster rate than its Fc-inactive counterpart. This observation is consistent with the concept that the Fc portion is actively involved in the antibody elimination process [225], [355] . This is also supported by the pharmacokinetics of the two bsAbs observed in a previous experiment (see Fig. 26 panels F and G).

To get a glimpse on the expression of the two bsAb targets in the TME of MC38 tumors, PD-L1 and CD47 expression levels were determined in different cell populations in the control (untreated) group at D10 and D16. As anticipated [101], [206], the highest PD-L1 expression levels were found on myeloid cells, while CD47 signal was highest on myeloid cells and the CD45-negative cell population most probably corresponding to tumor cells (Fig. S13)

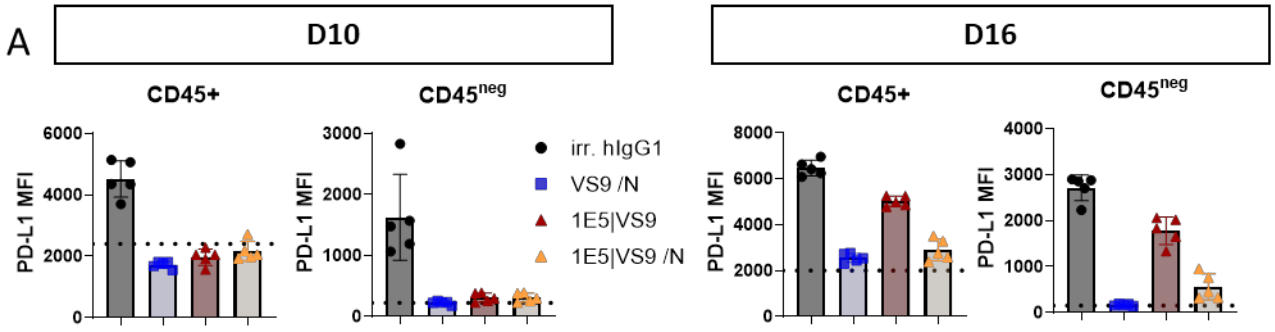

Figure 32: Quantification of PD-L1 expression on CD45+ and CD45^{neg} cells the tumor microenvironment. Mean fluorescence intensity was quantified on day 10 and on day 16 on CD45^{+} and CD45^{neg}. Dotted line represents the Fluorescence Minuse One (FMO) signal level. Values are displayed as mean ± SD.

3.2.5. BsAb efficacy, and pharmacokinetics, as compared to the parental mAbs

To compare the efficacity, the PK and the hematotoxicity profiles of bispecific antibodies versus their parental mAbs and a combination thereof, two consecutive *in vivo* experiments were run, one involving antibodies with a fully active Fc portion, the other one with Fc-silenced antibodies.

3.2.5.1. *Anti-tumor efficacy, PK and safety profile of antibodies with a silenced Fc portion*

With regards to efficacy, all treatment groups, except the anti-CD47 mAb, showed a delay in tumor growth (Fig. 33B). The bsAb and the PD-L1 mAb showed a similar efficacy, while the combination of CD47 and PD-L1 mAbs was even more potent (Fig. 33B and C – please note that the overall antibody dose in the latter group was two times higher than in the other treatment groups). As in the previous experiments, some mice showed tumor ulceration (without correlation with the treatment) and therefore had to be euthanized. No body weight loss was observed in any of the treatment groups, excluding mice with tumor ulceration (Fig. 33D)

The levels of antibody in the plasma measured by ELISA at three different time points showed strikingly diverse profiles (Fig. 33E). For both the control hIgG1 and the anti-PD-L1 mAb, elevated antibody levels were apparent, also at D18, i.e., 4 days after the last dose. On the contrary, antibodies targeting CD47, (both the mAb and the bsAb) were more rapidly eliminated from the circulation, probably reflecting a powerful TMDD resulting from ubiquitous and abundant expression of CD47 in healthy tissues ("antigen sink"), especially in blood cells. The antibody combination presented a mixed PK profile, reflecting different PK characteristics of the two constituent mAbs.

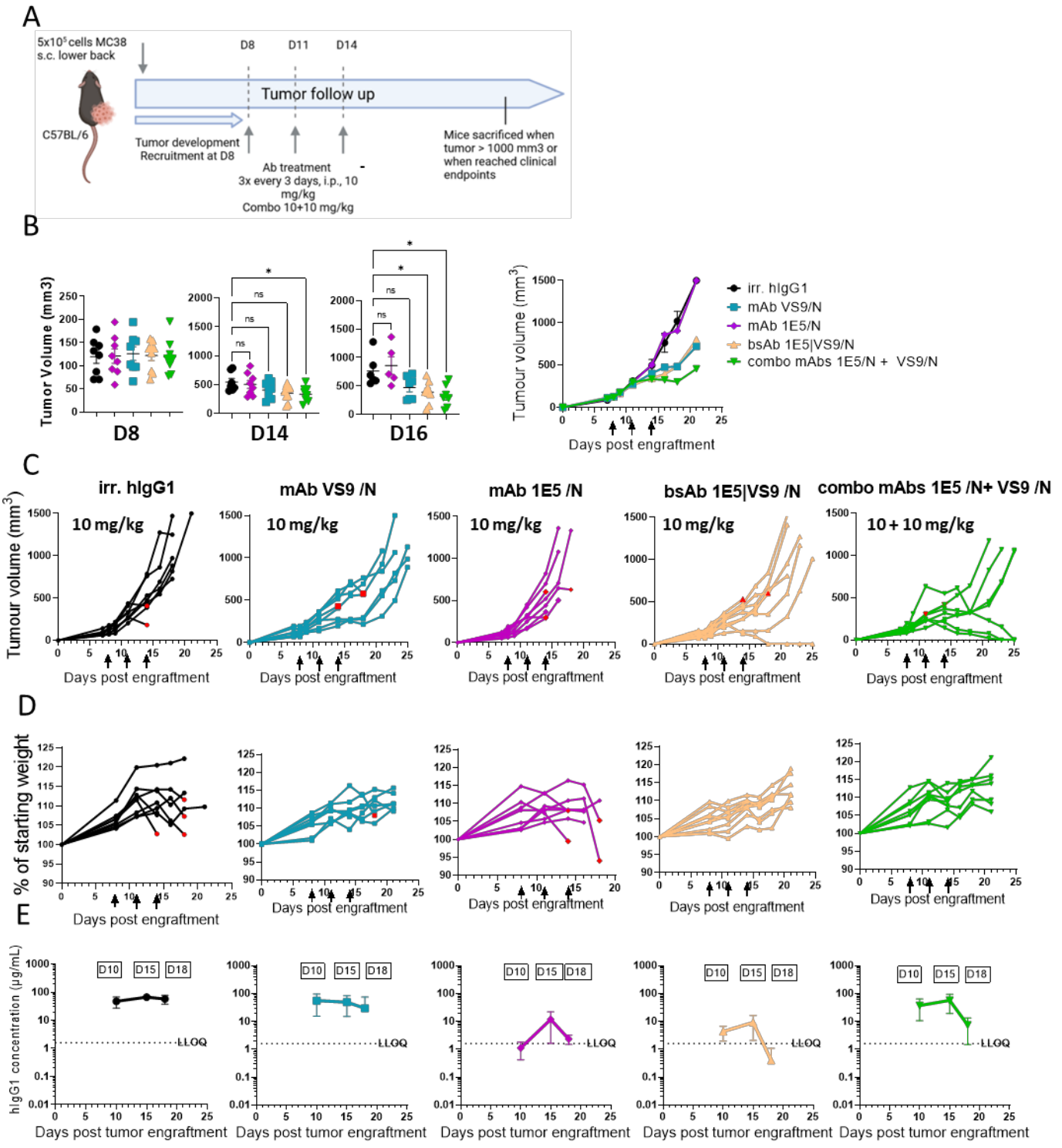

Figure 33: Therapeutic efficacy of the bsAb 1E5|VS9 /N and the corresponding mAbs in a MC38 tumor model. (A) Schematic illustrating the experimental design: 5x10^5 MC38 cells were injected above the hind leg (s.c. "high") into C57BL/6 female mice (n = 8-9 mice/group). Mice were randomized into treatment groups on day 8 (mean tumor volume around 120 mm^3) and were treated i.p. with either 200 µg of bsAb with the inactive Fc (1E5|VS9 /N), 200 µg of an anti-PD-L1 (VS9 /N), 200 µg of an anti-CD47 (1E5 /N), the combination of 200 µg of anti-PD-L1 (VS9 /N) and 200 µg of anti-CD47 mAb (1E5 /N) or 200 µg of an irrelevant hIgG1 control antibody on days 8, 11, and 14. (B) Individual tumor volume on day 8, 14 and 16 ± SEM and tumor growth as average

tumor size per group ± SEM. For average tumor size per group: once a mouse reached the volume endpoint, the following measurements were assigned a maximal value. (C) Individual tumor growth curves of control and treated groups. Mice with ulcerated tumors were indicated with a dot of a different color and were euthanized. (D) Percent of initial body weight. Mice that lost weight due to ulceration were identified with a dot of a different color. (E) Mean serum concentrations (n = 4-6) ± SD were determined using the FastELISA system (RD-Biotech) on day 10, day 15 or 18 after engraftment. n.s., not significant, *P<0.05 were obtained using the Brown-Forsythe and Welch ANOVA Dunnett's method for multiple comparison correction.

The effect of the bsAb and the mAbs on blood cells was evaluated in tumor bearing mice. In addition, the impact of the bsAb treatment was also evaluated in tumor-free mice (designated as "naïve mice", Fig. 34 and S14). Mice treated with the inactive Fc bsAb showed reduced red blood cell count (RBC), hemoglobin (HGB) and hematocrit (HCT) one day after the last (i.e., the third) dose. This decrease was correlated with an increase in reticulocyte (RET) count, which was even more pronounced five days after the last dose (Fig. 34). Intriguingly, a minor decrease in platelet count was seen with the anti-PD-L1 mAb, which is difficult to explain.

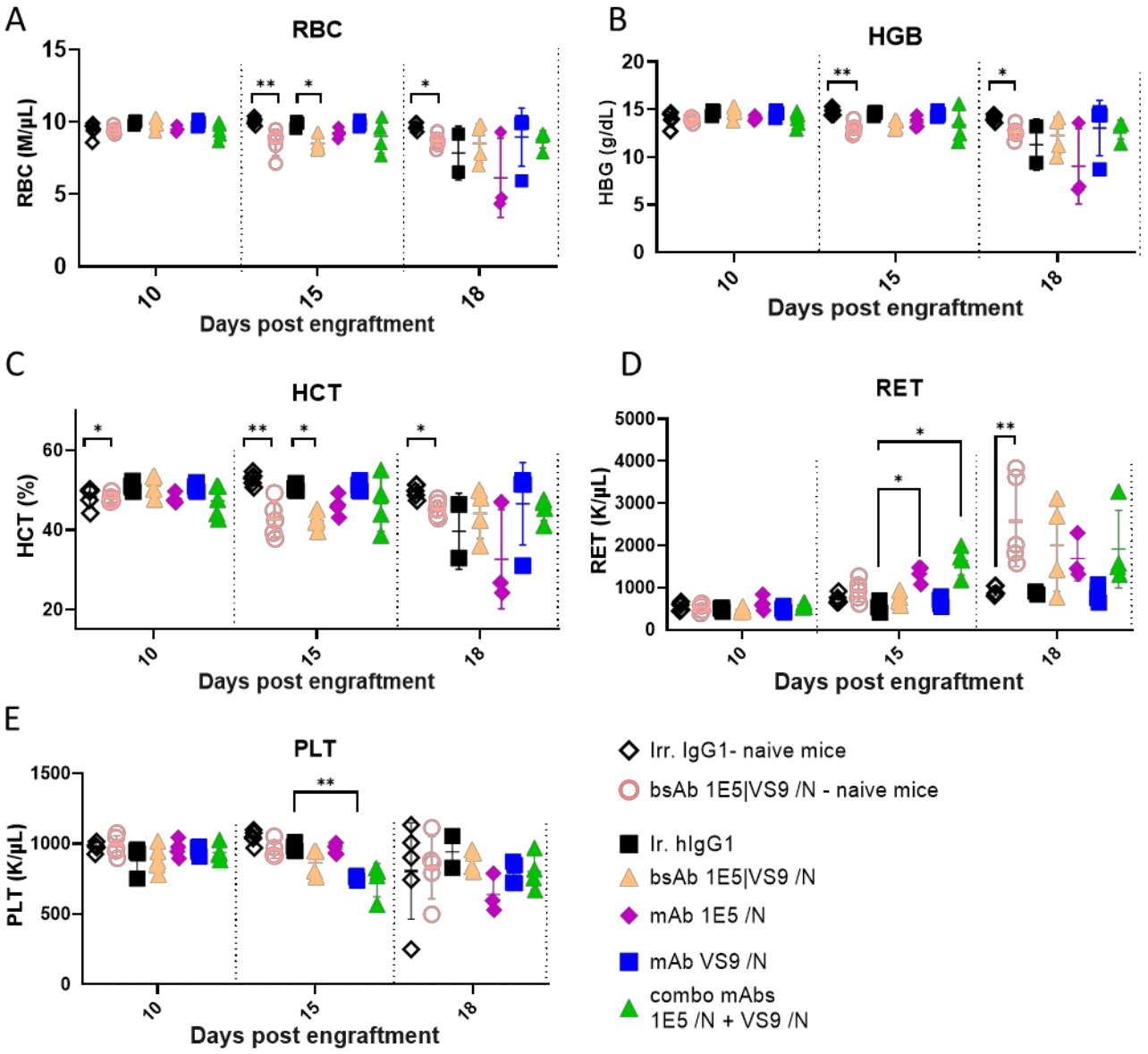

Figure 34: Blood parameters analysis following treatments. Mice were treated on day 8, 11 and 14 and blood was collected on day 10, day 15 and day 18. Samples were run on ProCyte Dx Haematology Analyser. A) Red blood cell (RBC), B) hemoglobin (HGB), C) hematocrit (HCT), D) reticulocytes (RET), and E) platelets were measured (n=3-5 mice per group). n.s., not significant, *P<0.05, **P<0.01, were obtained using the Kruskal-Wallis ANOVA with Dunn's method of multiple comparisons. Only significant differences were indicated on the graphs. Values are displayed as mean ± SD.

3.2.5.2. *Anti-tumor efficacy, PK and safety profile of active Fc bsAb and mAbs*

The anti-PD-L1 mAb with an active hIgG1 Fc portion induced an important and prolonged delay in tumor growth (Fig. 33B and C). The effect of the bsAb was smaller but also apparent, while the anti-CD47 mAb did not seem to have any effect on tumor progression. On the other hand, the administration of the anti-CD47 mAb with an active Fc portion resulted in transient body weight loss in some animals (Fig. 35D). Unfortunately, the anti-tumor efficacy of the combination therapy (mAb 1E5+VS9) could not be assessed at later time points due to tumor ulceration in 6 out of 8 animals in this group.

Antibody levels in the plasma suggested that Fcγ receptor binding importantly impacted the PK profiles by enhancing antibody elimination (Fig. 35E). That effect was apparent with the PD-L1 mAb when comparing with the previous experiment (see Fig. 33) but was even more pronounced for the bsAb and the anti-CD47 mAb.

Interestingly, in contrast to the experiment with antibodies bearing a silenced Fc portion, analysis of blood from animals treated with antibodies with a fully active Fc did not show any hematotoxic effect of the PD-L1/CD47 bsAb (Fig. 36 and S15). This discrepancy is counter intuitive, but could potentially be explained by the extremely poor PK of the active Fc bsAb, resulting in much lower levels of circulating antibody as compared to the inactive Fc bsAb (see Fig. 33 and 25). However, the anti-CD47 mAb – also rapidly eliminated from the circulation – induced a reduction in RBC, HGB, HCT on day 10, which was followed by a compensatory increase in reticulocytes observed at later time points (day 16 and day 18, the latter was also apparent with animals treated with the bsAb and the mAb combination therapy). Platelet counts were also impacted by the CD47 antibody bearing an active Fc. Overall, this picture is consistent with previous findings showing that the hematotoxicity profile of CD47 mAbs is dependent their affinity to the target and the Fc portion [242], [243], [279].

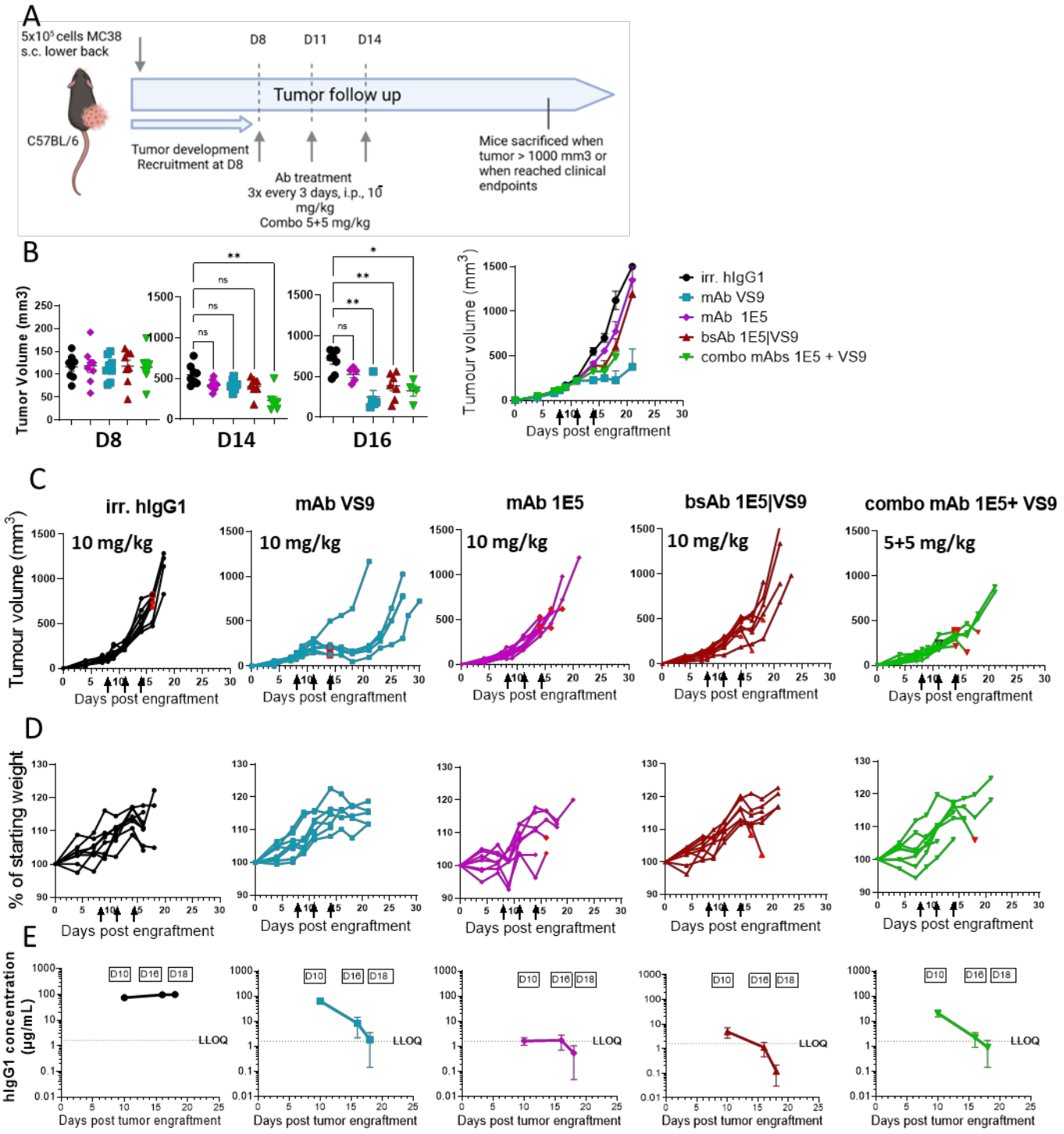

Figure 35: Therapeutic efficacy of the bsAb 1E5|VS9 and the corresponding mAbs in a MC38 tumor model. (A) Schematic illustrating the experimental design: 5x10^5 MC38 cells were injected above the hind leg (s.c. "high") into C57BL/6 female mice (n = 8-9 mice/group). Mice were randomized into treatment groups on day 8 (mean tumor volume around 120 mm^3) and were treated i.p. with either 200 µg of bsAb with the active Fc (1E5|VS9), 200 µg of an anti-PD-L1 (VS9) , 200 µg of anti-CD47 (1E5) the combination of 100 µg of anti-PD-L1 (VS9) and 100 µg of anti-CD47 mAb (1E5) or 200 ug of an irrelevant hIgG1 control antibody

on days 8, 11, and 14. (B) Individual tumor volume on day 8, 10 and 16 ± SEM and tumor growth as average tumor size per group ± SEM. For average tumor size per group: once a mouse reached the volume endpoint, the following measurements were assigned a maximal value. (C) Individual tumor growth curves of control and treated groups. Mice with ulcerated tumors were indicated with a dot of a different color and were euthanized. (D) Percent of initial body weight. Mice that lost weight due to ulceration were identified with a dot of a different color. (E) Mean serum concentrations (n = 4-6) ± SD were determined using the FastELISA system (RD-Biotech) on day 10, day 16 or 18 after engraftment. n.s., not significant, *P<0.05, **P<0.01 were obtained using the Brown-Forsythe and Welch ANOVA Dunnett's method for multiple comparison correction.

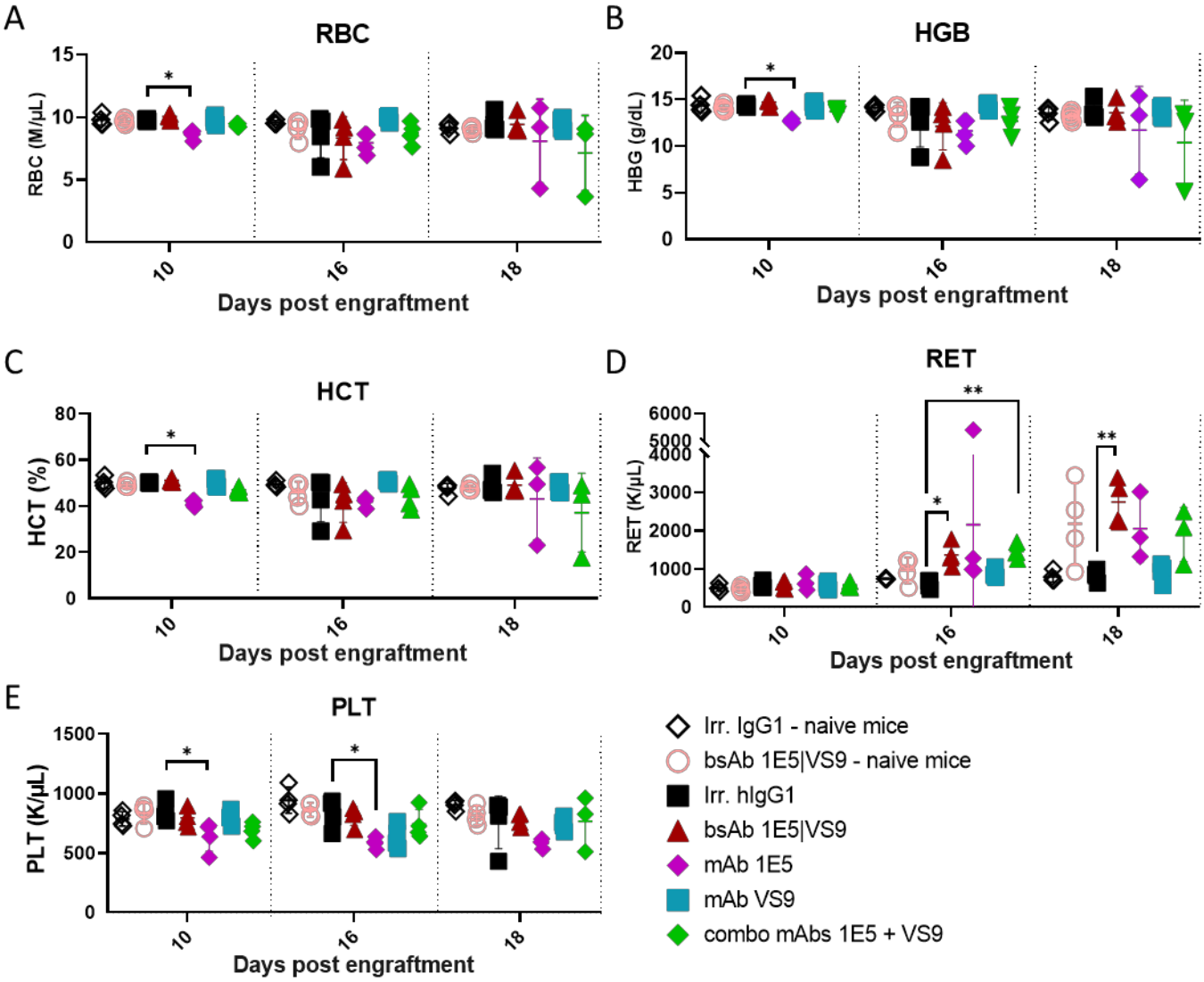

Figure 36: Blood parameters analysis following treatments. Mice were treated on day 8, 11 and 14 and blood was collected on day 10, day 16 and day 18. Samples were run on ProCyte Dx Haematology Analyser. (A) Red blood cell (RBC), (B) hemoglobin (HGB), (C) hematocrit (HCT), (D) reticulocytes (RET), and E) platelets were measured (n=3-5 mice per group). n.s., not significant, *P<0.05, **P<0.01, were obtained using the Kruskal-Wallis ANOVA with Dunn's method of multiple comparisons. Only significant differences were indicated on the graphs. Values are displayed as mean ± SD.

4. Discussion

4.1. Background

Immunotherapy breakthroughs in the early 2000s brought a new perspective for cancer treatment. Blockade of immune checkpoints, principally CTLA-4 or PD-1/PD-L1, via antagonizing antibodies has revolutionized the field of oncology. These new treatments resulted in long term patient survival in a broad range of cancers that were previously untreatable. However, despite tremendous responses observed in clinical trials, the efficacy of immune checkpoint inhibitors (ICI) is limited to a subset of patients[227]. In order to boost the anti-tumor response and circumvent resistance mechanisms, combination treatments are being evaluated in the clinic. In particular, anti-PD-1 or anti-PD-L1 combined with other T cell immune checkpoints such as anti-CTLA-4 showed enhanced therapeutic benefits [231], [356], [357]. Also, combining ICI with other treatments targeting non redundant tumor-promoting mechanisms may lead to increasingly efficient therapeutic strategies [358]. One example is innate immune checkpoint inhibitors, aimed at reversing immunosuppression in the TME such as anti-CD47 mAbs [358]–[360]. CD47 is expressed on virtually all cells and is considered as a marker of self for innate immune recognition [234]. By interacting with SIRPα present at the surface myeloid cells, CD47 provides a “don’t eat me” signal that protects the cell from destruction by innate immune phagocytes, principally macrophages [237].

Early preclinical studies have demonstrated that overexpression of CD47 on cancer cells allows the tumor to escape immune surveillance and is associated with poor prognosis [245], [269], [272]. Targeting CD47 with mAbs has shown promising effects in mouse tumor models, promoting phagocytosis of tumor cells and enhancing antigen cross presentation [242], [270], [280], [285], [288], [361]. Yet, this therapeutic strategy suffers from important drawbacks, principally related to ubiquitous expression of CD47 in healthy cells. As a consequence, anti-CD47 mAbs and SIRPα-Fc fusion proteins are characterized by poor pharmacokinetics (caused by an important “antigen sink”, mostly harbored by red blood cells) and by some toxic side effects. In particular, binding to red blood cells (RBC) and platelets may result in anemia or thrombocytopenia, principal hematologic adverse events observed in clinical trials with CD47 inhibitors [245], [291], [362]. In addition, the “antigen sink” mandates high and frequent antibody dosing, necessary to maintain acceptable drug exposure [295], [296].

While no CD47-targeting therapeutic is on the market yet, a multitude of experimental drugs are now at different stages of clinical development [242], [243], [245]. Both the affinity to the target and the binding of the Fc part to Fcγ receptors impact antibody safety, pharmacokinetic and efficacy [350], and

this applies in particular to CD47 inhibitors, given the abundant expression of this target on healthy tissues. To achieve an acceptable compromise between safety and efficacy of CD47 inhibitors, diverse approaches exist. The most common consists on downmodulating or silencing the antibody Fc portion. Such molecules, like the anti-CD47 mAb magrolimab (hu5F9-G4, the leading CD47-targeting drug, currently in phase III clinical trials) still require high and frequent dosage, but show manageable anemia and thrombocytopenia [243], [284], [294]. However, the tradeoff of increased safety with downmodulated or silenced effector functions is limited efficacy, especially when such antibody is used as a single agent. As a consequence, magrolimab is mainly investigated in combination therapies (e.g., with hIgG1 mAbs endowed with full Fc functionality, like Rituxan) [245], [293]. The same situation applies to SIRPα-Fc fusion proteins in clinical development, such as ALX148 [299] or TTI-622 [300]**.**

4.2. Targeting CD47 with bispecific antibodies

Another approach to overcome the problems arising from ubiquitous expression of CD47 consists of using bispecific antibodies (bsAb) with unbalanced affinities. This allows to restrain CD47 blockade to defined cell populations, with a low affinity anti-CD47 arm associated to a high affinity arm directed toward another cell surface molecule, typically a tumor-associated antigen (TAA) [301], [305], [363]. The unbalanced affinity promotes targeting of TAA-positive cells and avoids binding to CD47 expressed on (TAA-negative) healthy cells resulting in improved pharmacokinetic and safety properties. This restricted binding profile allows endowing the CD47|TAA bsAb with an active Fc portion, boosting effector functions and anti-tumor abilities [305], [306], [363]. Several such bsAbs have shown promising results in preclinical studies and are now in clinical trials [245], [301], [303].

Numerous preclinical studies combining the inhibition of the PD1/PD-L1 and CD47/SIRPα immune checkpoints delivered promising results [286], [316]. Current clinical trials usually study mAb combinations [245], [302]. However, there is a strong rationale for inhibiting both immune checkpoints with a bispecific antibody. Both CD47 and PD-L1 are overexpressed in tumor cells, which is associated with poor clinical outcome [176], [272]. In addition, their expression in tumor cells was found to be often co-regulated at transcriptional level by the MYC oncogene [313]. Last but not least, for reasons explained above, a bispecific antibody with unbalanced affinities is preferred to a mAb as far as CD47 targeting is concerned.

Our aim was to evaluate the anti-tumor efficacy, pharmacokinetics and safety of CD47|PD-L1 bsAbs *in vivo*, in syngeneic tumor mouse models. For bsAb generation, we principally used the bispecific antibody format developed at Novimmune, referred to as the κλ body [175]. These κλ bodies were designed to have a high affinity anti-PD-L1 arm with a dual function: first, potent blockade of the PD-1/PD-L1 interaction (the CPI function), and, second, driving the binding to PD-L1-positive cells (the "guide arm" function). The lower affinity anti-CD47 arm was aimed at blocking the CD47/SIRPα interaction upon PD-L1 coengagement at the cell surface, at the same time limiting monovalent binding to PD-L1 negative cells (i.e., the vast majority of CD47-positive cells). In the course of this project, successive waves of CD47|PD-L1 bsAbs were generated and tested *in vitro* and *in vivo*. In an attempt to improve upon the *in vivo* efficacy of bsAb treatment, anti-PD-L1 arms and anti-CD47 arms of various affinities were combined with active or inactive Fc portions, either of mouse or human origin. As a consequence, I generated and tested three different waves of bsAbs (the first wave bsAbs with mIgG2a Fc portion, 2nd and 3rd wave bsAbs with hIgG1 Fc portion). As expected, CD47|PD-L1 bsAbs bound strongly to double positive cells showing reduced binding to PD-L1-negative cells, in particular to erythrocytes. I also showed that the bsAbs co-engaged the two targets on double-positive cells, efficiently disrupting the CD47/SIRPα and the PD-1/PD-L1 checkpoints.

4.3. Anti-tumor efficacy of PD-L1 |CD47 bsAbs

To evaluate the anti-tumor efficacy of our bsAbs, we started by setting up two syngeneic mouse models, CT26 immunogenic cell lines described to be partially responsive to PD-1/PD-L1 inhibition, and a non-immunogenic cell line, 4T1. Unfortunately, after a series of pilot experiments and testing two alternative s.c. engraftment sites (Fig. 13), both models were eventually abandoned: 4T1 showed early tumor ulceration at low tumor volumes (data not shown), while CT26 was not responding to treatment with a "benchmark" anti-PD-L1 antibody widely used in preclinical research (Fig. 13-14) [331]. We therefore switched to the popular hypermutated colorectal cancer model MC38, known to respond well to ICI treatment [209], [338].

We then evaluated the efficacy of the first wave bsAbs, which had the same anti-PD-L1 arm (6E8), an immunologically active Fc portion (mIgGa) but different anti-CD47 arm, one of intermediate affinity (mC2) and one low affinity (GD1). Both bsAbs marginally delayed tumor growth and increasing the dose from 10 to 20 mg/kg did not result in a superior anti-tumor efficacy compared to the anti-PD-L1 mAb (Fig. 16). The effect of both bsAb was comparable, despite having anti-CD47 arms of significantly different

affinities (mC2, K_D= 108.2 nM; GD1, K_D= 2130 nM,). The lack of differentiation with the two bsAbs may have seemed surprising at a first glance, but it might just reflect the offset between the effect of a more potent CD47 inhibition (mC2) on one side, and a superior exposure (GD1). Of note, in a previous study comparing the *in vivo* efficacy of two CD47|TAA bsAbs with different CD47 arms in the B cell lymphoma A20 tumor model, the low affinity CD47 bsAb arm GD1 resulted in a superior anti-tumor efficacy, pharmacokinetics, and distribution profile than the intermediate affinity CD47 bsAb mC2 [305]. Importantly both bsAbs analyzed in the present study showed inferior (at least, not superior) to the anti-PD-L1 mAb, which starkly contrasts with recently published research using a similar experimental approach [320], [324].

I hypothesized that the poor performance of the bsAbs in the MC38 model could be due to insufficient affinity of the 6E8 anti-PD-L1 arm. While the 6E8 mAb blocked the PD-1/PD-L1 interaction *in vitro* with a similar potency as atezolizumab and the benchmark mAb 10F.9G2 (Fig. 12A), it was less efficacious *in vivo* (Fig. 17). What is more, I speculated that a CD47|PD-L1 bsAb might require a more potent PD-L1 arm for an efficient PD-L1 blockade in the TME, given the anticipated negative effect of the CD47 antigen sink on antibody distribution and on tumor penetration in particular.

In parallel with the 6E8-based bsAbs *in vivo* experiments, a new anti-PD-L1 arm with higher affinity was identified by phage display (VS9, Fig. 20). This allowed us to generate three VS9-based bsAbs: two bsAbs with an anti-CD47 arm of intermediate affinity (1E5), either an active or an inactive hIgG1 Fc part and one bsAb with the GD1 arm with an active Fc part (Table 4, Figs 21-23). As compared to 6E8, VS9-based antibodies showed a significantly higher PD-1/PD-L1 blocking potency, both in the mAb and in κλ body (bispecific and monovalent) formats (Fig. 24).

The accumulated experience with syngeneic tumor models demonstrates that variability in tumor growth kinetics reflects the complexity of the interactions between the immune system and the tumor and is a major factor influencing the efficacy of experimental immunotherapy [364]. When comparing MC38 tumor growth curves obtained in our laboratory with published data, we realized that, in general, these tumors were growing much faster and were less responsive to PD-L1 mAb treatment in our experiments [209], [320], [328]. This led us to test and subsequently adopt an alternative subcutaneous tumor engraftment technique (named here “s.c. high”) that resulted in a slower tumor growth and overall better responses to PD-L1 blockade (Fig. 25 and data not shown). According to a few published papers, this change might result in more immunogenic tumors, which would explain the slower growth and an increase in treatment efficacy [347]–[349].

Using the new engraftment protocol, several *in vivo* experiments were run to assess the therapeutic efficacy of the two CD47|PD-L1 bsAbs (bearing an active or a silenced Fc portion), safety, antibody pharmacokinetics, and treatment-induced changes in the MC38 tumor microenvironment (Figs 25-36).

From the point of view of treatment efficacy, it would be difficult to draw any definitive conclusions as to the superiority of any of the two Fc versions of the 15E|VS9 bsAbs. If subtle differences emerged in individual experiments, a clear distinction cannot be made based on the entire set of MC38 experiments performed in this study. Overall, the same could be said when comparing the bsAbs with the PD-L1 mAb treatment – no distinct superiority of one treatment versus another was apparent. In other terms, we were not able to confirm here the advantage of CD47|PD-L1 targeting over PD-L1 monotherapy, as recently described in two other studies [320], [324]. Likewise, the CD47 and PD-L1 mAb combination therapy showed superior to the bsAb in our hands in one of the experiments, with antibodies with silenced Fc portion (Fig. 33; the efficacy of the mAb combination in the context of an active Fc could not be established due to premature tumor ulceration in most of the animals in this group, see Fig. 35). As to the CD47 mAb, either with active or inactive Fc did not show any significant anti-tumor efficacy in this model, which confirms previous findings [320], [324]

I hypothesized that one of the reasons for insufficient anti-tumor efficacy of the bsAbs could be linked to short antibody half-life, which may result in insufficient exposure. Thus, a significantly higher dosing may be required for a superior therapeutic effect. Indeed, a recently described CD47|PD-L1 bsAb (with a high affinity CD47 arm and an active Fc portion, Chen et al., (JITC, October 2021, ref. [324]) required unusually high dosing — 6 doses at 40 mg/kg twice a week — to reach maximal efficacy in the MC38 models. This is significantly higher than the rather conventional dosing I used in my experiments, i.e., 3 to 4 doses at 10 or 20 mg/kg twice a week (I did not retest our bsAbs at such high doses, due to time and material constraints and potential hematotoxicity considerations, see next section). However, another relevant publication using a similar experimental approach suggested that a high bsAb dosing may not be necessary. In a paper published by Liu et al., (Cell. Rep, August 2018 ref. [320]) a remarkable anti-tumor efficacy of a PD-L1|SIRPα Fc fusion protein (bearing a wild-type hIgG1 Fc portion) was achieved after just two doses at 5 mg/kg, administered 4 days apart [320].

Notwithstanding, the MC38 tumors in the experiments published by Liu et al. [320] showed a significantly slower growth as compared to our experiments (the s.c. high protocol) and Chen et al. [324]. As already mentioned, slower tumor growth may reflect a more vigorous immune response against the implanted tumor and would be expected to allow for a better efficacy of immunotherapy, CPI in particular.

What is more, several factors affecting the immune competence of the host animals (mouse provider, gut microbiota, housing conditions) may largely affect inter-laboratory reproducibility and variability of *in vivo* preclinical experiments [365]. Last but not least, we cannot exclude that the MC38 cell line we have differs slightly but importantly from MC38 used in the other studies. Commercial availability of MC38 is restricted, and this cell line is usually passed from one lab to another, which probably results in genetic drift and heterogeneity [366], [367]. Finally, protocols for cancer cell line culture may differ between labs, which could account for additional variability and lack of reproducibility of *in vivo* data [367].

When comparing the therapeutic efficacy of the two 1E5|VS9 bsAbs differing by their Fc portion and associated effector functions, we have not noticed any significant and consistent difference. This again is in stark contrast with the results published by Chen et al., showing a net therapeutic advantage of the wild type mIgG2a Fc-endowed CD47|PD-L1 bsAb over its Fc-null counterpart [324]. The latter can be understood on the grounds that the IgG Fc contributes to bsAb efficacy by mediating the direct elimination of (PD-L1-positive) MC38 tumor cells by effector cells of innate immunity (macrophages, NK cells, NKT cells).

On the other hand, the active IgG Fc portion was found to negatively impacts the pharmacokinetics of our CD47|PD-L1 bsAb as shown in (Fig. 25, see below). Thus, in the end, the difference in antibody half-life and exposure in favor of silenced Fc variant may potentially compensate for the lack of tumor cell killing functions.

4.4. Pharmacokinetics and safety

We observed that an active Fc part had a negative impact on antibody half-life. When compared side by side, the wild type hIgG1 Fc bsAb showed faster elimination than the one with a silenced Fc portion (Fig.25). This was confirmed by an assessment of PD-L1 receptor occupancy in the TME two days after the third (i.e., the last) administration of bsAb, pointing at a significantly lower exposure with the Fc active bsAb variant (Fig. 32). A more rapid antibody elimination associated with an active Fc portion was also observed in subsequent experiments, both with the bsAbs but also with the CD47 and PD-L1 mAbs (Figs 33 and 35). While this could be easily explained for the CD47 mAbs and the bsAbs, given an expected TMDD effect (mediated by the CD47 antigen sink), it is less obvious for the PD-L1 mAb. Nonetheless, our findings correlate with clinical data on the PK of two PD-L1 ICI mAbs, atezolizumab and avelumab, attesting a significantly shorter half-life of the latter [225], [355]. The fact that avelumab has a wild-type hIgG1 Fc part and atezolizumab has a silenced Fc may well explain that difference, although other factors

(like the higher affinity of avelumab, different physicochemical properties, etc.,) could also be responsible for the observed difference in PK.

In the context of CD47 targeting, the Fc functionality is expected to significantly affect the hematotoxicity profile of the antibody. Indeed, several pre-clinical studies showed that CD47-targeting molecules associated with active Fc part trigger hematotoxicity (usually appearing as anemia or thrombocytopenia) while the same exact molecule but with an inactive Fc has no deleterious impact (i.e. ALX148 versus ALX377) [243], [279], [299]. Early clinical data from TTI-621, a SIRPα-Fc fusion protein endowed with an immunologically active Fc portion (hIgG1) showed dose-limiting toxicity at low dose (0.2 mg/kg) upon systemic administration in patients [291], [368]. Confirming published findings [243], the anti-CD47 mAb with an active Fc part triggered a partial depletion of platelets and lowered RBC levels, which was associated with body weight loss (Figs 35 and 36). In the case of the CD47|PD-L1 bsAbs, the three experiments in which we have analyzed blood parameters following antibody treatment did not give a clear indication as to the relationship between the antibody Fc part and hematotoxicity. In the first experiment comparing the two versions of the VS9/1E5 bsAb, we noticed that, contrary to the silenced Fc bsAb, the active Fc bsAb impacted RBC, HGB, HCT and platelet levels, especially when assessed soon after the cessation of the treatment (i.e., two days after the 3rd and last dose, Fig. 26). Intriguingly, the association of hematotoxicity with an active Fc portion was not confirmed in a subsequent experiment (aimed at comparing the bsAbs with the corresponding mAbs and the combination therapy, see Figs 35 and 36). I assume that a lower dosing (10 mg/kg, instead of 20 mg/kg in the first experiment) resulted in a quicker elimination of the antibody (compare Fig. 26 with Fig. 35 and see next section) which weakened the hematotoxic potential of the bsAb with an active Fc portion.

4.5. Effect of CD47|PD-L1 BsAbs on the tumor immune microenvironment

In order to evaluate if the nature of immune responses triggered by CD47|PD-L1 bsAbs, I analyzed the major immune populations infiltrating the tumor microenvironment (TME) and the tumor draining lymph nodes (TdLNs). Flow cytometry analysis was performed at two time points, two days after the 1st antibody dose (early timepoint) and two days after the 3rd and last dose (late timepoint).

Tumor infiltrating macrophages (TAMs) are a heterogeneous population that can exert both anti-tumor and pro-tumor functions in the TME, depending on their polarization state (M1-like or M2-like,

respectively). I showed here an increase in macrophage infiltration following treatment with CD47|PD-L1 bsAbs, which was associated with enhanced polarization towards the M1-like phenotype (iNOS+, MHC II+ CD206-) and decreased M2-like phenotype (MHCII-, CD206-). This change was observed at the late timepoint in two different experiments. At the same time, I also observed a decrease in monocytes, which could represent a differentiation to macrophages or, alternatively, could just reflect reduced monocyte recruitment into the tumor.

DCs are key for the generation of anti-tumor adaptive immune responses following treatment with ICIs, anti-CD47 mAbs, or bsAbs [280], [287], [320], [324]. I observed a net decrease in DC infiltration in the treatment groups at the late timepoint. I speculated that this could reflect, at least in part, the migration of mature DCs to the tumor draining lymph nodes, but I was unable to confirm this hypothesis due to technical limitations. At the same time, the DCs remaining in the TME displayed an intriguing increase in the expression of the costimulatory receptor ligand CD86, associated with a decrease in CD80 expression. The latter may possibly be due to the recently described phenomenon of CTLA-4 mediated removal of CD80 by transendocytosis [32]. *In vivo* experiments have shown that PD-L1 interacts in cis with its' ligand CD80 on the surface of an APC protecting it from removal by transendocytosis [194], which can, in turn, be blocked with a PD-L1 mAb. It is therefore possible that the CD47|PD-L1 bsAbs indirectly induced CTLA-4 mediated transendocytosis of CD80 expressed at the surface of DCs and macrophages in the TME.

Cellular immunity and in particular CD8+ T cells are the ultimate effectors of immunotherapies [320], [324]. At the late timepoint, the treatment with the bsAbs resulted in an increase of the CD8+ T cells and the CD8+ T cells to Treg ratio, a feature commonly associated with an efficient anti-tumor response and a good prognosis in the clinic [354]. Based on the analysis cell surface markers, CD8+ T cells displayed a mixed signature, between activation and exhaustion, suggesting that the bulk of this T cell population in the TME may represent a pre-dysfunctional state. No specific changes were observed with regard to the CD4+ T cells subsets neither in the TME nor in the TdLNs.

To summarize, the treatment with both CD47|PD-L1 bsAbs induced changes corresponding to a more tumor-hostile immune microenvironment, such as an increase in macrophages skewed towards the M1-like phenotype, as well as an increase in CD8+ cell infiltration. My observations were therefore similar to those published by Chen et al. [324]. However, contrary to my experiments, Chen et al. were able to show distinct changes restricted to the bsAb treatment group as compared to the PD-L1 mAb group. In my TME analysis, most of the changes observed following bsAb treatment were also apparent in the PD-

L1 mAb group. I speculate that the generally similar antitumor efficacy of bsAbs and PD-L1 mAbs seen in the present study could account for the observed similarity in immune cell infiltrates.

4.6. Perspectives and conclusion

In this work, I investigated the antitumor efficacy and the mechanism of action of CD47|PD-L1 neutralizing bispecific antibodies. Over the course of my thesis, I generated several versions of bsAbs, differing in the affinities of the arms and the effector functions of the Fc region. I was eventually able to demonstrate a partial bsAb-induced tumor growth inhibition in the MC38 model, but failed to confirm the net superiority of the bispecific approach over PD-L1 mAb monotherapy, as shown by three recent studies [308], [320], [324].). Unfortunately, the bsAb generation took – for unanticipated technical reasons – considerably more time than planned, and the same could be said of the multiple and long-lasting unsuccessful attempts to set up and optimize *in vivo* protocols. As a consequence, the project timelines become very tight, and I was unable to complete the *in vivo* analysis of all the bsAbs I had generated. So, even though I could confirm antitumor activity with several of these CD47|PD-L1 bsAbs in the MC38 model, the accumulated data does not allow drawing robust and unambiguous conclusions as to the impact of the CD47 arm or the PD-L1 arm affinity, or the effect of Fc-mediated effector functions on bsAb antitumor efficacy. In this context, it would be particularly interesting to continue comparative *in vivo* studies with the various 6E8-based and the VS9-based bsAbs. That could shed more light on the importance of the affinities of individual bsAb arms and the effector functions of the Fc portion, both on the efficacy and on the pharmacokinetics of individual bispecific antibodies. In particular, it would be interesting to assess the role of the CD47 arm affinity in association with a potent PD-L1 arm and an active Fc portion, by comparing head-to head the 1E5|VS9 bsAb and the GD1|VS9 bsAb. I speculate that the latter should show a more restricted, more PD-L1-dependent CD47 binding pattern resulting in less CD47-mediated TMDD, superior PK and tumor exposure, which, in turn, might result in better anti-tumor efficacy. Such an inverse relationship between CD47 arm affinity and bsAb efficacy has already been described by Dheilly et al with CD47|hCD19 bsAbs and hCD19-expressing A20 tumors. [305]. It could be interesting to address the affinity-efficacy relationship with the currently available tools, in the context of PD-L1 expressed both in the TME, by tumor and non-tumor cells, and in the periphery.

The importance of the Fc part for the PD-L1 mAb PK I observed in the present study (the active Fc resulting in a shorter half-life) suggests a more significant contribution of PD-L1 to TMDD than initially

expected. Overall, our experience with the different mAbs and bsAbs we have tested in this study suggests that testing the antibody PK to in syngeneic models could be an important preliminary step for the establishment of a correct dose/treatment schedule for subsequent efficacy studies.

Provided a reliable *in vivo* protocol allowing for a convincing, reproductible efficacious treatment with CD47|PD-L1 bsAb could be established, a number of studies using these reagents could be attempted. To further extend the characterization of the mode of action of the CD47|PD-L1 bsAb we should try to evaluate the importance of PD-L1 expression on the tumor cells versus host cells, by using a PD-L1 KO tumor cell line. Studies with KO cell lines might help us to better understand which cell populations are important for the antitumor efficacy of CD47|PD-L1 bsAb.

The effect of the bsAb on the TME would also deserve further investigation. Given the complexity of the TME, not only with regards to the different populations but also their differentiation and activation profiles, a subsequent TME analysis would ideally be performed using “big data” approaches [369], such as single-cell RNA-seq [324]. Treatment-induced changes in immune cells infiltrating the tumor or the tumor periphery could even better be addressed by spatial transcriptomics [69]. Treatment-induced changes in DCs would be of particular interest, as this cell population expresses high levels of PD-L1 and CD47 and constitutes the key link between the innate and adaptive immunity [280], [320], [370]. Last but not least, tumor cell lines expressing chicken ovalbumin (OVA) together with OVA-specific CD8+ T cells from OT-I mice would allow for mechanistic studies potentially helpful for the understanding of antigen specific cross-presentation, CD8+ T cell activation and expansion as well as the generation of tumor specific memory T cell pool induced by CD47|PD-L1 bsAb treatment.

5. Material and methods

5.1. Antibodies generation

The bsAbs generated during my thesis are based on one heavy chain and two different light chains (one κ and on λ) with distinct antigen specificity. The isolation of the single chain variable fragments (scFvs) of the κ and λ arms was performed using proprietary phage display libraries in which all the library members have the same heavy chain variable domain (VH) and different variable light chain (VL).

Screening and selections

For each target arm, the antibody sequences were identified following the protocol described in [175]. Selection strategies were performed on κ and λ phage library pools on recombinant proteins or on mouse native cell lines, as well as a combination of both approaches. Screening was conducted by evaluating the binding and the blocking properties of scFvs on recombinant proteins, native cells line and transfected cells using the CellInsight™ CX5 HCS imaging platform (ThermoFisher) associated with the HCS Studio™ Cell Analysis Software. Positive hits were reformatted into hIgG1 monoclonal antibodies for characterization. In order to obtain an anti-PD-L1 arm of higher affinity, three phage-display libraries were generated in the lead optimization step by introducing diversity into the CDR1, CDR2, and/or CDR3 of the variable light chain region of the 1h6 sequence. Three libraries were used for phage-display selections under stringent conditions with 1, 0.1, or 0.01 nM of recombinant mPD-L1 protein (ACROBiosystems).

Reformatting mAbs

VL gene of selected sequences were cloned into vectors already containing the VH and CH domains. The selected insert was amplified by PCR and purified with the MiniElute Gel Extraction kit (Qiagen). Vector and insert were digested using the BsRDI restriction enzyme. Final vectors were transiently transfected into mammalian cells.

Reformatting bsAbs

The VL CL kappa chains and the VL CL lambda chains from the selected candidate were cloned into a vector which already contained the VH CH regions. The expression of the three antibody chains was driven by three-promoter vector. Final vectors were transiently transfected into mammalian cells. The random pairing and assembly of the heavy and the two light chains led to the secretion of two mAbs and one bispecific antibody (the κλ body).

Transfection and purification

Small scale transfection was performed in Transformed Human Embryo Kidney monolayer epithelial cells (PEAK cells; Edge Bio). Transfection conditions and bsAb purification are detailed in Fischer et al., [175]. For *in vivo* material, Chinese Hamster Ovary (CHO) cells were transiently transfected using the FectoCHO® expression system (Polyplus Transfection). Cell cultures were supplemented every 2-3 days with glucose (Sigma). After 13 days of culture, cell supernatants were harvested and filtered using the Sartoclear Dynamics Lab® (Satorius). A three steps ligand affinity chromatography was used to recover the bispecific antibodies as described in [175]. For the bsAbs mIgG2a, the MabSelectSure (GE Healthcare), the CaptureSelect LC-kappa (mouse) (ThermoFisher), the CaptureSelect LC-lambda (mouse) (ThermoFisher) were used successively. For the bsAb hIgG1, the MabSelectSure, the KappaSelect, the CaptoL affinity resins (GE Healthcare) were employed. The knobs-into-holes construct was purified with FcXL and CH1 resins (ThermoFisher). After the last step, κλ bodies were formulated into a 25 mM histidine, 125 mM NaCl, pH 6.0 buffer.

Analytics

After purification, antibodies were analyzed by electrophoresis with the Agilent Bioanalyzer 2100 (Agilent Technologies) in denaturing and reducing conditions. The aggregate and the fragment levels were determined by SEC-HPLC. The MCS-LAL kit (Charles River Laboratories) was used to assess the endotoxin level. Antibodies were stored at -80 °C until use.

Affinity measurement

The affinities for each target protein were measured on an Octet Red96 biolayer interferometry (BLI) system (ForteBio) as described in [175], [305]. The recombinant proteins used were mouse PD-L1 (ACROBiosystems, PD1-M5220) and mouse CD47 (in house).

5.2. Cell lines and reagents

Cells lines

CT26 (murine colon carcinoma), 4T1 (murine breast carcinoma), L1.2 (murine pre-B lymphoma), HEPA 1.6 (murine hepatocellular carcinoma) and B16F10 (murine melanoma) cells lines were obtained from ATCC (Wesel, Germany). CT26 and 4T1 cells were cultured in RPMI-1640 supplemented with 10% heat-inactivated fetal bovine serum (FBS) and 2mM L-Glutamine. L1.2 cells were cultured in RPMI supplemented with 10% heat-inactivated FBS, 2mM L-Glutamine, 10 mM 4-(2-hydroxyethyl)-1-

piperazineethanesulfonic acid (HEPES) and 50 µM 2-mercaptoethanol (Gibco). HEPA 1.6 cells were cultured in DMEM (high glucose) supplemented with 10% FBS (not heat-inactivated).. B16F10 cells were cultured in DMEM (high glucose) supplemented with 10% heat-inactivated FBS, 4mM L-Glutamine and 1 mM Sodium Pyruvate. MC38 (murine colon carcinoma) cell line was provided by Walter Reith (University of Geneva) and cultured in DMEM supplemented with 10% heat-inactivated FBS. Cells were maintained at 37 °C in a humidified atmosphere containing 5% CO_2. All cell lines were tested negative for mycoplasma contamination. All reagents were purchased from Sigma.

PEAK mouse PD-L1 (mPD-L1) and PEAK mouse CD47 (mCD47) were generated in our laboratory. Briefly, the full-length sequence of mouse PD-L1 or mouse CD47 were cloned into OriGene vectors that target the AAVS1 loci. Guide RNA vector and the donor vector were transfected into PEAK cells and gene of interest was knocked in by using clustered regularly interspaced short palindromic repeats (CRISPR)/Cas9 technology. The final stable pool of positive cells was established after puromycin selection and one step of cell sorting. Transfected cells were cultured in DMEM high-glucose supplemented with 10% heat-inactivated FBS and 2mM Glutamine. Selection was maintained by adding puromycin at 0.5 µg/mL (Sigma).

Control mAbs

Different anti-PD-L1 monoclonal antibodies have been described as blocking the PD-1/PD-L1 interaction. They were used as control mAbs in *in vitro* and in *in vivo* experiments. Anti-mouse PD-L1 10F.9G2 (rat IgG2b) was purchased from BioXCell. Atezolizumab, a high-affinity monoclonal anti-human PD-L1 therapeutic antibody, is cross-reactive to mouse PD-L1 and is able to block the mouse PD-1/PD-L1 interaction [327]. The anti-PD-L1 atezolizumab was cloned and produced in house as scFv and as mAb either with a mouse IgG2a or with a human IgG1 backbone. This “in-house” atezolizumab analog is described as atezolizumab in the results sections. For the *in vivo* experiments, the anti-CD47 mAb MIAP301 (rat IgG2a) was purchased from BioXCell.

5.3. Syngeneic mouse models

Mice

Six- to eight-week-old female BALB/c mice were purchased from Charles River Laboratories (France). Six- to eight-week-old female C57BL/6 mice were obtained from Charles River (Italy or Germany) and Janvier laboratories (France). The animals were kept under conventional conditions in a temperature-controlled room under a 12-hour light/dark cycle. All animal experiments were performed in accordance

with the Swiss Federal Veterinary Office guidelines and as authorized by the Cantonal Veterinary Office. For the comparison of different engraftment protocols all the mice were coming from the same provider and were engrafted with the same batch of cells at the same day.

In vivo efficacy experiment

Cells were cultured as described above and resuspended in PBS at the desired concentration before injection. Mice were anesthetized either with isoflurane or with a mix of xylazine/ketamine depending on the engraftment technique. According to the experimental design the injection site was either the thoracic part or the back of the host mice and the depth of the engraftment varied. Tumor cells were injected subcutaneously in a volume of 100 µL and the number of injected cells is indicated in each figure. Tumors were allowed to grow for different periods of time as indicated in each experimental design. Tumors were measured every 2-3 days using a digital caliper and volumes were calculated using the formula: length x width^2 x 0.5. At the day of the recruitment, mice were randomized according to their tumor volume to obtain different treatment groups with similar mean tumor volume and standard deviation. The treatment frequency as well as the concentration used for each antibody are indicated in each figure's legend. All antibodies were diluted in PBS at either 10 mg/kg or 20 mg/kg and administered intraperitoneally (i.p.). Mice were euthanized when the tumor volume exceeded 1000 mm^3 or when the mice reached the endpoint criteria.

Tumor microenvironment analysis

Mice were euthanized by CO_2 at indicated time and tumors and tumor-draining lymph nodes (TdLNs) were harvested for immune cell infiltration flow cytometry analysis. Tumors and tumor-draining lymph nodes were cut with scissors and digested with a mix of collagenase D and DNAse I (Roche) in RMPI medium completed with 1% of FBS for 30 min at 37 °C. After digestion, lysates were processed through a 70 µm cell strainers (BD Falcon™). Dead cells and RBCs were removed from tumor digested samples using lympholyte M (Cedarlane Laboratory).

Single-cell suspensions were stained to identify the major myeloid and lymphoid subsets with the different panels. Cells were counted and 2 x 10^6 cells per sample were plated in a V bottom 96 well plate. Cells were incubated with Mouse BD Fc Block™ for 10 min at 4 °C. Surface staining was directly performed with antibodies and the viability dye resuspended in PBS in the dark for 20 min at 4 °C. Intracellular stainings were performed using the eBioscience™ Foxp3 / Transcription Factor Staining Buffer set (ThermoFisher). Cells were then washed with FACS buffer (PBS, 2% BSA) and resuspended in fixation buffer for 15 min at room temperature in the dark before intracellular staining. Cells were washed with

permeabilization buffer and antibodies for intracellular staining were resuspended in permeabilization buffer. Plates were incubated for 45 min at room temperature and protected from light. Cells were washed once with permeabilization buffer and twice with FACS buffer. For intracellular cytokines analyses, cells were restimulated for 4 hours at 37 °C and in complete RPMI medium in the presence of phorbol 12-myristate 13-acetate (Sigma; 100 ng/mL) and ionomycin (Sigma; 1 mg/mL) and golgi block. Data were acquired with a BD LSR Fortessa (BD Biosciences) instrument and were analyzed with FlowJo software (TreeStar). Antibodies used for extracellular and intracellular staining are listed below.

Marker	Fluorochrome	Manufacturer	Reference
CD11b	BV605	Biolegend	101237
CD11b	SB702	eBioscience	67-0112-82
CD11c	BUV737	BD Biosciences	612796
CD19	FITC	eBioscience	11-0193-82
CD206	APC	Biolegend	141707
CD4	BUV737	BD Biosciences	612761
CD4	BUV737	BD Biosciences	612761
CD44	PB	Biolegend	103020
CD45	BUV395	BD Biosciences	564279
CD47	BV650	BD Biosciences	740536
CD62L	BV510	Biolegend	104441
CD68	BV421	Biolegend	137017
CD69	APC	eBioscience	17-0691-82
CD80	PerCp710	eBioscience	46-0801-82
CD86	PE Cy7	Biolegend	105014
CD8a	PE Cy7	eBioscience	25-0081-82
CD8a	AF700	Invitrogen	56-0081-82
CTLA-4	PEe610	eBioscience	61-1522-82
F4/80	PEe610	eBioscience	61-4801-82
Foxp3	PE	eBioscience	12-5773-82
GranzB	PB	Biolegend	515408
IFNγ	BV786	Biolegend	505838

iNOS	PE	eBioscience	12-5920-82
Ki67	FITC	Invitrogen	11-5698-82
Ly6C	BV510	Biolegend	128033
Ly6G	BV605	Biolegend	127639
MHCII	AF700	Biolegend	107622
NK1.1	PEe610	eBioscience	61-5941-82
PD1	PerCp5.5	Biolegend	109119
PD-L1	APC	Biolegend	124312
PD-L1	SB780	eBioscience	78-5982-82
TCRβ	BV711	BD Biosciences	563135
TCRβ	BV510	Biolegend	109234
Tim3	PE Cy7	Invitrogen	25-5870-80
TNFα	Percp710	eBioscience	46-7321-80
viability	APC Cy7	BD Biosciences	565388

Table I: Antibodies and viability dye used for immunophenotyping analyses.

5.4. Flow cytometry

For all binding testing data were acquired on the CytoFLEX S flow cytometer (Beckman Coulter) and analyzed using FlowJo software (Tree Star).

Binding assays

To compare binding of bsAb, mAbs and monovalent control antibodies in dose-range experiments, increasing concentrations of test antibodies were incubated with 2 x 10^5 cells/well) in V bottom 96-well plates for 20 min at 4 °C in FACS buffer. Antibody-bound cells were then washed twice and stained for 20 min at 4 °C with the appropriate secondary antibody. After two washes with FACS buffer, cells were resuspended in FACS buffer (PBS, 2% BSA) and sytox blue (ThermoFisher) was added before acquisition to exclude dead cells from analysis. All the antibodies used for the *in vitro* characterization are hIgG1 with no mutation in the Fc portion. The antibodies generated with the inactive Fc portion showed results similar to their Fc active counterparts (data not shown).

Quantification of cell surface receptor density

PD-L1 and CD47 expression was determined with QIFIKIT (Dako K0078) according to the manufacturer's instructions. Atezolizumab mIgG2a mAb and high affinity anti-CD47 mIgG2a mAb

produced at Novimmune were used for testing. In order to modulate the PD-L1 cell surface expression, cell culture medium was supplemented with 40ng/mL of mouse IFN-γ (R&D Systems) 24 or 48 hours before staining.

Antibody selectivity

To assess antibody selectivity, WT cells were stained with Cell Trace Violet at 1 µM (Invitrogen) and mixed with cells KO either for mPD-L1 or for mCD47 in a ratio 1:1. Increasing concentrations of test antibodies in FACS buffer (PBS, 2% BSA) were incubated with the mix of cells (2 x 10^5 cells/well) in a 96-well-plate for 20 min at 4 °C. Cells were then washed and stained with an anti-human labeled IgG detection antibody AF647 (Jackson ImmunoResearch, 109-606-170) for 20 min at 4 °C. After two washes with FACS buffer, cells were resuspended in FACS buffer (PBS, 2% BSA) and sytox orange (ThermoFisher) was added before acquisition to exclude dead cells from analysis.

Binding to RBC

For RBC binding, whole blood from C57BL/6 was collected in heparinized EDTA tube and red blood cells were isolated after three steps of centrifugation and washing with PBS. The purified RBCs (3 x 10^5 cells) were incubated with test antibodies diluted for 20 min in FACS buffer (PBS, 2% BSA) in a 96-well-plate, washed once with FACS buffer and stained with an anti-human labeled IgG detection antibody (Jackson Immunoresearch 109-606-170) for 20 min. Cells were then washed two times in FACS buffer and antibody binding was measured.

5.5. CD47/SIRPα blocking assay

mCD47 positive cell suspensions were prepared and resuspended in PBS at a concentration of 1.5 x 10^6 cells /mL. Cells were stained with Cell Trace Violet at 1 µM (ThermoFischer) and incubated for 20 min at 37 °C. Cell concentration was then adjusted at 1.5 x 10^5 cells/mL in FACS buffer (PBS, 2% BSA) and cells were dispensed into 384-well clear-bottom plates (Corning) at 3000 cells per well (20 µL/well). 50 µL of increasing concentration of antibodies of interest were added to the cells and incubated for 1 hour at room temperature. In parallel, the blocking buffer was prepared by mixing one volume of recombinant SIRPα with 2 volumes of detection reagent (table below), Alexa Fluor 647-conjugated IgG Fc (Jackson Immunoresearch, 109-606-170). Different recombinant SIRPα proteins and detection were used (listed in the table below). 30 µL of this mixture were added in each well and the incubation continued for 3 hours at room temperature and protected from light. Binding of the soluble recombinant SIRPα to cells was

detected using the CellInsight™ CX5 HCS imaging platform (ThermoFisher) associated with the HCS Studio™ Cell Analysis Software. The blockade of the SIRPα binding by competing antibodies resulted in a decrease in fluorescence signal.

Rec. protein	Manufacturer	Reference	Detection	Manufacturer	Reference
mouse SIRPα HIS Tag	Sino Biological	50956-M08H	Penta HIS AF647	Quiagen	35370
mouse SIRPα mouse Fc	ACROBiosystems	SIA-M5252	anti-mFc AF647	Jackson ImmunoResearch	109-606-170
mouse SIRPα human Fc	ACROBiosystems	SIA-M5258	anti-hFc AF647	Jackson ImmunoResearch	115-605-008

Table II: SIRPα proteins and detections used in the blocking assay.

5.6. PD-1/PD-L1 blocking assay

On PEAK mouse PD-1

The PD-1/PD-L1 assay measures the binding of a fluorescently labelled PD-L1 protein at the surface PEAK cells expressing PD-1. Dose-response of anti-PD-L1 antibodies were diluted in PBS and mixed with the detection buffer containing the mouse PD-L1 biotinylated protein (produced in house) and streptavidin-AF750 (Invitrogen™). This mix was left for 1 hour incubation at room temperature and in the dark. In the meantime, PEAK mouse PD-1 cells were resuspended in PBS at a concentration of 1.5 x 10^6 cells /mL. Cells were stained with Cell Trace Violet at 1 µM (ThermoFischer) and incubated for 20 min at 37 °C. Cell concentration was then adjusted at 1 x 10^5 cells/mL in FACS buffer (PBS, 2%BSA) and cells were dispensed into 384-well clear-bottom plates (Corning) at 3000 cells per well (30 µL/well). 70 µL of the antibodies-detection mix was added in each well and the incubation continued for 2 hours at room temperature and protected from light. Binding of the soluble recombinant SIRPα to cells was detected using the CellInsight™ CX5 HCS imaging platform (ThermoFisher) associated with the HCS Studio™ Cell Analysis Software. Positive signal was measured in the absence of IgG or in the presence of a non-blocker antibody.

On PEAK mouse PD-L1 and on mouse native cell lines

The PD-1/PD-L1 assay measures the binding of a fluorescently labeled PD-1 protein at the surface of the cells expressing PD-L1. In the presence of an antibody that blocks the PD-1/PD-L1 interaction, the labelled PD-1 protein cannot bind, and no signal is measured. This assay requires the use of cells that highly expressed PD-L1 in order to obtain a strong PD-1 binding signal. *In vitro*, human PD-1 can bind to

mouse PD-L1 with a similar affinity as mouse PD-1 to mouse PD-L1 [327], [371], [372]. The high affinity human PD-1 described by Maute et al., [372] showed stronger enhanced binding on mouse PD-L1 positive cells compared to wild type mouse PD-1 (in house data and [372]). This high affinity human PD-1 was produced in house with a human IgG1 and a mouse IgG1 backbone and was used on mouse native cell lines induced with IFN-γ.

PEAK mouse PD-L1 or mouse native cells activated wit IFN-γ suspensions were prepared and resuspended in PBS at a concentration of 1.5 x 10^6 cells /mL. Cells were stained with Cell Trace Violet at 1 µM (ThermoFischer) and incubated for 20 min at 37 °C. Cell concentration was then adjusted at 1 x 10^5 cells/mL in FACS buffer (PBS, 2% BSA) and cells were dispensed into 384-well clear-bottom plates (Corning) at 3000 cells per well (30 µL/well). 50 µL of increasing concentration of antibody of interest were added to the cells and incubated for 30 min at room temperature. In parallel, the blocking buffer was prepared by mixing the recombinant PD-1 protein and the detection reagent. Different recombinant PD-1 proteins and detection antibodies were used (listed in the table below). 30 µL of this mixture were added in each well and the incubation continued for 2h at room temperature and protected from light. Binding of the soluble recombinant PD-1 to cells was detected using the CellInsight™ CX5 HCS imaging platform (ThermoFisher) associated with the HCS Studio™ Cell Analysis Software. Positive signal was measured in the absence of IgG or in the presence of a non-blocker antibody.

Rec. protein	Manufacturer	Reference	Detection	Manufacturer	Reference
mouse PD-1 human Fc	RD system	1021-PD	anti-hFc AF647	Jackson ImmunoResearch	109-606-170
human PD-1 human Fc	RD system	1086-PD	anti-hFc AF647	Jackson ImmunoResearch	109-606-170
hPD-1 high affinity human Fc	in house	NA	anti-hFc AF647	Jackson ImmunoResearch	109-606-170
hPD-1 high affinity mouse Fc	in house	NA	anti-mIgG1 Fc AF647	Jackson ImmunoResearch	115-605-205

Table III: PD-1 proteins and detections used in the blocking assay

5.7. Evaluation of blood parameters and bsAb concentrations in serum

Blood parameters as well the persistence of the antibody in the plasma of treated mice was evaluated at different time points. Briefly, mice were bled at the indicated timepoints in each experiment

and blood cell count was analyzed with the ProCyte Dx Haematology analyzer (IDEXX Laboratories, Inc., ME, USA). After centrifugation of the blood samples, the antibody concentrations in the plasma were determined using the FastELYSA system (RD-Biotech) according to the manufacturer instructions.

5.8. Statistics

GraphPad Prism (GraphPad Software, CA, USA) was used for all statistical analysis and detailed analysis are specified under each graph.

5.9. Illustrations

All the illustrations in the figures were created with BioRender.com

6. Appendices

A

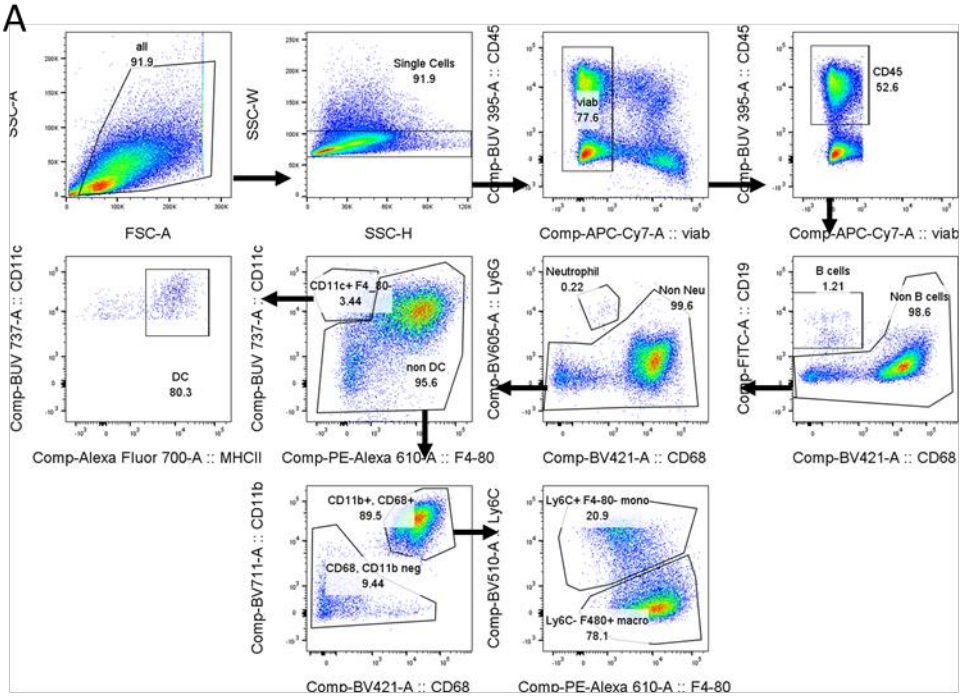
all
91.9
FSC-A
SSC-A
Single Cells
91.9
SSC-H
SSC-W
viab
77.6
Comp-APC-Cy7-A :: viab
Comp-BUV 395-A :: CD45
CD45
52.6
DC
80.3
Comp-Alexa Fluor 700-A :: MHCII
Comp-BUV 737-A :: CD11c
CD11c+ F4_80-
3.44
non DC
95.6
Comp-PE-Alexa 610-A :: F4-80
Neutrophil
0.22
Non Neu
99.6
Comp-BV421-A :: CD68
Comp-BV605-A :: Ly6G
B cells
1.21
Non B cells
98.6
Comp-FITC-A :: CD19
CD11b+, CD68+
89.5
CD68, CD11b neg
9.44
Comp-BV711-A :: CD11b
Ly6C+ F4-80- mono
20.9
Ly6C- F480+ macro
78.1
Comp-BV510-A :: Ly6C

B

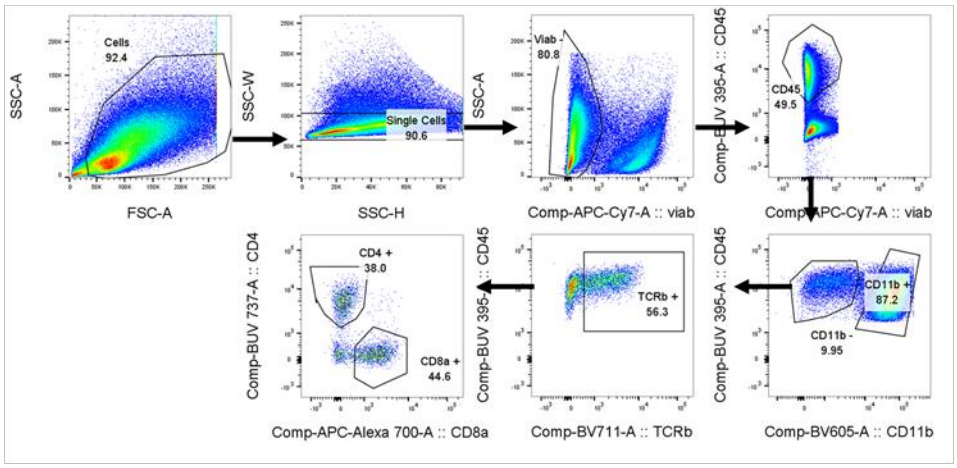
Cells
92.4
FSC-A
SSC-A
Single Cells
90.6
SSC-H
SSC-W
Viab -
80.8
Comp-APC-Cy7-A :: viab
SSC-A
CD45
49.5
Comp-BUV 395-A :: CD45
CD4 +
38.0
CD8a +
44.6
Comp-APC-Alexa 700-A :: CD8a
Comp-BUV 737-A :: CD4
TCRb +
56.3
Comp-BV711-A :: TCRb
CD11b +
87.2
CD11b -
9.95
Comp-BV605-A :: CD11b

C

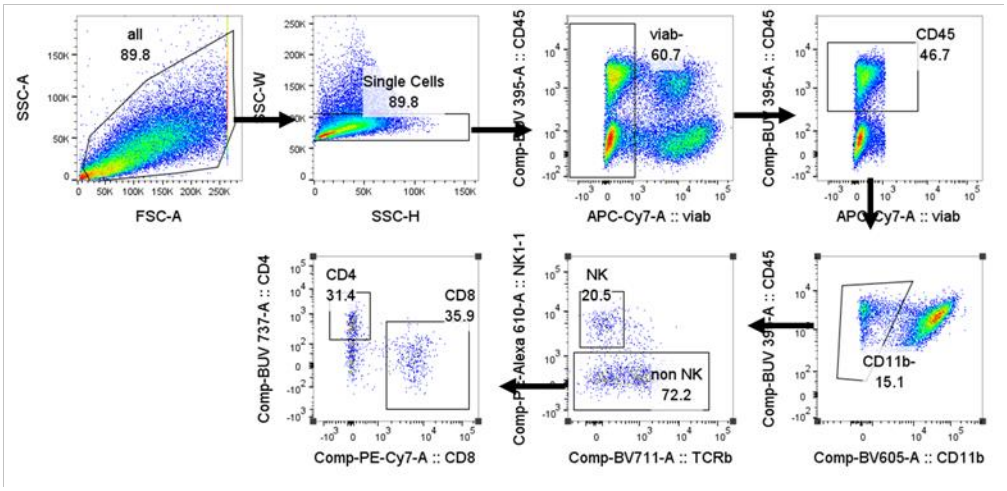
all
89.8
FSC-A
SSC-A
Single Cells
89.8
SSC-H
SSC-W
viab-
60.7
APC-Cy7-A :: viab
Comp-BUV 395-A :: CD45
CD45
46.7
CD4
31.4
CD8
35.9
Comp-PE-Cy7-A :: CD8
Comp-BUV 737-A :: CD4
NK
20.5
non NK
72.2
Comp-BV711-A :: TCRb
Comp-PE-Alexa 610-A :: NK1-1
CD11b-
15.1
Comp-BV605-A :: CD11b

Supplemental Figure S1: Gating strategy to identify the main infiltrating leucocyte populations in tumors. Single-cells suspensions were prepared from tumors of control and treated mice. After exclusion of debris, doublets, and dead cells, immune cells were isolated by gating on the CD45+ group. (A) Sequential gating strategy was used to identify to the main myeloid subsets: B cell (CD19+), neutrophils (Ly6G+), DCs (CD11c+ MHCII+), monocytes (CD11b+ CD68+ Ly6C+), macrophages (CD11b+ CD68+ F4/80^{pos}). (B) Sequential gating strategy was used to identify the T cell subsets: T cells (TCRβ+), subsequently split depending on CD8+ or CD4+ expression. Exhaustion and activation makers were analyzed for each T cell subsets. (C) Proliferative and cytokine production capacity of T cells subsets were analyzed following a unspecific *ex vivo* stimulation with PMA/ionomycin. Sequential gating strategy was used to identify NK cells (NK1-1), and T cells subsets (CD8+ or CD4+ subsets). Antibody list for each panel is described in the material and methods.

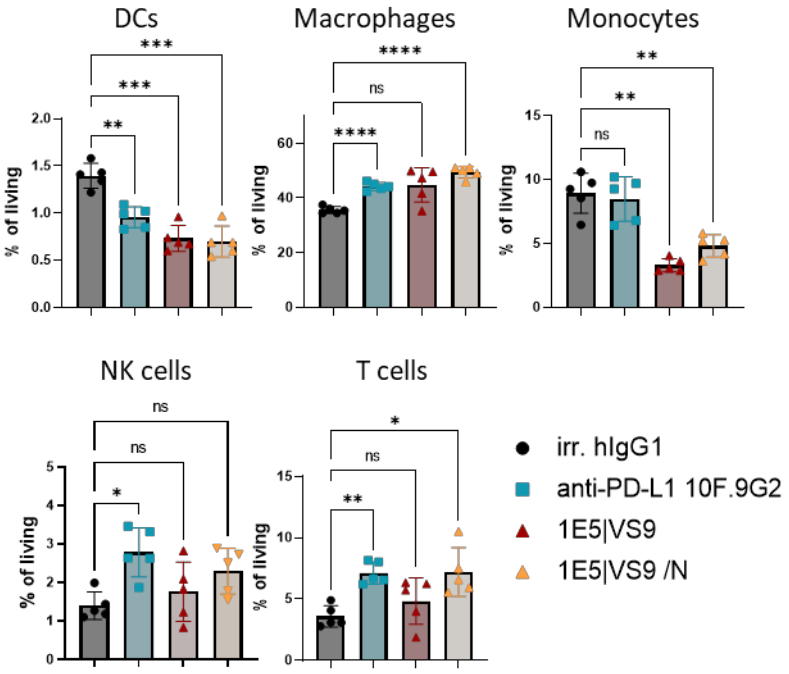

Supplemental Figure S2: Lymphoid and myeloid populations in the TME showed major changes in response to treatment. Proportion of the dendritic cells (DCs), macrophages, monocytes, natural killer (NK) cells and T cells among living cells. n.s., not significant, *P<0.05, **P<0.01, ***P<0.001, ****P<0.0001 were obtained using the Brown-Forsythe and Welch ANOVA with Dunnett's method for multiple comparisons correction. Values are displayed as mean ± SD.

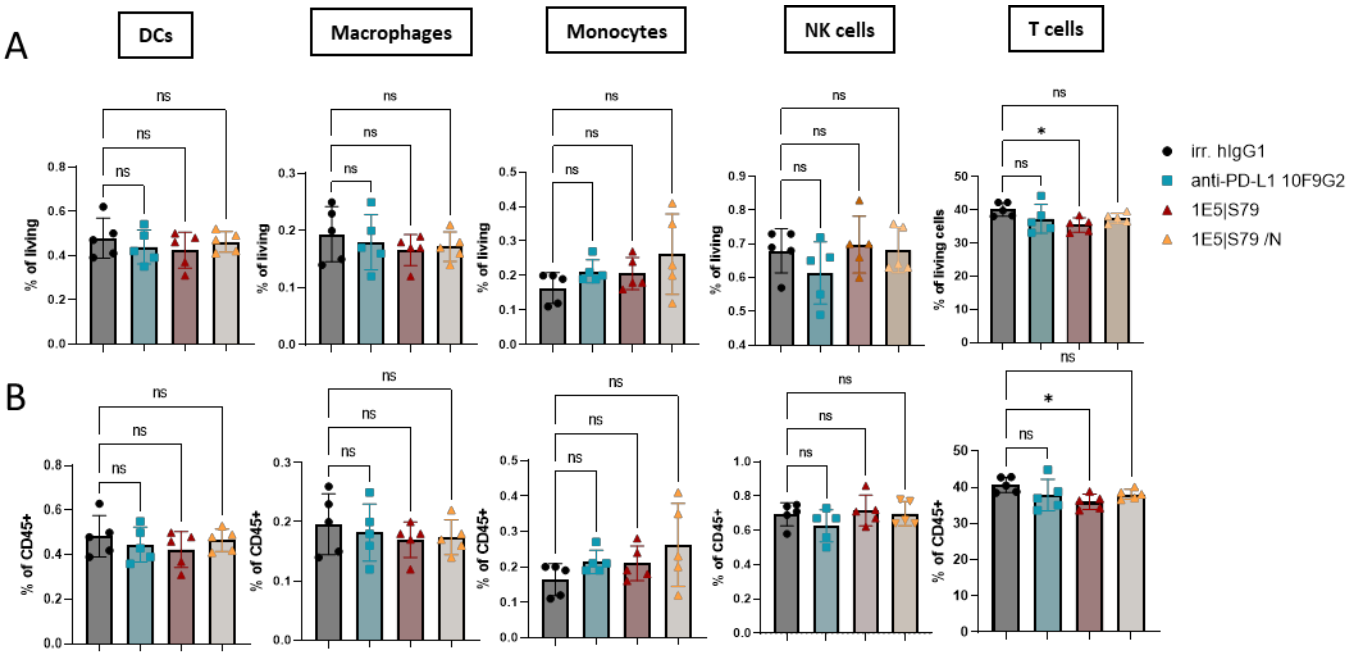

Supplemental Figure S3: Lymphoid and myeloid populations in the TdLN did not change in response to treatment. (A) Proportion of the main immune subgroups among (A) living cells and (B) immune cells (CD45+). n.s., not significant, *P<0.05, were obtained using the Brown-Forsythe and Welch ANOVA with Dunnett's method for multiple comparisons correction. Abbreviations: dendritic cells (DCs), natural killer (NK) cells. Values are displayed as mean ± SD.

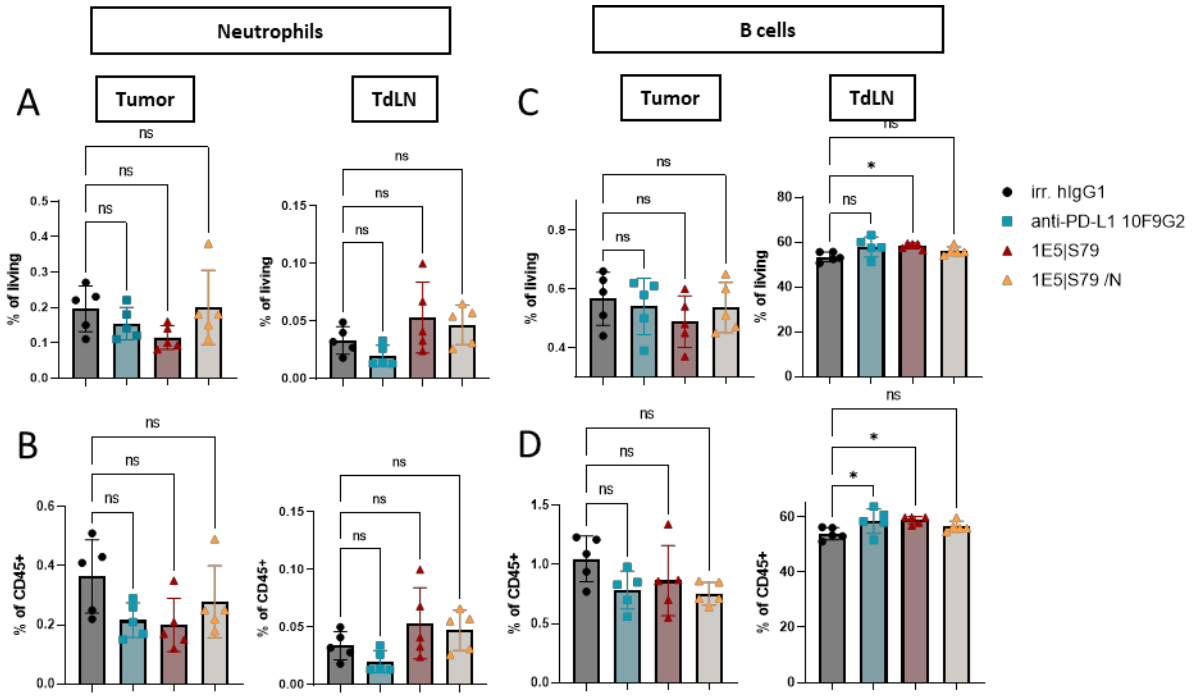

Supplemental Figure S4: B cells and neutrophils populations in the tumors and in the tumor draining lymph nodes showed no changes in response to the treatment. (A-B) Proportion of neutrophils in tumor and TdLN among (A) living cells and (B) immune cells (CD45+). (C-D) Proportion of B cells in tumor and TdLN among (C) living cells and (D) immune cells (CD45+). n.s., not significant, *P<0.05, were obtained using the Brown-Forsythe and Welch ANOVA with Dunnett's method for multiple comparisons correction. Values are displayed as mean ± SD.

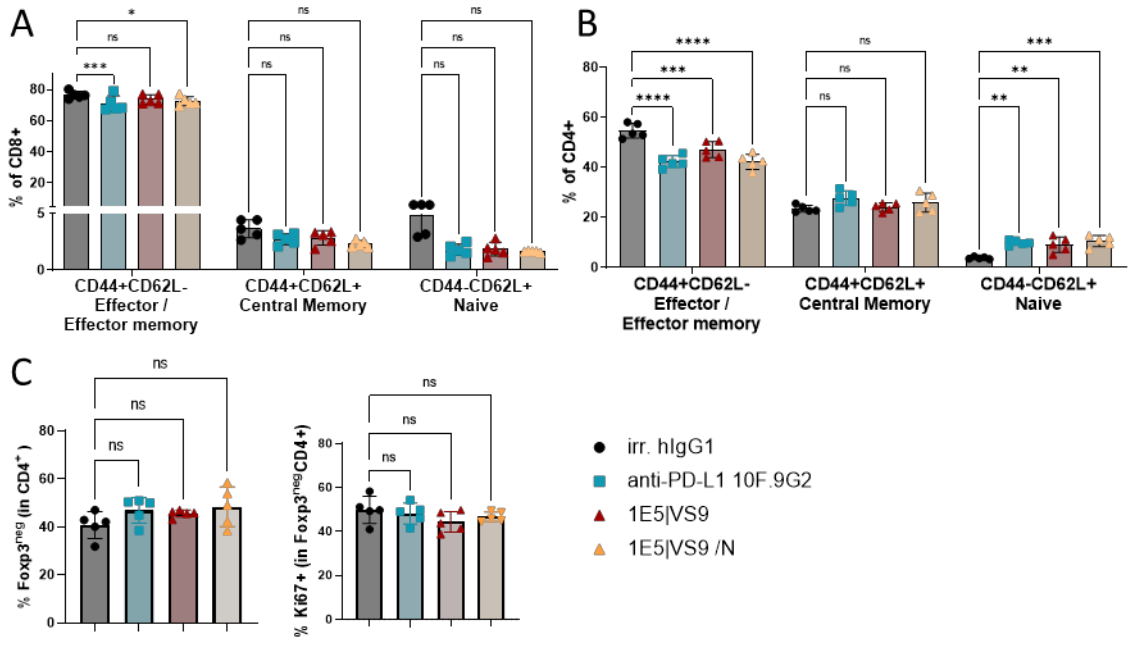

Supplemental Figure S5: CD8+ and CD4+ T cells subset in MC38 tumors following treatment with bsAbs and PD-L1. (A) Analysis of the T cells subsets among CD8+ T cells. (B) Proportion of Foxp3^{neg} CD4+ T cells and analysis of their proliferative capacity (Ki67+). (C) Analysis of the T cells subsets among CD4+ T cells. n.s., not significant, *P<0.05, **P<0.01, ***P<0.001, ****P<0.0001 were

obtained using the Brown-Forsythe and Welch ANOVA with Dunnett's method for multiple comparisons correction. Values are displayed as mean ± SD.

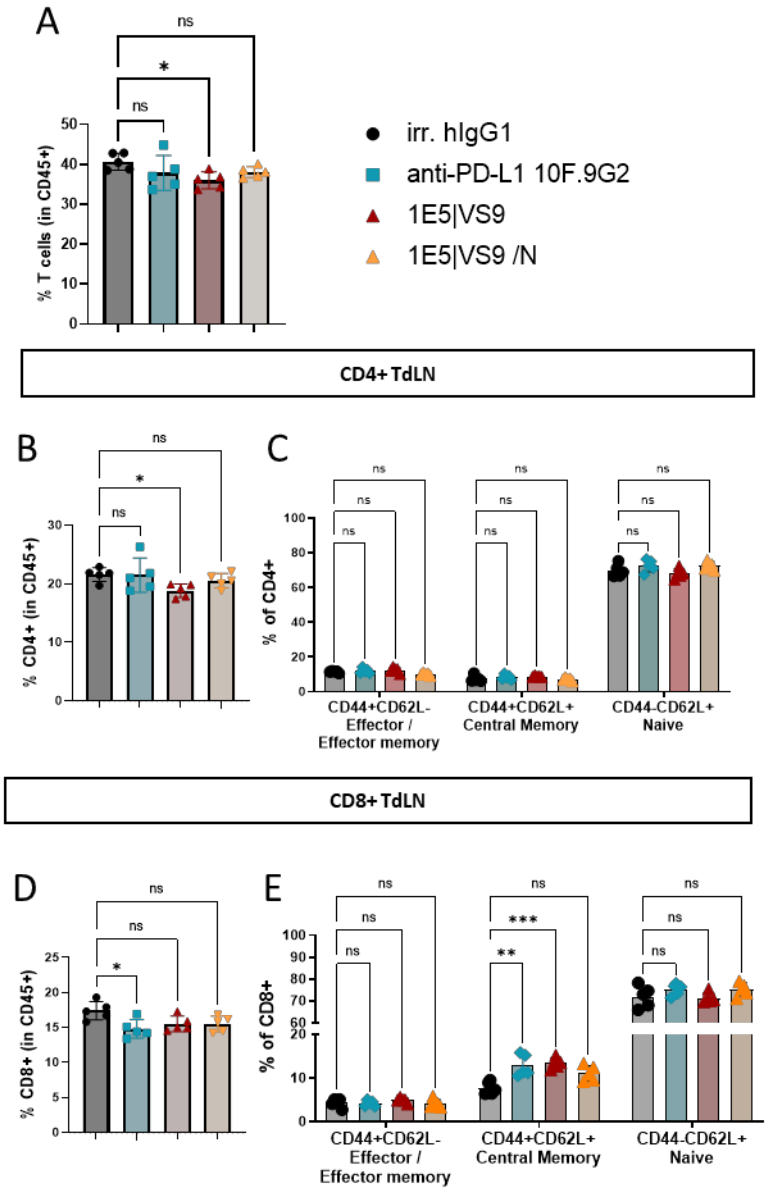

Supplemental Figure S6: T cells subset in TdLN following treatment with bsAbs and PD-L1. (A) Proportion of total T cells among CD45+ cells. (B) Proportion of CD4+ among CD45+ and (C) proportion of different subsets among CD4+ T cells (D) Proportion of CD8+ among CD45+ and (E) proportion of different subsets among CD8+ T cells. n.s., not significant, *P<0.05, **P<0.01, ***P<0.001 were obtained using the Brown-Forsythe and Welch ANOVA with Dunnett's method for multiple comparisons correction. Values are displayed as mean ± SD.

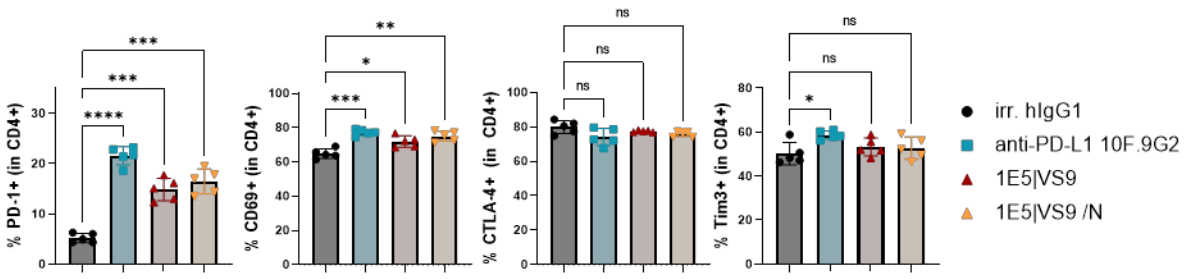

Supplemental Figure S7: Analysis of activation and exhaustion markers on CD4+ in MC38 tumor after *ex vivo* restimulation. Proportion of PD-1+, CD69+, CTLA-4+ positive cells among CD4+ T cells. *P<0.05, **P<0.01, ***P<0.001, ****P<0.0001 were obtained using the Brown-Forsythe and Welch ANOVA with Dunnett's method for multiple comparisons correction. Values are displayed as mean ± SD.

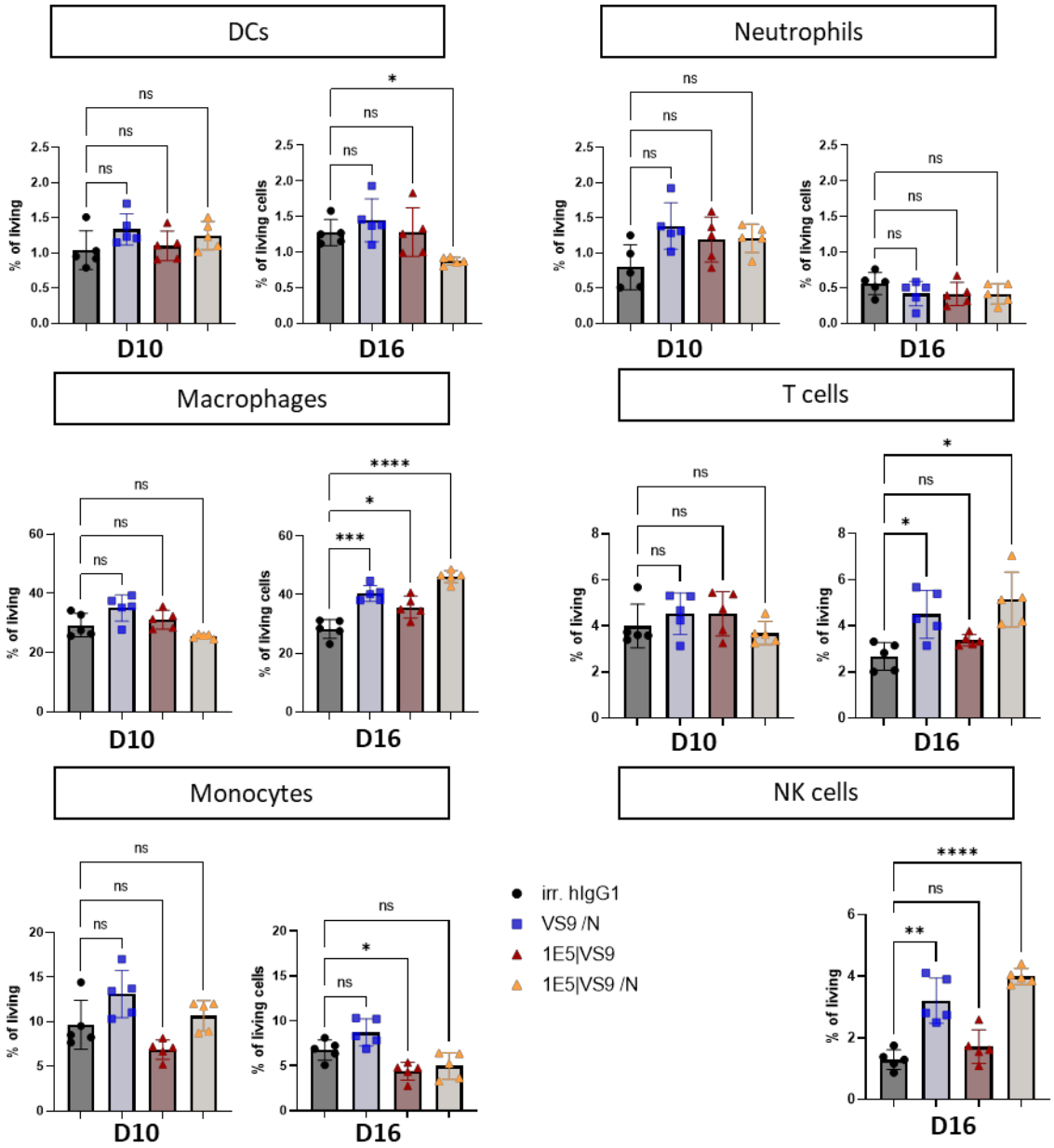

Supplemental Figure S8: Analysis of myeloid and lymphoid populations in the TME following treatment with bsAbs and anti-PD-L1. Proportion of the main immune subgroups among living cells on day 10 and day 16. Values are displayed as mean ± SD. n.s., not significant *P<0.05, **P<0.01, ***P<0.001, ****P<0.0001 were obtained using the Brown-Forsythe and Welch ANOVA Dunnett's method for multiple comparison correction. NK cells data for D10 were not available due to a technical issue.

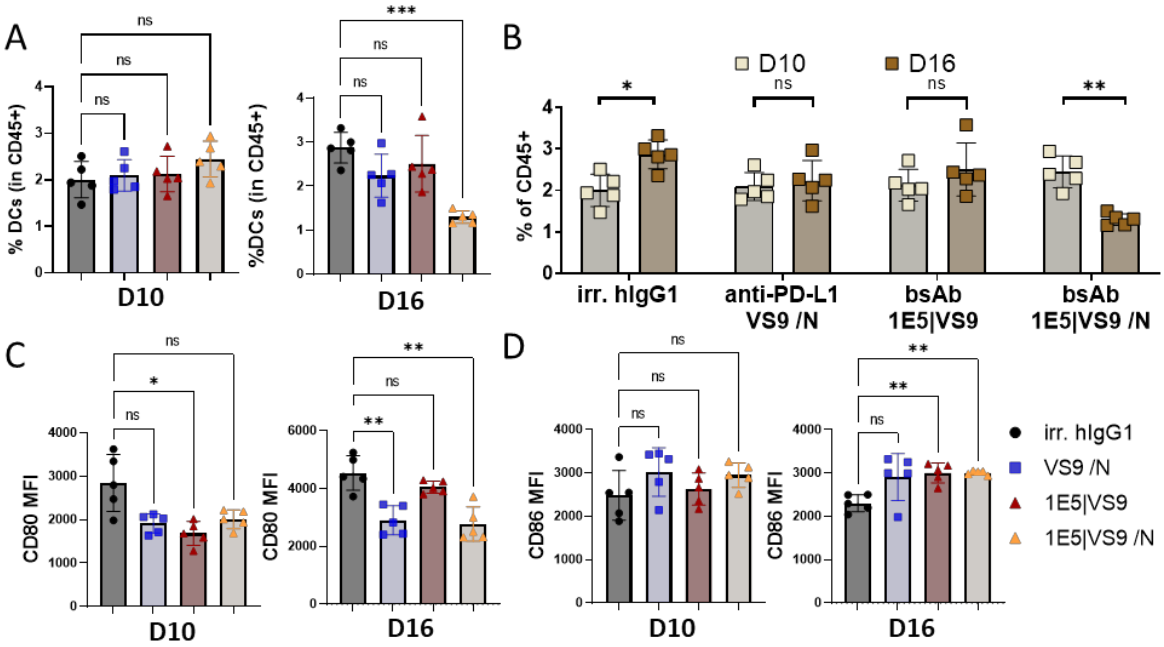

Supplemental Figure S9: DC characterization in MC38 tumors following treatment with bsAbs and anti-PD-L1.. (A) Comparison of proportion between groups at a given time point. B) Comparison of proportion within groups between time points. (C) CD80 and (D) CD86 MFI were measured on DCs on day 10 and day 16. n.s., not significant, *P<0.05, **P<0.01 were determined using the Brown-Forsythe and Welch ANOVA with Dunnett's method for multiple comparison correction except for panel B, where they were determined by one-tailed non-parametric Mann-Whitney U t-test. Values are displayed as mean ± SD.

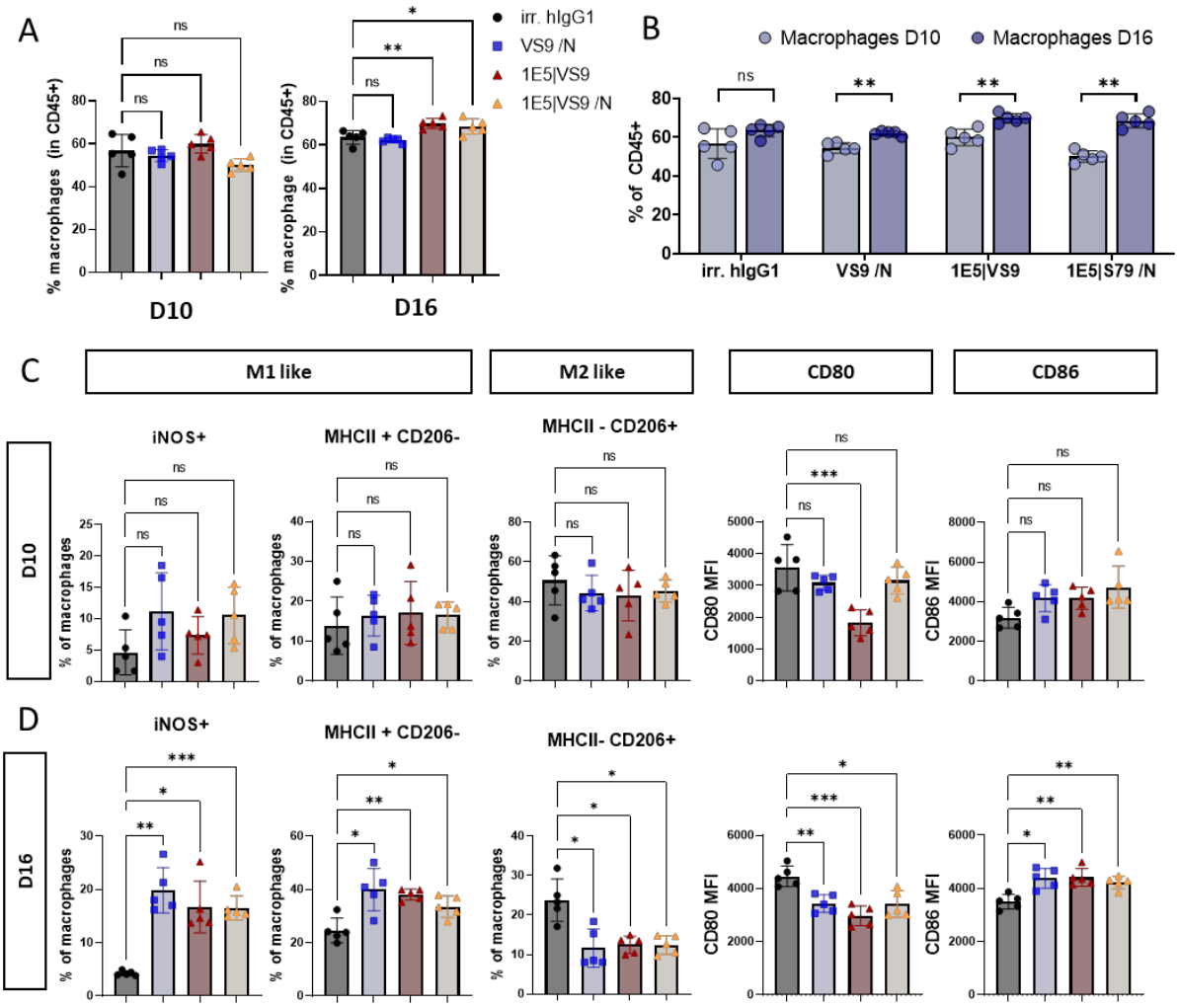

Supplemental Figure S10: Macrophage characterization in MC38 tumors following treatment with bsAbs and anti-PD-L1. (A) Comparison of proportion between groups at a given timepoint. (B) Comparison of proportion within groups between timepoints. (C-D) Proportion of iNOS+, MHCII+CD206-, MHCII-CD206+ macrophages and CD80 and CD86 MFI were measured on (C) day 10 and (D) day 16. n.s., not significant, *P<0.05, **P<0.01 were determined using the Brown-Forsythe and Welch ANOVA Dunnett's method for multiple comparison correction except for panel B, where they were determined by one-tailed non-parametric Mann-Whitney U t-test. Values are displayed as mean ± SD.

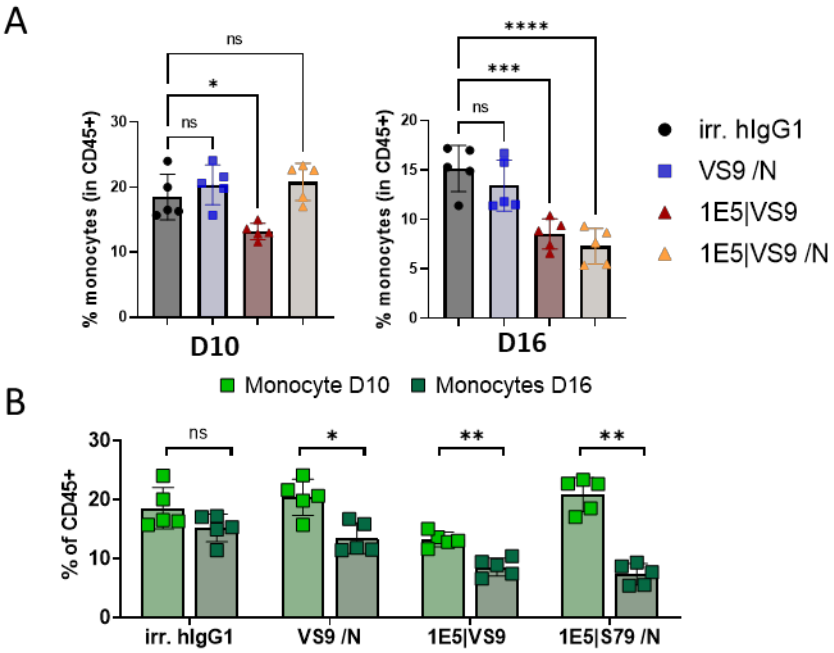

Supplemental Figure S11: Monocytes in MC38 tumors following treatment with bsAbs and anti-PD-L1. (A) Comparison between groups at a given timepoint. (B) Comparison between timepoints. n.s., not significant, *P<0.05, **P<0.01, ***P<0.001, ****P<0.0001 were obtained using the Brown-Forsythe and Welch ANOVA Dunnett's method for multiple comparison correction for panel (A) while for panel (B), where they were determined by one-tailed non-parametric Mann-Whitney U t-test. Values are displayed as mean ± SD.

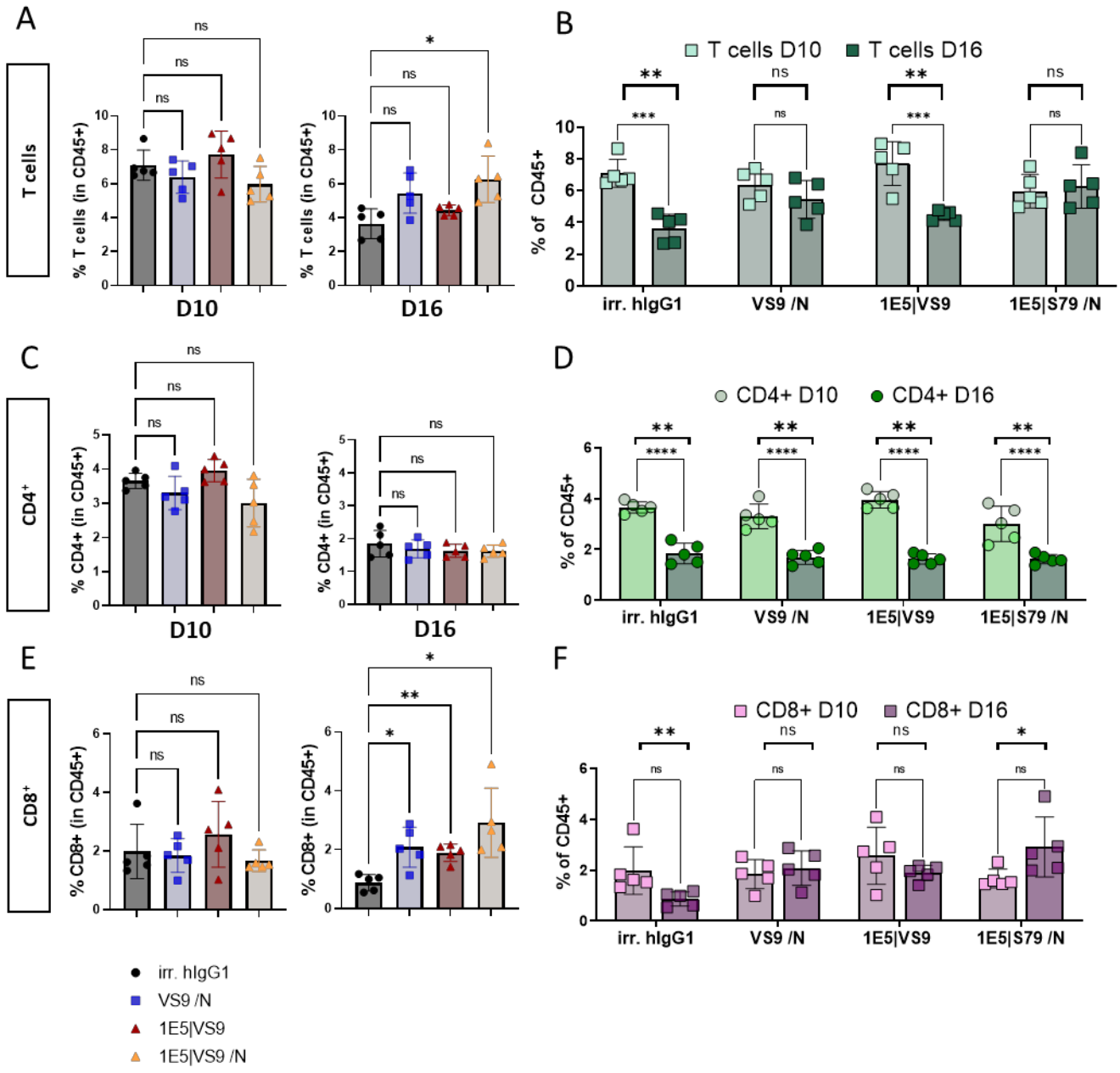

Supplemental Figure S12: T cells in MC38 tumors following treatment with bsAbs and anti-PD-L1. (A) Comparison between groups of (A) T cells, (C) CD4+ and (E) CD8+ subsets at a given timepoint. Comparison of (B) T cells, (D) CD4+ and (F) CD8+ T cells subsets within a group between timepoints. n.s., not significant, *P<0.05, **P<0.01, ***P<0.001, ****P<0.0001 were obtained using the Brown-Forsythe and Welch ANOVA with Dunnett's method for multiple comparison correction. Values are displayed as mean ± SD.

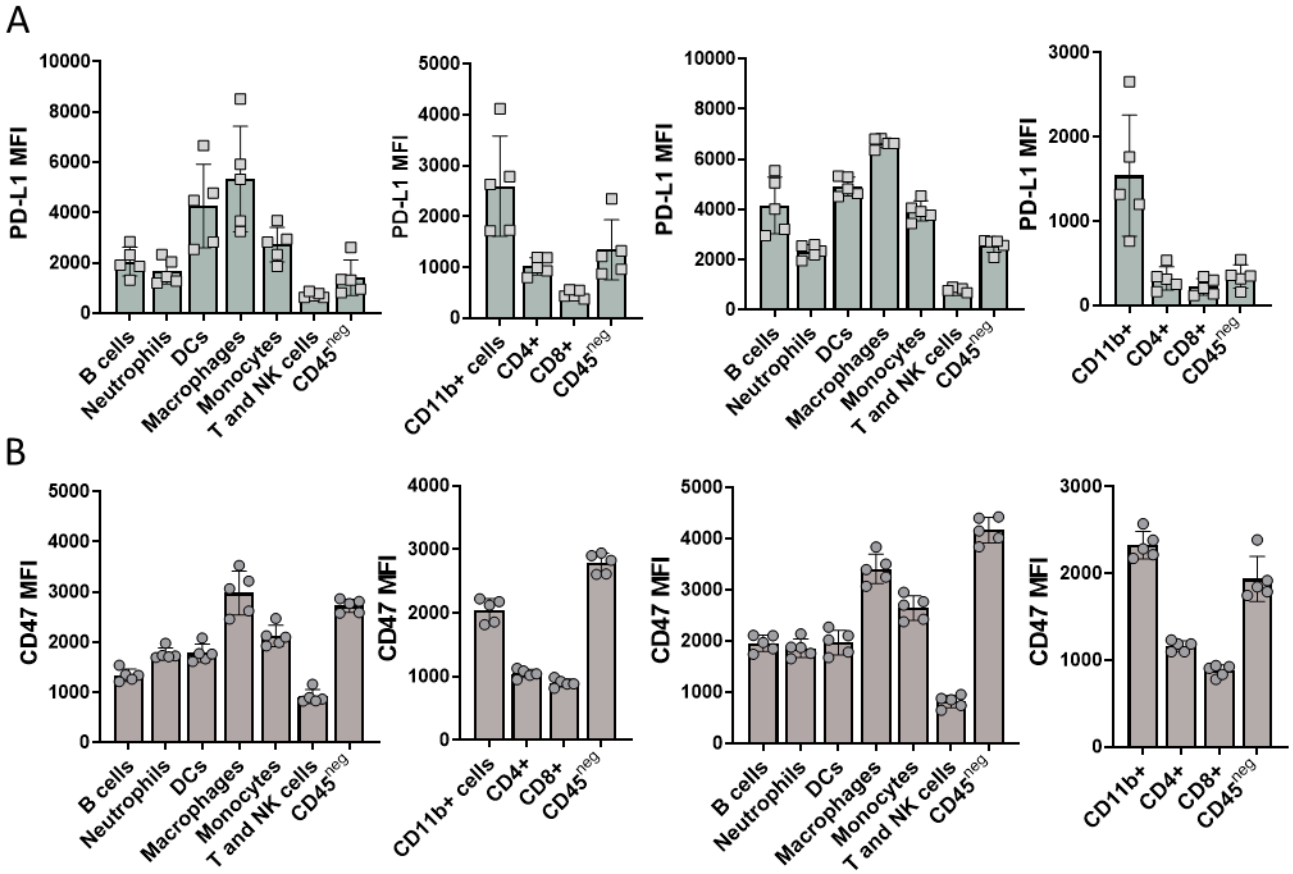

Supplemental Figure S13: Quantification of PD-L1 and CD47 expression in the tumor microenvironment of untreated animals
(A) PD-L1 and (B) CD47 cell surface expression were quantified on the main myeloid and lymphoid subgroups on day 10 (left panel) and on day 16 (right panel).

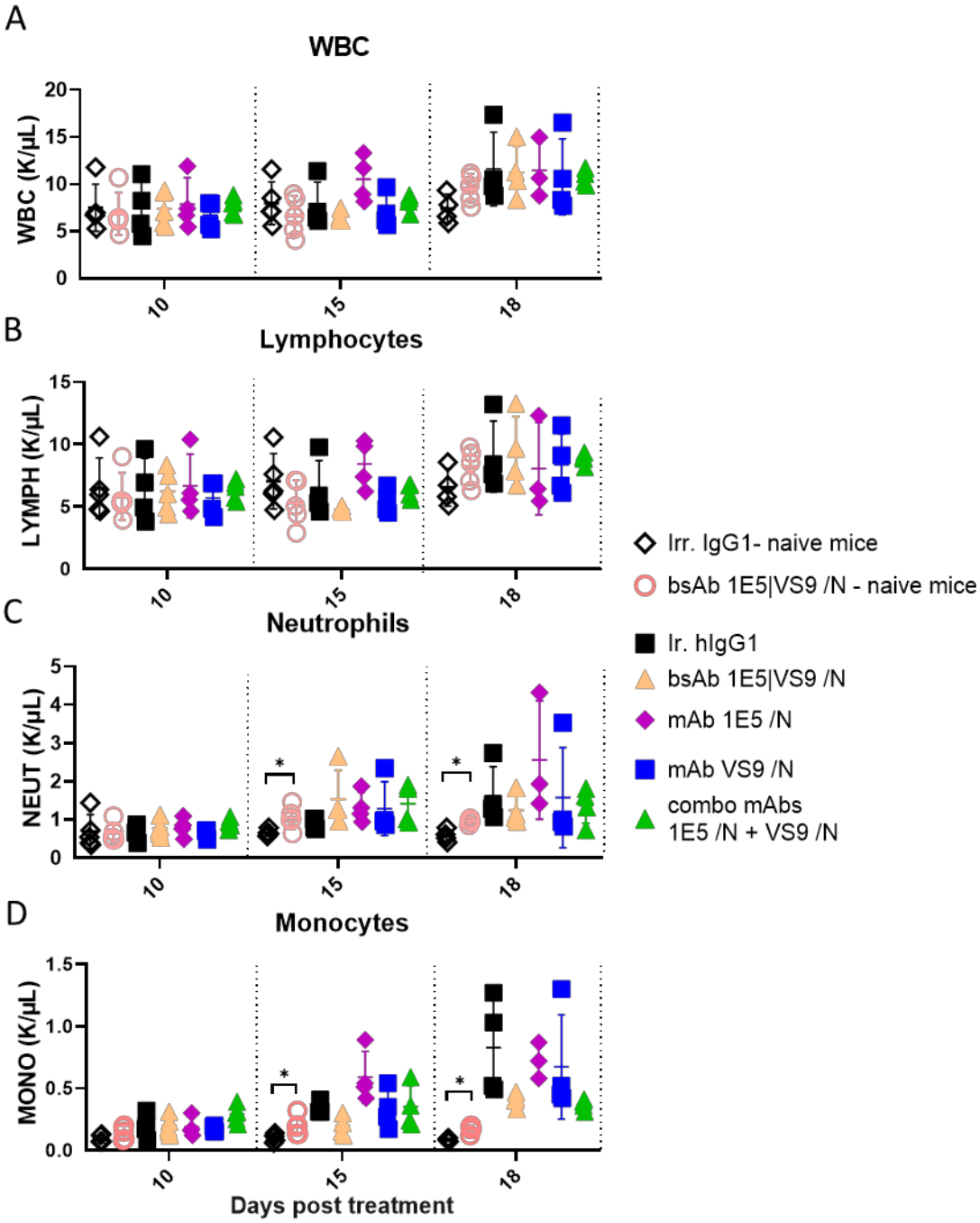

Supplemental Figure S14: White blood cell analysis following treatment with antibodies bearing a silenced Fc portion. Mice were treated on day 8, 11 and 14 and blood was collected on day 10, day 15 and day 18. Samples were run on ProCyte Dx Haematology Analyser. (A) Total white blood cells (WBC), (B) lymphocyte, (C) neutrophil and (D) monocyte counts were measured (n=3-5 mice per group). *P<0.05 were obtained using the Kruskal-Wallis ANOVA with Dunn's method of multiple comparisons. Only significant differences were indicated on the graphs.

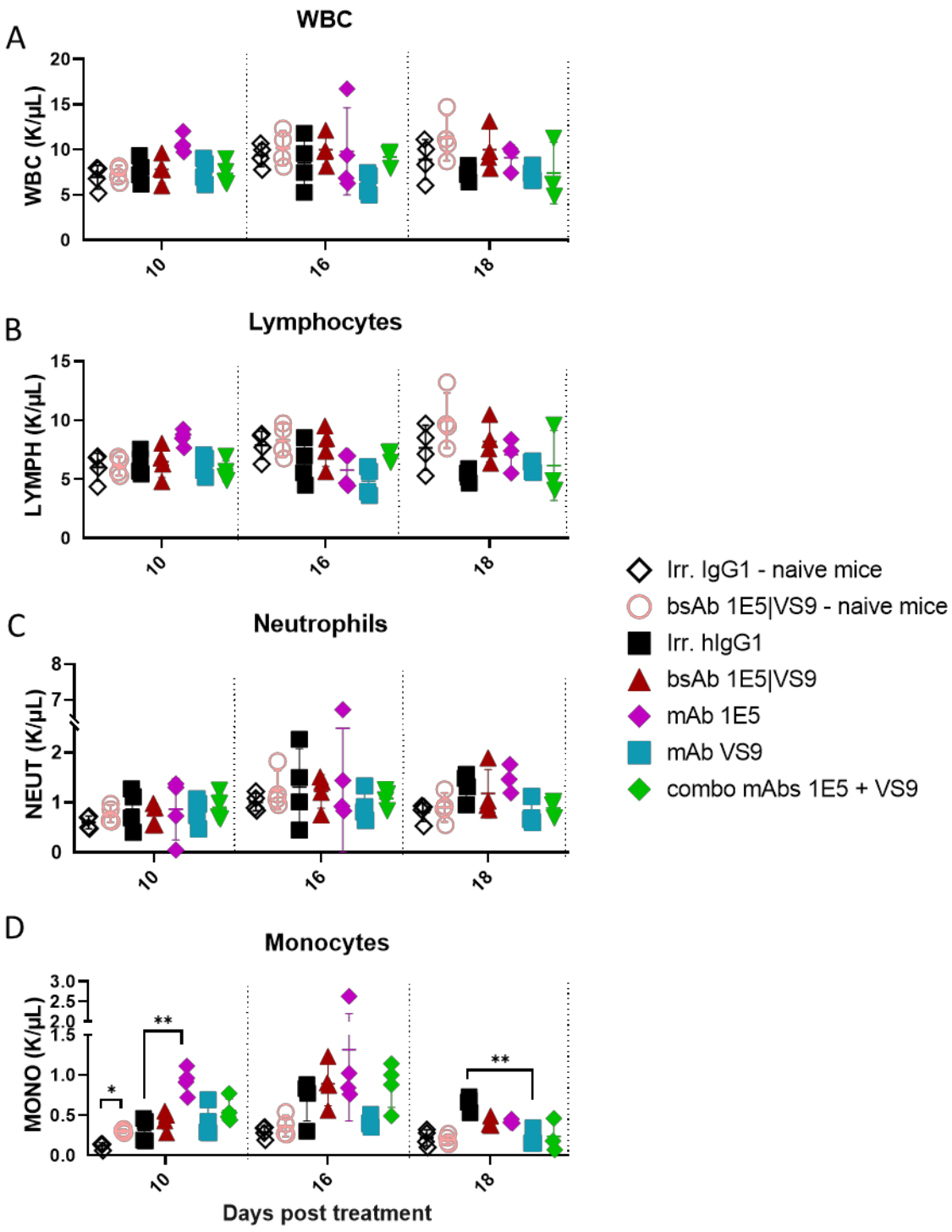

Supplemental Figure S15 : White blood cell analysis following treatment with antibodies with an active Fc portion. Mice were treated on day 8, 11 and 14 and blood was collected on day 10, day 16 and day 18. Samples were run on ProCyte Dx Haematology Analyser. A) Total white blood cell (WBC), B) lymphocyte, C) neutrophil and D) monocyte counts were measured (n=3-5 mice per group). n.s., not significant, *P<0.05, **P<0.01, were obtained using the Kruskal-Wallis ANOVA with Dunn's method of multiple comparisons. Only significant differences were indicated on the graphs.

7. List of Abbreviations

Ab: antibody

ADA: anti-drug antibody

ADCC: antibody-dependent cell-mediated cytotoxicity

ADCP: Antibody-dependent cell-mediated phagocytosis

APC: antigen presenting cell

Arg1: arginase 1

Blimp-1: B lymphocyte induced maturation protein 1

bsAb: bispecific antibody

CD: cluster of differentiation

CDC: complement dependent cytotoxicity

CDR: complementarity determining region

CH: immunoglobulin constant heavy chain domain

CPI: checkpoint inhibitor

CSF: colony stimulating factor

CTLA-4: cytotoxic T-lymphocyte–associated antigen 4

DAMP: damage-associated molecular pattern

DC: dendritic cell

ELISA: enzyme-linked immunosorbent assay

Fab: fragment antigen-binding

FACS: fluorescence activated cell sorting

FasL: Fas ligand

Fc: fragment crystallizable

FcγR: Fc gamma receptor

FcR: Fc receptor

FDA: food and drug administration

FMO: fluorescence minus one

FOXP3: forkhead box P3

GITR: glucocorticoid-induced TNFR-related protein

GM-CSF: granulocyte macrophage colony-stimulating factor

HA: hemagglutinin

HIF1α: hypoxia-inducible factor 1-alpha

ICI: immune checkpoint inhibitor

IFN: interferon

Ig: immunoglobulin

IL: interleukin

ITAM: immunoreceptor tyrosine-based activation motif

ITIM: immunoreceptor tyrosine-based inhibitory motif

ITSM: immunoreceptor tyrosine-based switch motif

KO: knock-out

LAG-3: lymphocyte-activation protein 3

LN: lymph nods

mAb: monoclonal antibody

MDSC: myeloid derived suppressor cell

MHC: major histocompatibility complex

NK cell: natural killer cell

NO: nitric oxide

OVA: ovalbumin

PAMP: pathogen-associated molecular pattern

POC: proof-of-concept

PD-1: programmed cell death 1

pDC: plasmacytoid dendritic

PD-L1: programmed death-ligand 1

PK: pharmacokinetic

RBC: red blood cell

RNA: ribonucleic acid

scfv: single-chain variable fragment

SD: standard deviation

SEM: standard error of the mean

SHP-1: Src homology region 2 domain-containing phosphatase-1

SIRP: signal-regulatory protein

SLO: secondary lymphoid organs

TAA: tumor associated antigen

TAM: tumor-associated macrophages

T-bet: T-box expressed in T cells

TCF-1 : T cell factor 1

TIGIT: T-Cell Immunoglobulin and ITIM Domain

TCR: T-cell receptor

Th: helper T cell

TIGIT: T cell immunoreceptor with Ig and ITIM domains

TIL: tumor infiltrating lymphocytes

Tim-3: T-cell immunoglobulin and mucin-domain-containing molecule 3

TLR: toll like receptor

TME: tumor microenvironment

TMDD: target mediated drug disposition

TNF: tumor necrosis factor

TRAIL: tumor-necrosis-factor related apoptosis inducing ligand

Treg: regulatory T cells

TSP1: thrombospondin-1

VEGF: vascular endothelial growth factor

VH: immunoglobulin variable heavy chain domain

VL: immunoglobulin variable light chain domain

8. References

[1] C. Mattiuzzi and G. Lippi, "Current cancer epidemiology," *J. Epidemiol. Glob. Health*, vol. 9, no. 4, pp. 217–222, 2019.

[2] L. Falzone, S. Salomone, and M. Libra, "Evolution of Cancer Pharmacological Treatments at the Turn of the Third Millennium," *Front. Pharmacol.*, vol. 9, no. NOV, Nov. 2018.

[3] S. D. Kim *et al.*, "Baicalein inhibits agonist- and tumor cell-induced platelet aggregation while suppressing pulmonary tumor metastasis via cAMP-mediated VASP phosphorylation along with impaired MAPKs and PI3K-Akt activation," *Biochem. Pharmacol.*, vol. 92, no. 2, pp. 251–265, 2014.

[4] Y. Zhang and Z. Zhang, "The history and advances in cancer immunotherapy: understanding the characteristics of tumor-infiltrating immune cells and their therapeutic implications," *Cell. Mol. Immunol.*, vol. 17, no. 8, pp. 807–821, 2020.

[5] J. Galon and D. Bruni, "Tumor Immunology and Tumor Evolution: Intertwined Histories.," *Immunity*, vol. 52, no. 1, pp. 55–81, 2020.

[6] I. Mellman, G. Coukos, and G. Dranoff, "Cancer immunotherapy comes of age," *Nature*, vol. 480, no. 7378, pp. 480–489, Dec. 2011.

[7] Y. Iwai, M. Ishida, Y. Tanaka, T. Okazaki, T. Honjo, and N. Minato, "Involvement of PD-L1 on tumor cells in the escape from host immune system and tumor immunotherapy by PD-L1 blockade," *Proc. Natl. Acad. Sci. U. S. A.*, vol. 99, no. 19, pp. 12293–12297, 2002.

[8] L. D. R., K. M. F., and A. J. P., "Enhancement of Antitumor Immunity by CTLA-4 Blockade," *Science (80-.).*, vol. 271, no. 5256, pp. 1734–1736, Mar. 1996.

[9] S. C. Wei, C. R. Duffy, and J. P. Allison, "Fundamental mechanisms of immune checkpoint blockade therapy," *Cancer Discov.*, vol. 8, no. 9, pp. 1069–1086, 2018.

[10] A. Ribas and J. D. Wolchok, "Cancer immunotherapy using checkpoint blockade," *Science (80-.).*, vol. 359, no. 6382, pp. 1350–1355, 2018.

[11] A. K. Abbas, A. H. Lichtman, and S. Pillai, *Cellular and molecular immunology*. Elsevier Health Sciences, 2018.

[12] J. Banchereau *et al.*, "Immunobiology of dendritic cells," *Annu. Rev. Immunol.*, vol. 18, pp. 767–811, 2000.

[13] I. Mellman and R. M. Steinman, "Dendritic cells: Specialized and regulated antigen processing machines," *Cell*, vol. 106, no. 3, pp. 255–258, 2001.

[14] S. K. Wculek, F. J. Cueto, A. M. Mujal, I. Melero, M. F. Krummel, and D. Sancho, "Dendritic cells in cancer immunology and immunotherapy," *Nat. Rev. Immunol.*, vol. 20, no. 1, pp. 7–24, 2020.

[15] J. E. Smith-Garvin, G. A. Koretzky, and M. S. Jordan, "T cell activation," *Annu. Rev. Immunol.*, vol. 27, pp. 591–619, 2009.

[16] M. L. Bettini *et al.*, "Membrane Association of the CD3ε Signaling Domain Is Required for Optimal T Cell Development and Function," *J. Immunol.*, vol. 193, no. 1, pp. 258–267, 2014.

[17] C. S. Guy and D. A. A. Vignali, "Organization of proximal signal initiation at the TCR:CD3 complex," *Immunol. Rev.*, vol. 232, no. 1, pp. 7–21, 2009.

[18] L. Chen and D. B. Flies, "Molecular mechanisms of T cell co-stimulation and co-inhibition," *Nat. Rev. Immunol.*, vol. 13, no. 4, pp. 227–242, Apr. 2013.

[19] R. Spolski, P. Li, and W. J. Leonard, "Biology and regulation of IL-2: from molecular mechanisms to human therapy," *Nat. Rev. Immunol.*, vol. 18, no. october, 2018.

[20] R. H. Schwartz, "T cell anergy," *Annu. Rev. Immunol.*, vol. 21, pp. 305–334, 2003.

[21] J. M. Curtsinger and M. F. Mescher, “Inflammatory cytokines as a third signal for T cell activation,” *Curr. Opin. Immunol.*, vol. 22, no. 3, pp. 333–340, Jun. 2010.

[22] D. S. M. Chatzileontiadou, H. Sloane, A. T. Nguyen, S. Gras, and E. J. Grant, “The many faces of CD4+ T cells: Immunological and structural characteristics,” *Int. J. Mol. Sci.*, vol. 22, no. 1, pp. 1–27, 2021.

[23] F. Sallusto and A. Lanzavecchia, “The instructive role of dendritic cells on T-cell responses.,” *Arthritis Res.*, vol. 4 Suppl 3, no. 3, pp. S127-32, 2002.

[24] A. D. Waldman, J. M. Fritz, and M. J. Lenardo, “A guide to cancer immunotherapy: from T cell basic science to clinical practice,” *Nat. Rev. Immunol.*, vol. 20, no. 11, pp. 651–668, 2020.

[25] S. Sakaguchi, N. Mikami, J. B. Wing, A. Tanaka, K. Ichiyama, and N. Ohkura, “Regulatory T Cells and Human Disease,” *Annu. Rev. Immunol.*, vol. 38, pp. 541–566, 2020.

[26] J. D. Fontenot, M. A. Gavin, and A. Y. Rudensky, “Foxp3 programs the development and function of CD4+CD25+ regulatory T cells,” *J. Immunol.*, vol. 198, no. 3, pp. 986–992, 2017.

[27] D. Perkins *et al.*, “Regulation of CTLA-4 expression during T cell activation.,” *J. Immunol.*, vol. 156, no. 11, pp. 4154–9, 1996.

[28] T. Takahashi *et al.*, “Immunologic self-tolerance maintained by CD25+CD4+ regulatory T cells constitutively expressing cytotoxic T lymphocyte-associated antigen 4,” *J. Exp. Med.*, vol. 192, no. 2, pp. 303–309, 2000.

[29] C. T. Huang *et al.*, “Role of LAG-3 in regulatory T cells,” *Immunity*, vol. 21, no. 4, pp. 503–513, 2004.

[30] Y. Togashi, K. Shitara, and H. Nishikawa, “Regulatory T cells in cancer immunosuppression — implications for anticancer therapy,” *Nat. Rev. Clin. Oncol.*, vol. 16, no. 6, pp. 356–371, 2019.

[31] M. F. Krummel and J. P. Allison, “CD28 and CTLA-4 have opposing effects on the response of T cells to stimulation.,” *J. Exp. Med.*, vol. 182, no. 2, pp. 459–465, Aug. 1995.

[32] O. S. Qureshi *et al.*, “Trans-endocytosis of CD80 and CD86: A molecular basis for the cell-extrinsic function of CTLA-4,” *Science (80-.).*, vol. 332, no. 6029, pp. 600–603, 2011.

[33] L. Strauss, C. Bergmann, M. Szczepanski, W. Gooding, J. T. Johnson, and T. L. Whiteside, “A unique subset of CD4+CD25highFoxp3+ T cells secreting interleukin-10 and transforming growth factor-β1 mediates suppression in the tumor microenvironment,” *Clin. Cancer Res.*, vol. 13, no. 15, pp. 4345–4354, 2007.

[34] T. Chinen *et al.*, “An essential role for the IL-2 receptor in Treg cell function,” *Nat. Immunol.*, vol. 17, no. 11, pp. 1322–1333, 2016.

[35] S. M. Kaech, E. J. Wherry, and R. Ahmed, “Effector and memory T-cell differentiation: Implications for vaccine development,” *Nat. Rev. Immunol.*, vol. 2, no. 4, pp. 251–262, 2002.

[36] V. Golubovskaya and L. Wu, “Different subsets of T cells, memory, effector functions, and CAR-T immunotherapy,” *Cancers (Basel).*, vol. 8, no. 3, 2016.

[37] S. M. Kaech and W. Cui, “Transcriptional control of effector and memory CD8+ T cell differentiation,” *Nat. Rev. Immunol.*, vol. 12, no. 11, pp. 749–761, 2012.

[38] I. Raphael, R. R. Joern, and T. G. Forsthuber, “Memory CD4+ T Cells in Immunity and Autoimmune Diseases,” *Cells*, vol. 9, no. 3, pp. 1–23, 2020.

[39] L. Kok, D. Masopust, and T. N. Schumacher, “The precursors of CD8+ tissue resident memory T cells: from lymphoid organs to infected tissues,” *Nat. Rev. Immunol.*, vol. 22, no. May, pp. 283–293, 2021.

[40] B. M. Carreno and M. Collins, “The B7 family of ligands and its receptors: New pathways for costimulation and inhibition

of immune responses," *Annu. Rev. Immunol.*, vol. 20, pp. 29–53, 2002.

[41] S. C. Wei, C. R. Duffy, and J. P. Allison, "Fundamental Mechanisms of Immune Checkpoint Blockade Therapy," *Cancer Discov.*, vol. 8, no. 9, 2018.

[42] D. M. Pardoll, "The blockade of immune checkpoints in cancer immunotherapy," *Nat. Rev. Cancer*, vol. 12, no. 4, pp. 252–264, 2012.

[43] M. A. ElTanbouly and R. J. Noelle, "Rethinking peripheral T cell tolerance: checkpoints across a T cell's journey," *Nat. Rev. Immunol.*, vol. 21, no. 4, pp. 257–267, 2021.

[44] T. Honda, J. G. Egen, T. Lämmermann, W. Kastenmüller, P. Torabi-Parizi, and R. N. Germain, "Tuning of Antigen Sensitivity by T Cell Receptor-Dependent Negative Feedback Controls T Cell Effector Function in Inflamed Tissues," *Immunity*, vol. 40, no. 2, pp. 235–247, Feb. 2014.

[45] A. C. Anderson, N. Joller, and V. K. Kuchroo, "Lag-3, Tim-3, and TIGIT: Co-inhibitory Receptors with Specialized Functions in Immune Regulation," *Immunity*, vol. 44, no. 5, pp. 989–1004, 2016.

[46] A. Schnell, L. Bod, A. Madi, and V. K. Kuchroo, "The yin and yang of co-inhibitory receptors: toward anti-tumor immunity without autoimmunity," *Cell Res.*, vol. 30, no. 4, pp. 285–299, 2020.

[47] R. I. Nurieva, X. Liu, and C. Dong, "Yin-Yang of costimulation: Crucial controls of immune tolerance and function," *Immunol. Rev.*, vol. 229, no. 1, pp. 88–100, 2009.

[48] N. Chihara *et al.*, "Induction and transcriptional regulation of the co-inhibitory gene module in T cells," *Nature*, vol. 558, no. 7710, pp. 454–459, Jun. 2018.

[49] L. M. Francisco, P. T. Sage, and A. H. Sharpe, "The PD-1 Pathway in Tolerance and Autoimmunity," *Immunol. Rev.*, vol. 236, no. 1, pp. 219–242, 2010.

[50] L. Baitsch *et al.*, "Extended co-expression of inhibitory receptors by human CD8 T-cells depending on differentiation, antigen-specificity and anatomical localization," *PLoS One*, vol. 7, no. 2, pp. 1–10, 2012.

[51] A. H. Sharpe and G. J. Freeman, "The B7-CD28 superfamily," *Nat. Rev. Immunol.*, vol. 2, no. 2, pp. 116–126, 2002.

[52] P. S. Linsley, J. L. Greene, W. Brady, J. Bajorath, J. A. Ledbetter, and R. Peach, "Human B7-1 (CD80) and B7-2 (CD86) bind with similar avidities but distinct kinetics to CD28 and CTLA-4 receptors.," *Immunity*, vol. 1, no. 9, pp. 793–801, Dec. 1994.

[53] E. Hui *et al.*, "T cell costimulatory receptor CD28 is a primary target for PD-1-mediated inhibition," *Science (80-.).*, vol. 355, no. 6332, pp. 1428–1433, 2017.

[54] R. Mizuno *et al.*, "PD-1 primarily targets TCR signal in the inhibition of functional T cell activation," *Front. Immunol.*, vol. 10, no. MAR, pp. 1–14, 2019.

[55] Y. Agata *et al.*, "Expression of the PD-1 antigen on the surface of stimulated mouse T and B lymphocytes," *Int. Immunol.*, vol. 8, no. 5, pp. 765–772, 1996.

[56] G. J. Freeman *et al.*, "Engagement of the Pd-1 Immunoinhibitory Receptor by a Novel B7 Family Member Leads to Negative Regulation of Lymphocyte Activation," *J. Exp. Med.*, vol. 192, no. 7, pp. 1027–1034, 2000.

[57] Y. Latchman *et al.*, "PD-L2 is a second ligand for PD-1 and inhibits T cell activation," *Nat. Immunol.*, vol. 2, no. 3, pp. 261–268, 2001.

[58] P. Ritprajak and M. Azuma, "Intrinsic and extrinsic control of expression of the immunoregulatory molecule PD-L1 in epithelial cells and squamous cell carcinoma," *Oral Oncol.*, vol. 51, no. 3, pp. 221–228, 2015.

[59] M. J. Eppihimer *et al.*, "Expression and regulation of the PD-L1 immunoinhibitory molecule on microvascular endothelial

cells.," *Microcirculation*, vol. 9, no. 2, pp. 133–45, 2002.

[60] T. Yamazaki *et al.*, "Expression of Programmed Death 1 Ligands by Murine T Cells and APC," *J. Immunol.*, vol. 169, no. 10, pp. 5538–5545, 2002.

[61] M. E. Keir *et al.*, "Tissue expression of PD-L1 mediates peripheral T cell tolerance," *J. Exp. Med.*, vol. 203, no. 4, pp. 883–895, 2006.

[62] E. Ahn *et al.*, "Role of PD-1 during effector CD8 T cell differentiation," *Proc. Natl. Acad. Sci.*, no. 29, p. 201718217, 2018.

[63] N. M. Durham *et al.*, "Lymphocyte activation gene 3 (LAG-3) modulates the ability of CD4 T-cells to be suppressed In Vivo," *PLoS One*, vol. 9, no. 11, pp. 1–13, 2014.

[64] Y. Wolf, A. C. Anderson, and V. K. Kuchroo, "TIM3 comes of age as an inhibitory receptor," *Nat. Rev. Immunol.*, vol. 20, no. 3, pp. 173–185, 2020.

[65] S. Qin, L. Xu, M. Yi, S. Yu, K. Wu, and S. Luo, "Novel immune checkpoint targets: Moving beyond PD-1 and CTLA-4," *Mol. Cancer*, vol. 18, no. 1, pp. 1–14, 2019.

[66] D. Hanahan and R. A. Weinberg, "The Hallmarks of Cancer," *Cell*, vol. 100, no. 1, pp. 57–70, Jan. 2000.

[67] D. S. Chen and I. Mellman, "Oncology meets immunology: The cancer-immunity cycle," *Immunity*, vol. 39, no. 1, pp. 1–10, 2013.

[68] D. Mittal, M. M. Gubin, R. D. Schreiber, and M. J. Smyth, "New insights into cancer immunoediting and its three component phases-elimination, equilibrium and escape," *Curr. Opin. Immunol.*, vol. 27, no. 1, pp. 16–25, 2014.

[69] N. A. Giraldo *et al.*, "The clinical role of the TME in solid cancer," *Br. J. Cancer*, vol. 120, no. 1, pp. 45–53, 2019.

[70] D. S. Chen and I. Mellman, "Elements of cancer immunity and the cancer-immune set point," *Nature*, vol. 541, no. 7637, pp. 321–330, 2017.

[71] L. Bejarano, M. J. C. Jordão, and J. A. Joyce, "Therapeutic targeting of the tumor microenvironment," *Cancer Discov.*, vol. 11, no. 4, pp. 933–959, 2021.

[72] K. E. De Visser, A. Eichten, and L. M. Coussens, "Paradoxical roles of the immune system during cancer development," *Nat. Rev. Cancer*, vol. 6, no. 1, pp. 24–37, 2006.

[73] T. Wu, X. Wu, H. Y. Wang, and L. Chen, "Immune contexture defined by single cell technology for prognosis prediction and immunotherapy guidance in cancer," *Cancer Commun.*, vol. 39, no. 1, pp. 1–9, 2019.

[74] J. Galon *et al.*, "Type, Density, and Location of Immune Cells Within Human Colorectal Tumors Predict Clinical Outcome," *Science (80-.).*, vol. 313, no. 5795, pp. 1960–1964, Sep. 2006.

[75] D. Bruni, H. K. Angell, and J. Galon, "The immune contexture and Immunoscore in cancer prognosis and therapeutic efficacy," *Nat. Rev. Cancer*, vol. 20, no. 11, pp. 662–680, 2020.

[76] P. B. Narasimhan, P. Marcovecchio, A. A. J. Hamers, and C. C. Hedrick, "Nonclassical Monocytes in Health and Disease," *Annu. Rev. Immunol.*, vol. 37, pp. 439–456, 2019.

[77] F. Veglia, E. Sanseviero, and D. I. Gabrilovich, "Myeloid-derived suppressor cells in the era of increasing myeloid cell diversity," *Nat. Rev. Immunol.*, vol. 21, no. 8, pp. 485–498, 2021.

[78] C. Schulz *et al.*, "A lineage of myeloid cells independent of myb and hematopoietic stem cells," *Science (80-.).*, vol. 335, no. 6077, pp. 86–90, 2012.

[79] C. Varol, A. Mildner, and S. Jung, *Macrophages: Development and tissue specialization*, vol. 33. 2015.

[80] C. D. Mills, K. Kincaid, J. M. Alt, M. J. Heilman, and A. M. Hill, "M-1/M-2 Macrophages and the Th1/Th2 Paradigm," *J. Immunol.*, vol. 164, no. 12, pp. 6166–6173, Jun. 2000.

[81] X. Huang, Y. Li, M. Fu, and H. B. Xin, “Polarizing macrophages in vitro,” *Methods Mol. Biol.*, vol. 1784, pp. 119–126, 2018.

[82] A. J. Boutilier and S. F. Elsawa, “Macrophage polarization states in the tumor microenvironment,” *Int. J. Mol. Sci.*, vol. 22, no. 13, 2021.

[83] A. R. Poh and M. Ernst, “Targeting macrophages in cancer: From bench to bedside,” *Front. Oncol.*, vol. 8, no. MAR, pp. 1–16, 2018.

[84] A. Mantovani, S. Sozzani, M. Locati, P. Allavena, and A. Sica, “Macrophage polarization: Tumor-associated macrophages as a paradigm for polarized M2 mononuclear phagocytes,” *Trends Immunol.*, vol. 23, no. 11, pp. 549–555, 2002.

[85] P. J. Murray *et al.*, “Macrophage Activation and Polarization: Nomenclature and Experimental Guidelines,” *Immunity*, vol. 41, no. 1, pp. 14–20, 2014.

[86] N. Cortese, R. Carriero, L. Laghi, A. Mantovani, and F. Marchesi, “Prognostic significance of tumor-associated macrophages: past, present and future,” *Semin. Immunol.*, vol. 48, no. July, p. 101408, 2020.

[87] Ö. Canli *et al.*, “Myeloid Cell-Derived Reactive Oxygen Species Induce Epithelial Mutagenesis,” *Cancer Cell*, vol. 32, no. 6, pp. 869-883.e5, 2017.

[88] N. J. Neubert *et al.*, “T cell-induced CSF1 promotes melanoma resistance to PD1 blockade,” *Sci. Transl. Med.*, vol. 10, no. 436, 2018.

[89] X. Zhong, B. Chen, and Z. Yang, “The Role of Tumor-Associated Macrophages in Colorectal Carcinoma Progression,” *Cell. Physiol. Biochem.*, vol. 45, no. 1, pp. 356–365, 2018.

[90] L. Cassetta and J. W. Pollard, “Targeting macrophages: Therapeutic approaches in cancer,” *Nat. Rev. Drug Discov.*, vol. 17, no. 12, pp. 887–904, 2018.

[91] Z. Duan and Y. Luo, “Targeting macrophages in cancer immunotherapy,” *Signal Transduct. Target. Ther.*, vol. 6, no. 1, pp. 1–21, 2021.

[92] F. Kotsias, I. Cebrian, and A. Alloatti, “Antigen processing and presentation,” *Int. Rev. Cell Mol. Biol.*, vol. 348, pp. 69–121, 2019.

[93] M. Cabeza-Cabrerizo, A. Cardoso, C. M. Minutti, M. Pereira Da Costa, and C. Reis E Sousa, “Dendritic Cells Revisited,” *Annu. Rev. Immunol.*, vol. 39, pp. 131–166, 2021.

[94] A. Schlitzer, N. McGovern, and F. Ginhoux, “Dendritic cells and monocyte-derived cells: Two complementary and integrated functional systems,” *Semin. Cell Dev. Biol.*, vol. 41, pp. 9–22, 2015.

[95] P. F. Rodrigues, L. Alberti-Servera, A. Eremin, G. E. Grajales-Reyes, R. Ivanek, and R. Tussiwand, “Distinct progenitor lineages contribute to the heterogeneity of plasmacytoid dendritic cells,” *Nat. Immunol.*, vol. 19, no. 7, pp. 711–722, 2018.

[96] A. Gardner, Á. de Mingo Pulido, and B. Ruffell, “Dendritic Cells and Their Role in Immunotherapy,” *Front. Immunol.*, vol. 11, no. May, pp. 1–14, 2020.

[97] Y. S. Lee and K. J. Radford, *The role of dendritic cells in cancer*, 1st ed., vol. 348. Elsevier Inc., 2019.

[98] D. Gabrilovich, “Mechanisms and functional significance of tumour-induced dendritic-cell defects,” *Nat. Rev. Immunol.*, vol. 4, no. 12, pp. 941–952, 2004.

[99] F. Veglia and D. I. Gabrilovich, “Dendritic cells in cancer: the role revisited,” *Curr. Opin. Immunol.*, vol. 45, pp. 43–51, 2017.

[100] L. A. Norian *et al.*, “Tumor-Infiltrating regulatory dendritic cells inhibit CD8+ T cell function via L-Arginine metabolism,” *Cancer Res.*, vol. 69, no. 7, pp. 3086–3094, 2009.

[101] Q. Peng *et al.*, "PD-L1 on dendritic cells attenuates T cell activation and regulates response to immune checkpoint blockade," *Nat. Commun.*, vol. 11, no. 1, pp. 1–8, 2020.

[102] C. R. Perez and M. De Palma, "Engineering dendritic cell vaccines to improve cancer immunotherapy," *Nat. Commun.*, vol. 10, no. 1, pp. 1–10, 2019.

[103] A. M. Mujal, R. B. Delconte, and J. C. Sun, "Natural Killer Cells: From Innate to Adaptive Features," *Annu. Rev. Immunol.*, vol. 39, pp. 417–447, 2021.

[104] C. Pasero *et al.*, "Highly effective NK cells are associated with good prognosis in patients with metastatic prostate cancer," *Oncotarget*, vol. 6, no. 16, pp. 14360–14373, 2015.

[105] G. Habif, A. Crinier, P. André, E. Vivier, and E. Narni-Mancinelli, "Targeting natural killer cells in solid tumors," *Cell. Mol. Immunol.*, vol. 16, no. 5, pp. 415–422, 2019.

[106] W. Wang, A. K. Erbe, J. A. Hank, Z. S. Morris, and P. M. Sondel, "NK cell-mediated antibody-dependent cellular cytotoxicity in cancer immunotherapy," *Front. Immunol.*, vol. 6, no. JUL, 2015.

[107] J. P. Böttcher *et al.*, "NK Cells Stimulate Recruitment of cDC1 into the Tumor Microenvironment Promoting Cancer Immune Control," *Cell*, vol. 172, no. 5, pp. 1022-1037.e14, 2018.

[108] M. G. Morvan and L. L. Lanier, "NK cells and cancer: You can teach innate cells new tricks," *Nat. Rev. Cancer*, vol. 16, no. 1, pp. 7–19, 2016.

[109] N. Shimasaki, A. Jain, and D. Campana, "NK cells for cancer immunotherapy," *Nat. Rev. Drug Discov.*, vol. 19, no. 3, pp. 200–218, 2020.

[110] O. Melaiu, V. Lucarini, L. Cifaldi, and D. Fruci, "Influence of the Tumor Microenvironment on NK Cell Function in Solid Tumors," *Front. Immunol.*, vol. 10, no. January, 2020.

[111] S. Viel *et al.*, "TGF-β inhibits the activation and functions of NK cells by repressing the mTOR pathway," *Sci. Signal.*, vol. 9, no. 415, pp. 1–14, 2016.

[112] L. Quatrini, F. R. Mariotti, E. Munari, N. Tumino, P. Vacca, and L. Moretta, "The immune checkpoint PD-1 in natural killer cells: Expression, function and targeting in tumour immunotherapy," *Cancers (Basel).*, vol. 12, no. 11, pp. 1–21, 2020.

[113] J. Hsu *et al.*, "Contribution of NK cells to immunotherapy mediated by PD-1/PD-L1 blockade," *J. Clin. Invest.*, vol. 128, no. 10, pp. 4654–4668, 2018.

[114] J. Galon and D. Bruni, "Approaches to treat immune hot, altered and cold tumours with combination immunotherapies," *Nat. Rev. Drug Discov.*, vol. 18, no. 3, pp. 197–218, 2019.

[115] B. Farhood, M. Najafi, and K. Mortezaee, "CD8+ cytotoxic T lymphocytes in cancer immunotherapy: A review," *J. Cell. Physiol.*, vol. 234, no. 6, pp. 8509–8521, 2019.

[116] L. M. McLane, M. S. Abdel-Hakeem, and E. J. Wherry, "CD8 T Cell Exhaustion During Chronic Viral Infection and Cancer," *Annu. Rev. Immunol.*, vol. 37, pp. 457–495, 2019.

[117] Y. Jiang, Y. Li, and B. Zhu, "T-cell exhaustion in the tumor microenvironment," *Cell Death Dis.*, vol. 6, no. 6, pp. 1–9, 2015.

[118] D. S. Thommen and T. N. Schumacher, "T Cell Dysfunction in Cancer," *Cancer Cell*, vol. 33, no. 4, pp. 547–562, 2018.

[119] Z. Zhang, S. Liu, B. Zhang, L. Qiao, Y. Zhang, and Y. Zhang, "T Cell Dysfunction and Exhaustion in Cancer," *Front. Cell Dev. Biol.*, vol. 8, no. February, 2020.

[120] Z. Yang *et al.*, " Expression of Lag-3 Defines Exhaustion of Intratumoral Pd-1 + T Cells and Correlates With Poor Outcome in Follicular Lymphoma ," *Hematol. Oncol.*, vol. 35, no. 37, pp. 260–261, 2017.

[121] M. Sade-Feldman *et al.*, "Defining T Cell States Associated with Response to Checkpoint Immunotherapy in Melanoma,"

Cell, vol. 175, no. 4, pp. 998-1013.e20, 2018.

[122] E. J. Wherry, "T cell exhaustion," *Nat. Immunol.*, vol. 12, no. 6, pp. 492–499, 2011.

[123] J. L. Collier, S. A. Weiss, K. E. Pauken, D. R. Sen, and A. H. Sharpe, "Not-so-opposite ends of the spectrum: CD8+ T cell dysfunction across chronic infection, cancer and autoimmunity," *Nat. Immunol.*, vol. 22, no. 7, pp. 809–819, 2021.

[124] E. J. Wherry and M. Kurachi, "Molecular and cellular insights into T cell exhaustion," *Nat. Rev. Immunol.*, vol. 15, no. 8, pp. 486–499, 2015.

[125] A. Schietinger and P. D. Greenberg, "Tolerance and exhaustion: Defining mechanisms of T cell dysfunction," *Trends Immunol.*, vol. 35, no. 2, pp. 51–60, 2014.

[126] H. Kaminski, M. Lemoine, and T. Pradeu, "Immunological exhaustion: How to make a disparate concept operational?," *PLoS Pathog.*, vol. 17, no. 9, pp. 1–16, 2021.

[127] J. Duraiswamy *et al.*, "Phenotype, Function, and Gene Expression Profiles of Programmed Death-1 hi CD8 T Cells in Healthy Human Adults," *J. Immunol.*, vol. 186, no. 7, pp. 4200–4212, 2011.

[128] S. Woo *et al.*, "Immune inhibitory molecules LAG-3 and PD-1 synergistically regulate T-cell function to promote tumoral immune escape.," *Cancer Res.*, vol. 72, no. 4, pp. 917–27, Feb. 2012.

[129] K. Sakuishi, L. Apetoh, J. M. Sullivan, B. R. Blazar, V. K. Kuchroo, and A. C. Anderson, "Targeting Tim-3 and PD-1 pathways to reverse T cell exhaustion and restore anti-tumor immunity," *J. Exp. Med.*, vol. 207, no. 10, pp. 2187–2194, 2010.

[130] P. A. Ascierto *et al.*, "Initial efficacy of anti-lymphocyte activation gene-3 (anti–LAG-3; BMS-986016) in combination with nivolumab (nivo) in pts with melanoma (MEL) previously treated with anti–PD-1/PD-L1 therapy.," *J. Clin. Oncol.*, vol. 35, no. 15_suppl, p. 9520, May 2017.

[131] G. Plitas and A. Y. Rudensky, "Regulatory T Cells in Cancer," *Annu. Rev. Cancer Biol.*, vol. 4, pp. 459–477, 2020.

[132] K. S. Peggs, S. A. Quezada, C. A. Chambers, A. J. Korman, and J. P. Allison, "Blockade of CTLA-4 on both effector and regulatory T cell compartments contributes to the antitumor activity of anti-CTLA-4 antibodies," *J. Exp. Med.*, vol. 206, no. 8, pp. 1717–1725, 2009.

[133] V. K. Sondak, K. S. M. Smalley, R. Kudchadkar, S. Grippon, and P. Kirkpatrick, "Ipilimumab," *Nat. Rev. Drug Discov.*, vol. 10, no. 6, pp. 411–412, 2011.

[134] J. A. Seidel, A. Otsuka, and K. Kabashima, "Anti-PD-1 and anti-CTLA-4 therapies in cancer: Mechanisms of action, efficacy, and limitations," *Front. Oncol.*, vol. 8, no. MAR, pp. 1–14, 2018.

[135] G. Biffi and D. A. Tuveson, "Deciphering cancer fibroblasts," *J. Exp. Med.*, vol. 215, no. 12, pp. 2967–2968, 2018.

[136] H. V. Newnes, J. D. Armitage, K. M. Audsley, A. Bosco, and J. Waithman, "Directing the future breakthroughs in immunotherapy: The importance of a holistic approach to the tumour microenvironment," *Cancers (Basel).*, vol. 13, no. 23, 2021.

[137] G. Ishii, A. Ochiai, and S. Neri, "Phenotypic and functional heterogeneity of cancer-associated fibroblast within the tumor microenvironment," *Adv. Drug Deliv. Rev.*, vol. 99, pp. 186–196, 2016.

[138] D. Ribatti, A. Vacca, and F. Dammacco, "The Role of the Vascular Phase in Solid Tumor Growth: A Historical Review," *Neoplasia*, vol. 1, no. 4, pp. 293–302, 1999.

[139] F. De Sanctis, S. Ugel, J. Facciponte, and A. Facciabene, "The dark side of tumor-associated endothelial cells," *Semin. Immunol.*, vol. 35, no. February, pp. 35–47, 2018.

[140] A. C. Dudley, "Tumor endothelial cells," *Cold Spring Harb. Perspect. Med.*, vol. 2, no. 3, 2012.

[141] P. Carmeliet and R. K. Jain, "Angiogenesis in cancer and other diseases," *Nature*, vol. 407, no. 6801, pp. 249–257, Sep.

2000.

[142] G. Helmlinger, F. Yuan, M. Dellian, and R. K. Jain, “Interstitial pH and pO2 gradients in solid tumors in vivo: High-resolution measurements reveal a lack of correlation,” *Nat. Med.*, vol. 3, no. 2, pp. 177–182, Feb. 1997.

[143] L. Nagl, L. Horvath, A. Pircher, and D. Wolf, “Tumor Endothelial Cells (TECs) as Potential Immune Directors of the Tumor Microenvironment – New Findings and Future Perspectives,” *Front. Cell Dev. Biol.*, vol. 8, no. August, pp. 1–18, 2020.

[144] N. Rodig *et al.*, “Endothelial expression of PD-L1 and PD-L2 down-regulates CD8+T cell activation and cytolysis,” *Eur. J. Immunol.*, vol. 33, no. 11, pp. 3117–3126, 2003.

[145] R. J. Brezski and G. Georgiou, “Immunoglobulin isotype knowledge and application to Fc engineering,” *Curr. Opin. Immunol.*, vol. 40, no. May 2015, pp. 62–69, 2016.

[146] L. M. Weiner, R. Surana, and S. Wang, “Monoclonal antibodies: Versatile platforms for cancer immunotherapy,” *Nat. Rev. Immunol.*, vol. 10, no. 5, pp. 317–327, 2010.

[147] G. Vidarsson, G. Dekkers, and T. Rispens, “IgG subclasses and allotypes: From structure to effector functions,” *Front. Immunol.*, vol. 5, no. OCT, pp. 1–17, 2014.

[148] P. Gogesch, S. Dudek, G. van Zandbergen, Z. Waibler, and M. Anzaghe, “The role of fc receptors on the effectiveness of therapeutic monoclonal antibodies,” *Int. J. Mol. Sci.*, vol. 22, no. 16, 2021.

[149] P. Bruhns, “Properties of mouse and human IgG receptors and their contribution to disease models,” *Blood*, vol. 119, no. 24, pp. 5640–5649, 2012.

[150] M. Lo *et al.*, “Effector-attenuating Substitutions That Maintain Antibody Stability and Reduce Toxicity in Mice.,” *J. Biol. Chem.*, vol. 292, no. 9, pp. 3900–3908, 2017.

[151] T. Schlothauer *et al.*, “Novel human IgG1 and IgG4 Fc-engineered antibodies with completely abolished immune effector functions.,” *Protein Eng. Des. Sel.*, vol. 29, no. 10, pp. 457–466, 2016.

[152] X. Chen, X. Song, K. Li, and T. Zhang, “FcγR-binding is an important functional attribute for immune checkpoint antibodies in cancer immunotheraphy,” *Front. Immunol.*, vol. 10, no. FEB, pp. 1–13, 2019.

[153] A. Lux and F. Nimmerjahn, “Of mice and men: The need for humanized mouse models to study human igg activity in Vivo,” *J. Clin. Immunol.*, vol. 33, no. SUPPL.1, pp. 4–8, 2013.

[154] G. KÖHLER and C. MILSTEIN, “Continuous cultures of fused cells secreting antibody of predefined specificity,” *Nature*, vol. 256, no. 5517, pp. 495–497, Aug. 1975.

[155] D. Zahavi and L. Weiner, “Monoclonal Antibodies in Cancer Therapy,” *Antibodies*, vol. 9, no. 3, p. 34, Jul. 2020.

[156] J. K. H. Liu, “The history of monoclonal antibody development - Progress, remaining challenges and future innovations,” *Ann. Med. Surg.*, vol. 3, no. 4, pp. 113–116, 2014.

[157] C. Sgro, “Side-effects of a monoclonal antibody, muromonab CD3/orthoclone OKT3: bibliographic review,” *Toxicology*, vol. 105, no. 1, pp. 23–29, 1995.

[158] R. M. Lu *et al.*, “Development of therapeutic antibodies for the treatment of diseases,” *J. Biomed. Sci.*, vol. 27, no. 1, pp. 1–30, 2020.

[159] S. L. Morrison, M. J. Johnson, L. A. Herzenberg, and V. T. Oi, “Chimeric human antibody molecules: Mouse antigen-binding domains with human constant region domains,” *Proc. Natl. Acad. Sci. U. S. A.*, vol. 81, no. 21 I, pp. 6851–6855, 1984.

[160] P. T. Jones, P. H. Dear, J. Foote, M. S. Neuberger, and G. Winter, “Replacing the complementarity-determining regions in a human antibody with those from a mouse,” *Nature*, vol. 321, no. 6069, pp. 522–525, May 1986.

[161] F. Ducancel and B. H. Muller, “Molecular engineering of antibodies for therapeutic and diagnostic purposes,” *MAbs*, vol. 4, no. 4, pp. 445–457, 2012.

[162] J. McCafferty, A. D. Griffiths, G. Winter, and D. J. Chiswell, “Phage antibodies: filamentous phage displaying antibody variable domains,” *Nature*, vol. 348, no. 6301, pp. 552–554, Dec. 1990.

[163] M. A. Alfaleh *et al.*, “Phage Display Derived Monoclonal Antibodies: From Bench to Bedside,” *Front. Immunol.*, vol. 11, no. August 2020, 2020.

[164] N. Clementi, N. Mancini, L. Solforosi, M. Castelli, M. Clementi, and R. Burioni, “Phage display-based strategies for cloning and optimization of monoclonal antibodies directed against human pathogens,” *Int. J. Mol. Sci.*, vol. 13, no. 7, pp. 8273–8292, 2012.

[165] H. R. Hoogenboom, “Selecting and screening recombinant antibody libraries,” *Nat. Biotechnol.*, vol. 23, no. 9, pp. 1105–1116, 2005.

[166] G. Housman *et al.*, “Drug resistance in cancer: An overview,” *Cancers (Basel).*, vol. 6, no. 3, pp. 1769–1792, 2014.

[167] M. E. Valsecchi, “Combined Nivolumab and Ipilimumab or Monotherapy in Untreated Melanoma,” *N. Engl. J. Med.*, vol. 373, no. 13, pp. 1270–1271, 2015.

[168] J. Larkin *et al.*, “Combined Nivolumab and Ipilimumab or Monotherapy in Untreated Melanoma,” *N. Engl. J. Med.*, vol. 373, no. 1, pp. 23–34, 2015.

[169] P. Sharma, S. Hu-Lieskovan, J. A. Wargo, and A. Ribas, “Primary, Adaptive, and Acquired Resistance to Cancer Immunotherapy,” *Cell*, vol. 168, no. 4, pp. 707–723, 2017.

[170] A. F. Labrijn, M. L. Janmaat, J. M. Reichert, and P. W. H. I. Parren, “Bispecific antibodies: a mechanistic review of the pipeline,” *Nat. Rev. Drug Discov.*, 2019.

[171] U. Brinkmann and R. E. Kontermann, “The making of bispecific antibodies,” *MAbs*, vol. 9, no. 2, pp. 182–212, 2017.

[172] A. F. Labrijn, M. L. Janmaat, J. M. Reichert, and P. W. H. I. Parren, “Bispecific antibodies: a mechanistic review of the pipeline,” *Nat. Rev. Drug Discov.*, vol. 18, no. 8, pp. 585–608, 2019.

[173] Y. Wu, M. Yi, S. Zhu, H. Wang, and K. Wu, “Recent advances and challenges of bispecific antibodies in solid tumors,” *Exp. Hematol. Oncol.*, vol. 10, no. 1, pp. 1–14, 2021.

[174] G. Riethmüller, “Symmetry breaking: Bispecific antibodies, the beginnings, and 50 years on,” *Cancer Immun.*, vol. 12, no. May, pp. 1–7, 2012.

[175] N. Fischer *et al.*, “Exploiting light chains for the scalable generation and platform purification of native human bispecific IgG,” *Nat. Commun.*, vol. 6, pp. 1–12, 2015.

[176] J. H. Cha, L. C. Chan, C. W. Li, J. L. Hsu, and M. C. Hung, “Mechanisms Controlling PD-L1 Expression in Cancer,” *Mol. Cell*, vol. 76, no. 3, pp. 359–370, 2019.

[177] M. E. Keir, M. J. Butte, G. J. Freeman, and A. H. Sharpe, “PD-1 and its ligands in tolerance and immunity,” *Annu. Rev. Immunol.*, vol. 26, pp. 677–704, 2008.

[178] A. P. R. Bally, J. W. Austin, and J. M. Boss, “Genetic and epigenetic regulation of PD-1 expression,” *J. Immunol.*, vol. 196, no. 6, pp. 2431–2437, 2016.

[179] D. Sauce *et al.*, “PD-1 expression on human CD8 T cells depends on both state of differentiation and activation status,” *Aids*, vol. 21, no. 15, pp. 2005–2013, 2007.

[180] A. H. Sharpe and K. E. Pauken, “The diverse functions of the PD1 inhibitory pathway,” *Nat. Rev. Immunol.*, vol. 18, no. 3, pp. 153–167, 2018.

[181] J. M. Chemnitz, R. V. Parry, K. E. Nichols, C. H. June, and J. L. Riley, "SHP-1 and SHP-2 Associate with Immunoreceptor Tyrosine-Based Switch Motif of Programmed Death 1 upon Primary Human T Cell Stimulation, but Only Receptor Ligation Prevents T Cell Activation," *J. Immunol.*, vol. 173, no. 2, pp. 945–954, 2004.

[182] C. Kao *et al.*, "Transcription factor T-bet represses expression of the inhibitory receptor PD-1 and sustains virus-specific CD8+ T cell responses during chronic infection," *Nat. Immunol.*, vol. 12, no. 7, pp. 663–671, 2011.

[183] R. Kratchmarov, A. M. Magun, and S. L. Reiner, "TCF1 expression marks self-renewing human CD8+ T cells," *Blood Adv.*, vol. 2, no. 14, pp. 1685–1690, 2018.

[184] W. H. Hudson *et al.*, "Proliferating Transitory T Cells with an Effector-like Transcriptional Signature Emerge from PD-1+ Stem-like CD8+ T Cells during Chronic Infection," *Immunity*, vol. 51, no. 6, pp. 1043-1058.e4, 2019.

[185] H. Dong, G. Zhu, K. Tamada, and L. Chen, "B7-H1, a third member of the B7 family, co-stimulates T-cell proliferation and interleukin-10 secretion," *Nat. Med.*, vol. 5, no. 12, pp. 1365–1369, 1999.

[186] K. Bardhan, T. Anagnostou, and V. A. Boussiotis, "The PD1: PD-L1/2 pathway from discovery to clinical implementation," *Front. Immunol.*, vol. 7, no. DEC, 2016.

[187] T. Yokosuka, M. Takamatsu, W. Kobayashi-Imanishi, A. Hashimoto-Tane, M. Azuma, and T. Saito, "Programmed cell death 1 forms negative costimulatory microclusters that directly inhibit T cell receptor signaling by recruiting phosphatase SHP2," *J. Exp. Med.*, vol. 209, no. 6, pp. 1201–1217, 2012.

[188] E. Hui *et al.*, "T cell costimulatory receptor CD28 is a primary target of PD-1 mediated inhibition," *Science (80-.).*, vol. 4, no. March, pp. 1–14, 2016.

[189] A. J. Korman, S. C. Garrett-Thomson, and N. Lonberg, "The foundations of immune checkpoint blockade and the ipilimumab approval decennial," *Nat. Rev. Drug Discov.*, 2021.

[190] L. Wang, K. Pino-Lagos, V. C. De Vries, I. Guleria, M. H. Sayegh, and R. J. Noelle, "Programmed death 1 ligand signaling regulates the generation of adaptive Foxp3+CD4+ regulatory T cells," *Proc. Natl. Acad. Sci. U. S. A.*, vol. 105, no. 27, pp. 9331–9336, 2008.

[191] Y. Zhao, D. L. Harrison, Y. Song, J. Ji, J. Huang, and E. Hui, "Antigen-Presenting Cell-Intrinsic PD-1 Neutralizes PD-L1 in cis to Attenuate PD-1 Signaling in T Cells," *Cell Rep.*, vol. 24, no. 2, pp. 379-390.e6, 2018.

[192] A. Chaudhri, Y. Xiao, A. N. Klee, X. Wang, B. Zhu, and G. J. Freeman, "PD-L1 Binds to B7-1 only in cis on the same cell surface," *Cancer Immunol. Res.*, vol. 6, no. 8, pp. 921–929, 2018.

[193] D. Sugiura *et al.*, "Restriction of PD-1 function by cis-PD-L1/CD80 interactions is required for optimal T cell responses," *Science (80-.).*, vol. 364, no. 6440, pp. 558–566, 2019.

[194] Y. Zhao *et al.*, "PD-L1:CD80 Cis-Heterodimer Triggers the Co-stimulatory Receptor CD28 While Repressing the Inhibitory PD-1 and CTLA-4 Pathways," *Immunity*, vol. 51, no. 6, pp. 1059-1073.e9, 2019.

[195] M. Ahmadzadeh *et al.*, "Tumor antigen – specific CD8 T cells infiltrating the tumor express high levels of PD-1 and are functionally impaired," *Blood*, vol. 114, no. 8, pp. 1537–1544, 2009.

[196] H. Raskov, A. Orhan, J. P. Christensen, and I. Gögenur, "Cytotoxic CD8+ T cells in cancer and cancer immunotherapy," *Br. J. Cancer*, vol. 124, no. 2, pp. 359–367, 2021.

[197] S. R. Gordon *et al.*, "PD-1 expression by tumour-associated macrophages inhibits phagocytosis and tumour immunity," *Nature*, 2017.

[198] M. Qorraj *et al.*, "The PD-1/PD-L1 axis contributes to immune metabolic dysfunctions of monocytes in chronic lymphocytic leukemia," *Leukemia*, vol. 31, no. 2, pp. 470–478, 2017.

[199] C. Sun, R. Mezzadra, and T. N. Schumacher, "Regulation and Function of the PD-L1 Checkpoint," *Immunity*, vol. 48, no. 3, pp. 434–452, 2018.

[200] T. Noguchi *et al.*, "Temporally Distinct PD-L1 Expression by Tumor and Host Cells Contributes to Immune Escape," *Cancer Immunol. Res.*, vol. 5, no. 2, pp. 106–117, 2017.

[201] H. Dong *et al.*, "Tumor-associated B7-H1 promotes T-cell apoptosis: A potential mechanism of immune evasion," *Nat. Med.*, vol. 8, no. 8, pp. 793–800, 2002.

[202] R. S. Herbst *et al.*, "Predictive correlates of response to the anti-PD-L1 antibody MPDL3280A in cancer patients," *Nature*, vol. 515, no. 7528, pp. 563–567, 2016.

[203] J. Lau *et al.*, "Tumour and host cell PD-L1 is required to mediate suppression of anti-tumour immunity in mice," *Nat. Commun.*, vol. 8, pp. 1–11, 2017.

[204] H. Tang *et al.*, "PD-L1 on host cells is essential for PD-L1 blockade – mediated tumor regression," *J. Clin. Invest.*, vol. 128, no. 2, pp. 580–588, 2018.

[205] J. W. Kleinovink, K. A. Marijt, M. J. A. Schoonderwoerd, T. van Hall, F. Ossendorp, and M. F. Fransen, "PD-L1 expression on malignant cells is no prerequisite for checkpoint therapy," *Oncoimmunology*, vol. 6, no. 4, p. e1294299, 2017.

[206] H. Lin *et al.*, "Host expression of PD-L1 determines efficacy of PD-L1 pathway blockade – mediated tumor regression," *J. Clin. Invest.*, vol. 128, no. 2, pp. 1–11, 2018.

[207] S. A. Oh *et al.*, "PD-L1 expression by dendritic cells is a key regulator of T-cell immunity in cancer," *Nat. Cancer*, 2020.

[208] J. Borst, J. Busselaar, D. M. T. Bosma, and F. Ossendorp, "Mechanism of action of PD-1 receptor/ligand targeted cancer immunotherapy," *Eur. J. Immunol.*, vol. 51, no. 8, pp. 1911–1920, 2021.

[209] V. R. Juneja *et al.*, "PD-L1 on tumor cells is sufficient for immune evasion in immunogenic tumors and inhibits CD8 T cell cytotoxicity," *J. Exp. Med.*, vol. 214, no. 4, pp. 895–904, 2017.

[210] F. Tang and P. Zheng, "Tumor cells versus host immune cells: Whose PD-L1 contributes to PD-1/PD-L1 blockade mediated cancer immunotherapy?," *Cell Biosci.*, vol. 8, no. 1, pp. 1–8, 2018.

[211] M. F. Fransen *et al.*, "Tumor-draining lymph nodes are pivotal in PD-1/PD-L1 checkpoint therapy.," *JCI insight*, vol. 3, no. 23, pp. 1–7, 2018.

[212] F. Dammeijer *et al.*, "The PD-1/PD-L1-Checkpoint Restrains T cell Immunity in Tumor-Draining Lymph Nodes," *Cancer Cell*, vol. 38, no. 5, pp. 685-700.e8, Nov. 2020.

[213] M. K. Callahan and J. D. Wolchok, "Recruit or Reboot? How Does Anti-PD-1 Therapy Change Tumor-Infiltrating Lymphocytes?," *Cancer Cell*, vol. 36, no. 3, pp. 215–217, 2019.

[214] J. Borst, T. Ahrends, N. Bąbała, C. J. M. Melief, and W. Kastenmüller, "CD4+ T cell help in cancer immunology and immunotherapy," *Nat. Rev. Immunol.*, vol. 18, no. 10, pp. 635–647, 2018.

[215] N. Budimir, G. D. Thomas, J. S. Dolina, and S. Salek-Ardakani, "Reversing T-cell Exhaustion in Cancer: Lessons Learned from PD-1/PD-L1 Immune Checkpoint Blockade," *Cancer Immunol. Res.*, vol. 10, no. 2, pp. 146–153, 2022.

[216] Y. Simoni *et al.*, "Bystander CD8+ T cells are abundant and phenotypically distinct in human tumour infiltrates," *Nature*, vol. 557, no. 7706, pp. 575–579, 2018.

[217] A. Gros *et al.*, "PD-1 identifies the patient-specific CD8+ tumor-reactive repertoire infiltrating human tumors," *J. Clin. Invest.*, vol. 124, no. 5, pp. 2246–2259, 2014.

[218] B. C. Miller *et al.*, "Subsets of exhausted CD8+ T cells differentially mediate tumor control and respond to checkpoint blockade," *Nat. Immunol.*, vol. 20, no. 3, pp. 326–336, 2019.

[219] J. Busselaar, S. Tian, H. van Eenennaam, and J. Borst, "Helpless Priming Sends CD8+ T Cells on the Road to Exhaustion," *Front. Immunol.*, vol. 11, no. October, pp. 1–12, 2020.

[220] I. Siddiqui *et al.*, "Intratumoral Tcf1 + PD-1 + CD8 + T Cells with Stem-like Properties Promote Tumor Control in Response to Vaccination and Checkpoint Blockade Immunotherapy," *Immunity*, vol. 50, no. 1, pp. 195-211.e10, 2019.

[221] A. M. van der Leun, D. S. Thommen, and T. N. Schumacher, "CD8+ T cell states in human cancer: insights from single-cell analysis," *Nat. Rev. Cancer*, vol. 20, no. 4, pp. 218–232, 2020.

[222] S. J. Im *et al.*, "Defining CD8+ T cells that provide the proliferative burst after PD-1 therapy," *Nature*, vol. 537, no. 7620, pp. 417–421, 2016.

[223] S. Kurtulus *et al.*, "Checkpoint Blockade Immunotherapy Induces Dynamic Changes in PD-1 − CD8 + Tumor-Infiltrating T Cells," *Immunity*, vol. 50, no. 1, pp. 181-194.e6, 2019.

[224] Gravbrot *et al.*, "Therapeutic Monoclonal Antibodies Targeting Immune Checkpoints for the Treatment of Solid Tumors," *Antibodies*, vol. 8, no. 4, p. 51, 2019.

[225] Y. Chen, Y. Pei, J. Luo, Z. Huang, J. Yu, and X. Meng, "Looking for the Optimal PD-1/PD-L1 Inhibitor in Cancer Treatment: A Comparison in Basic Structure, Function, and Clinical Practice," *Front. Immunol.*, vol. 11, no. May, 2020.

[226] S. L. Topalian *et al.*, "Safety, Activity, and Immune Correlates of Anti–PD-1 Antibody in Cancer," *N. Engl. J. Med.*, vol. 366, no. 26, pp. 2443–2454, Jun. 2012.

[227] S. Bagchi, R. Yuan, and E. G. Engleman, "Immune Checkpoint Inhibitors for the Treatment of Cancer: Clinical Impact and Mechanisms of Response and Resistance," *Annu. Rev. Pathol. Mech. Dis.*, vol. 16, pp. 223–249, 2021.

[228] P. Sharma, S. Hu-Lieskovan, J. A. Wargo, and A. Ribas, "Primary, Adaptive, and Acquired Resistance to Cancer Immunotherapy," *Cell*, vol. 168, no. 4, pp. 707–723, 2017.

[229] R. W. Jenkins, D. A. Barbie, and K. T. Flaherty, "Mechanisms of resistance to immune checkpoint inhibitors," *Br. J. Cancer*, vol. 118, no. 1, pp. 9–16, 2018.

[230] S. Koyama *et al.*, "Adaptive resistance to therapeutic PD-1 blockade is associated with upregulation of alternative immune checkpoints," *Nat. Commun.*, vol. 7, pp. 1–9, 2016.

[231] S. Upadhaya, S. T. Neftelinov, J. Hodge, and J. Campbell, "Challenges and opportunities in the PD1/PDL1 inhibitor clinical trial landscape.," *Nature reviews. Drug discovery*. England, Feb-2022.

[232] M. Yi, X. Zheng, M. Niu, S. Zhu, H. Ge, and K. Wu, "Combination strategies with PD-1/PD-L1 blockade: current advances and future directions," *Mol. Cancer*, vol. 21, no. 1, pp. 1–27, 2022.

[233] P.-A. Oldenborg, "CD47: A Cell Surface Glycoprotein Which Regulates Multiple Functions of Hematopoietic Cells in Health and Disease," *ISRN Hematol.*, vol. 2013, p. 614619, 2013.

[234] E. J. Brown and W. A. Frazier, "Integrin-associated protein (CD47) and its ligands," *Trends Cell Biol.*, vol. 11, no. 3, pp. 130–135, 2001.

[235] S. M. G. Hayat, V. Bianconi, M. Pirro, M. R. Jaafari, M. Hatamipour, and A. Sahebkar, "CD47: role in the immune system and application to cancer therapy," *Cell. Oncol.*, vol. 43, no. 1, pp. 19–30, 2020.

[236] R. K. Tsai and D. E. Discher, "Inhibition of 'self' engulfment through deactivation of myosin-II at the phagocytic synapse between human cells," *J. Cell Biol.*, vol. 180, no. 5, pp. 989–1003, Mar. 2008.

[237] P.-A. Oldenborg, A. Zheleznyak, Y.-F. Fang, C. F. Lagenaur, H. D. Gresham, and F. P. Lindberg, "Role of CD47 as a marker of self on red blood cells," *Science (80-.).*, vol. 288, 2000.

[238] F. P. Lindberg, H. D. Gresham, E. Schwarz, and E. J. Brown, "Molecular cloning of Integrin-Associated Protein: an

immunoglobulin family member with multiple membrane spanning domains implicated in avB3-dependent ligand binding," *J. Cell Biol.*, vol. 123, no. 2, pp. 485–496, 1993.

[239] M. P. Chao, I. L. Weissman, and R. Majeti, "The CD47-SIRP alpha pathway in cancer immune evasion and potential therapeutic implications," *Curr. Opin. Immunol.*, vol. 24, no. 2, pp. 225–232, 2012.

[240] H. Okazawa *et al.*, "Negative Regulation of Phagocytosis in Macrophages by the CD47-SHPS-1 System," *J. Immunol.*, vol. 174, no. 4, pp. 2004–2011, 2005.

[241] S. Khandelwal, N. Van Rooijen, and R. K. Saxena, "Reduced expression of CD47 during murine red blood cell (RBC) senescence and its role in RBC clearance from the circulation," *Transfusion*, vol. 47, no. 9, pp. 1725–1732, 2007.

[242] Z. Jiang, H. Sun, J. Yu, W. Tian, and Y. Song, "Targeting CD47 for cancer immunotherapy," *J. Hematol. Oncol.*, vol. 14, no. 1, pp. 1–18, 2021.

[243] R. Maute, J. Xu, and I. L. Weissman, "CD47–SIRPα-targeted therapeutics: status and prospects," *Immuno-Oncology Technol.*, vol. 13, no. C, p. 100070, Mar. 2022.

[244] T. M. Kim *et al.*, "A Phase 1 Study of ALX148, a CD47 Blocker, in Combination with Rituximab in Patients with Non-Hodgkin Lymphoma," *Blood*, vol. 134, no. Supplement_1, p. 1953, Nov. 2019.

[245] T. Qu, B. Li, and Y. Wang, "Targeting CD47/SIRPα as a therapeutic strategy, where we are and where we are headed," *Biomark. Res.*, vol. 10, no. 1, pp. 1–18, 2022.

[246] D. R. Soto-Pantoja, S. Kaur, and D. D. Roberts, "CD47 signaling pathways controlling cellular differentiation and responses to stress," *Crit. Rev. Biochem. Mol. Biol.*, vol. 50, no. 3, pp. 212–230, 2015.

[247] F. P. Lindberg, H. D. Gresham, E. Schwarz, and E. J. Brown, "Molecular cloning of integrin-associated protein: An immunoglobulin family member with multiple membrane-spanning domains implicated in α(v)β3- dependent ligand binding," *J. Cell Biol.*, vol. 123, no. 2, pp. 485–496, 1993.

[248] G. Brooke, J. D. Holbrook, M. H. Brown, and A. N. Barclay, "Human Lymphocytes Interact Directly with CD47 through a Novel Member of the Signal Regulatory Protein (SIRP) Family," *J. Immunol.*, vol. 173, no. 4, pp. 2562–2570, 2004.

[249] Z. Li, L. He, K. E. Wilson, and D. D. Roberts, "Thrombospondin-1 Inhibits TCR-Mediated T Lymphocyte Early Activation," *J. Immunol.*, vol. 166, no. 4, pp. 2427–2436, 2001.

[250] V. Q. Van *et al.*, "CD47high Expression on CD4 Effectors Identifies Functional Long-Lived Memory T Cell Progenitors," *J. Immunol.*, vol. 188, no. 9, pp. 4249–4255, 2012.

[251] S. Jaiswal *et al.*, "CD47 Is Upregulated on Circulating Hematopoietic Stem Cells and Leukemia Cells to Avoid Phagocytosis," *Cell*, vol. 138, no. 2, pp. 271–285, Jul. 2009.

[252] L. B. Cham *et al.*, "Immunotherapeutic Blockade of CD47 Inhibitory Signaling Enhances Innate and Adaptive Immune Responses to Viral Infection," *Cell Rep.*, vol. 31, no. 2, p. 107494, 2020.

[253] Y. Liu, D. Merlin, S. L. Burst, M. Pochet, J. L. Madara, and C. A. Parkos, "The Role of CD47 in Neutrophil Transmigration," *J. Biol. Chem.*, vol. 276, no. 43, pp. 40156–40166, Oct. 2001.

[254] V. Azcutia *et al.*, "Neutrophil expressed CD47 regulates CD11b/CD18-dependent neutrophil transepithelial migration in the intestine in vivo," *Mucosal Immunol.*, no. April, pp. 1–11, 2020.

[255] V. Q. Van *et al.*, "Expression of the self-marker CD47 on dendritic cells governs their trafficking to secondary lymphoid organs," *EMBO J.*, vol. 25, no. 23, pp. 5560–5568, 2006.

[256] S. Dehmani *et al.*, "SIRPγ-CD47 Interaction Positively Regulates the Activation of Human T Cells in Situation of Chronic Stimulation," *Front. Immunol.*, vol. 12, no. December, pp. 1–17, 2021.

[257] M. I. Reinhold, F. P. Lindberg, G. J. Kersh, P. M. Allen, and E. J. Brown, "Costimulation of T cell activation by integrin-associated protein (CD47) is an adhesion-dependent, CD28-independent signaling pathway," *J. Exp. Med.*, vol. 185, no. 1, pp. 1–11, 1997.

[258] M.-N. Avice, M. Rubio, M. Sergerie, G. Delespesse, and M. Sarfati, "CD47 Ligation Selectively Inhibits the Development of Human Naive T Cells into Th1 Effectors," *J. Immunol.*, vol. 165, no. 8, pp. 4624–4631, 2000.

[259] J. M. Baumgartner, B. E. Palmer, A. Banerjee, and M. D. McCarter, "Role of melanoma secreted thrombospondin-1 on induction of immunosuppressive regulatory T cells through CD47," *J. Cancer Mol.*, vol. 4, no. 5, pp. 145–152, 2008.

[260] L. B. Cham, T. Adomati, F. Li, M. Ali, and K. S. Lang, "CD47 as a Potential Target to Therapy for Infectious Diseases," *Antibodies*, vol. 9, no. 3, p. 44, 2020.

[261] S. Adams *et al.*, "Signal-regulatory protein is selectively expressed by myeloid and neuronal cells.," *J. Immunol.*, vol. 161, no. 4, pp. 1853–9, Aug. 1998.

[262] Y. Fujioka *et al.*, "A novel membrane glycoprotein, SHPS-1, that binds the SH2-domain-containing protein tyrosine phosphatase SHP-2 in response to mitogens and cell adhesion," *Mol. Cell. Biol.*, vol. 16, no. 12, pp. 6887–6899, 1996.

[263] A. Veillette, E. Thibaudeaut, and S. Latour, "High expression of inhibitory receptor SHPS-1 and its association with protein-tyrosine phosphatase SHP-1 in macrophages," *J. Biol. Chem.*, vol. 273, no. 35, pp. 22719–22728, 1998.

[264] T. Ishikawa-Sekigami *et al.*, "SHPS-1 promotes the survival of circulating erythrocytes through inhibition of phagocytosis by splenic macrophages," *Blood*, vol. 107, no. 1, pp. 341–348, 2006.

[265] P. R. Taylor, L. Martinez-Pomares, M. Stacey, H. H. Lin, G. D. Brown, and S. Gordon, "Macrophage receptors and immune recognition," *Annu. Rev. Immunol.*, vol. 23, pp. 901–944, 2005.

[266] S. J. Gardai *et al.*, "Cell-surface calreticulin initiates clearance of viable or apoptotic cells through trans-activation of LRP on the phagocyte," *Cell*, vol. 123, no. 2, pp. 321–334, 2005.

[267] M. P. Chao *et al.*, "Calreticulin is the dominant pro-phagocytic signal on multiple human cancers and is counterbalanced by CD47," *Sci. Transl. Med.*, vol. 2, no. 63, 2010.

[268] A. Veillette and J. Chen, "SIRPα–CD47 Immune Checkpoint Blockade in Anticancer Therapy," *Trends Immunol.*, pp. 1–12, 2018.

[269] M. P. Chao *et al.*, "Anti-CD47 Antibody Synergizes with Rituximab to Promote Phagocytosis and Eradicate Non-Hodgkin Lymphoma," *Cell*, vol. 142, no. 5, pp. 699–713, 2010.

[270] S. B. Willingham *et al.*, "The CD47-signal regulatory protein alpha (SIRPa) interaction is a therapeutic target for human solid tumors," *Proc. Natl. Acad. Sci.*, vol. 109, no. 17, pp. 6662–6667, 2012.

[271] M. P. Chao *et al.*, "Therapeutic antibody targeting of CD47 eliminates human acute lymphoblastic leukemia," *Cancer Res.*, vol. 71, no. 4, pp. 1374–1384, 2011.

[272] R. Majeti *et al.*, "CD47 Is an Adverse Prognostic Factor and Therapeutic Antibody Target on Human Acute Myeloid Leukemia Stem Cells," *Cell*, vol. 138, no. 2, pp. 286–299, 2009.

[273] H. Kim *et al.*, "Correlation of cd47 expression with adverse clinicopathologic features and an unfavorable prognosis in colorectal adenocarcinoma," *Diagnostics*, vol. 11, no. 4, 2021.

[274] R. M. Brightwell *et al.*, "The CD47 'don't eat me signal' is highly expressed in human ovarian cancer," *Gynecol. Oncol.*, vol. 143, no. 2, pp. 393–397, 2016.

[275] H. L. Matlung, K. Szilagyi, N. A. Barclay, and T. K. van den Berg, "The CD47-SIRPα signaling axis as an innate immune checkpoint in cancer," *Immunol. Rev.*, vol. 276, no. 1, pp. 145–164, 2017.

[276] M. E. W. Logtenberg, F. A. Scheeren, and T. N. Schumacher, "The CD47-SIRPα Immune Checkpoint," *Immunity*, vol. 52, no. 5, pp. 742–752, 2020.

[277] K. Weiskopf *et al.*, "Engineered SIRPα Variants as Immunotherapeutic Adjuvants to Anticancer Antibodies," *Science (80-.).*, vol. 341, no. 6141, pp. 88–91, Jul. 2013.

[278] X. W. Zhao *et al.*, "CD47-signal regulatory protein-α (SIRPα) interactions form a barrier for antibody-mediated tumor cell destruction," *Proc. Natl. Acad. Sci. U. S. A.*, vol. 108, no. 45, pp. 18342–18347, 2011.

[279] E. C. Pietsch *et al.*, "Anti-leukemic activity and tolerability of anti-human CD47 monoclonal antibodies," *Blood Cancer J.*, vol. 7, no. 2, pp. e536-8, 2017.

[280] X. Liu *et al.*, "CD47 blockade triggers T cell-mediated destruction of immunogenic tumors," *Nat. Med.*, vol. 21, no. 10, pp. 1209–1215, 2015.

[281] T. C. Kuo *et al.*, "Targeting the myeloid checkpoint receptor SIRPα potentiates innate and adaptive immune responses to promote anti-tumor activity," *J. Hematol. Oncol.*, vol. 13, no. 1, pp. 1–19, 2020.

[282] J. R. Ingram *et al.*, "Localized CD47 blockade enhances immunotherapy for murine melanoma," *Proc. Natl. Acad. Sci.*, vol. 114, no. 38, pp. 10184–10189, Sep. 2017.

[283] M. Olsson, P. Bruhns, W. A. Frazier, J. V. Ravetch, and P. A. Oldenborg, "Platelet homeostasis is regulated by platelet expression of CD47 under normal conditions and in passive immune thrombocytopenia," *Blood*, vol. 105, no. 9, pp. 3577–3582, 2005.

[284] J. Liu *et al.*, "Pre-clinical development of a humanized anti-CD47 antibody with anti-cancer therapeutic potential," *PLoS One*, vol. 10, no. 9, pp. 1–23, 2015.

[285] Y. Huang, Y. Ma, P. Gao, and Z. Yao, "Targeting CD47: the achievements and concerns of current studies on cancer immunotherapy," *J. Thorac. Dis.*, vol. 9, no. 2, pp. E168–E174, Feb. 2017.

[286] J. T. Sockolosky *et al.*, "Durable antitumor responses to CD47 blockade require adaptive immune stimulation," *Proc. Natl. Acad. Sci.*, vol. 113, no. 19, p. 201604268, 2016.

[287] M. M. Xu *et al.*, "Dendritic Cells but Not Macrophages Sense Tumor Mitochondrial DNA for Cross-priming through Signal Regulatory Protein α Signaling," *Immunity*, vol. 47, no. 2, pp. 363-373.e5, Aug. 2017.

[288] D. Tseng *et al.*, "Anti-CD47 antibody-mediated phagocytosis of cancer by macrophages primes an effective antitumor T-cell response," *Proc. Natl. Acad. Sci.*, vol. 110, no. 27, pp. 11103–11108, 2013.

[289] J. R. Ingram *et al.*, "Localized CD47 blockade enhances immunotherapy for murine melanoma," *Proc. Natl. Acad. Sci.*, p. 201710776, 2017.

[290] P. S. Petrova *et al.*, "TTI-621 (SIRPαFc): A CD47-blocking innate immune checkpoint inhibitor with broad antitumor activity and minimal erythrocyte binding," *Clin. Cancer Res.*, vol. 23, no. 4, pp. 1068–1079, 2017.

[291] S. M. Ansell *et al.*, "Phase I study of the CD47 blocker TTI-621 in patients with relapsed or refractory hematologic malignancies," *Clin. Cancer Res.*, vol. 27, no. 8, pp. 2190–2199, 2021.

[292] S. Ansell *et al.*, "A Phase 1 Study of TTI-621, a Novel Immune Checkpoint Inhibitor Targeting CD47, in Patients with Relapsed or Refractory Hematologic Malignancies," *Blood*, vol. 128, no. 22, p. 1812, Dec. 2016.

[293] R. Advani *et al.*, "CD47 Blockade by Hu5F9-G4 and Rituximab in Non-Hodgkin's Lymphoma," *N. Engl. J. Med.*, vol. 379, no. 18, pp. 1711–1721, 2018.

[294] C. K. Brierley *et al.*, "The effects of monoclonal anti-CD47 on RBCs, compatibility testing, and transfusion requirements in refractory acute myeloid leukemia," *Transfusion*, vol. 59, no. 7, pp. 2248–2254, 2019.

[295] N. J. Lakhani *et al.*, "Evorpacept alone and in combination with pembrolizumab or trastuzumab in patients with advanced solid tumours (ASPEN-01): a first-in-human, open-label, multicentre, phase 1 dose-escalation and dose-expansion study," *Lancet Oncol.*, vol. 22, no. 12, pp. 1740–1751, 2021.

[296] B. I. Sikic *et al.*, "First-in-human, first-in-class phase i trial of the anti-CD47 antibody Hu5F9-G4 in patients with advanced cancers," *J. Clin. Oncol.*, vol. 37, no. 12, pp. 946–953, 2019.

[297] D. A. Sallman *et al.*, "The first-in-class anti-CD47 antibody Hu5F9-G4 is active and well tolerated alone or with azacitidine in AML and MDS patients: Initial phase 1b results.," *J. Clin. Oncol.*, vol. 37, no. 15_suppl, p. 7009, May 2019.

[298] R. Upton *et al.*, "Combining CD47 blockade with trastuzumab eliminates HER2-positive breast cancer cells and overcomes trastuzumab tolerance," *Proc. Natl. Acad. Sci. U. S. A.*, vol. 118, no. 29, pp. 1–8, 2021.

[299] S. E. Kauder *et al.*, "ALX148 blocks CD47 and enhances innate and adaptive antitumor immunity with a favorable safety profile," *PLoS One*, vol. 13, no. 8, p. e0201832, Aug. 2018.

[300] K. Patel *et al.*, "CD47-Blocker TTI-622 Shows Single-Agent Activity in Patients with Advanced Relapsed or Refractory Lymphoma: Update from the Ongoing First-in-Human Dose Escalation Study," *Blood*, vol. 138, no. Supplement 1, pp. 3560–3560, Nov. 2021.

[301] B. Zhang *et al.*, "Advances in the study of CD47-based bispecific antibody in cancer immunotherapy," *Immunology*, vol. 15, no. 32, pp. 4–6, May 2022.

[302] S. Kaur, K. V Cicalese, R. Banerjee, and D. D. Roberts, "Preclinical and clinical development of therapeutic antibodies targeting functions of CD47 in the tumor microenvironment," *Antib. Ther.*, vol. 3, no. 3, pp. 179–192, Jul. 2020.

[303] Y. Yang, Z. Yang, and Y. Yang, "Potential Role of CD47-Directed Bispecific Antibodies in Cancer Immunotherapy," *Front. Immunol.*, vol. 12, no. July, pp. 1–10, Jul. 2021.

[304] A. Zhang *et al.*, "Dual targeting of CTLA-4 and CD47 on Treg cells promotes immunity against solid tumors.," *Sci. Transl. Med.*, vol. 13, no. 605, pp. 1–16, Aug. 2021.

[305] E. Dheilly *et al.*, "Tumor-directed blockade of CD47 with bispecific antibodies induces adaptive anti-tumor immunity," *Antibodies*, vol. 7, no. 3, pp. 3–15, 2018.

[306] V. Buatois *et al.*, "Preclinical development of a bispecific antibody that safely and effectively targets CD19 and CD47 for the treatment of B-cell lymphoma and leukemia," *Mol. Cancer Ther.*, vol. 17, no. 8, pp. 1739–1751, 2018.

[307] E. Dheilly *et al.*, "Selective Blockade of the Ubiquitous Checkpoint Receptor CD47 Is Enabled by Dual-Targeting Bispecific Antibodies," *Mol. Ther.*, vol. 25, no. 2, 2017.

[308] Y. Wang *et al.*, "Tumor-selective blockade of CD47 signaling with a CD47/PD-L1 bispecific antibody for enhanced anti-tumor activity and limited toxicity," *Cancer Immunol. Immunother.*, vol. 70, no. 2, pp. 365–376, 2021.

[309] M. J. Pittet, O. Michielin, and D. Migliorini, "Clinical relevance of tumour-associated macrophages.," *Nat. Rev. Clin. Oncol.*, vol. 0123456789, no. Box 1, 2022.

[310] M. Feng, W. Jiang, B. Y. S. Kim, C. C. Zhang, Y. X. Fu, and I. L. Weissman, "Phagocytosis checkpoints as new targets for cancer immunotherapy," *Nat. Rev. Cancer*, vol. 19, no. 10, pp. 568–586, 2019.

[311] Z. Yang *et al.*, "PD-L1 and CD47 co-expression predicts survival and enlightens future dual-targeting immunotherapy in non-small cell lung cancer," *Thorac. Cancer*, vol. 12, no. 11, pp. 1743–1751, 2021.

[312] Z. Yang, J. Xu, R. Li, Y. Gao, and J. He, "PD-L1 and CD47 co-expression in pulmonary sarcomatoid carcinoma: a predictor of poor prognosis and potential targets of future combined immunotherapy," *J. Cancer Res. Clin. Oncol.*, vol. 145, no. 12, pp. 3055–3065, 2019.

[313] S. C. Casey *et al.*, "MYC regulates the antitumor immune response through CD47 and PD-L1," *Science (80-.).*, vol. 352, no. 6282, pp. 227–231, 2016.

[314] H. Zhang *et al.*, "HIF-1 regulates CD47 expression in breast cancer cells to promote evasion of phagocytosis and maintenance of cancer stem cells," *Proc. Natl. Acad. Sci. U. S. A.*, vol. 112, no. 45, pp. E6215–E6223, 2015.

[315] M. Z. Noman *et al.*, "PD-L1 is a novel direct target of HIF-1α, and its blockade under hypoxia enhanced: MDSC-mediated T cell activation," *J. Exp. Med.*, vol. 211, no. 5, pp. 781–790, 2014.

[316] S. Lian *et al.*, "Simultaneous blocking of CD47 and PD-L1 increases innate and adaptive cancer immune responses and cytokine release," *EBioMedicine*, vol. 42, pp. 281–295, 2019.

[317] R. T. Manguso *et al.*, "In vivo CRISPR screening identifies Ptpn2 as a cancer immunotherapy target," *Nature*, 2017.

[318] B. I. Sikic *et al.*, "First-in-human, first-in-class phase i trial of the anti-CD47 antibody Hu5F9-G4 in patients with advanced cancers," *J. Clin. Oncol.*, vol. 37, no. 12, pp. 946–953, 2019.

[319] N. J. Lakhani *et al.*, "A phase Ib study of the anti-CD47 antibody magrolimab with the PD-L1 inhibitor avelumab (A) in solid tumor (ST) and ovarian cancer (OC) patients.," *J. Clin. Oncol.*, vol. 38, no. 5_suppl, p. 18, Feb. 2020.

[320] X. Liu *et al.*, "Dual Targeting of Innate and Adaptive Checkpoints on Tumor Cells Limits Immune Evasion," *Cell Rep.*, vol. 24, no. 8, pp. 2101–2111, 2018.

[321] B. Liu *et al.*, "Elimination of tumor by CD47/PD-L1 dual-targeting fusion protein that engages innate and adaptive immune responses," *MAbs*, vol. 10, no. 2, pp. 315–324, Feb. 2018.

[322] M. A. Postow, M. K. Callahan, and J. D. Wolchok, "Immune checkpoint blockade in cancer therapy," *J. Clin. Oncol.*, vol. 33, no. 17, pp. 1974–1982, 2015.

[323] A. E. Vilgelm, D. B. Johnson, and A. Richmond, "Combinatorial approach to cancer immunotherapy: strength in numbers," *J. Leukoc. Biol.*, vol. 100, no. 2, pp. 275–290, 2016.

[324] S.-H. Chen *et al.*, "Dual checkpoint blockade of CD47 and PD-L1 using an affinity-tuned bispecific antibody maximizes antitumor immunity," *J. Immunother. Cancer*, vol. 9, no. 10, p. e003464, Oct. 2021.

[325] K. Abiko *et al.*, "PD-L1 on tumor cells is induced in ascites and promotes peritoneal dissemination of ovarian cancer through CTL dysfunction," *Clin. Cancer Res.*, vol. 19, no. 6, pp. 1363–1374, 2013.

[326] F. Gueneau, U. Ravn, and N. Fischer, "Round optimization for improved discovery of native bispecific antibodies," *Methods*, vol. 154, no. November 2018, pp. 51–59, 2019.

[327] K. Magiera-Mularz *et al.*, "Human and mouse PD-L1: similar molecular structure, but different druggability profiles," *iScience*, vol. 24, no. 1, p. 101960, 2021.

[328] H. Tang *et al.*, "Facilitating T Cell Infiltration in Tumor Microenvironment Overcomes Resistance to PD-L1 Blockade," *Cancer Cell*, vol. 29, no. 3, pp. 285–296, 2016.

[329] L. Baudino *et al.*, "Crucial Role of Aspartic Acid at Position 265 in the CH2 Domain for Murine IgG2a and IgG2b Fc-Associated Effector Functions," *J. Immunol.*, vol. 181, no. 9, pp. 6664–6669, 2008.

[330] W. Zhong *et al.*, "Comparison of the molecular and cellular phenotypes of common mouse syngeneic models with human tumors," *BMC Genomics*, vol. 21, no. 1, pp. 1–17, 2020.

[331] S. I. S. Mosely *et al.*, "Rational Selection of Syngeneic Preclinical Tumor Models for Immunotherapeutic Drug Discovery," *Cancer Immunol. Res.*, 2017.

[332] M. A. Taylor *et al.*, "Longitudinal immune characterization of syngeneic tumor models to enable model selection for immune oncology drug discovery," *J. Immunother. Cancer*, vol. 7, no. 1, pp. 1–16, 2019.

[333] M. J. Selby *et al.*, "Preclinical development of ipilimumab and nivolumab combination immunotherapy: Mouse tumor models, In vitro functional studies, and cynomolgus macaque toxicology," *PLoS One*, vol. 11, no. 9, pp. 1–19, 2016.

[334] M. G. Lechner, S. S. Karimi, K. Barry-holson, and T. E. Angell, "Immunogenicity of murine solid tumor models as a defining feature of in vivo behavior and response to immunotherapy," *J. Immunother.*, vol. 36, no. 9, pp. 477–489, 2013.

[335] M. Yadav *et al.*, "Predicting immunogenic tumour mutations by combining mass spectrometry and exome sequencing," *Nature*, vol. 515, no. 7528, pp. 572–576, 2014.

[336] R. Dahan, E. Sega, J. Engelhardt, M. Selby, A. J. Korman, and J. V. Ravetch, "FcγRs Modulate the Anti-tumor Activity of Antibodies Targeting the PD-1/PD-L1 Axis," *Cancer Cell*, vol. 28, no. 3, pp. 285–295, 2015.

[337] J. Duraiswamy, K. M. Kaluza, G. J. Freeman, and G. Coukos, "Dual blockade of PD-1 and CTLA-4 combined with tumor vaccine effectively restores T-cell rejection function in tumors," *Cancer Res.*, vol. 73, no. 12, pp. 3591–3603, 2013.

[338] B. Homet Moreno *et al.*, "Response to Programmed Cell Death-1 Blockade in a Murine Melanoma Syngeneic Model Requires Costimulation, CD4, and CD8 T Cells," *Cancer Immunol. Res.*, vol. 4, no. 10, pp. 845–857, 2016.

[339] Sivan Ayelet *et al.*, "Commensal Bifidobacterium promotes antitumor immunity and facilitates anti–PD-L1 efficacy," *Science (80-.).*, vol. 350, no. 6264, pp. 1084–1089, 2015.

[340] M. Vétizou *et al.*, "Anticancer immunotherapy by CTLA-4 blockade relies on the gut microbiota," *Science (80-.).*, vol. 350, no. 6264, pp. 1079–1084, 2015.

[341] K. M. Kokolus *et al.*, "Baseline tumor growth and immune control in laboratory mice are significantly influenced by subthermoneutral housing temperature.," *Proc. Natl. Acad. Sci. U. S. A.*, vol. 110, no. 50, pp. 20176–81, Dec. 2013.

[342] S. de Silva *et al.*, "CD40 Enhances Type I Interferon Responses Downstream of CD47 Blockade, Bridging Innate and Adaptive Immunity.," *Cancer Immunol. Res.*, 2019.

[343] A. M. Merchant *et al.*, "An efficient route to human bispecific IgG," *Nat. Biotechnol.*, vol. 16, no. 7, pp. 677–681, 1998.

[344] B. D. Wines, M. S. Powell, P. W. H. I. Parren, N. Barnes, and P. M. Hogarth, "The IgG Fc Contains Distinct Fc Receptor (FcR) Binding Sites: The Leukocyte Receptors FcγRI and FcγRIIa Bind to a Region in the Fc Distinct from That Recognized by Neonatal FcR and Protein A," *J. Immunol.*, vol. 164, no. 10, pp. 5313–5318, 2000.

[345] J. Lund *et al.*, "Human Fc gamma RI and Fc gamma RII interact with distinct but overlapping sites on human IgG.," *J. Immunol.*, vol. 147, no. 8, pp. 2657–62, Oct. 1991.

[346] R. L. Shields *et al.*, "High Resolution Mapping of the Binding Site on Human IgG1 for FcγRI, FcγRII, FcγRIII, and FcRn and Design of IgG1 Variants with Improved Binding to the FcγR," *J. Biol. Chem.*, vol. 276, no. 9, pp. 6591–6604, 2001.

[347] N. T. Joncker, S. Bettini, D. Boulet, M. Guiraud, and S. Guerder, "The site of tumor development determines immunogenicity via temporal mobilization of antigen-laden dendritic cells in draining lymph nodes," *Eur. J. Immunol.*, vol. 46, no. 3, pp. 609–618, 2016.

[348] P. M. Carlson *et al.*, "Depth of tumor implantation affects response to in situ vaccination in a syngeneic murine melanoma model," *J. Immunother. cancer*, vol. 9, no. 4, 2021.

[349] B. Bonnotte *et al.*, "Intradermal injection, as opposed to subcutaneous injection, enhances immunogenicity and suppresses tumorigenicity of tumor cells," *Cancer Res.*, vol. 63, no. 9, pp. 2145–2149, 2003.

[350] L. Liu, "Pharmacokinetics of monoclonal antibodies and Fc-fusion proteins," *Protein Cell*, vol. 9, no. 1, pp. 15–32, Jan. 2018.

[351] M. Chaib, S. C. Chauhan, and L. Makowski, "Friend or Foe? Recent Strategies to Target Myeloid Cells in Cancer," *Front. Cell Dev. Biol.*, vol. 8, no. May, pp. 1–18, May 2020.

[352] D. Lu *et al.*, "Beyond T Cells: Understanding the Role of PD-1/PD-L1 in Tumor-Associated Macrophages," *J. Immunol. Res.*, vol. 2019, 2019.

[353] Y. Pan, Y. Yu, X. Wang, and T. Zhang, "Tumor-Associated Macrophages in Tumor Immunity," *Front. Immunol.*, vol. 11, no. December, 2020.

[354] S. A. Quezada, K. S. Peggs, M. A. Curran, and J. P. Allison, "CTLA4 blockade and GM-CSF combination immunotherapy alters the intratumor balance of effector and regulatory T cells," *J. Clin. Invest.*, vol. 116, no. 7, pp. 1935–1945, Jul. 2006.

[355] H. Jin *et al.*, "Avelumab internalization by human circulating immune cells is mediated by both Fc gamma receptor and PD-L1 binding," *Oncoimmunology*, vol. 10, no. 1, 2021.

[356] K. Wu, M. Yi, S. Qin, Q. Chu, X. Zheng, and K. Wu, "The efficacy and safety of combination of PD-1 and CTLA-4 inhibitors: A meta-analysis," *Exp. Hematol. Oncol.*, vol. 8, no. 1, pp. 1–12, 2019.

[357] S. Vafaei *et al.*, "Combination therapy with immune checkpoint inhibitors (ICIs); a new frontier," *Cancer Cell Int.*, vol. 22, no. 1, pp. 1–27, 2022.

[358] J. A. Marin-Acevedo, E. M. O. Kimbrough, and Y. Lou, "Next generation of immune checkpoint inhibitors and beyond," *J. Hematol. Oncol.*, vol. 14, no. 1, pp. 1–29, 2021.

[359] L. F. Campesato, C.-H. Weng, and T. Merghoub, "Innate immune checkpoints for cancer immunotherapy: expanding the scope of non T cell targets," *Ann. Transl. Med.*, vol. 8, no. 16, pp. 1031–1031, 2020.

[360] R. W. Lentz, M. D. Colton, S. S. Mitra, and W. A. Messersmith, "Innate immune checkpoint inhibitors: The next breakthrough in medical oncology?," *Mol. Cancer Ther.*, vol. 20, no. 6, pp. 961–974, 2021.

[361] D. R. Soto-Pantoja *et al.*, "CD47 in the Tumor Microenvironment Limits Cooperation between Antitumor T-cell Immunity and Radiotherapy," *Cancer Res.*, vol. 74, no. 23, pp. 6771–6783, Dec. 2014.

[362] M. P. Chao *et al.*, "Therapeutic Targeting of the Macrophage Immune Checkpoint CD47 in Myeloid Malignancies," *Front. Oncol.*, vol. 9, no. January, p. 1380, Jan. 2020.

[363] E. Dheilly *et al.*, "Selective Blockade of the Ubiquitous Checkpoint Receptor CD47 Is Enabled by Dual-Targeting Bispecific Antibodies - supplementary," *Mol. Ther.*, vol. 25, no. 2, 2017.

[364] B. Mao, S. Guo, D. Ouyang, and H. Li, "Abstract 265: Evaluating variation in drug efficacy endpoints in a syngeneic mouse model (CT26.WT) under immune checkpoint blockade," *Cancer Res.*, vol. 81, no. 13_Supplement, pp. 265–265, Jul. 2021.

[365] A. Mullard, "Half of top cancer studies fail high-profile reproducibility effort," *Nature*, vol. 600, no. 7889, pp. 368–369, Dec. 2021.

[366] Y. Liu *et al.*, "Multi-omic measurements of heterogeneity in HeLa cells across laboratories," *Nat. Biotechnol.*, vol. 37, no. 3, pp. 314–322, 2019.

[367] U. Ben-David *et al.*, "Genetic and transcriptional evolution alters cancer cell line drug response," *Nature*, vol. 560, no. 7718, pp. 325–330, 2018.

[368] S. M. Ansell *et al.*, "TTI-621 (SIRPαFc), an Immune Checkpoint Inhibitor Blocking the CD47 'Do Not Eat' Signal, Induces Objective Responses in Patients with Advanced, Relapsed/Refractory Diffuse Large B-Cell Lymphoma (DLBCL)," *Blood*, vol. 130, no. Supplement 1, p. 4116, Dec. 2017.

[369] Y. Xu, G. H. Su, D. Ma, Y. Xiao, Z. M. Shao, and Y. Z. Jiang, "Technological advances in cancer immunity: from immunogenomics to single-cell analysis and artificial intelligence," *Signal Transduct. Target. Ther.*, vol. 6, no. 1, 2021.

[370] H. Lin *et al.*, "Host expression of PD-L1 determines efficacy of PD-L1 pathway blockade – mediated tumor regression," *J. Clin. Invest.*, vol. 128, no. April, pp. 805–815, 2018.

[371] D. Y. Lin *et al.*, “The PD-1 / PD-L1 complex resembles the antigen-binding Fv domains of antibodies and T cell receptors,” *Proc. Natl. Acad. Sci.*, vol. 105, no. 8, pp. 3011–3016, 2008.

[372] R. L. Maute *et al.*, “Engineering high-affinity PD-1 variants for optimized immunotherapy and immuno-PET imaging,” *Proc. Natl. Acad. Sci.*, vol. 112, no. 47, pp. E6506–E6514, 2015.